

# INAUGURAL - DISSERTATION

ZUR ERLANGUNG DER DOKTORWÜRDE DER  
NATURWISSENSCHAFTLICH - MATHEMATISCHEN  
GESAMTFAKULTÄT DER RUPRECHT-KARLS-UNIVERSITÄT  
HEIDELBERG

vorgelegt von  
M.Sc. Michael Andreas Thaller  
aus Freising

Tag der mündlichen Prüfung: 1. März 2016



# Hyaluronan hydrogel modified intraocular implants for glaucoma treatment

## Gutachter

Prof. Dr. Joachim P. Spatz

Physikalisch-Chemisches Institut  
Ruprecht-Karls-Universität Heidelberg,  
Max-Planck-Institut für Intelligente  
Systeme Stuttgart

Prof. Dr. Reiner Dahint

Physikalisch-Chemisches Institut  
Ruprecht-Karls-Universität Heidelberg





## **Abstract**

Glaucoma is a very prevalent eye disease with more than 60 million people affected worldwide. The only form of therapy is the artificial lowering of the intraocular pressure of the aqueous humor, which is the main cause for the disease. This can be achieved for example by the application of an intraocular implant to drain excess liquid. Due to a non-optimal biocompatibility these intraocular stents often induce inflammation and fibrosis of their surrounding tissue. This subsequently blocks the outflow of liquid through the implant and results in long-term failure of the therapy.

The goal of this thesis was the development of a new type of glaucoma implant made from titanium enhanced by hyaluronan hydrogels. The basic concept was the coating of the outer surfaces of a small tube with hydrogels made from hyaluronic acid to enhance cell adhesion for a better biocompatibility and a lower occurrence of inflammation and fibrosis. Simultaneously the interior was to be filled with hyaluronan hydrogels with slightly different properties to block a clogging of the drainage path by cell growth and act as a valve to regulate the intraocular pressure. In addition the economical and work safety aspects for an industrial mass production and biomedical application of these implants were considered.

In order to achieve this goal, a number of methods to fabricate, and tools to analyze, hydrogel-enhanced glaucoma implants have been investigated in this thesis. Reaction sequences were developed to simultaneously crosslink and immobilize hyaluronan hydrogels on glass and titanium surfaces by a combination of several established methods. In addition, fluoresceinamine was integrated into the process to generate fluorescently labeled hydrogels, which was an effective tool for further analysis. Also, a number of methods were designed to observe the behavior of the hydrogel-modified implants when exposed to external pressures. It was possible, by using these methods, to verify the stability of the immobilization, with hydrogels within the tubes being able to withstand the pressures encountered in the glaucomatous eye without breaking apart. Furthermore it was shown that a regulation of external liquid pressures by these hydrogel-filled tubes was possible which illustrated these implants' potential to drain excess intraocular fluid from the glaucomatous eye without causing hypotony. The mechanism of the pressure regulation was further explored and related to the presence of channels within the hydrogels that enabled liquid flow at certain pressure levels. Since the natural occurrence of these channels during the production process of the implants was initially random, two methods were developed to allow their artificial and reproducible creation. This was achieved either by the use of a laser to burn channels into the hydrogels or by the implementation of small glass fibers prior to the gel formation within the tubes.

The methods established and the results gained in this thesis provide the means to generate hydrogel-enhanced implants and illustrate their general usability in glaucoma therapy by reducing intraocular pressure. In addition the process for the implant creation was successfully streamlined to allow for a cost effective, low-hazard production on an industrial scale. Future research based on the established concept will comprise the optimization of the hydrogels' capabilities to either improve or resist cell adhesion as

necessary. Also setups will have to be designed for a miniaturization and industrial mass fabrication of the implants.

## Zusammenfassung

Das Glaukom, oder grüner Star, umfasst eine Reihe von Augenkrankheiten, die mehr als 60 Millionen mal weltweit diagnostiziert wurden. Hauptursache für die Entstehung eines Glaukoms ist ein erhöhter Augeninnendruck. Die einzige bisher angewendete Behandlungsmethode besteht in einer künstlichen Reduktion des Augeninnendrucks. Hierfür kann zum Beispiel ein Implantat, das überschüssiges Kammerwasser aus dem Auge abfließen lässt, eingesetzt werden. Häufig kommt es jedoch auf Grund unzureichender Biokompatibilität zu Entzündungen und Narbenbildung im umliegenden Gewebe des Implantats. Hierdurch wird der Flüssigkeitsfluss blockiert und die Therapie muss abgebrochen bzw. das Implantat erneuert werden.

Im Rahmen dieser Doktorarbeit sollten Glaukomimplantaten einer neuen Generation entwickelt und, deren Biokompatibilität mit Hyaluronsäure basierten Hydrogeln verbessert werden. Das Grundkonzept sah vor, die Außenseite kleiner Titanröhrchen mit diesen Biopolymeren so zu beschichten, dass eine Zellbesiedlung vereinfacht und das Auftreten von Entzündungen und die Bildung von Narbengewebe reduziert wird. Im Inneren der Röhrchen sollten Gele mit anderen Eigenschaften immobilisiert werden, um einen Zellbewuchs zu verhindern und den Augeninnendruck zu regulieren. Bei der Methodenentwicklung wurden außerdem wirtschaftliche und sicherheitstechnische Aspekte für eine industrielle Massenproduktion berücksichtigt.

Es wurde eine Reihe von Methoden entwickelt, um solche neuartigen Implantate herzustellen und deren Eigenschaften zu charakterisieren. Zunächst wurde eine Auswahl von Reaktionen aus bereits etablierten Methoden kombiniert um eine gleichzeitige Gelbildung und Immobilisierung von Hyaluronsäure auf Glas- und Titanoberflächen zu erreichen. Weiterhin wurde Fluoresceinamin in den Herstellungsprozess der modifizierten Hyaluronäsure integriert. Dies ermöglichte die Synthese fluoreszierender Hyaluronsäure bzw. HA-Gele, die besser beobachtet werden konnten. Außerdem wurde eine Reihe von Methoden entwickelt, die es erlaubten die Reaktionen der hydrogel-modifizierten Implantate zu beobachten, wenn diese externen Flüssigkeitsdrücken ausgesetzt werden. Die Stabilität der Immobilisierung der Hydrogele auf den Implantatoberflächen konnte damit getestet und überprüft werden, ob die Gele einem typischen glaukomatösem Augeninnendruck stand halten können, ohne zerstört zu werden. Außerdem konnte gezeigt werden, dass die HA-Gel gefüllten Röhrchen prinzipiell einen externen Flüssigkeitsdruck regulieren können und damit geeignet sind überschüssiges Kammerwasser aus dem Auge zu entfernen ohne einen Unterdruck zu verursachen. Der zugrunde liegende Mechanismus dieser Druckregulation wurde aufgeklärt und mit dem Auftreten von Kanälen innerhalb der Hydrogele in Verbindung gebracht. Diese lassen einen Flüssigkeitsfluss ab einem bestimmten Druck zu. Da die Kanäle während dem Herstellungsprozess der Implantate zunächst nur zufällig auftraten, wurden zwei Methoden entwickelt um eine künstliches und reproduzierbares Entstehen der Kanäle zu gewährleisten. Die Kanäle wurden entweder nachträglich mit einem Laser in die Hydrogele "gebrannt" oder durch die Implementierung dünner Glasfasern im Inneren der Röhrchen während der Gelbildung ermöglicht.

Die in dieser Arbeit entwickelten Methoden und gewonnenen Erkenntnisse bilden die Grundlage um Intraokularimplantate einer neuer Generation herzustellen. Modellimplantate wurden außen und innen mit Hydrogelen beschichtet und es wurde gezeigt, dass diese in der Lage sind Drücke zu regulieren. Implantate, die sich in Zukunft an diesen Modellen orientieren, werden in der Lage sein den Augeninnendruck zu regulieren und damit als Therapie des Glaukoms einsetzbar sein. Nächste Forschungsschritte sind die Optimierung hinsichtlich der Zelladhäsion, sowie die Miniaturisierung der Implantate.

1.	Introduction .....	1
1.1.	Thesis Overview .....	1
1.2.	The glaucoma disease .....	3
1.3.	Biomaterials and biocompatibility .....	8
1.4.	Hyaluronan hydrogels .....	11
1.5.	Titanium: An efficient biomaterial .....	17
1.6.	General challenges and their proposed solutions .....	20
2.	Results & Discussion .....	26
2.1.	Chemical modification of hyaluronan .....	26
2.1.1.	Fluorescent labeling .....	26
2.1.2.	Modification of hyaluronan with thiol groups .....	28
2.1.3.	Combination of thiolation and fluorescent labeling of hyaluronan .....	31
2.1.4.	Summary and conclusion .....	36
2.2.	Immobilization of hyaluronan to glass and titanium surfaces .....	37
2.2.1.	Development of a silanization protocol .....	37
2.2.2.	Immobilization of hyaluronan to flat glass and titanium surfaces .....	40
2.2.3.	Selective Immobilization of hyaluronan to small glass tubes .....	42
2.2.4.	Summary and Conclusion .....	44
2.3.	Formation and immobilization of hyaluronan hydrogels .....	45
2.3.1.	Synthesis of acrylamide-crosslinked hydrogels .....	45
2.3.2.	Immobilizing hyaluronan hydrogels to epoxide modified surfaces .....	49
2.3.3.	Summary and conclusion .....	52
2.4.	Development of analytical tools for determining the pressure resistance of HA hydrogel-modified tubes .....	53
2.4.1.	Constrained swelling of hydrogels in small tubes .....	53
2.4.2.	Continuous pressure application .....	57
2.4.3.	Hydrostatic pressure measurements .....	72
2.4.4.	Summary and conclusion .....	75
2.5.	Optimization of the concept for a creation of intraocular stents .....	77
2.5.1.	The mechanism of liquid flow through gel-filled tubes .....	77
2.5.2.	Exploration of physical methods for the creation of small channels in hyaluronan hydrogels .....	85

2.5.3. Summary and conclusion .....	92
3. Summary and Outlook.....	93
3.1.1. Summary and Discussion .....	93
3.2. Outlook.....	99
4. Materials and Methods .....	101
4.1. Modification of Hyaluronan.....	101
4.1.1. Materials.....	101
4.1.2. Modification of hyaluronan with thiol groups.....	101
4.1.3. Modification of HA with fluorescent markers .....	104
4.1.4. Combined modification of HA with fluorescein and thiol groups.....	105
4.2. Immobilization of hyaluronan to glass and titanium surfaces.....	106
4.2.1. Materials.....	106
4.2.2. Basic silanization protocol .....	106
4.2.3. Immobilization of HA on partially silanized flat surfaces .....	108
4.2.4. Selective HA immobilization on the outer and inner surfaces of small glass and titanium tubes.....	109
4.3. Creation and immobilization of HA hydrogels .....	110
4.3.1. Materials.....	110
4.3.2. Formation of hydrogels .....	110
4.4. Swelling behavior of hydrogels.....	113
4.4.1. Materials.....	113
4.4.2. Experimental procedure.....	113
4.5. Pressure resistance measurements of HA-hydrogel modified tubes .....	114
4.5.1. Materials.....	114
4.5.2. CPA measurements .....	114
4.6. Hydrostatic pressure measurements .....	116
4.6.1. Materials.....	116
4.6.2. Measurements.....	116
4.7. Microscopic pressure-flow experiments.....	118
4.7.1. Materials.....	118
4.7.2. Measurements.....	118
4.8. Artificial creation of channels in hydrogels .....	120
4.8.1. Materials.....	120

4.8.2. Channel creation and HPA measurement.....	120
5. Literature .....	124
6. Appendix .....	135
6.1. List of abbreviations .....	135
6.2. Additional <sup>1</sup> H-NMR's of DTPH and unmodified HA .....	136
6.3. pH changes in unbuffered BSS due to diluting HS-HA.....	137
6.4. Molds for creating macroscopic gels .....	137
6.5. Blueprints of sample holder for CPA measurements .....	138
6.6. Blueprints of setup for partially silanizing glass and titanium slides.....	139
6.7. Blueprints for the setup for filling large glass tubes (ID = 5 mm; OD = 7 mm; L = 10 mm) with hydrogels .....	140
6.8. Publication derived from this thesis .....	141

## **1. Introduction**

### **1.1. Thesis Overview**

The impact of glaucoma on our healthcare system is considerable and with an aging population the problem is bound to increase. One form of therapy is the use of an implant to reduce intraocular pressure, which is considered to be the main risk factor for the development and progress of the affliction. However, the failure rate of these implants is not acceptable, creating the need for further improvements for an improved application (See Section 1.2 for further discussion).

The main problem surrounding implant failure is non-optimal biocompatibility (See Sections 1.2 and 1.3). The aim of the thesis was the development of a new type of intraocular implant, modified with hydrogels made from hyaluronan enhancing the therapeutic properties. Hydrogels made from hyaluronan have already been used successfully in tissue engineering, and have also shown promise in a glaucoma stent with enhanced capabilities (see Section 1.4). The basic concept relied on a small tube made from titanium, a biocompatible biomaterial, which is already used in many biomedical applications (see Section 1.5). On the outer surface of the tubes hyaluronan (HA) hydrogels are grafted for promoting cell proliferation, reducing inflammatory responses of the surrounding tissue and further enhancing biocompatibility. For the interior of the tube, the idea was to fill it with a hyaluronan-based hydrogel possessing cell repellent characteristics for preventing clotting due to cell growth. Additionally this hydrogel should perform as a valve and regulate intraocular pressure within the glaucomatous eye (Figure 1).

In this thesis the methods for immobilization of hydrogels made from hyaluronic acid to small glass and titanium tubes, acting as model implants were developed. Furthermore it was investigated, whether a controlled regulation of an external liquid pressure was possible.

To that end, an already established method for modifying hyaluronan with thiol groups (Section 2.1.2) to generate hydrogels using crosslinkers containing multiple acrylamide functions (Section 2.3) was adapted and refined. For visualization on a small scale, a combined modification of hyaluronan with thiols and fluorescein was established in order to generate hydrogels with fluorescent properties (Section 2.2.2). Following that, the selective immobilization of hydrogels to glass and titanium surfaces was developed. The goal was creating “model” or “prototype” implants in the form of small tubes carrying hydrogels selectively on their inner and/or outer surfaces (Section 2.3.2). In order to evaluate a resistance to external liquid pressure, two methods were established: the first utilized constant pressure buildup in a syringe while the second employed the hydrostatic pressure of a liquid column (Sections 2.4.2 and 2.4.3). Measurements with these methods showed that liquid flow through the hydrogel-filled model implants and regulation of the external liquid pressure was possible. Subsequent experiments with fluorescence revealed pressure regulatory abilities in some samples due to the presence of small channels within the hydrogels (Section 2.5.1).

## 1. Introduction

Subsequently an artificial generation of these channels was successfully established, either mechanically or by the application of lasers (Section 2.5.2). Provided that future miniaturization is feasible, the methods developed within this thesis showed that the manufacture of these new types of implants is possible.

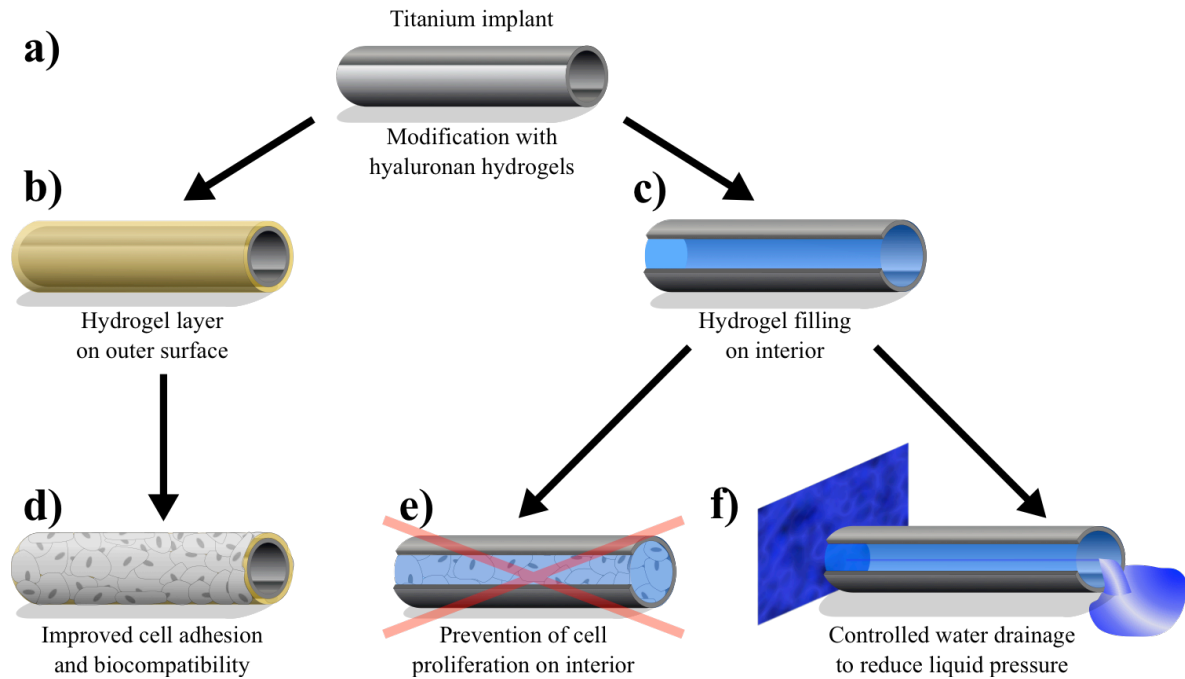


**Figure 1:** Basic principle for the creation of a new type of glaucoma implant. The basic design is a titanium tube (a) capable of draining fluid from the glaucomatous eye in order to reduce the intraocular pressure. Hydrogels made from hyaluronan are selectively grafted on the outer surface (b) and into the interior (c) of the tube. These modifications should on the one hand enable an improved cell proliferation to increase the biocompatibility of the tube (d) while preventing a blockade of the interior through cell proliferation (e). The hydrogel on the interior further acts as a valve and control the amount of liquid drained from the eye for a regulated decrease of intraocular pressure. (f)

### 1.2. The glaucoma disease

#### Overview

The term “glaucoma” encompasses a group of progressive diseases that affect the eye, which share the common symptom of a slow degeneration of the visual nerve.<sup>1</sup> All variations are progressive and can potentially lead to a total loss of vision.<sup>2</sup> The occurrence of glaucoma is very low before the age of 40 and increases with the age of the patient.<sup>3</sup> This affliction comes in different variations<sup>2</sup>, but the most prevalent manifestation of glaucoma in the western hemisphere is “Primary Open-Angle Glaucoma” (POAG).<sup>4</sup> A main risk factor for the development of POAG is increased intraocular pressure<sup>1</sup>, and so far the main therapy is a reduction of this pressure, even when no increased values were detected<sup>5</sup>.

Glaucoma is a prevalent disease and its impact on healthcare is not to be underestimated; studies conducted by the WHO in 2010 estimated that around 57 million people worldwide suffered from vision loss from this disease with more than 3 million afflicted by acute blindness due to glaucoma, elevating the disease to the second highest cause of blindness.<sup>6</sup> Estimations for 2020 and 2040 expect 76 million and 111.8 million cases, respectively, of glaucoma worldwide due to an aging population.<sup>4</sup> For that reason it is important to further develop therapies to cure or slow the progression of the disease.

#### Pathophysiology

The cause of visual loss in POAG is the gradual and progressive degeneration of the retinal ganglion cells.<sup>2,7</sup> These neurons are part of the retinal nerve fiber layer, converge at the optic disc where they form the optic nerve that exits the eye through the lamina cribrosa.<sup>1</sup> They are responsible for the transfer of visual signals to the brain and rely on a supply of trophic factors to survive.<sup>8</sup> During the development of POAG, a gradual apoptosis of these ganglion cells is induced, leading to a deformation and loss of functionality of the optical disc and irreversible damage of the visual nerve (Figure 2).<sup>7</sup> There are different factors contributing to the development of POAG<sup>9</sup> and the pathophysiology has not yet been fully understood.<sup>1,2,7</sup> However, it has been shown that one of the main contributors to the outbreak and progress of the disease is elevated intraocular pressure (IOP) of the aqueous humor (Figure 2).<sup>1,2,10</sup> This phenomena is often caused by an increased resistance of the trabecular meshwork to an outflow of liquid from the aqueous humor into the Schlemm’s canal<sup>11</sup>, resulting in the IOP rising to levels above the normal values of 21 mmHg<sup>12</sup>. This can result in a deformation of the lamina cribrosa<sup>13</sup> and a blockade of axonal transport of trophic factors.<sup>14</sup> As a result of this trophic deficiency an apoptosis of retinal ganglion cells is induced, leading to a gradual loss of vision.<sup>15,16</sup> Furthermore, this initial loss of ganglion cells can amplify further degeneration due to the formation of a toxic environment, accelerating the progress of the disease.<sup>9</sup>

# 1. Introduction

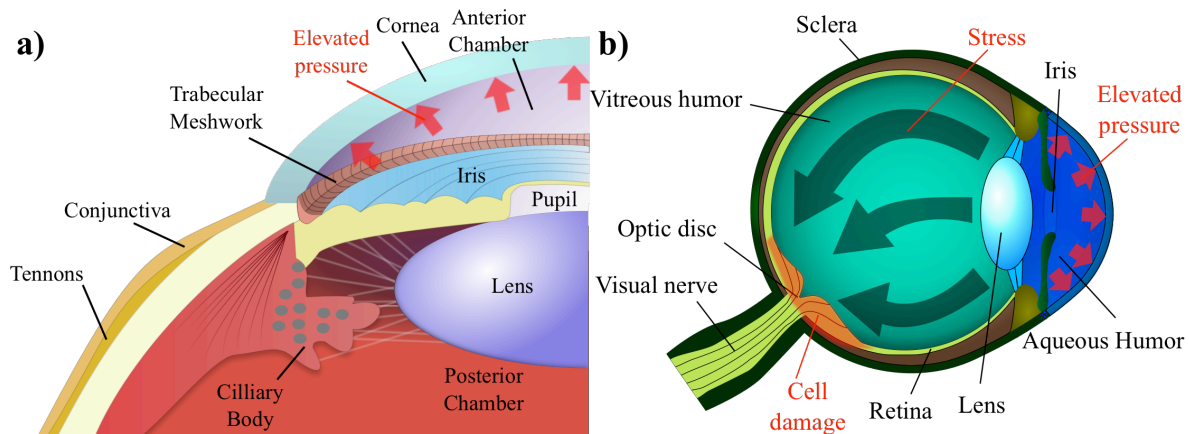


**Figure 2:** (a): Depiction of a cross section of part of the human eye illustrating the origin of the disease being an elevated pressure within the aqueous humor of the anterior chamber. (b): This increase pressure puts a strain on rest of the eye causing damage to the optic disc. The retinal ganglion cells degrade ultimately resulting in a loss of vision.

As already outlined, the whole pathophysiology has not been fully understood<sup>17</sup> and patients can develop symptoms similar to POAG at normal pressure levels (“normal tension glaucoma”).<sup>18</sup> Still, the main risk factor for the development of the disease is elevated intraocular pressure<sup>2</sup> and the main focus of therapies is a reduction of this intraocular pressure, even when values are at normal levels.<sup>1,5,9,19</sup>

## Treatment

The visual loss from glaucoma is irreversible<sup>1</sup>, but the progression can be impeded by a reduction of the intraocular pressure.<sup>19</sup> Currently pressure reduction is the only established therapy even for people with normal levels of IOP<sup>5</sup>. To that end, several different therapies have been utilized:

### *Pharmaceutical treatment*

Usually, the first line of treatment in the progress of glaucoma is the use of medical agents, most commonly in the form of eye drops.<sup>9</sup> They consist, for example, of prostaglandins that can directly reduce the intraocular pressure of the glaucomatous eye.<sup>20</sup> While this method is relatively cheap and the application to the glaucomatous eye is rather simple to perform<sup>21</sup>, the issue of side effects<sup>22</sup> and a low compliancy of the patients, with more than half of them failing to follow their prescribed medication schedule<sup>23</sup>, proves to be a recurring problem.

## 1. Introduction

---

### *Laser application*

The use of lasers to reduce intraocular pressures (“laser trabeculoplasty”) was found to be an effective alternative to medical treatment.<sup>24</sup> In this form of therapy, laser light is used to lower the resistance of the trabecular meshwork to liquid outflow from the aqueous humor (Figure 3a).<sup>25</sup> The mechanism of the pressure lowering effect is not yet fully understood<sup>26</sup> and a number of different methods have been established with different laser types and pulsing times without any showing clear superiority to the others.<sup>25</sup> Still, laser trabeculoplasty is a sufficient alternative or addition to medical treatment for a reduction of the intraocular pressure.<sup>24</sup> The main drawback preventing the method to be the gold standard in glaucoma treatment is the relatively high failure rate, with up to 42% of patients regaining elevated IOP after five years.<sup>27</sup>

### *Surgical treatment*

Another method that was established separately from medical treatment was the surgical removal of a small part of the trabecular meshwork and its surrounding tissue in order to enhance aqueous outflow, called trabeculectomy (Figure 3b).<sup>28</sup> While the treatment was successful in reducing IOP<sup>29</sup>, some studies showed significant side effects, such as infections<sup>30</sup>, the formation of cataracts<sup>31</sup>, and hypotony due to an uncontrolled leakage<sup>32</sup> which often necessitated extensive postoperative care.

### *Application of intraocular implants*

A method that was established as an alternative to trabeculectomy was the implementation of an intraocular implant in order to create an artificial channel for the drainage of excess fluid within the aqueous humor.<sup>33</sup> This concept was first introduced by Molteno in 1969<sup>34</sup> and later refined<sup>35</sup> to treat patients suffering from glaucoma. The implant that Molteno designed consisted of a small tube connected to a plate. The tip of the tube was inserted into the anterior chamber and the plate attached to the sclera, creating a pocket that contained a spherical cavity filled with drained intraocular fluid (“bleb”). Fibrous tissue formed around the bleb, allowing a slow drainage of the excess liquid via diffusion and resulting in a decrease of the intraocular pressure (Figure 3c).<sup>34,35</sup>

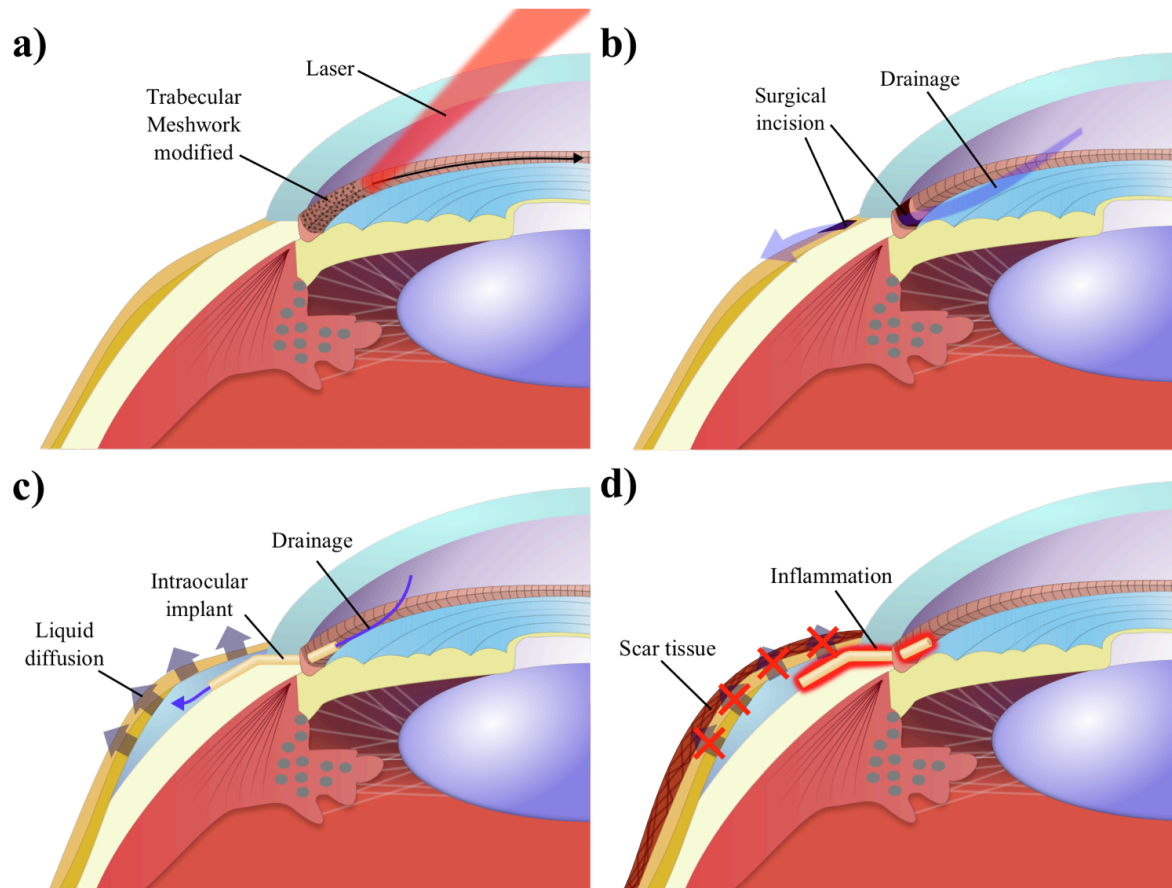


**Figure 3:** (a-c) Basic concepts of the glaucoma treatment using different methods: **(a) Laser trabeculoplasty:** The trabecular meshwork is treated with a laser to improve the natural drainage of intraocular fluid. **(b) Trabeculectomy:** An artificial channel is created surgically to drain excess fluid and lower the intraocular pressure. **(c) Intraocular implant:** Application of an intraocular implant to reduce the pressure by draining liquid from the anterior chamber into a small pocket (“bleb”) from where it is expelled by diffusion. **(d):** Main cause for the failure of these implants due to non-optimal biocompatibility: An inflammatory reaction of the body results in the formation of scar tissue around the bleb blocking the outflow of intraocular liquid.

While these early implants were able to lower the intraocular pressure in glaucomatous eyes and slow the progress of the disease<sup>35</sup>, they did not come without several of problems which led to a number of modifications of the original design; among other things, they offered no resistance to aqueous outflow, which often led to hypotony through uncontrolled drainage.<sup>33</sup> This resulted in the introduction of pressure-sensitive valves to increase pressure resistance.<sup>36</sup> The other important modification was the increase of surface area improving implant’s ability to lower the intraocular pressure compared to the original concept by Molteno.<sup>37</sup> Today, the designs of modern implants are derived from these early concepts and used regularly in glaucoma therapies.<sup>33</sup>

Still, a number of issues persist that limit the effectiveness of this treatment, both short- and long-term. While less frequent with the introduction of valves, pressure regulation is still not optimal and in some cases hypotony was observed.<sup>36</sup> Also, it was found that certain types of implants can diplopia, probably related to the form of the implant’s end plate.<sup>37,38</sup> Moreover, with some models using pressure-sensitive valves to prevent hypotony, obstructing that valve could result in a blockade of the outflow, making the mechanical parts of the implant an additional risk factor for therapy failure.<sup>39</sup> However, the main reason for implant failure was related to bleb infection and fibrosis<sup>33</sup>.

## *1. Introduction*

---

It has been shown that the permeability of the bleb wall was related to its thickness and extensive formation of scar tissue could hinder the diffusion of liquid through the bleb. This would subsequently prevent the implant from performing its required function (Figure 3d).<sup>40,41</sup> While the distribution of intraocular fluid into the subconjunctival space of the eye itself already triggers a fibrous response from the surrounding cells<sup>42</sup>, non-optimal biocompatibility and suboptimal design of the implants are considered to be the main risk factors for extensive scarring, resulting in the long-term failure of intraocular implants.<sup>33</sup> Even with all the different concepts and modifications available today, an optimal design has not been found and even modern designs showcase suboptimal success rates<sup>43</sup> with the main hindrance being the formation of scar tissue around the bleb. Therefore further optimizations are necessary with future research necessitates an improvement of material biocompatibility and implant design.<sup>33,44</sup>

The modification of the implants surfaces with hyaluronan hydrogels is an attempt to solve the three issues of hypotony, implant occlusion, and bleb fibrosis. Coating the outer walls of the tubular implant with a layer of hydrogel would make the surface more attractive for cells and lower the occurrence of an immunogenic reaction of the surrounding tissue. This in turn could result in the development of an inflammatory reaction and bleb fibrosis should be lowered. As a result, the stent's biocompatibility with its environment and its performance in glaucoma therapy would be improved. Preventing cells from migrating into the tube a blocking the drainage path for excess intraocular fluid should be possible by filling hydrogels to the interior. Furthermore, by regulating the amount of drained liquid with a hydrogel, instead of a mechanical valve, the failure rate of the implants could be reduced by avoiding the mechanical stress inherent with the use of valves.

### 1.3. Biomaterials and biocompatibility

The concept of using a biomaterial, or a material designed to interact with tissues of the human body without causing unacceptable damage<sup>45</sup>, is as old as human civilization. In Ancient Egypt around 2500 B.C., golden wire was used to link teeth together and artificial replacements for missing teeth made from brass, ivory, gold and wood were already being commonly used.<sup>46</sup> With advancing technology, the use of biomaterials became more sophisticated. While early prosthetics were of a simple design, utilizing mostly one-jointed pieces, and made from basic materials such as wood and leather and simple multi-jointed metallic devices later in history, modern prosthetics can be very complex and are manufactured using advanced materials.<sup>47</sup> The improvement of existing biomaterials in order to enhance their performance was often done for medical reasons, due to often unwanted side-effects. Early metallic implants, including screws to aid the healing of fractures<sup>48</sup>, were made from low grade steel or chromium alloys.<sup>49,50</sup> However, the application of these devices produced a number of undesirable side-effects, such as corrosion<sup>49</sup>, physical wear<sup>51</sup>, or the release of metal ions into the surrounding tissue.<sup>52</sup> This could subsequently cause adverse reactions in the biomaterial's host, including inflammation and osteolysis<sup>53</sup>, metal sensitivity<sup>50</sup> or even toxic reactions to the metal ions released from the implants<sup>54</sup>. As a result, efforts have been made to find less chemically reactive biomaterials in order to reduce these adverse effects, with later generation metallic implants being made from stainless steel, cobalt-chromium and titanium alloys<sup>55</sup>. Today's biomaterials are even more evolved and diverse with implants being created from polymers<sup>56</sup>, ceramics<sup>57</sup> or even living cells<sup>58</sup>, and hybrid materials such as metals coated with ceramic<sup>59</sup> or polymeric<sup>60</sup> layers.

Concerning the previously mentioned adverse side effects, the concept of “biocompatibility” was coined in 1970<sup>61,62</sup>, and since then has gained massive popularity, especially in the new millennium (Figure 4).

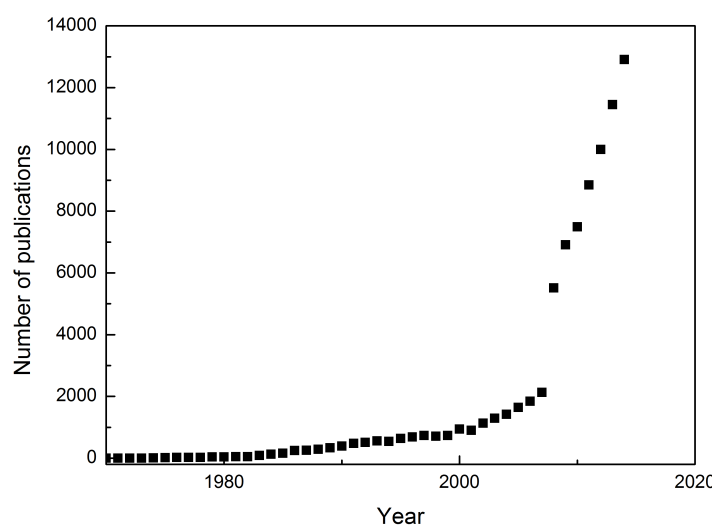


**Figure 4:** Number of publications with “biocompatibility” as topic. The data was taken from the “Web of Science” database<sup>63</sup> by searching for “biocompatibility” and refining the results for each individual year.

## 1. Introduction

---

The concept of biocompatibility in the most basic levels is concerned with the way in which biomaterials interact with tissues and how to minimize the potential negative effects from the application of biomaterials as a therapy.<sup>45</sup> The main desired biocompatibility properties in early biomaterial studies required components that were non-toxic, non-allergenic, non-carcinogenic, had low inflammatory response from the surrounding tissue, and minimized other negative effects on the body.<sup>62</sup> For example, early orthopedic implants made from low grade stainless steel had non-optimal biocompatibility due to corrosion.<sup>49</sup> As a result, modern implants are made from less corrosive materials, such as high grade stainless steel, Co-Cr alloys or titanium, thereby increasing the biocompatibility of these devices.<sup>55</sup>

Over time, however, the concept of biocompatibility evolved from being only a material-specific constant, with the best biocompatible materials being as chemically inert as possible, to a more synergistic system utilizing a broad understanding of several factors<sup>45</sup>. First, the biocompatibility of a material was not an intrinsic property of the material but rather one dependent on its application. PTFE, for example, is a popular biomaterial due to its inertness to chemical reactions and is being used for different types of medical applications.<sup>64</sup> However, when PTFE was used for hip implants, an abrasion of the material due to wear caused adverse reactions in the surrounding tissue and led to therapy failure.<sup>65,66</sup> Furthermore, in medical cases where a specific reaction of the tissue to the implant was actually desired for a successful therapy, chemically inert materials, such as the aforementioned PTFE, sometimes led to non-optimal outcomes as a result of their inertness<sup>67</sup>. As a result, the concept of biocompatibility was expanded from simply material properties to a broader understanding that the biocompatibility of a material is always dependent on the intended application.<sup>45,68</sup> Therefore in 1987 biocompatibility was defined as *“the ability of a material to perform with an appropriate host response”* and more recently expanded by Williams to *“the ability of a biomaterial to perform its desired function with respect to a medical therapy, without eliciting any undesirable local or systemic effects in the recipient or beneficiary of that therapy, but generating the most appropriate beneficial cellular or tissue response in that specific situation, and optimising the clinically relevant performance of that therapy.”*<sup>45</sup>

Recently, this new way of thinking resulted in a wholly new concept for developing biocompatible materials, as proposed by Williams<sup>68</sup>. In short, when a biomaterial is considered for a given therapy, researchers must evaluate desired cell reactions (cell proliferation on surface material, protein adsorption etc.) and negative responses (inflammation, calcification etc.). Furthermore, cells interacting with the biomaterial can be placed into three distinct groups:

- *Target cells*: Cells that are the target of the therapy with the biomaterial. A specific reaction from these is desired.
- *Defensive cells*: Mostly immunogenic cells who can create adverse reactions to the implementation of the biomaterial
- *Interfering cells*: Cells that don't resist the biomaterial but generally hinder the therapy

## *1. Introduction*

---

In order to achieve good biocompatibility, the desired effects of the therapy should be maximized while minimizing adverse reactions and side effects. In other words, the response of the target cells should be positive while the response of defensive and interfering cells should be as low as possible. A more in-depth discussion of this concept can be found in the respective literature and extends the scope of this chapter.<sup>68,69</sup> Today, biocompatibility is more important than ever and the concept plays an important role in almost all biomedical applications.<sup>45</sup>

As outlined in Section 1.2, non-optimal biocompatibility of glaucoma implants currently in use has been determined to be the main culprit for therapy failure. The goal of this project was to possibly enhance the biocompatibility of glaucoma stents by coating their outer surfaces and filling their interiors with hydrogels made from hyaluronan. The intention was to increase the biocompatibility of glaucoma implants through a reduction of inflammatory reactions from the defensive cells and bleb fibrosis by using hydrogel layers promoting cell adhesion, making the stent's surface more attractive to cells and possibly enhancing the performance of the implants and improving the chances of positive outcomes when used as therapy for glaucoma.

### 1.4. Hyaluronan hydrogels

#### Hydrogels

One very important class of biomaterials that have already been utilized in various applications<sup>70</sup> and were used in this project are hydrogels. They consist of three dimensional networks of interconnected polymers, carrying hydrophilic groups, with a defining ability to contain large amounts of water.<sup>70</sup> These networks can be made from various starting materials, including but not limited to natural polymers like alginate<sup>71</sup>, gelatin<sup>72</sup> or hyaluronan<sup>73</sup>, synthetic sources like polyethylene glycol (PEG)<sup>74</sup>, Poly(N-isopropylacrylamide) (PNIPAM)<sup>75</sup> and poly(hydroxyethyl methacrylate) (PHEMA)<sup>76</sup>, or composite materials like Zinkoxide<sup>77</sup>.

Hydrogels were first recognized as a potential biomaterial by Wichterle in 1960<sup>78</sup>, and since then have found a wide range of applications in various scientific and industrial fields<sup>70</sup>. In biomedical sciences they achieved broad use in tissue engineering<sup>79</sup>, including the creation of artificial muscles<sup>80</sup>, as a therapy against thrombosis after arterial damage<sup>81</sup>, and as an effective agent for wound dressing<sup>82</sup>. In pharmaceutical applications, environmentally sensitive hydrogels were used as a means for controlled drug release.<sup>83</sup> In biotechnology, surfaces modified with hydrogels have been used to manipulate cell adhesion<sup>84</sup> or as biosensors<sup>85</sup>. Potential applications for hydrogels also include the purification of water<sup>86</sup> or use as a delivery system for the controlled release of fertilizers<sup>87</sup> and water<sup>88</sup> to crops in order to enhance the efficacy of agricultural techniques. Almost every modern diaper utilizes superabsorbent hydrogels for an enhanced intake of liquid.<sup>89</sup> These examples are only a small fraction of possible applications and many more can be found in corresponding literature.<sup>70,84,90-92</sup>

The types and classes of hydrogels are as diverse as their applications, with differences ranging from their physical properties, their source materials (natural, synthetic, etc.), and rates of biodegradation over their generation methods, nature of crosslinking, and swelling behavior to properties such as pH responsiveness, net ionic charge, and biodegradation (Figure 5).<sup>70</sup> The most basic distinction between different types relates to their method of creation, differentiating between physical and chemical hydrogels<sup>90</sup>. In physical, or reversible, hydrogels, crosslinking between the individual polymer chains is a function of physical interactions between these chains, such as ionic forces, hydrogen bonding, physical entanglements, or hydrophilic and hydrophobic forces (Figure 6a/b).<sup>70</sup> Calcium ions, for example, were used to crosslink alginate chains together via ionic forces<sup>93</sup>, while soft hydrogels made from chitosan used only hydrophobic forces and hydrogen bonding to bind together the polysaccharides<sup>94</sup>. While hydrogels are usually considered to be rather soft and brittle materials, recently developed physical hydrogels made from polyampholytes, utilizing ionic bonds of varying strengths between polymers, show a relatively high toughness and viscoelasticity.<sup>95</sup> These interactions are dependent on characteristics of the corresponding environment, such as pH, temperature, presence of detergents etc., resulting in the formation of physical hydrogels being reversible, which potentially allows for controlled dissolution.<sup>90</sup>

# 1. Introduction

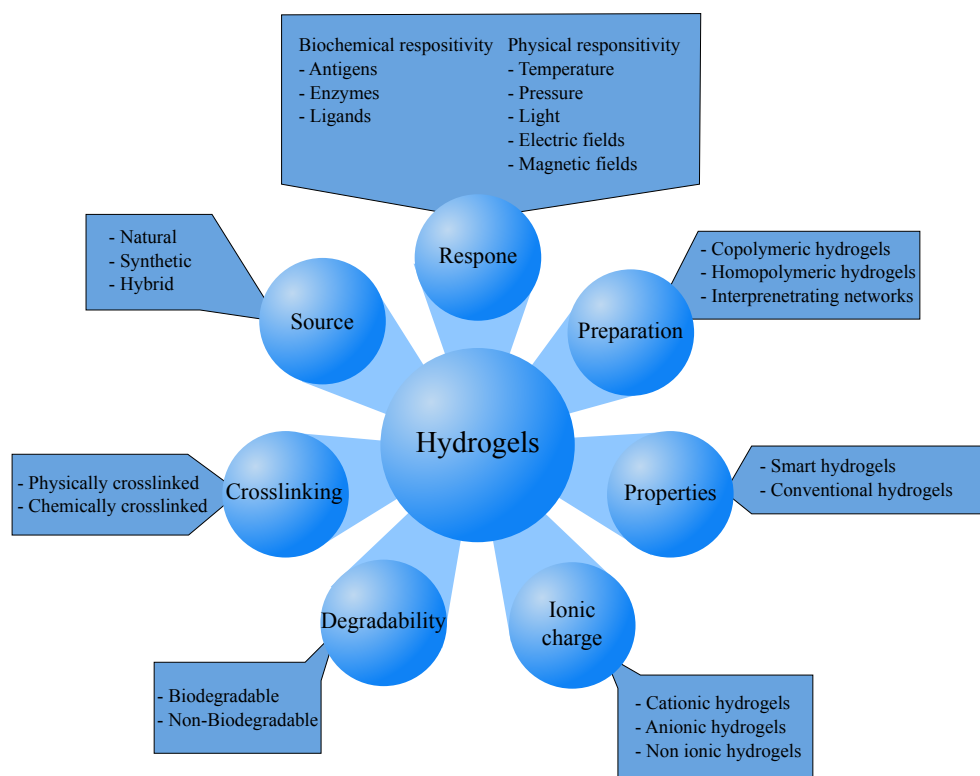


**Figure 5:** Overview of the different types and classes of hydrogels based on different parameters. Picture adapted from Ullah.<sup>70</sup>

Chemical, or permanent, hydrogels are formed by the formation of covalent links between the original polymers, either by a direct reaction between functional groups connected to the polymers or the application of bi- or multifunctional crosslinkers to create the networks.<sup>70</sup> The nature of the chemical reactions used for hydrogel generation can be diverse and is only limited by the available chemistry. Free radical reactions with specific monomers (acrylates, etc.) and crosslinkers (Figure 6c) have been used to create polyethylene glycol<sup>96</sup> or PNIPAM<sup>97</sup> hydrogels, among others. The radical chain reaction was initiated by “classical”, such as Azobisisobutyronitrile (AIBN)<sup>97</sup>, or photosensitive initiators allowing for photopolymerizable hydrogels, which have found broad use in bioengineering.<sup>98</sup> Alternatively, all kinds of condensation reactions between polymers and crosslinkers carrying chemically active groups have been employed to create different hydrogels (Figure 6d). Chemical strategies for hydrogel fabrication include a reaction between isocyanate groups and alcohols to form urea and urethane bonds<sup>99</sup>, Michael reactions between amines<sup>100</sup> or thiols<sup>101</sup> and acrylic groups, disulfide formation from thiols<sup>102</sup>, reactions between amines, alcohols or carboxylic acids and epoxides<sup>103</sup>, between amines and active esters<sup>104</sup> or the application of click chemistry<sup>105</sup>. Through a combination of different polymers and methods, including the co-polymerization of two different polymers<sup>106</sup> (Figure 7a) or the formation of interpenetrating networks by first creating a swollen hydrogel followed by the polymerization of a second intermeshing network<sup>107</sup> (Figure 7b), even more complex hydrogels were obtained. This diversity in starting materials and polymerization chemistry allows for a large amount of hydrogels with different features and makes this type of biomaterial extremely useful for various applications.<sup>70</sup>

# 1. Introduction

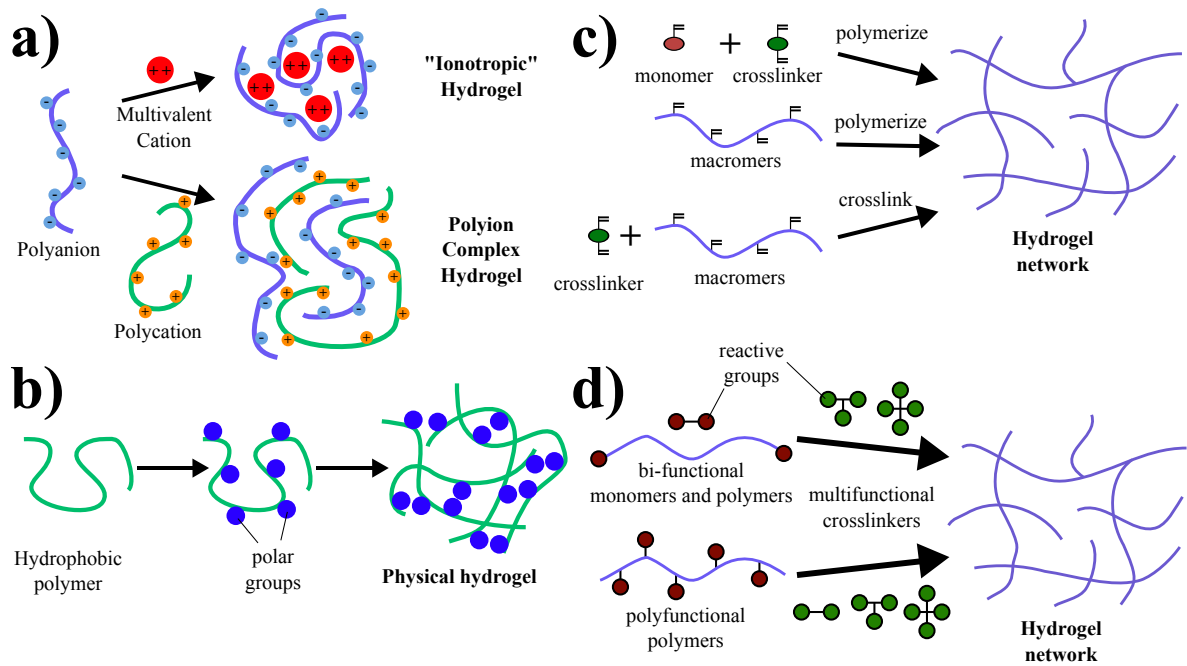


**Figure 6:** Overview of different methods for the creation of hydrogels. **(a):** Physical hydrogels using ionic interactions from charged polymers combined with ions or polymers containing the opposite charges. **(b):** Physical hydrogel using hydrophilic interactions from a hydrophobic polymer modified with hydrophilic groups. **(c):** Chemical hydrogels using radical reactions from monomers or polymers containing groups capable of radical chain reactions. **(d):** Permanent hydrogels using chemical reactions such as Michael-Additions, peptide couplings etc. from polymers and multifunctional crosslinkers. Pictures redrawn from Hoffman et al.<sup>90</sup>

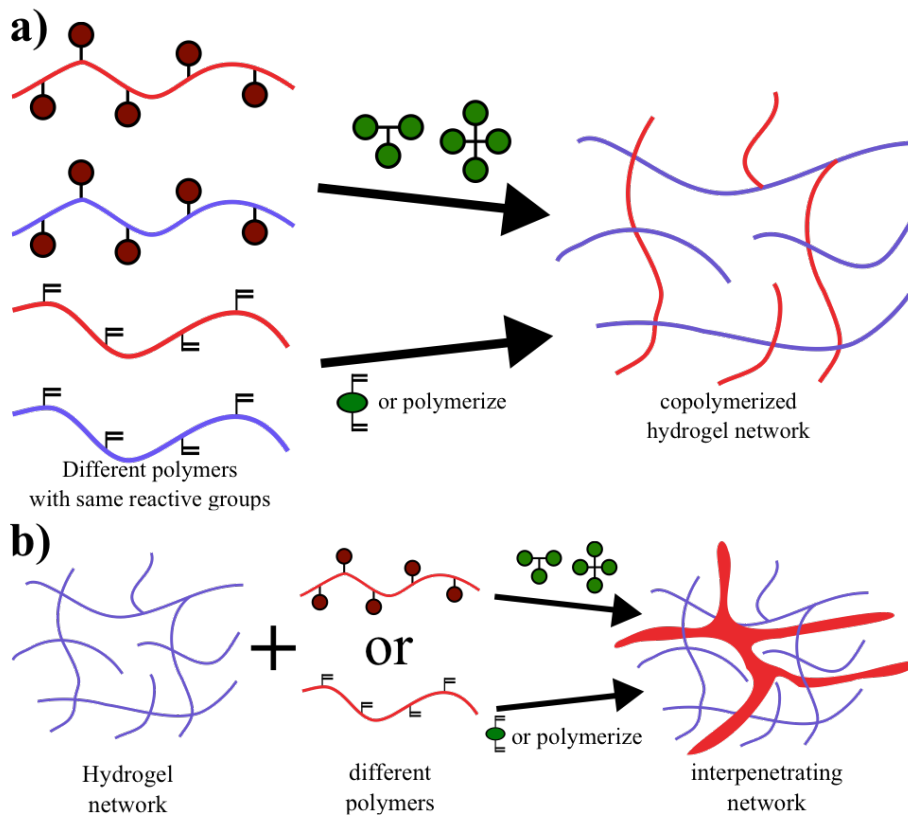


**Figure 7:** Creation of more complex hydrogels by **(a):** The co-polymerization of two different starting polymers **(b):** The polymerization of one hydrogel into a pre-existing second one. Pictures adapted from Hoffman et al.<sup>90</sup>

## 1. Introduction

As already outlined, a defining feature of hydrogels is their ability to take in large amounts of water, resulting in swelling of the hydrophilic polymer networks.<sup>108</sup> The kinetics of this swelling behavior can be complex and are highly dependent on the hydrogel's properties.<sup>109</sup> Briefly<sup>90</sup>, due to the presence of hydrophilic groups within the polymer networks, water can infiltrates dry hydrogels, hydrating these hydrophilic groups ("primary bound water"). This starts an initial swelling of the networks and exposes hydrophobic groups, which can also bind water using hydrophobic interactions ("secondary bound water"). Due to osmotic forces, more water, which is not bound to the network and therefore can move more freely, infiltrates the network, further swelling it further ("free water" or "bulk water"). This swelling continues until a balance between osmotic forces that try to further dilute the network even more and the physical retractive force of the polymer chains is reached (Flory-Rehner theory).<sup>92</sup> At that point the gel either starts to disintegrate (when degradable) or remains in a steady equilibrium swelling state.<sup>90</sup> As already mentioned, the kinetics of the swelling can be rather complex and are highly dependent on the parameters of the hydrogel (ionic charge, mesh size, crosslinking density chain length, etc.) and the environment (ionic concentrations, temperature pH etc.).<sup>92,109</sup> The swelling behavior further influences other gel properties, such as elasticity, the average pore size, and diffusion rates of smaller molecules within the polymer network.<sup>110,111</sup> This contributes to the capabilities of hydrogels for the intake of nutrients for cells<sup>90</sup>, the release of drugs<sup>112</sup>, or cell adhesion on the gel's surface<sup>96</sup> and therefore is an important parameter for the use of hydrogels in different types of applications.

### Hyaluronan hydrogels

One type of material that has been successfully used to generate hydrogels is hyaluronan (hyaluronic acid, hyaluronate, HA).<sup>113</sup> This polysaccharide is a glycosaminoglycan (GAGs) that consists of unbranched, often high molecular weight chains of alternating  $\beta$ -1,3- and  $\beta$ -1,4 linked units of glucuronic acid and N-acetylglucosamine (Figure 8).<sup>114</sup>

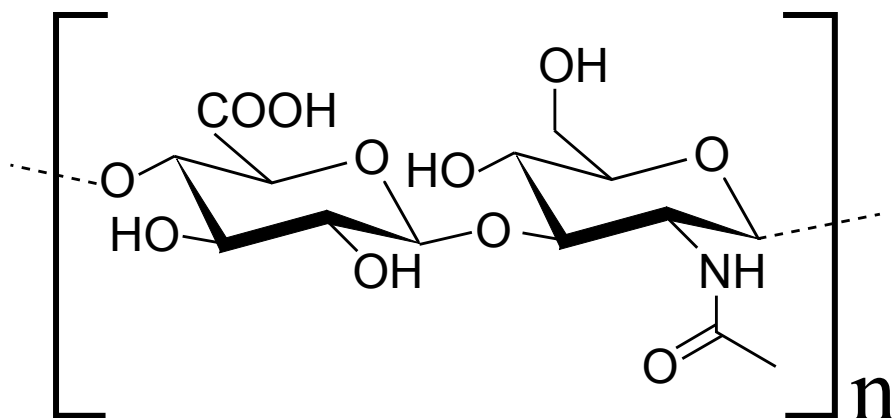


**Figure 8:** Molecular structure of the repeating unit of hyaluronan. It consists of glucuronic acid and N-acetylglucosamine connected with  $\beta$ -1,3 and  $\beta$ -1,4 links.

Hyaluronan is predominantly found in connective tissues (synovial fluid, etc.)<sup>115</sup>, skin tissues<sup>116</sup>, and the aqueous humor of the human eye<sup>117</sup>, but is also present in smaller amounts in all parts of the body<sup>115</sup>. HA differentiates itself in a number of ways from other GAGs. First, it is synthesized in the plasma membrane instead of the Golgi apparatus.<sup>114</sup>

## 1. Introduction

---

Furthermore, it is neither covalently modified with core proteins<sup>118</sup>, although some serum-derived proteins do bind covalently with the GAG<sup>119</sup>. It is furthermore not sulfated, giving hyaluronen the simplest primary structure of all GAGs.<sup>120</sup> While most GAGs are rather short, forming chains with a molecular mass of <50 kDa, HA usually generates huge molecules with a mass of up to  $7 \cdot 10^6$  kDa.<sup>115</sup> HA is known for possessing some peculiar properties, such as the ability to bind around one thousand times its own weight in water, resulting in viscous and elastic solutions at concentrations as low as 1 mg/ml.<sup>121</sup> Viscosity increases exponentially with HA concentration<sup>110</sup>, although it does not form solid gels at high concentrations.<sup>114</sup> Furthermore, HA networks exhibit water homeostasis (prevention of bulk water flow), a non-ideal osmotic pressure which increases exponentially with the concentration, and the ability to prevent other macromolecules from diffusing within the polysaccharides.<sup>122</sup> These properties of hyaluronan are related to its structure in solution. While the primary structure is rather simple compared to other GAGs, the secondary and tertiary structures are much more complex and indeed not yet fully understood.<sup>121</sup> Earlier models proposed the secondary structure to be a stiff ribbon-like helix, formed due to intramolecular hydrogen bonds,<sup>123</sup> which create entangled networks at higher concentrations,<sup>124</sup> resulting in the previously described rheological properties. However, solid state X-ray and NMR measurements also showed the HA's ability to form double-helical structures<sup>125</sup> while liquid NMR and simulations found even more stable conformations with only minimal differences in energy states.<sup>126</sup> As a result, it is more likely that hyaluronan rapidly undergoes different conformations with passing intermolecular interactions instead of remaining in the stiff ribbon-like helical structure for extended times.<sup>127</sup> However, the hydrodynamic structure of hyaluronan is not yet fully explained,<sup>121</sup> and its architecture *in vivo* may differ from what is observed in the lab.<sup>128</sup> Nonetheless, it is remarkable how a molecule with a seemingly simple architecture is capable of rather complex secondary and tertiary structures.

This same trend, complexity from simplicity, continues when looking at the biological functions of hyaluronan. While in earlier times it was mostly disregarded as a filler material and lubricant for joints, this point of view changed with the discovery of hyaladherins, proteins which specifically react with hyaluronan.<sup>129</sup> Today it is known that HA plays a role in a large amount of biological processes, at times with opposing roles depending on its size, including but not limited to simple space filling properties, hydration of the skin, anti-inflammatory and anti-angiogenic functions, a suppression of cell-cell or ligand-receptor interactions, embryogenesis, inflammatory inducement, and wound repair.<sup>128</sup> This participation in a vast amount of functions makes this seemingly simple molecule an integral part of the ECM<sup>130</sup> and allows it to play an important role in many biological processes.

Due to these properties and biological functions hyaluronan has also found use in many biomedical applications. The physical properties of HA have been used as a protective layer in cataract surgery<sup>131</sup>, the treatment of joint diseases<sup>132</sup>, or the promotion of wound healing<sup>118</sup>. Of note is also the ability to obtain the GAG from non-animal (e.g. bacterial) sources.<sup>133</sup> Chemically modified HA was successfully used in the surgical reduction of adhesions induced by physical trauma, for tissue augmentations, and for therapeutic applications by linking biologically active agents.<sup>134</sup>

## 1. Introduction

Furthermore, and perhaps most importantly with respect to this thesis, hyaluronic acid hydrogels also found use as biomaterials in biomedical applications like tissue engineering<sup>135</sup>. HA is an excellent candidate for the creation of biomaterials due to its excellent biocompatibility, which is a result of its non-immunogenic and anti-inflammatory characteristics<sup>132</sup> and the fact that it is naturally a component of the extracellular matrix. Also, the potential to chemically modify the polysaccharide in various ways allows the adaptation of the polysaccharide for a number of different purposes (Figure 9).<sup>113,135</sup>

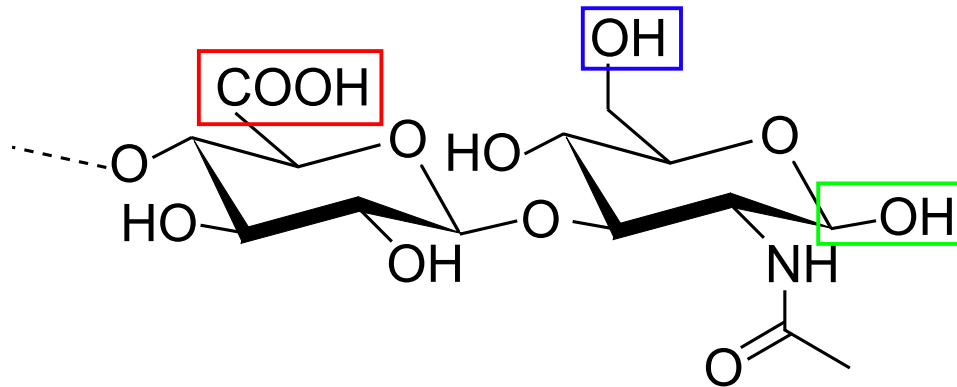


**Figure 9:** HA-molecule with outlined functional groups on which chemical modifications are usually performed: The carboxyl function of the D-glucuronic acid (red), the hydroxyl group of the D-N-acetylglucosamine (blue) and the reducing end of the polysaccharide chain (green).

Specifically the idea of manipulating cell adhesion to hydrogel-modified surfaces is an already well-established concept. Poly(ethylene glycol) (PEG) hydrogels showed good cell repellent properties<sup>136</sup> and investigations of hyaluronan hydrogels illustrated their potential to create cell adhesive surfaces.<sup>101,137</sup> Furthermore the group of Spatz demonstrated the ability to switch between cell adhesive and cell resistant PEG hydrogel properties by the introduction of additional functional groups.<sup>138</sup>

For these beneficial properties, specifically its good biocompatibility and availability for chemical modifications, hyaluronic acid hydrogels were used in this thesis for the development of enhanced glaucoma implants. As outlined before (see Section 1.2), the main reason for the failure of glaucoma therapy with intraocular implants is an immunogenic reaction of the body to the implant, resulting in the formation of fibrous tissue and subsequent blockage of liquid drainage. Since hyaluronan is already present within the human eye and possesses the aforementioned (size-dependent) anti-inflammatory and anti-immunogenic properties, it is an ideal candidate for a potential reduction of the immunogenic reaction of the host tissue to the implant by masking its surfaces with hydrogels made from hyaluronic acid and facilitating cell adhesion on its outer surfaces. Moreover, it was already shown that modified hyaluronan enhanced the biocompatibility of metallic surfaces,<sup>139</sup> and Shu et al. has already demonstrated positive cell proliferation on the surface of hyaluronan hydrogels.<sup>101,102,137</sup> The diversity of possible crosslinkers (see Section 1.6) and the potential to further modify hyaluronan with other reactive groups enables the potential creation of HA hydrogels with different properties, allowing for a great deal of optimization. For these reasons, hyaluronan was the ideal candidate to be used in this project for an enhancement of glaucoma stents.

### 1.5. Titanium: An efficient biomaterial

#### Properties of titanium

Titanium is one of the most established biomaterials in medicine due to its inherent beneficial properties as an implant material for medical applications.<sup>140</sup> Titanium, discovered in the second half of the 18<sup>th</sup> century<sup>141</sup>, makes up 0.6% of the earth's crust, mostly in the form of FeTiO<sub>3</sub> and TiO<sub>2</sub>, and is among the most common structural metals, along with magnesium, aluminum, and iron.<sup>142</sup> The first industrial method of producing the material was invented in 1937 (the Kroll process), in which solid TiO<sub>2</sub> is first transformed into gaseous TiCl<sub>4</sub> followed by a reduction with magnesium at high temperatures (Figure 10)<sup>142</sup>. Although it has been optimized, this method is cost intensive<sup>143</sup> but remains the predominant way of obtaining pure titanium on an industrial scale.<sup>144</sup>

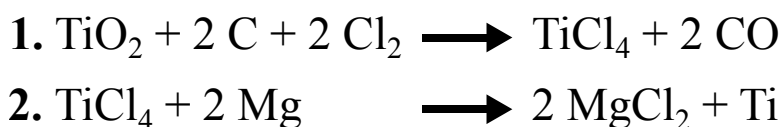


**Figure 10:** Reaction equations for the production of titanium from Ti(IV)-oxide in a two step process: First TiO<sub>2</sub> is transformed into gaseous TiCl<sub>4</sub> followed by a reduction to Ti(0) with magnesium at high temperatures.

The metal found its use in many different fields of application, including the automobile and aerospace industry, due to its low density<sup>143,145</sup>. In medical sciences, titanium and its alloys have gained rapid popularity as a very biocompatible biomaterial<sup>140</sup>, and is used in hip<sup>146</sup>, dental<sup>147</sup> or joint<sup>148</sup> implants. The biocompatibility of the metal comes from a number of intrinsic properties. Titanium offers good resistance to corrosion<sup>149</sup> and physical wear<sup>150</sup>, minimizing the potential release of metal ions and debris into the surrounding tissue that trigger adverse reactions (See Section 1.3). Furthermore, it offers a general inertness to chemical reactions<sup>151</sup>, a lower (pure titanium) or higher (alloys) density and Young's modulus than other metallic biomaterials (steel, etc.)<sup>152</sup>. It also has the ability to induce protein adsorption and cell proliferation on its surface, potentially increasing the acceptance of surrounding tissue to implants made from titanium<sup>151,153</sup>. Most of these features originate from surface properties of the metal. Titanium has a high affinity for oxygen, and as a result, pure titanium and most of its alloys readily form a layer of TiO<sub>2</sub> on its surface through a gradual oxidation of the Ti(0) to Ti<sup>4+</sup> by the environment. This is followed by association with O<sup>2-</sup>, resulting in a Rutil structure that allows oxygen diffusion and a gradual growth of the layer into the bulk material from the surface (Figure 11).<sup>142</sup> This layer is resistant to most chemical reactions and prevents the relatively aggressive physical environment in tissues from further dissolving implants made from titanium, including via complexation of the metal ions.<sup>140,142</sup> As a result, titanium is chemically inert and withstands corrosion well for extended amounts of time, making it a desirable biomaterial.<sup>148</sup> Furthermore, water and acids as well as basic hydroxyl groups are part of the TiO<sub>2</sub> layer, making the surface hydrophilic and allowing it to act as an amphoteric.<sup>154</sup> In addition, organic molecules are able to adsorb or covalently bind to the surface, as well as small, oxygen containing molecules such as phosphate or nitrate.<sup>140</sup>

## 1. Introduction

The hydroxyl groups result in a slightly negative surface charge at physical conditions (pH = 7.4), resulting in the adhesion of  $\text{Ca}^{2+}$  ions<sup>155</sup> which aid in the attachment of more biological macromolecules including glycosaminoglycans<sup>156</sup> or proteins<sup>157</sup>. *In vivo* these surface properties allow for the creation of a protein layer around an implant which promotes the attachment and proliferation of cells on its surface, which together with the non-toxicity and chemical inertness of the material, contributes to the overall good performance and biocompatibility of titanium implants in tissues.<sup>140</sup>

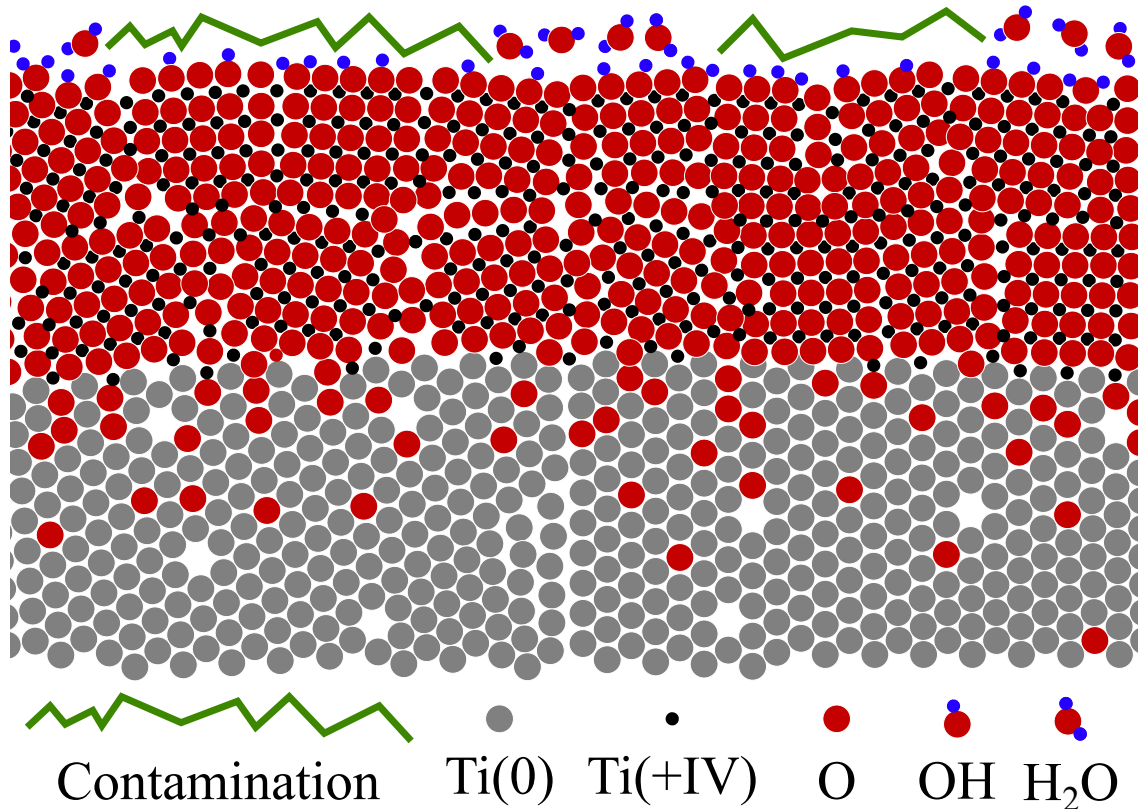


**Figure 11:** Depiction of the surface structure of unmodified titanium showing the metallic bulk with an oxygen gradient near the interface and a passivating  $\text{TiO}_2$  layer with bound hydroxyl groups and adhered  $\text{H}_2\text{O}$  as well as organic contaminations at the surface. Picture adapted from Brunette.<sup>140</sup>

### Surface modifications

While titanium itself has good biocompatibility, the pure metal often has suboptimal performance in practical biomedical applications. Contamination and non-uniform surfaces often occur during the manufacture of these implants.<sup>158</sup> For long-term applications (>10 years), physical wear of the metallic devices is still an unsolved problem.<sup>159</sup> Furthermore, for different applications different surface properties such as specific roughness levels for optimal bone attachment are required.<sup>160</sup> The concept of “hemocompatibility”<sup>161</sup> introduced a number of new requirements for titanium implants with respect to contact with blood.<sup>162,163</sup> As a result, a host of surface modifications have been established<sup>140,158</sup>, including physical methods like laser polishing<sup>164</sup> and sandblasting<sup>165</sup> of the surfaces, chemical methods like acidic<sup>166</sup> or basic<sup>167</sup> treatment, the application of inorganic coatings like hydroxyapatite<sup>59</sup> or silica<sup>168</sup>, or the use of chemical vapor deposition processes to create diamond coatings<sup>169</sup>.

## *1. Introduction*

---

One concept for the surface modification of titanium that has been also applied for this thesis is the attachment of biological molecules to enhance the implant's performance. This can contribute to lowering inflammatory responses of the surrounding tissue, triggering specific cellular reactions, resisting bacterial infections, and increasing the long-term stability.<sup>153</sup> Among these modifications were the immobilization of peptides to provide better osseointegration<sup>170</sup>, the use of hyaluronan and chitosan to improve resistance to bacterial growth<sup>171</sup>, the immobilization of enzymes to create bioactive interfaces<sup>166</sup>, and many more.<sup>140,153,158</sup> In order to permanently attach these molecules to titanium surfaces, a number of methods have been successfully developed. These include the adhesion of phosphates to create self-assembled monolayers or the reaction with silanes<sup>166</sup> to graft reactive groups to the titanium surfaces which subsequently reacted with the biological molecules resulting in a covalent immobilization of these molecules.<sup>172,173,174</sup>

Due to these properties of chemical inertness, tendency for cell adhesion, and chemical modifiability, titanium is a great biomaterial that is already being used in a large number of biomedical applications.<sup>140</sup> Therefore, it was also selected as the main body for the model glaucoma implants developed in this thesis.

### 1.6. General challenges and their proposed solutions

For the development of the hyaluronan hydrogel enhanced glaucoma implants, a number of basic problems had to be solved. A method for the creation of the hyaluronan hydrogels and a protocol for the immobilization of these hydrogels to titanium surfaces had to be established. Furthermore, analytical techniques had to be developed for determining a potential controlled reduction of external pressure through the hydrogel-filled tubes. Finally, the parameters of the intraocular stents had to be optimized to reduce the external pressure to specific desired levels.

Additionally, since the hydrogel-modified devices were ultimately meant to be manufactured on an industrial scale and used as intraocular implants in glaucoma therapy, some extra general requirements had to be fulfilled for the establishment of the methods used to generate them. For work safety reasons, a low cost of waste disposal and for the prevention of potential complications in a medical context the use of harmful materials had to be avoided. For the same reasons, the use of potentially hazardous chemicals also had to be minimized. Furthermore, also due to cost reasons and in order to reduce the occurrence of potential errors during a large scale manufacturing process, a goal of fabricating the intraocular implants in as few steps as possible was established. In addition, each of these steps ideally should be at a minimum level of complexity. For that reason, the concepts used in this thesis to realize the goal for the implant creation were developed with respect to a minimal complexity, a reduction of production steps, and an avoidance of toxic and harmful reagents whenever possible.

#### Implant design and hydrogel generation

For the formation of the hyaluronan hydrogels, a number of concepts were already established in literature (see Section 1.4). Among these, a method developed by Shu et al. was selected to be used for the design of the glaucoma implants:<sup>101,102,137</sup> In the first step, hyaluronan was modified with thiol groups by coupling dithiobis(propionic hydrazide) (DTPH) to the HA carboxylic acid groups followed by a reduction of the disulfide bond via dithiothreitol (DTT) (Figure 12a). The thiolated hyaluronan (HS-HA) was then mixed with crosslinkers containing acrylic groups to initiate a Thiol-Michael addition (Figure 12b)<sup>175</sup>, forming connections between the individual hyaluronan chains and creating the hydrogel (Figure 12c).

## 1. Introduction

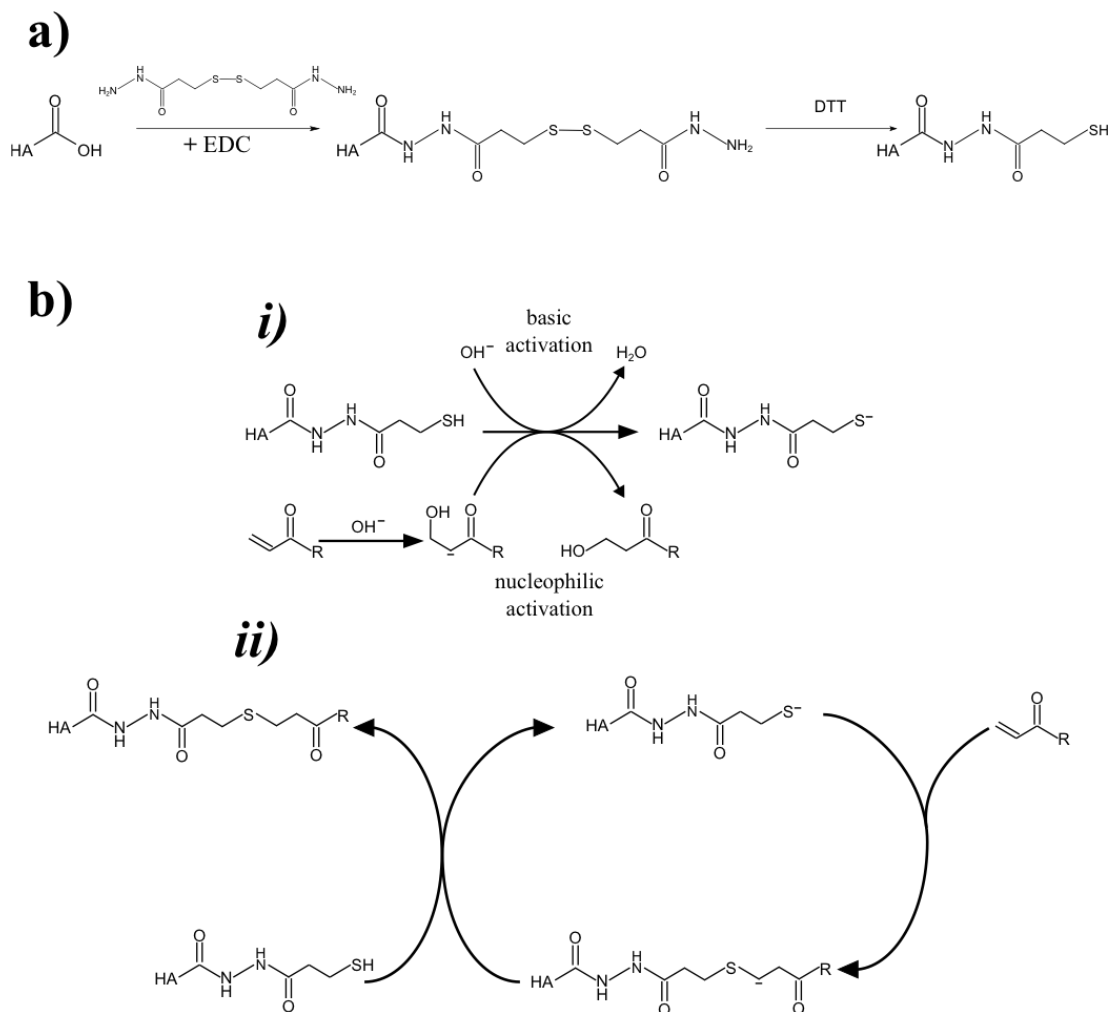


**Figure 12:** Schematic drawing of the chemical reactions for generating hyaluronan hydrogels, which was adapted in this thesis. **(a):** Two-step reaction of the modification of HA with thiol groups using an EDC mediated peptide coupling reaction of DTPH to HA carboxyl groups followed by a reduction of the disulfide bonds to thiols. **(b):** Reaction mechanism of the Thiol-Michael addition between thiols and acrylic groups that was used to crosslink the hyaluronan chains. In the first step the thiols are de-protonated by the hydroxyl groups either via the basic or nucleophilic method **(i)** followed by the nucleophilic attack at the  $\beta$ -carbon of the acrylic function **(ii)**. Mechanisms adapted from literature.<sup>102,175</sup>

This method came with a number of advantages. DTPH was easily synthesized from dithiobis(propionic acid) (DTPA), which is inexpensive, in non-hazardous conditions with ethyl acetate as the only organic solvent, and catalytic amounts of sulfuric acid being the most dangerous chemical involved (See Section 4.1.2). The HA modification itself also could be performed in a simple two-step synthesis mostly in non-toxic conditions (See Section 2.1.2) and minimal use of harmful chemicals with the exception of DTT. These conditions make the method viable with respect to an industrial application as discussed before. The only downside of this concept is the potential re-oxidation of the thiols to disulfides in the presence of oxygen under basic conditions<sup>102</sup>, requiring careful pH control and the exclusion of oxygen during the hydrogel synthesis, as well as some specific preparation requirements for long-term storage (see Section 4.1.2).

## 1. Introduction

---

Furthermore, the Thiol-Michael addition can be performed on any kind of crosslinker containing multiple acrylic groups. Shu et al. has already used poly(ethylene) glycol derivatives<sup>101</sup> and Hagel et al. successfully generated HA hydrogels using crosslinkers derived from desmosine<sup>176</sup>, and in this thesis N,N'-Methylenebisacrylamide (BIS, MBAA) was successfully used for hydrogel synthesis as well (See Section 2.3.1), illustrating the flexibility of the method for creating hydrogels. This potentially enables the generation of hydrogels with different properties depending on the type of crosslinker used and later allows an optimization of the characteristics of the glaucoma implant with respect to cell adhesion (outer surfaces) or repellence (implant interiors). For example ionic crosslinkers were used to change the net charge density within the hydrogel. As outlined before (Section 1.4), a successful cell adhesion onto the HA hydrogel modified surfaces was already demonstrated by Shu et al.<sup>101</sup>, further illustrating this method's potential for the enhancement of the biocompatibility of the glaucoma implants.

### **Immobilization strategy**

A few possibilities for the immobilization of the hyaluronan were considered. They all included the modification of the titanium surfaces with reactive groups using silanes followed by a covalent reaction of the hyaluronan with these reactive groups. Similar to silica surfaces<sup>177</sup>, the silanization method was used on titanium and other metal oxides<sup>173</sup> due to the presence of surface-bound hydroxyl groups reacting with alkoxy silanes. For the reaction between the hyaluronan and the silanized surfaces, several options were available. For example, a method that has been successfully applied by Thierry.<sup>178</sup> It proposed the coupling between a carboxylate terminated hyaluronan and surface-bound amino groups form a stable peptide bond. However, this would have demanded for an additional modification of the hyaluronan with functional groups at the terminal end, complicating the synthesis protocol in the process. Additionally thiols are not stable in basic conditions over a longer period of time. Thus, a multiple-step grafting process would be required, starting with the immobilization of HA still carrying non-cleaved DTPH, followed by incubation in a DTT solution to (re-)activate the thiol groups before the hydrogels are formed (Figure 14). The whole concept, and similar ones that involve additional reactive groups would be too elaborate, so other options that would not necessitate further modifications of the hyaluronan itself were considered. For example, the grafting of either thiol or acrylic functions to the metal and the use of either a direct (surface acrylic) or crosslinker-mediated (surface thiol) Michael Addition were explored. The advantage of this approach is the combination of the immobilization and the hydrogel generation in a one-step reaction, allowing for fewer required production steps. However, this creates competition between surface-bound and HA-bound reactive groups, making the kinetics of the hydrogel formation more dependent on the amount of active groups on the titanium surface. In order to mitigate this effect, epoxides were grafted to the surface (Figure 13a). These epoxides can subsequently react with hydroxyl groups of the hyaluronan in a nucleophilic ring-opening mechanism (Figure 13b)<sup>103</sup>.

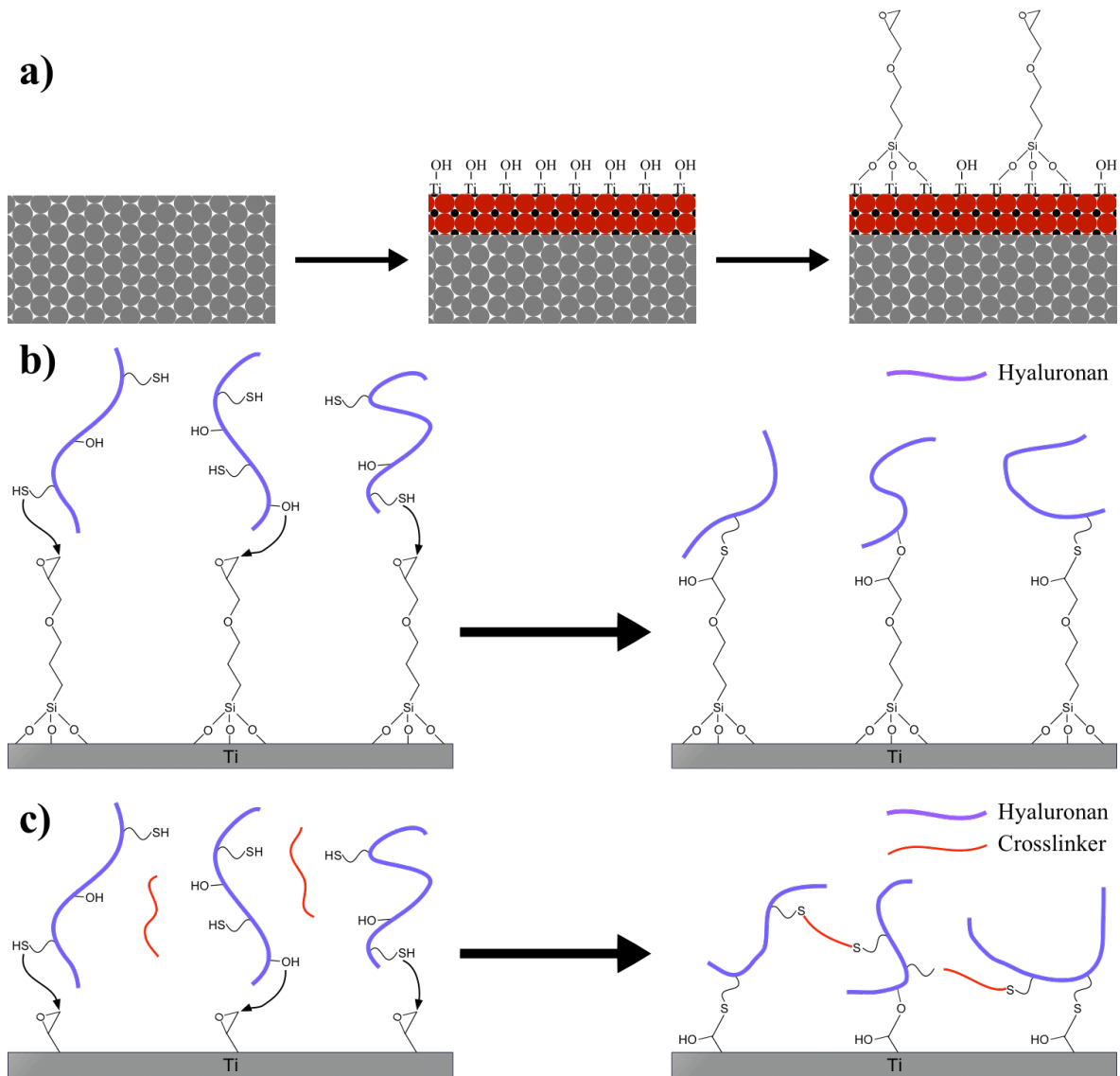


**Figure 13:** Schematic drawing over the concept of the combined hyaluronan hydrogel formation and surface immobilization on titanium. **(a):** Titanium naturally forms an oxide layer containing hydroxide groups (simplified) which can react with (3-glycidyloxypropyl)trimethoxysilane to create a layer of epoxide groups on the surface. **(b):** Hydroxyl and thiol groups of hyaluronan can react with the epoxides, subsequently immobilizing the HA on the Ti surface. **(c):** The Thiol-Michael Addition and epoxide ring-opening reaction can both be conducted with the same reactions parameters allowing for the immobilization and hydrogel formation to be done in one step.

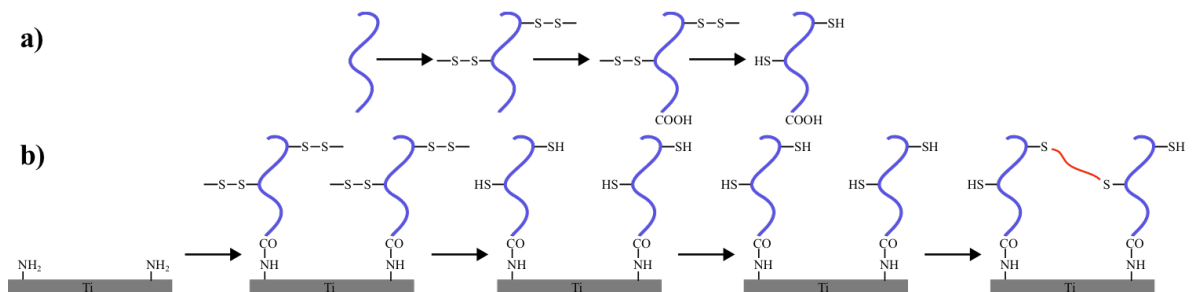


**Figure 14:** Schematic drawing of a potential concept adapted from Thierry<sup>178</sup> for the immobilization of HA hydrogels. It involves the immobilization of a carboxyl function at the terminal end of the saccharide chain reacting with surface bound amino-groups. Due to the sensitivity of the thiol groups to re-oxidation into disulfides, multiple steps would have been required to modify the hyaluronan and to conduct the immobilization of the hydrogel as opposed to the pathway used in this thesis (**Figure 13**).

## 1. Introduction

---

The described strategy allowed for immobilization and hydrogel formation in a single step (Figure 13c), lowering potential costs in an industrial setup while including more reactive groups in addition to the thiols, which would also react with the epoxides<sup>179</sup>. Moreover, epoxides decay over time in alkaline conditions by a ring opening reaction with hydroxides<sup>180</sup>. The number of covalent links formed between the titanium substrate and the hydrogel might not be as high as in other immobilization concepts due to the competing reactions, but it also eliminates all unreacted surface bound-groups that might otherwise cause reactions with the surrounding environment and cause adverse reactions within the host tissue. Nevertheless, this approach was selected since it promised the easiest route to the generation of hydrogel-modified model implants. In this case the only downside was the fact that the immobilization might not be as strong compared to other concepts without competing reactions.

### Analytical methods

Some analytical methods used in this thesis were already well established. <sup>1</sup>H-NMR was applied to monitor the synthesis of the starting materials (DTPH, HS-HA), and for the degree of HA modification with thiols the Ellman's test was used.<sup>102</sup> To ascertain the success of the silanization on flat surfaces contact angle measurements<sup>181</sup> could easily be conducted in order to determine changes in the surface energy by the introduction of new functional groups.<sup>182</sup> However, for some parts of the projects, custom made analytical methods were developed. In order to verify a successful immobilization of hyaluronan on a small scale and on rounded surfaces (e.g. small tubes), the polysaccharide was modified with fluorescein in addition to thiols to create HA with fluorescent properties in addition to the crosslinking capabilities (HS-FA-HA). This allowed for visualization of hyaluronan immobilized to the outer and inner surfaces of small tubes and on titanium surfaces. Furthermore, the fluorescent hydrogels could be visualized even on a small scale, e.g. layers with a small thickness and the interiors of small tubes, allowing for a better visual analysis of hydrogel formation. In addition, the non-toxicity of fluoresceinamine<sup>183</sup> would potentially allow for further potential applications of HS-FA-HA and their respective hydrogels in a biomedical context, making this the ideal fluorescent dye for this project.

Evaluating the behavior of hydrogel-modified prototype implants to external liquid pressures also required custom made setups that were capable of quickly evaluating whether the hydrogels would permit liquid flow at all, as well as how a change of certain parameters (e.g. dimensions and hydrogel properties) would influence this behavior. Another setup was necessary to see, in the case that a liquid flow through the intraocular implants was achieved, whether they were able to regulate the outflow to attain certain pressures, and how the parameters of the implant and the accompanying hydrogels could be modified to achieve these pressure levels. To verify and optimize these pressure regulatory properties was of great importance since one required ability of the implants was to decrease the intraocular pressure of the glaucomatous eye without causing hypotony (see Section 1.2). In order to fulfill these requirements for analytical methods to ascertain the pressure regulation of the hydrogel-modified implants two custom-made setups were created. One used a constant pressure buildup in a syringe connected to the samples for a

## 1. Introduction

quick evaluation of the general ability of the model implants to permit a liquid flow. In addition the immobilization stability of the hydrogels in the tube's interiors could be quantified. The other method applied a hydrostatic pressure in a column to evaluate the absolute values for the pressure regulation (see Section 2.4.3 for more information). With these methods it was possible to characterize the properties of model stents. And they provided helpful tools for future optimizations of the new intraocular implants to achieve an ideal level of pressure regulation for an improved biocompatibility.

### Summary

In this chapter a concept is proposed which allows creating a new type of intraocular implants. It is based on a surface modification of titanium with epoxides using a reaction between surface-bound hydroxyl groups and alkoxy silanes and the modification of hyaluronan with thiols. These initial steps are necessary for the crosslinking reaction with multifunctional acrylic groups and the surface immobilization of HA, using a nucleophilic ring-opening on the epoxides (Figure 15). Both reactions can be performed under the same conditions, allowing for hydrogel formation and surface binding in a single step, simplifying the process considerably, as opposed to a multi-step process.

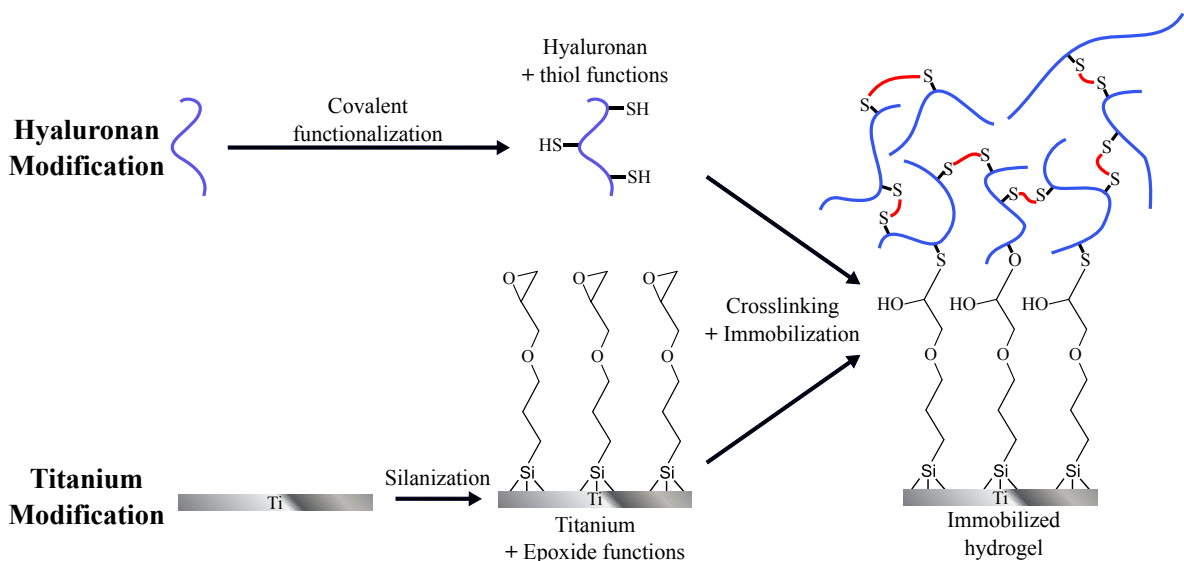


**Figure 15:** Schematic drawing of the concept used for creating hydrogel-modified glaucoma stents. In two separate steps, hyaluronan is modified with thiol groups and the surface of titanium with epoxides. Following that, the hydrogel formation via a Thiol-Michael Addition and the surface immobilization via a nucleophilic ring-opening of the epoxides can be done in one single step.

This combined concept enables the creation of glaucoma stents using a simple reaction pathway utilizing mostly non-harmful and low cost ingredients. By varying the type of crosslinker and the modification grade of HA with thiols and enabling different crosslinking densities, hydrogels with varying properties can be generated. This allows for a simple optimization of the model glaucoma implants with respect to cell adhesion and pressure reduction.

## 2. Results & Discussion

### 2.1. Chemical modification of hyaluronan

#### 2.1.1. Fluorescent labeling

As outlined in section 1.6, hyaluronan was labeled with a fluorescent dye to generate HA and hydrogels with fluorescent properties for an improved analysis of its immobilization to surfaces (Section 2.2.2) and model implants (Section 2.2.3). Furthermore the fluorescent labeling helped understanding the mechanism of the liquid flow through HA hydrogel-filled tubes (Section 2.5.1). In order to attain the labeling, 5-aminofluorescein (fluoresceinamine, FA) (Figure 16) was linked covalently to hyaluronan.

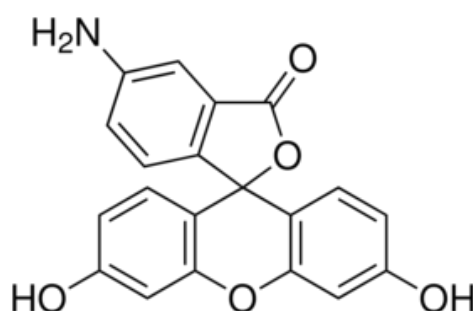


**Figure 16:** Molecular structure of 5-aminofluorescein

FA had a number of properties advantageous to the work with the hydrogels. Notably, it operated in the visible spectrum (pH = 9:  $\lambda_{\text{ex}} = 485 \text{ nm}$   $\lambda_{\text{em}} = 514 \text{ nm}$ ) with a high quantum yield and good photosensitivity.<sup>184</sup> Furthermore, FA possessed a rather low toxicity<sup>183</sup>, which made handling of the fluorophores easier without extra precautions, as opposed to quantum dots<sup>185</sup>, and it prevented any interference with possible cell experiments. In order to link FA to hyaluronan, a peptide coupling reaction between the amine groups of FA and the carboxylic groups of the hyaluronan backbone was used. It was mediated by N-(3-Dimethylaminopropyl)-N'-ethylcarbodiimide (EDC) and N-Hydroxysuccinimide (NHS) (Figure 17), a method that has already been employed previously for modifying HA with FA.<sup>186,187</sup>

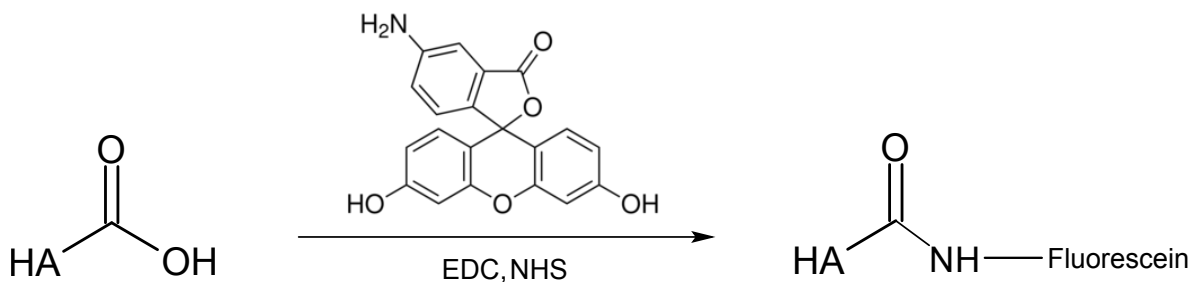


**Figure 17:** Reaction used to modify hyaluronan with fluoresceinamine: An EDC/NHS mediated peptide coupling reaction was employed to bind the amine group of fluorescein to the carboxyl groups of the HA disaccharide units.

## 2. Results & Discussion

Modifying HA with fluoresceinamine competed with introducing anchor groups for crosslinking the hydrogels (see section 2.1.3 for further discussion). The reaction could further influence hydrogel properties by changing the hydrophobicity of the network by reducing the amount of carboxylic  $-OH$  groups.<sup>188</sup> For that reasons parameters were chosen to achieve a low degree of substitution with FA (see Section 4.1.3). The experimental outline followed the work of Sehgal et al. who investigated the degree of substitution of EDC-mediated peptide couplings based on several parameters.<sup>189</sup>

The reaction yielded a product (FA-HA) in form of a yellow substance with wool-like consistency (Figure 18a), fluorescent properties (Figure 18c) and average product yields ranging from 70% to 90% (w/w).

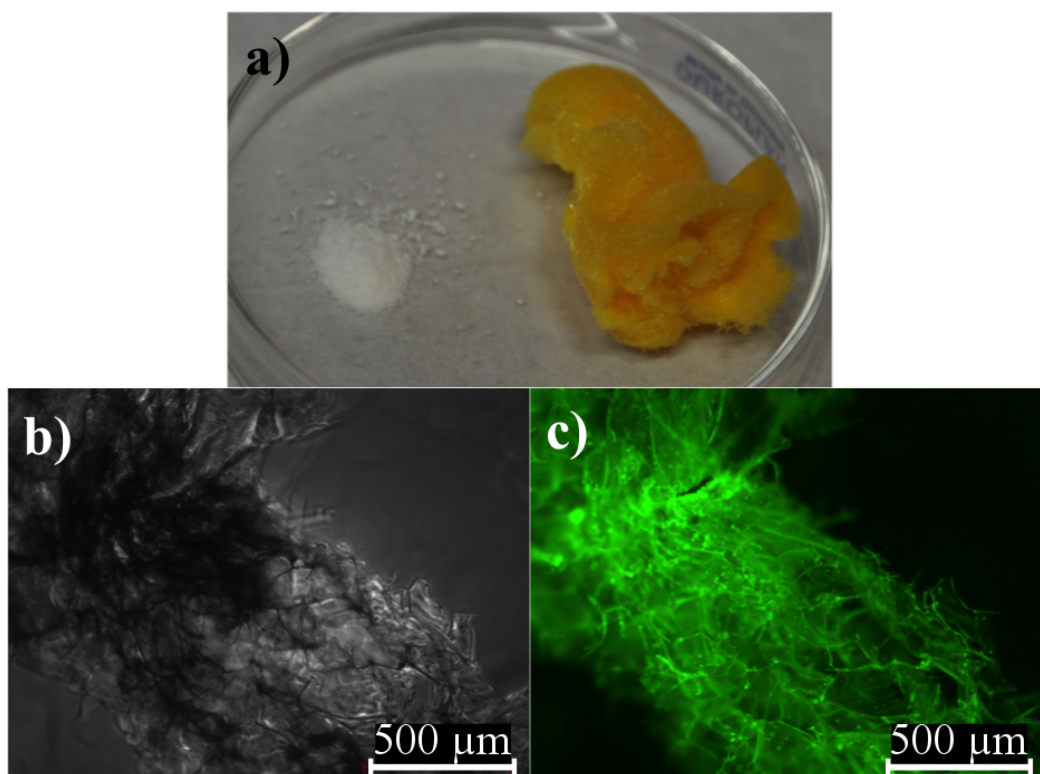


**Figure 18:** (a): Image of unmodified hyaluronan (white powder) and HA labeled with fluoresceinamine (yellow wool) illustrating the changes in color due to the labeling reaction with FA. (b): Bright-field microscopy image of dry fluorescent hyaluronan. (c): Fluorescence microscopy image ( $\lambda_{ex} = 470$  nm,  $\lambda_{em} = 525$  nm) of the same sample revealing the fluorescent properties of FA-HA.

Degrees of substitution, defined as the amount of FA divided by the number of disaccharide units within the hyaluronan, were generally between 0.006 and 0.012 (n/n). These values were low due to the choice of reaction parameters ( $n(NH_2)/n(COOH) = 1.46$ ;  $n(EDC)/n(NHS) = 0.5$ ; reaction time = 5h; pH = 7).<sup>189</sup> They were selected for generally achieving the desired low yield of FA modification. Additionally the low observed solubility of FA in aqueous medium contributed to these low degrees of substitution. However, they were sufficient for visualizing hyaluronan using fluorescence microscopy (Figure 18c). Subsequently FA-HA was used for immobilization experiments with non-crosslinked HA on glass and titanium surfaces (Section 2.2.2) and small model implants (Section 2.2.3). Analyzing the mechanism of the observed pressure reduction (Section 2.5.1) was also possible with this degree of fluorescent labeling. Therefore no further optimizations of the reaction parameters were undertaken.

## 2. Results & Discussion

### 2.1.2. Modification of hyaluronan with thiol groups

As outlined in Section 1.6, the strategy for generating hyaluronan hydrogels included the modification of HA chains with thiol groups. For this, a method developed by Shu et al. was used, in which dithiobis (butanoic hydrazide) (DTBH, Figure 19a) or dithiobis (propanoic hydrazide) (DTPH, Figure 19b) were covalently linked to hyaluronic acid. In a subsequent step selective oxidation of the disulfide bonds via dithiothreitol (DTT) yielded hyaluronan modified with thiol groups (HS-HA) (Figure 19c).<sup>101,102,137</sup> The group of Shu et al. further showed that the EDC-mediated peptide coupling was more effective when hydrazides were used instead of amides and that DTPH generally had a higher reactivity than DTBH due to a lower pKa.<sup>102</sup> Taking this into account, DTPH was used instead of DTBH to prepare HS-HA in this thesis. It was subsequently used for generating and immobilizing hyaluronan hydrogels to different solid surfaces (See Section 2.3.1).

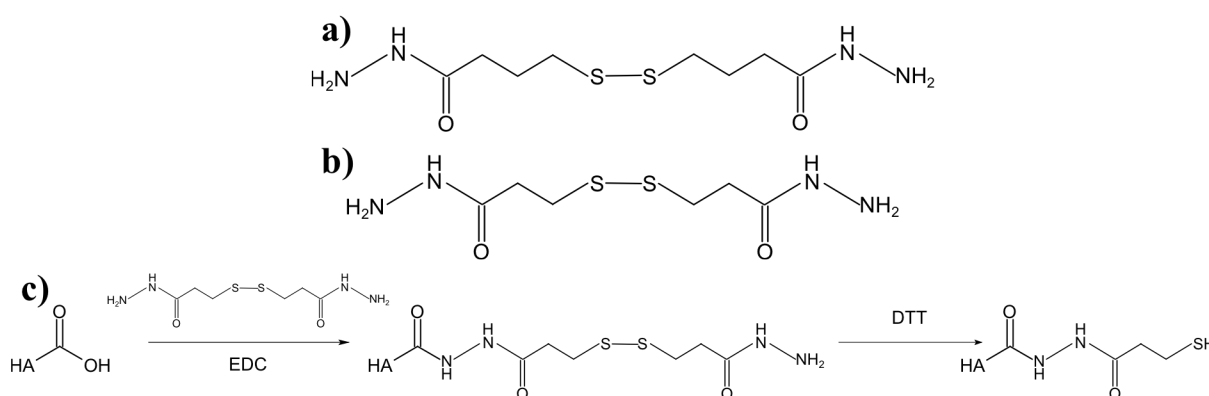


**Figure 19:** (a): Chemical structure of dithiobis (butanoic hydrazide). (b): Chemical structure of dithiobis (propanoic hydrazide) (DTPH). (c): Overview of the reaction pathway for creating hyaluronan with thiol groups including a EDC mediated peptide coupling reaction between hyaluronan and DTPH followed by a reduction of the disulfide groups with DTT.

DTPH was synthesized from dithiobis(propanoic acid) according to the protocol developed by Shu et al.<sup>190</sup> and analyzed using <sup>1</sup>H-NMR (300 MHz, D<sub>2</sub>O). The thiolation reaction was performed according to Shu et al.<sup>102</sup> with some minor alterations (See Section 4.1.2). The biggest change in the protocol was the use of HA with lower molecular weights ( $M_n = 100$  kDa, 60 kDa, 10 kDa) compared to the size Shu used ( $M_n = 120$  kDa)<sup>101,102,137</sup>. The amount of HA bound thiol groups was controlled by varying reaction times: 5 – 30 minutes for a low to medium degree of substitution and 1 – 2 hours for a higher degree of substitution, defined as the amount of thiol groups divided by the amount of disaccharide units.

## 2. Results & Discussion

The general success of the thiolation was confirmed by nuclear resonance spectroscopy on protons in deuterated water ( $^1\text{H-NMR}$  ( $\text{D}_2\text{O}$ )).

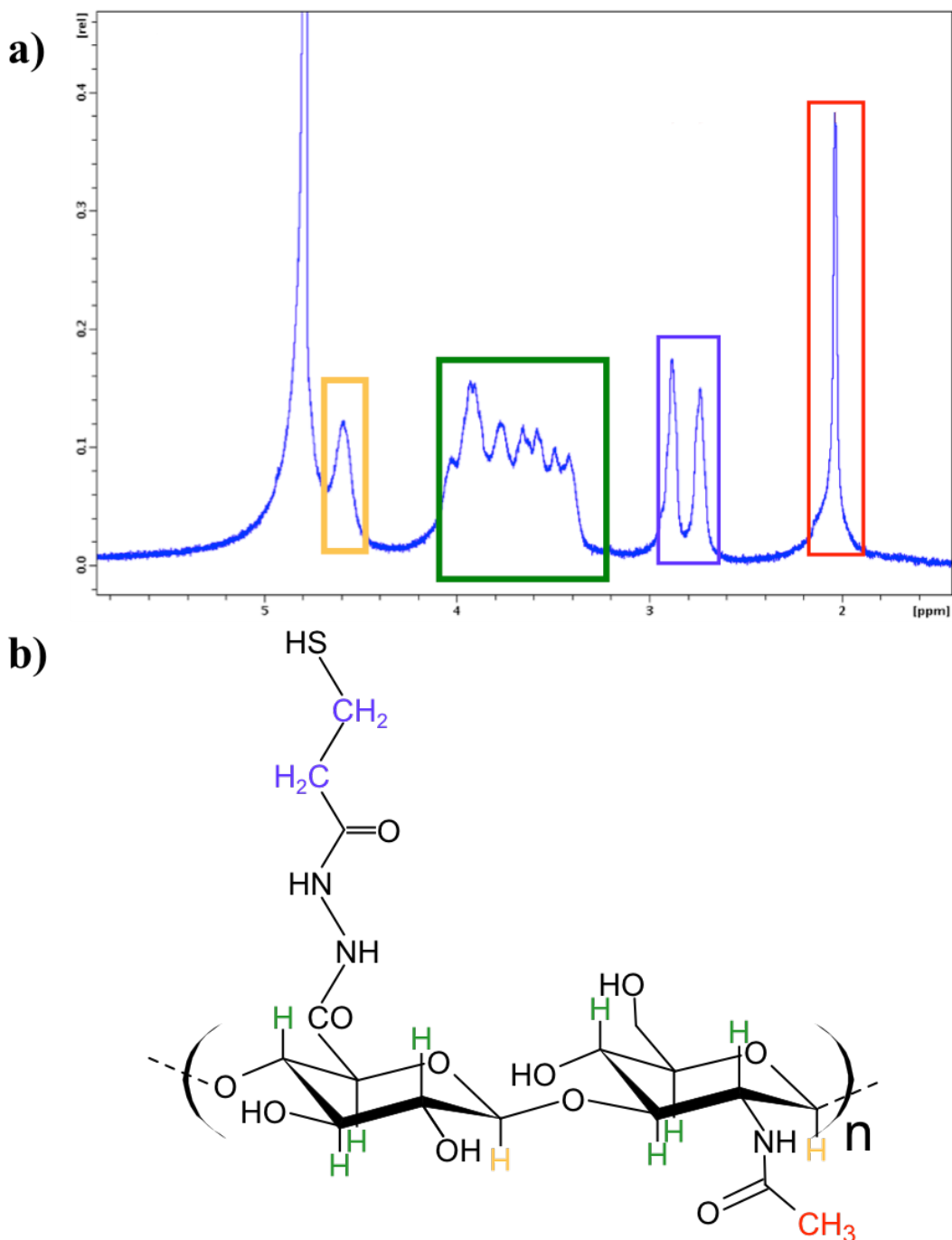


**Figure 20:** (a):  $^1\text{H-NMR}$  (300 MHz) of HS-HA. (b): The peaks were attributed to the individual H-atoms according to Shu et al. and Son et al.<sup>102,191</sup>

Spectra were analyzed according to Shu et al. and Son et al.<sup>102,191</sup> The multiple overlapping signals shown in Figure 20a at  $\delta = 4.1 - 3.3$  ppm and 4.6 ppm originated from the pyranose  $-\text{CH}-$  groups of the disaccharide units. The singlet at  $\delta = 2.03$  ppm belonged to the *N*-acetyl methyl protons and the peaks seen at  $\delta = 2.88$  ppm and 2.74 ppm were attributed to the  $-\text{CH}_2-\text{CH}_2$  groups of the thio(propanoic hydrazide) (TPH) chains. These results were similar to  $^1\text{H-NMR}$  of HS-HA published by Shu et al.<sup>102</sup>, confirming that the modification of HA with DTPH was a success.

## 2. Results & Discussion

For verifying success of the disulfide oxidation, which resulted in the thiols required for subsequent hydrogel generation, and to determine the degree of substitution with thiol groups (“thiolation grade”, “TG”), a modified Ellman’s test was applied (See 4.1.2).<sup>192,193</sup> HA of varying sizes ( $M_n = 10$  kDa; 60 kDa; 100 kDa) was reacted with DTPH for different times followed by sample analysis using Ellman’s test (Figure 21).

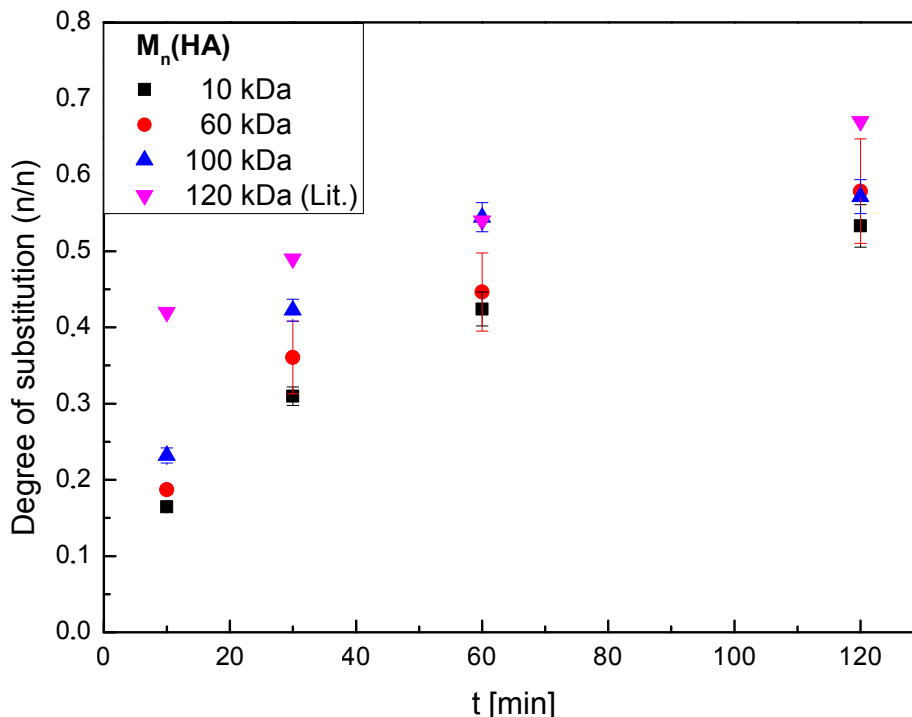


**Figure 21:** Degree of substitutions with thiol groups using DTPH for hyaluronan of varying sizes and for different reaction times. The values of 120 kDa were taken from Shu et al. for comparison<sup>102</sup>. The results show a tendency for a slower reaction speed for hyaluronan with a smaller size. Average thiolation grades were determined by at least three individual Ellman’s tests each with the standard deviation as error bars.

The results clearly showed that generating different thiolation grades was achieved by a modulation of the reaction times of the peptide coupling between HA and DTPH. This enabled creating hydrogels with different degrees of crosslinking by these variable amounts of thiol groups. Furthermore, at  $M_n = 100$  kDa, a gelation of the reaction solution during the peptide coupling was observed over the course of the modification. This was attributed to the both hydrazide groups of DTPH reacting with different hyaluronan chains forming crosslinks. This effect has been described before by Shu et al.<sup>102</sup> and was also observed with the DTPH modification of the  $M_n = 60$  kDa, although less pronounced with viscosity only increasing partially. This was also the explanation for comparatively lower TG of  $M_n = 100$  kDa at  $t = 120$  min. On the one hand maintaining the pH at 4.75 in the viscous solution was not possible, leading to lower reaction velocities and the movement of HA was potentially also slowed down within the network. As a result, no experiments with the thiolation of larger size HA were conducted in order to retain maximum level of control of the reaction parameters. Instead hyaluronan of  $M_n = 10$ -100 kDa was evaluated further for creating hydrogels.

## 2. Results & Discussion

---

The results further indicated a possible dependency thiolation grades on the sizes of hyaluronan used, with a lower thiolation grade of smaller HA after the same reaction time than fractions of larger size. This was not fully explained (See Section 3.1.1) and further research (HA of bigger sizes ( $M_n > 100$  kDa), different reactions) needs to be conducted for fully exploring this mechanism. Nonetheless, the results show clearly, that modifying hyaluronan chains of variable lengths with thiol groups was possible and hydrogels formed for almost all examined HS-HA fractions, excluding  $M_n = 10$  kDa (See Section 2.3.1).

### 2.1.3. Combination of thiolation and fluorescent labeling of hyaluronan

In the previous sections it was shown that fluorescent labeling (Section 2.1.1) and modification of HA with thiol groups (Section 2.1.2) was achieved individually. In order to create fluorescent hydrogels for an improved visibility, a simultaneous modification of HA with FA and thiols was required. To that end, a reaction sequence was established that allowed for a reproducible addition of both molecules (Figure 22). This sequence was set up that way for preparing HA with reproducible thiolation grades. It was shown, that some properties (elasticity, swelling behavior etc.) of hydrogels were dependent on crosslinking density<sup>176</sup>. In turn, this crosslinking density was dependent on the amount of anchor groups available for crosslinking, in this case the thiol groups. Therefore it was important to also create HS-FA-HA in a way for ensuring reproducible thiolation grades. The fluorescent labels, at least in the scope of this thesis, were only added for general visualization of the hyaluronan and not required for crosslinking or quantitative measurements. As a result a reproducible modification of HA with FA was not as important in the context of this project. Therefore, the reaction sequence for HS-FA-HA was established with a goal of ensuring maximum reproducibility of the thiolation grade.

## 2. Results & Discussion

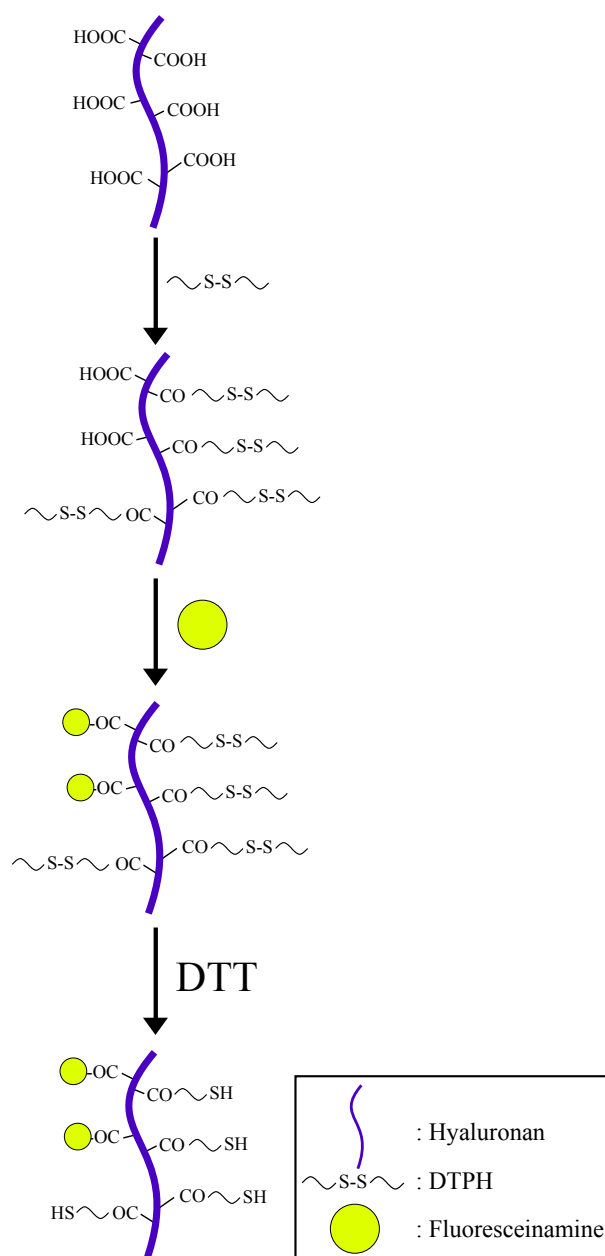


**Figure 22:** Overview of the combined modification of hyaluronan with a fluorescent dye and thiol groups. First hyaluronan was reacted with DTPH followed by a binding of fluoresceinamine to get fluorescent DTPH-HA. In a last step the disulfide bonds were cleaved to yield HS-FA-HA. This sequence was established to get a maximum reproducibility for the thiol group addition.

The first consideration concerning establishing reaction sequence was the order in which FA and DTPH should be connected to the hyaluronan (Figure 23). Both modifications targeted the carboxyl groups of the HA disaccharide units. Consequentially, after the first reaction step, the amount of available reaction partners for the second modification is decreased, resulting in a lower degree of substitution (Figure 23).

## 2. Results & Discussion

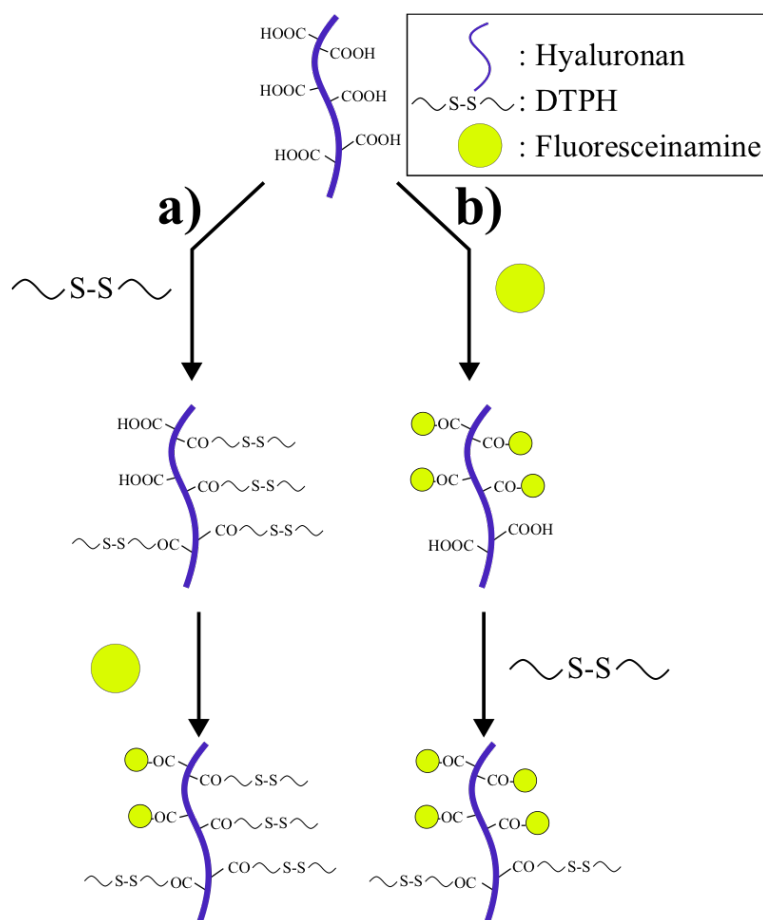


**Figure 23:** Overview of the two possible reaction paths to generate HS-FA-HA involving either **(a)** the modification first with DTPH followed by FA or **(b)** the addition of FA as a first and the reaction with DTPH as a second step. Depending on the sequence, the grade of modification of **(a)** FA would be influenced by DTPH or **(b)** DTPH would depend on the amount of FA bound to HA. Since the degree of substitution for the thiol groups was more important for the hydrogel properties, option **(a)** was selected.

Modifying HA with DTPH as a first reaction has an impact on the degree of substitution with FA (Figure 23a) conducted in a second step and vice versa. As mentioned before, the degree of substitution with thiol groups was the defining parameter for crosslink density.<sup>101</sup> For that reason the reaction pathway involving DTPH binding in the first step followed by the fluorescent labeling reaction (Figure 23a) was selected.

The other consideration determining the sequence of reaction steps shown in Figure 22 was, whether the DTT disulfide reaction would be performed before (Figure 24a) or after (Figure 24b) the fluorescent labeling with FA.

## 2. Results & Discussion

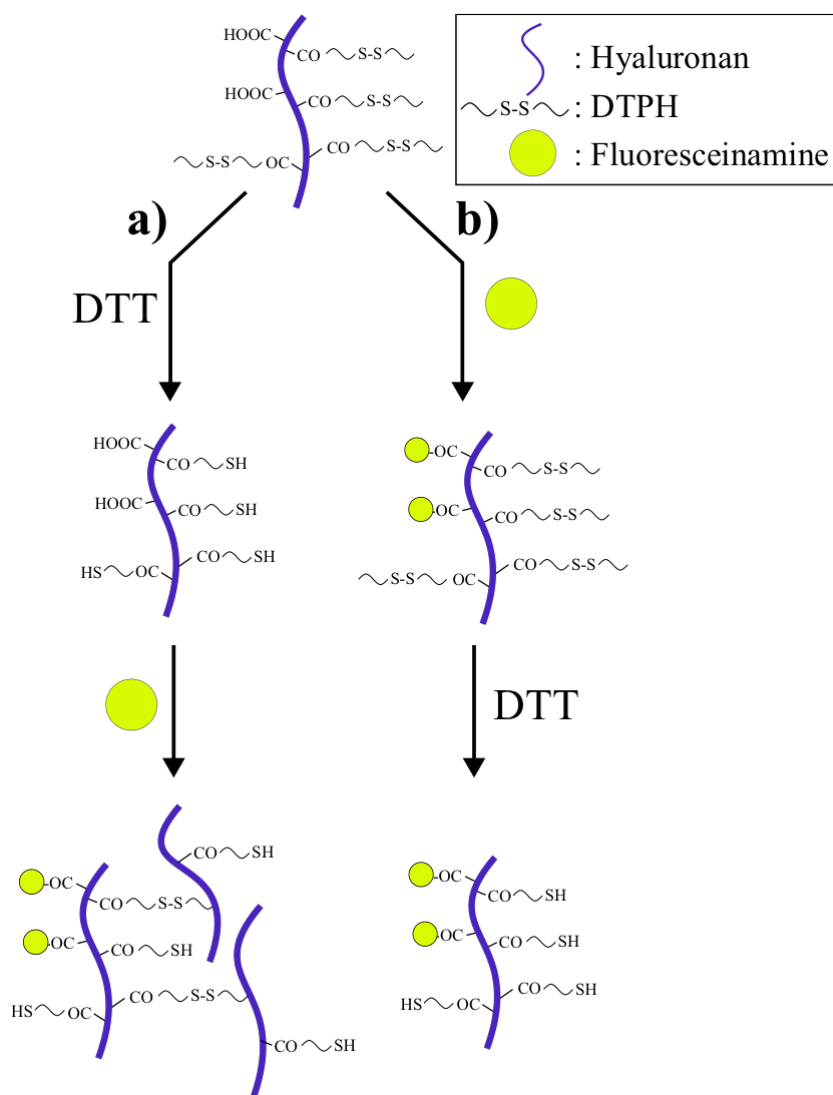


**Figure 24:** Overview of the possible reaction pathways involving disulfide reduction to thiols by DTT and fluorescent labeling with either the disulfide reaction (a) or the labeling (b) as a first step. Since thiols are vulnerable to a re-oxidation, and would re-form disulfides during the reaction between HA and FA, the disulfide reduction was conducted as the last step.

Under basic conditions and in the presence of oxygen, thiols start re-oxidizing disulfide formation, which would result in changes of thiolation grades and the formation of crosslinks between HA chains.<sup>102</sup> Therefore, if the disulfide reduction was performed before the binding of FA (Figure 24a), which was done in a neutral to basic medium (see 4.1.3), a prevention of the re-oxidation of the resulting thiols would require working under oxygen exclusion. This would have necessitated more elaborate experimental setups. Hence, disulfide reduction with DTT (Figure 24b) was performed as last step following the modification of the HA with FA.

These considerations resulted in the combined reaction sequence shown in Figure 22. It required more purification steps in between the individual reactions (see Section 4.1.4), as opposed to a modification with only thiols.<sup>137</sup> But it also ensured reproducible thiolation grades and was therefore chosen for the production of fluorescently labeled HS-HA (HS-FA-HA). This allowed for the creation of fluorescent hydrogels for analytical purposes (Section 2.3.1).

## 2. Results & Discussion

These results confirmed, that the chosen reaction pathway was suitable for preparing HS-FA-HA which thiol groups required to generate hydrogels fluorescence properties necessary for more elaborate analytical experiments. Simultaneously modifying HA with both groups also did not influence the thiolation grade. This was confirmed by creating HS-HA and HS-FA-HA from the same fraction of DTPH modified hyaluronan for different reaction times and analysis by Ellman's test (Figure 25; see Section 4.1.4 for further details).

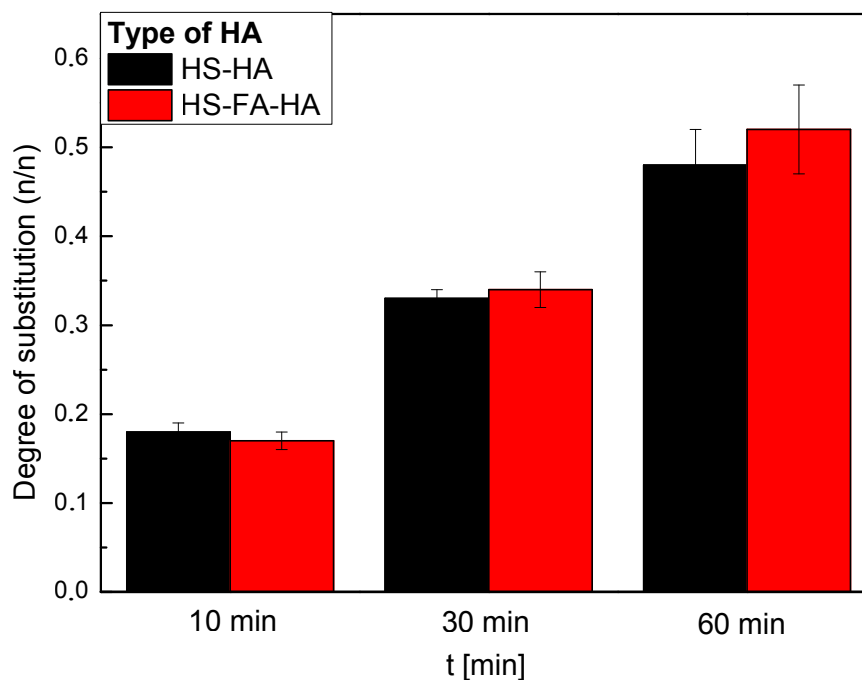


**Figure 25:** Comparison of the thiolation grades of HS-HA and HS-FA-HA ( $M_n = 60$  kDa) from the same fraction of DTPH modified hyaluronan for different reaction times. Average thiolation grades were gained from at least three individual Ellman's tests each with standard deviations as error bars.

The data showed that, apart from random errors during synthesis and purification of the individual HS-HA and HS-FA-HA fractions, covalently binding fluoresceinamine in addition to modifying HA with thiols using the developed reaction sequence (Figure 22) had no significant influence on thiolation grades. Therefore it was used for all further preparations of HS-FA-HA.

## 2. Results & Discussion

---

### 2.1.4. Summary and conclusion

In this section the different methods used to synthesize starting materials for creating hyaluronan hydrogels with or without fluorescent properties were presented. For fluorescent labeling, fluoresceinamine was linked to hyaluronan via an EDC mediated peptide-coupling reaction (See Section 2.1.1). FA was chosen for this because of its non-toxicity, which decreased potential hazards during the handling process and may be important for future cell experiments. The resulting degrees of substitution with the fluorescent dye were kept low (0.6%-1.2% (n/n)) because of the selected reaction parameters and low solubility of fluoresceinamine in aqueous solutions (See Section 4.1.3). However, degrees of substitution were similar to the values gained by Ogamo et al., who proposed a method for reacting HA with FA involving a 3:1 mixture of hydrochloric acid and pyridine<sup>186</sup>. In the reaction pathway developed in this thesis no organic solvent was used, which reduced the number of potential issues for safety and waste disposal in potential mass fabrication. Later measurements involving fluorescent hyaluronan showed the amounts of fluorescent dye bound to HA to be sufficient for generating detectable signals.

For creating anchor groups necessary for establishing crosslinks between HA chains resulting in hydrogel formation, a method developed by Shu et al.<sup>101</sup> was successfully adapted. This method involved EDC-mediated peptide coupling between hydrazide functions of DTPH and carboxyl groups of HA. By varying the reaction times, different thiolation grades were achieved and reaction kinetics for the thiolation were size dependent with lower size HA reacting more slowly with DTPH.

Furthermore, both reactions were combined to generate HA with both FA and thiol modifications (Section 2.1.3). The reaction sequence was chosen to ensure reproducible degrees of modification with thiols, which influenced both crosslinking densities and hydrogel properties.<sup>176</sup> The reproducibility of the degree of substitution with FA was neglected because the dye produced the necessary signals for detection. Furthermore, fluorescent labeling was only used for qualitative measurements in this thesis (See Sections 2.2, 2.3.2 and 2.5.1) and a reproducible degree of substitution was therefore not necessary. Also FA modification via the reaction sequence presented in this section (Figure 22) did not noticeably influence thiolation grades (Figure 25).

The methods established in this chapter were applicable to generate the required starting materials for the subsequent generation and immobilization of (fluorescent) hydrogels (Section 2.3). Moreover, these methods were also utilizable for potential mass fabrication of glaucoma stents since they required mostly inexpensive and non-toxic materials as well as no harmful organic solvents. This would significantly lower hazard safety and waste disposal requirements. For these advantages, these methods were used in the following chapters to covalently immobilize hyaluronan and HA hydrogels to model implants and analyze their properties.

### 2.2. Immobilization of hyaluronan to glass and titanium surfaces

#### 2.2.1. Development of a silanization protocol

In order to reliably perform as a possible treatment for the glaucoma disease, it was required of the potential glaucoma stents to enable a regulation of intraocular pressure for long periods of time.<sup>19</sup> Therefore it had to be ensured, that the performance of intraocular implants would not deteriorate over time. One aspect contributing to a potential long-term stability was, that hydrogel parts of these implants would consistently remain in place. For that reason, it was necessary to permanently immobilize hydrogels to implant surfaces. As outlined in Section 1.6 reacting HS-HA to surface-bound epoxide groups was selected to achieve immobilization. The epoxides themselves were bound to surfaces via silanization with (3-Glycidyloxypropyl)trimethoxy-silane (GPS) (Figure 26).

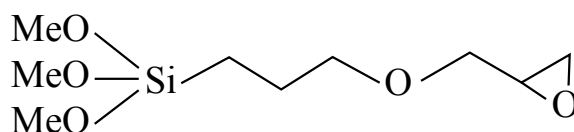


**Figure 26:** Chemical structure of Glycidyloxypropyl)trimethoxy-silane.

The use of silanes for grafting reactive groups to solid surfaces was applicable to both glass<sup>177</sup> and titanium<sup>166</sup> since both materials shared a similar surface chemistry.<sup>140,177</sup> Glass samples were used as model surfaces in addition to titanium for their transparency, which enabled a microscopic analysis of further stent parameters (See also Sections 2.2.3, 2.3.2 and 2.5.1) by using HS-FA-HA.

For cleaning and activation of the surfaces, the commercially available “Extran<sup>®</sup> MA01” (Extran) was used, an alkaline solution containing washing detergents. Immersion in a basic solution was sufficient to hydroxylate the surface of titanium<sup>194</sup> and with Extran this step was combined with additional cleaning. The detergent solution also had the advantage of being cheap and non-hazardous, both beneficial for a potential industrial application. Other methods, like the exposure of the surfaces to H<sub>2</sub>SO<sub>4</sub>/H<sub>2</sub>O<sub>2</sub> (3:1 v/v) (Caro’s solution)<sup>195</sup>, plasma treatment<sup>170</sup> or plasma treatment followed by immersion in nitric acid and H<sub>2</sub>O<sup>173</sup> were also considered. However, they were not further followed up for several reasons: Treating glass tubes with Caro’s solution was attempted but resulted in small bubbles forming on their interiors, which resulted in a non-reproducible inner surface activation. This could have been circumvented by using a syringe pump to remove bubbles. However, due to the dangerous nature of Caro’s solution<sup>196</sup> this path was not further pursued. Especially in an industrial environment this would not have been feasible, where extra safety precautions might have meant a considerable increase in production costs.

The use of a plasma machine brought up similar problems: The plasma was generated locally at the top of the machine and reactive species spread out from there into the plasma chamber (Figure 27). For the glass tubes, with the interiors being partially shielded from the plasma, it also was not guaranteed, that the activation on the inside would be uniform and reproducible. Additionally, maintaining a plasma machine was potentially more expensive than simply using an alkaline solvent.

## 2. Results & Discussion

Taking all this into account a basic solution was used for the surface activation,<sup>194</sup> since it guaranteed an equal concentration of active species all over the tube's surfaces while minimizing potential hazards.

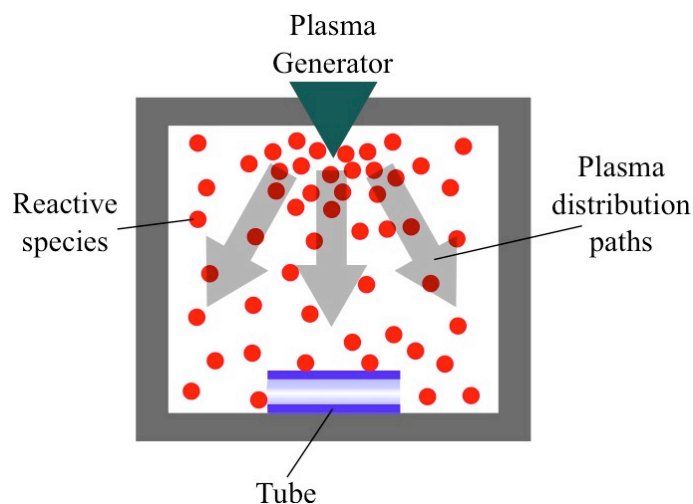


**Figure 27:** Simplified sketch of the plasma activation of small tubes. The plasma was generated locally at the top of the machine. The tube's inside was partially shielded from the reactive species possibly resulting in a non-uniform and non-reproducible surface activation.

For the silanization process itself, a method involving the immersion in a silane/toluene solution was selected. It was shown, that forming monolayers of GPS on silicon substrates was possible<sup>197</sup> and therefore this method was adapted for the use on titanium and the model glass surfaces. In order to verify the applicability of this method flat titanium and glass slides were modified with different silanes and the surface energies of these samples determined via contact angle measurements<sup>198</sup>. Besides GPS a hydrophobic silane in the form of 1H,1H,2H,2H-Perfluoro-trichlorosilane (PFS) (Figure 28a) and a hydrophilic silane ((3-Aminopropyl)triethoxysilane (APTES) (Figure 28b) were used for comparison.

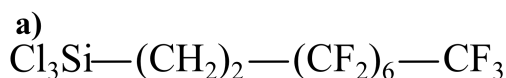


**Figure 28:** Chemical structures of PFS (a) and APTES (b).

The application of these silanes would result in surfaces with different energies due to the different active groups. Especially PFS was known to result in very hydrophobic surfaces<sup>199</sup> and was expected to show the biggest changes in surface energies compared to APTES and GPS. The liquids used for contact angle measurements were ddH<sub>2</sub>O, ethyleneglycol and mixtures of MilliQ and ethyleneglycol, which covered a liquid/vapor tension range of 49.15 mN/m (100% ethyleneglycol) to 72.58 mN/m (100% MilliQ).<sup>200</sup> The energies were calculated based on the young's equation using an equation of state approach according to Balkenende.<sup>198</sup>

## 2. Results & Discussion

The relation between the contact angle of a liquid and the surface energies was given by the formula

$$\cos \theta = -1 + 2 \sqrt{\frac{\gamma_{SV}}{\gamma_{LV}}} e^{-0,0001247(\gamma_{LV}-\gamma_{SV})} \quad \text{Equation 2:1}$$

with  $\Theta$  being the contact angle,  $\gamma_{SV}$  the surface-vapor energy and  $\gamma_{LV}$  the liquid-vapor energy. The formula was simplified by excluding the exponential part since it would be almost equal to one. It was aimed for only a qualitative comparison between the differently modified surfaces instead of an accurate determination of their energies. Therefore this decrease of accuracy by this simplification was acceptable on this context and allowed for a linear fit, which was more easily performed with a lower amount of data-points compared to an exponential fit. In turn this reduced the time required to gather enough data for a reasonable surface energy determination.

The results of these contact angle measurements (Figure 29) showed a distinctive variation of the surface energies for glass and titanium substrates, depending on the silanes.

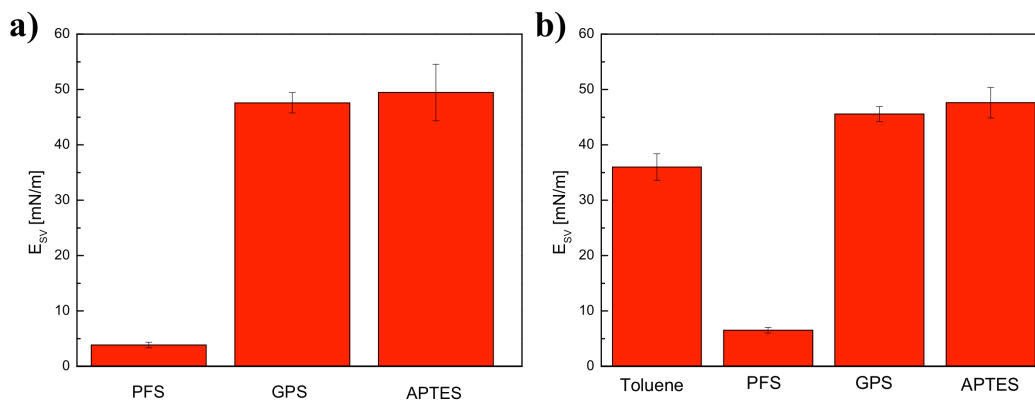


**Figure 29:** Surface energies of flat glass (a) and titanium (b) samples modified with different silanes using surface activation by Extran and silanization in a silane/toluene solution. The surface energy of the non-silanized glass sample was not determined since contact angles were too low for all tested solutions to be recorded. Average contact angles were calculated from ten drops with errors obtained from the variance of the linear fits and the standard deviations of the average contact angles.

For both materials the surface energies of samples modified with GPS and APTES were similar to each other. Modifications with PFS however caused a significant difference of the energy compared to the other silanes. This confirms the applicability of the developed protocol using Extran® MA01 for activation followed by immersing samples in silane/toluene solutions. In subsequent chapters the efficiency of the silanization was further confirmed by covalently immobilizing hyaluronan (Sections 2.2.2 and 2.2.3) and HA hydrogels (Section 2.3.2) to silanized surfaces.

## 2. Results & Discussion

### 2.2.2. Immobilization of hyaluronan to flat glass and titanium surfaces

In Section 2.2.1 a method to graft epoxide groups to titanium and glass surfaces was established. It was also shown before, that reacting epoxides to the primary alcohols of saccharides in solution was possible<sup>103</sup> and GPS was already successfully used to immobilize dextran to surfaces<sup>201</sup>. Due to these findings, immobilizing hyaluronan to epoxide-modified surfaces should be feasible. However the concept had to be verified experimentally. Furthermore, it was necessary to see, whether the hyaluronan would adhere to the surfaces due to an unspecific absorption, which would not be stable in the long term, or covalently link to the silanes. To that end, small glass and titanium sheets were silanized partially using a custom-made reaction chamber (Figure 30). The chamber was fastened on top of the sample in the holder covering it partially. By filling it with silane/toluene solutions only a small part in the middle of the substrate's surface was exposed to GPS. Afterwards the samples were immersed in a HS-FA-HA solution and incubated in the presence of oxygen.

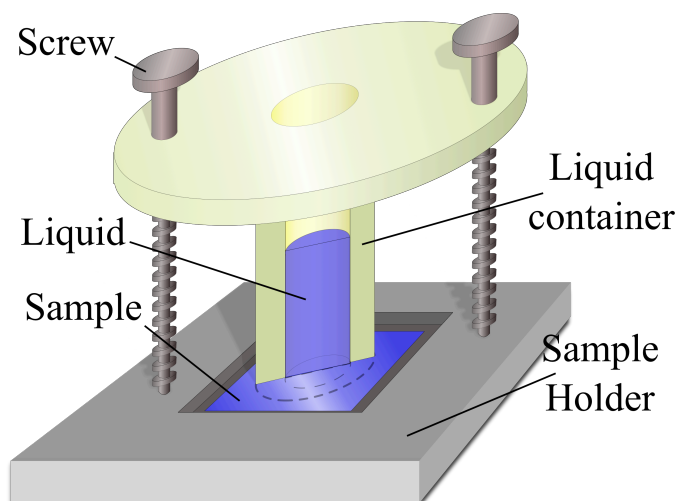


**Figure 30:** Schematic drawing of the custom-made chamber for partially modifying surfaces of flat glass and titanium slides with silanes. The liquid container covered only part of the samples and exposed only that part to silane solutions.

Fluorescently labeled HA was used for detecting a successful immobilization, either visually or by fluorescence microscopy. HS-FA-HA was used instead of FA-HA to allow for a partial re-oxidation of thiols to disulfides resulting in a gel formation. This also resulted in an increased number of HA molecules bound to the surface, amplifying the signals due to the presence of a higher number of fluorophores (Figure 31a/b). Careful rinsing in water removed the gel layer from the samples except for the silanized parts (Figure 31c/d). After drying the samples they were also analyzed by fluorescence microscopy, which further verified a strong presence of hyaluronan in the previously silanized area of the sample (Figure 31e/f).

## 2. Results & Discussion

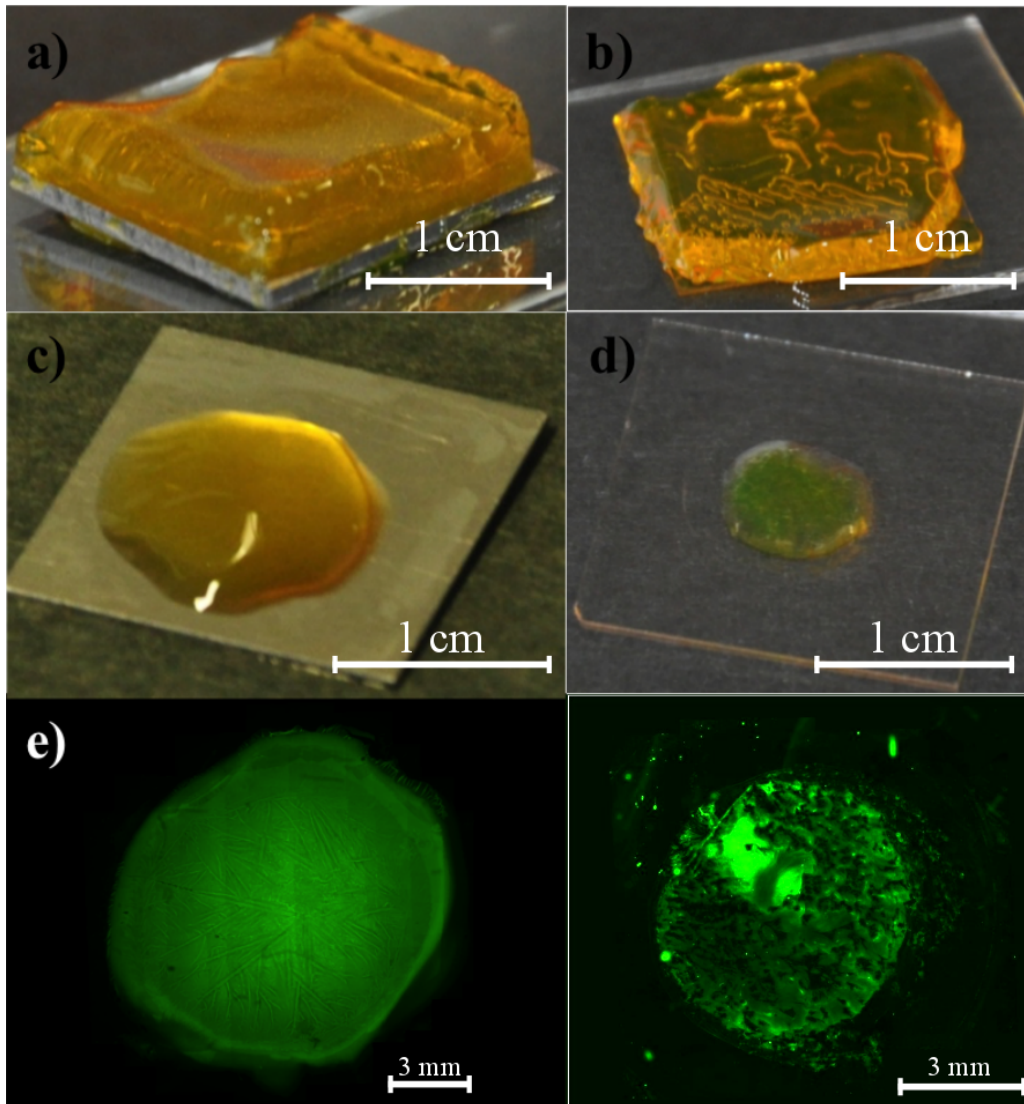


**Figure 31:** Results of immersing partially silanized glass and titanium slides in HS-FA-HA solutions. A layer of HA gel formed on the titanium (a) and glass (b) samples due to disulfide formation. After rinsing in water HS-FA-HA only remained on silanized parts of titanium (c) and glass (d). This was further visualized by fluorescence microscopy ( $\lambda_{\text{ex}} = 470 \text{ nm}$ ,  $\lambda_{\text{em}} = 525 \text{ nm}$ ) on titanium (e) and glass surfaces (f).

These results on the one hand further verified, in addition to the surface energy measurements (Section 2.2.1), that silanization using Extran for the surface activation and silane solutions in toluene were applicable to graft GPS to glass and titanium surfaces. Since the improved attachment of HA to silanized parts compared to blank surfaces illustrated the strength of the covalent links and verified the applicability of the established method.

## 2. Results & Discussion

### 2.2.3. Selective Immobilization of hyaluronan to small glass tubes

In section 2.2.2 the selective and covalent immobilization of hyaluronan to flat glass and titanium surfaces modified with epoxide groups was established. However, the intraocular stents would be in the shape of small tubes (see Section 1.6). Therefore the next step was to check, whether the methods presented in 2.2.1 and 2.2.2 were applicable as well to tubes. Furthermore, it was necessary to modify the outer and inner surfaces of the stents individually with HA hydrogels possessing potentially different properties in respect to cell adhesion (see Section 1.6). For that, immobilizing hyaluronan selectively to the outer or inner surfaces of the small tubes had to be developed.

Small glass tubes ( $L = 10$  mm,  $ID = 0,5$  mm,  $OD = 1$  mm) were manufactured by the glass workshop of the Max Planck Institute as models for the intraocular stents. They were used instead of titanium tubes most of the time since the later were non-transparent. Therefore immobilizing HA successfully to the inner surfaces of titanium would not have been possible. Since silanization and covalent HA immobilization was applicable for both materials (Section 2.2.2) glass was used as model substrates for most further experiments. Additionally FA-HA was used instead of HS-FA-HA, since properly removing the resulting gels on the tubes' interiors was not guaranteed. Instead FA-HA was used and weaker fluorescent signals detected by longer excitation times. Two different setups were designed for immobilizing hyaluronan selectively only to outer or inner surfaces of these glass tubes (Figure 32).

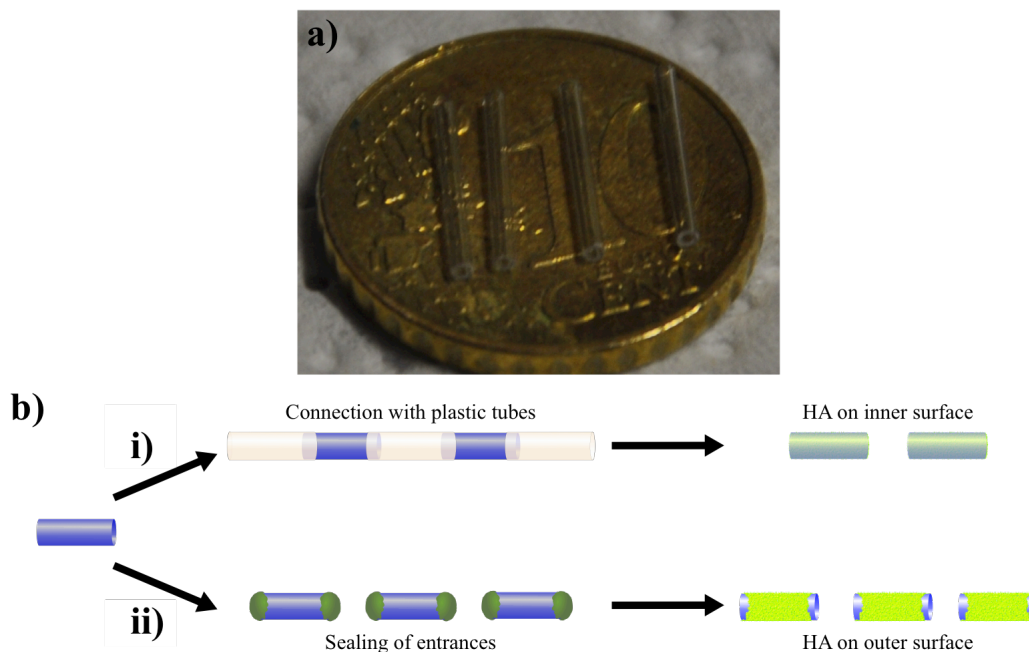


**Figure 32:** (a): Picture of the small glass tubes ( $L = 10$  mm,  $ID = 0,5$  mm,  $OD = 1$  mm) that were used for the directed immobilization of hyaluronan and most other experiments in this thesis. (b): Experimental setup for the immobilization of hyaluronan to either the inner (i) or outer (ii) surfaces of these small glass tubes.

For modifying the tubes' inner surfaces with fluorescent hyaluronan, silanized samples were connected to each other in series using small pieces of elastic QCMD tubing (Figure 32b, i). A FA-HA solution was then injected into the setup bringing only the interiors of the samples into contact with the fluorescently labeled hyaluronan.

## 2. Results & Discussion

For grafting FA-HA to outer surfaces, the entrances of the tubes were sealed using elastic polymer resistant to the infiltration of watery solutions (Figure 32b, ii). By fully immersing silanized glass tubes in a FA-HA solution exposed only their outsides while the polymer shielded the inner parts. After immobilization was finished, this polymer was easily removed, which potentially allowed for further modifying the insides.

After extensive washing samples they were examined using fluorescence microscopy. It was necessary to distinguish between possible fluorescence signals originating from HA covalently linked to the surfaces or from an unspecific adsorption. To that end tubes modified with GPS and non-silanized samples were incubated side-by-side in an FA-HA solution and subjected to the same washing protocols (See Section 4.2.4) before analyzing them by fluorescence microscopy (Figure 33).

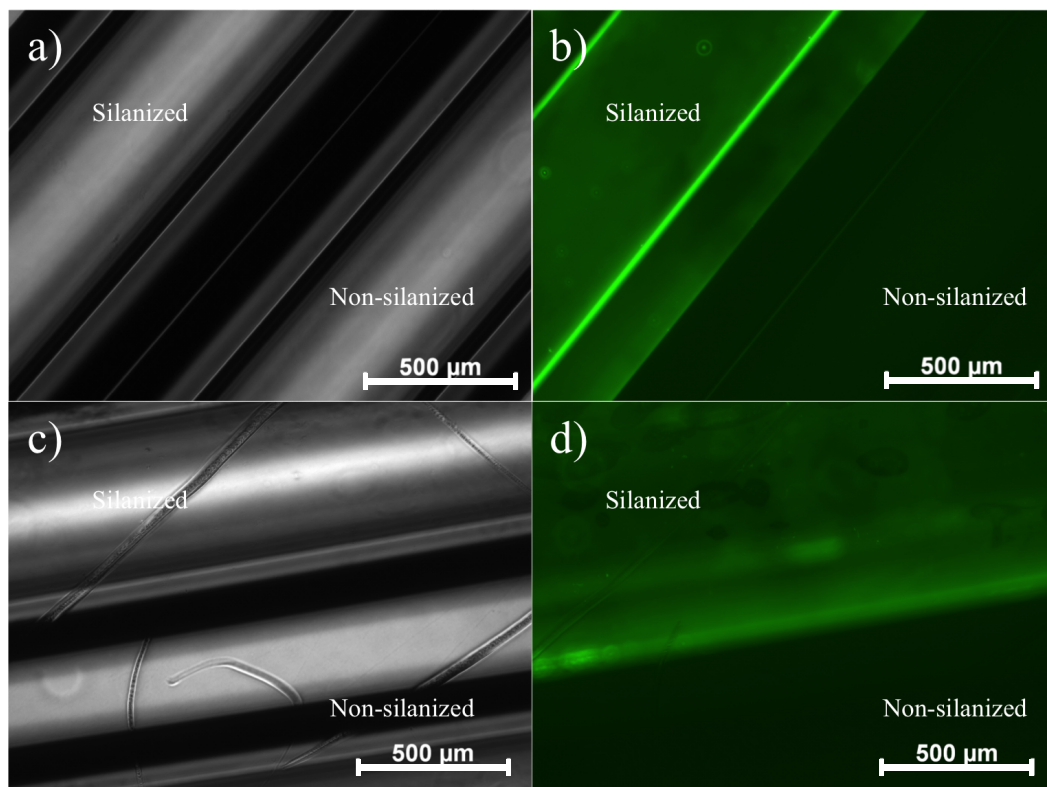


**Figure 33:** Brightfield (a + c) and fluorescence (b + d) ( $\lambda_{\text{ex}} = 470 \text{ nm}$ ,  $\lambda_{\text{em}} = 525 \text{ nm}$ ) microscopy images of silanized (GPS) and non-silanized glass tubes, that were selectively exposed to FA-HA on their inner (a + b) and outer (c + d) surfaces. Both silanized and non-silanized tubes are visible in brightfield images (a + c) but fluorescence signals were only detected from the silanized samples (b + d).

The images showed a clear difference of fluorescent signals between silanized and non-silanized samples. GPS modified glass tubes were visible under fluorescence while unmodified ones did not show significant signals. These results verified that the hyaluronan was bound selectively and covalently to surfaces carrying epoxides. They further ruled out unspecific adsorption since non-silanized samples did not show any fluorescent signal. It was concluded, that the silanization and immobilization protocols developed in Sections 2.2.1 and 2.1.2 were applicable also to the model implants. Furthermore individual modification of the inner (Figure 33b) or outer (Figure 33d) surfaces of the tubes with these methods could be demonstrated. These setups were later also used to selectively immobilize HA hydrogels on the inner and outer surfaces of glass and Ti tubes (Section 2.3.2).

### 2.2.4. Summary and Conclusion

In this section the concept proposed in Section 1.6 for immobilizing hyaluronan to glass and titanium surfaces was successfully established. The polysaccharides were covalently and selectively immobilized by modifying the target surfaces with silanes bearing epoxide groups (Section 2.2.1), followed exposing them to hyaluronic acid solutions (Section 2.2.2). Surface activation and silanization were performed in liquid environments because the alternatives proved to be disadvantageous when compared. By using fluorescently labeled hyaluronan, the applicability of the immobilization to glass and titanium surfaces was confirmed (Section 2.1.1).

The method was developed further for selectively immobilizing hyaluronan to glass tubes (Section 2.2.3). To that end two simple methods were established to specifically target only their outer or inner surfaces. Fluorescent hyaluronan was successfully immobilized on these parts of the silanized samples individually (Figure 33). Also, by comparing silanized and non-silanized tubes immersed in FA-HA a specific and covalent immobilization could be verified (Figure 33).

These collected results show the feasibility of the methods proposed in Section 1.6 for covalently and selectively immobilizing HA to glass and titanium surfaces. While the individual concepts, reacting hyaluronan with epoxides in solution<sup>103</sup> and immobilizing similar molecules on solid surfaces using GPS<sup>201</sup>, were already known, a combination of both was not done before for this system. This concept promises long-term stability for the intraocular implants, which was necessary for a successful therapy, by covalently attaching potential hydrogels. Furthermore, in terms of an industrial application, the method could be applied easily to a higher number of samples enabling a high-throughput modification of intraocular implants using non-expensive and mostly non-toxic materials. At this point of the thesis no information was available for the relative strength of the immobilization, but measurements on gel-modified tubes were performed to gain further insights into this issue (Section 2.4.2).

### 2.3. Formation and immobilization of hyaluronan hydrogels

#### 2.3.1. Synthesis of acrylamide-crosslinked hydrogels

As outlined in Section 1.1, developing a new implant for glaucoma therapy enhanced by hydrogels made from hyaluronic acid was the aim for this thesis. To that end, methods for modifying hyaluronan with thiol (Section 2.1.2) and fluorescent (Section 2.1.1) groups were already established and a combination of both processes successfully implemented (Section 2.1.3). Furthermore, immobilizing fluorescent hyaluronan to flat glass and titanium surfaces (Section 2.2.2) and small glass tubes acting as model implants (Section 2.2.3) was demonstrated. Forming (fluorescent) hydrogels from HS-(FA)-HA and enabling a selective immobilization to the outer and inner surfaces of glass and titanium tubes was the next step, discussed in this section.

As outlined in Section 1.6 the method published by Shu et al.<sup>101</sup>, utilizing a base-catalyzed Thiol-Michael reaction<sup>175,202</sup> (Figure 34), was adapted and modified for the hydrogel creation. The crosslinkers Shu used carried multiple acrylamide groups that were able to react with the thiols of HS-FA-HA, thus establishing crosslinks between the polysaccharides.

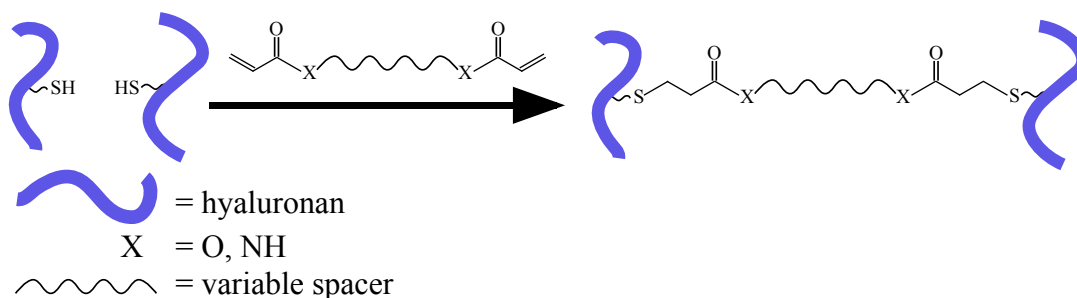


**Figure 34:** Concept for crosslinking HA hydrogels by a Thiol-Michael reaction between the SH groups of hyaluronan and acrylic groups of multifunctional crosslinkers.

Several parameters were considered and adapted for developing the synthesis protocol:

#### *Solvent properties:*

Shu et al. created their hydrogels by first dissolving HS-HA in a Phosphate Buffered Saline (PBS) solution followed by a manual adjustment of the pH to 7.4.<sup>101</sup> Hagel et al. similarly formed their hydrogels by adjusting the pH to 9.0 and incubating HS-HA/crosslinker solutions over night.<sup>176</sup> This manual adjustment posed a problem for transferring these methods to the creation of hydrogel-enhanced implants. Only small amounts of HA (3-15 mg) in small volumes of solvent (100-1000  $\mu$ L) were usually prepared in this thesis, since the tubes are small, and no modified HA was to be wasted. Since no micro pH electrodes for measuring such small volumes were available at that time it was difficult to manually adjust the pH after dissolving HS-HA. However without these manual adjustments of the pH this step led to an acidification of the solution (Figure 83).

To cope with this problem, the reaction parameters used by Hagel et al.<sup>176</sup> were adapted by including a buffer of Tris(hydroxymethyl)aminomethane (TRIS) in Balanced Saline Solution (BSS) at a pH of 8.5 to 9.0: BSS was used instead of water because it is commonly used in medicine for eye irrigation, mimicking the ion concentrations of the intraocular fluid.<sup>203</sup>

## 2. Results & Discussion

As a result gels were synthesized in an environment similar to the physical environments. In addition gel formation was conducted in oxygen-depleted solvents to prevent re-oxidation of thiols to disulfides due to the basic environment<sup>102,176</sup>.

### Crosslinker:

Two commonly used model crosslinkers were considered for generating the hydrogels. Poly(ethylene glycol) diacrylamide (PEGDAA), which was already employed by the Shu et al. group and had a rather long chain-length.<sup>101</sup> N,N'-Ethylenebis(acrylamide) (MBAA) was selected as a short crosslinker with a size similar to the desmosine inspired acrylamides developed by Hagel et al.<sup>176</sup> (Figure 35).

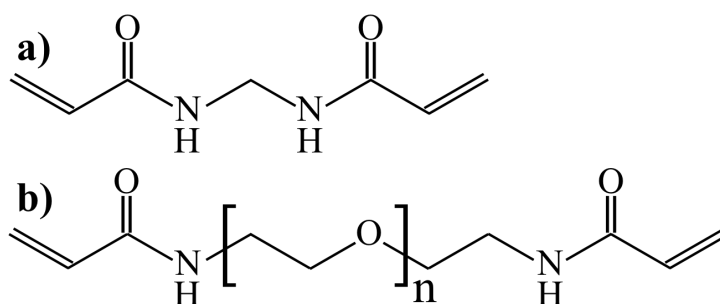


**Figure 35:** Chemical structures of the N,N'-Ethylenebis(acrylamide) (a) and Poly(ethylene glycol) diacrylamide (b) crosslinkers which were used for initial studies on the formation of HA hydrogels.

Acrylamides were selected over potential acrylate derivatives due to a better long-term stability of the hydrogels. Shu et al. reported, that stability of hydrogels formed with Poly(ethylene glycol) diacrylate (PEGDA) and PEGDAA was similar<sup>101</sup>. Hagl et al. however, reported a decomposition of the hydrogels with their desmosine-inspired crosslinkers when acrylates were used for preparing their hydrogels.<sup>176</sup> Since they had to perform in a long-term function as part of glaucoma implants it was expected of them to be stable over longer periods of time. Since acrylamides reportedly showed a better performance in that respect MBAA and PEGDAA were therefore selected as crosslinkers.

### Hyaluronan size:

As mentioned in Section 2.1.2, the modification of HA with thiols was performed on three different sizes ( $M_n = 10$  kDa, 60 kDa and 100 kDa). Consequently they were also used to generate hydrogels and further choices narrowed down depending on the results.

## 2. Results & Discussion

Small molds (diameter = 10 mm, depth = 5 mm,) were manufactured for synthesizing hydrogels using a 3D printer. In a first experiment, the performances of MBAA and PEGDAA for gel formation were tested with  $M_n = 60$  kDa HS-HA. Both crosslinkers readily formed hydrogels, albeit with vastly different gelation times. Solutions of HS-HA and MBAA remained in a liquid state for >30 min and solid gels were retrieved after 24 h of incubation time at 37° C (Figure 36c). Using PEGDAA on the other hand induced a gelation process very quickly, with an increase in viscosity after less than one minute and solid gels after less than five minutes (Figure 36d), which was also reported by Shu<sup>101</sup>. The gel formation was extended to ten minutes by cooling down both HS-HA and crosslinker solutions to 0° C prior to mixing. The modification of model implants with hydrogels sometimes necessitated a prolonged handling of HS-HA/crosslinker mixtures before gelation occurred (see Sections 2.3.2 and 4.3.2). Since MBAA gelation times as PEGDAA it was selected as model crosslinker for further experiments.

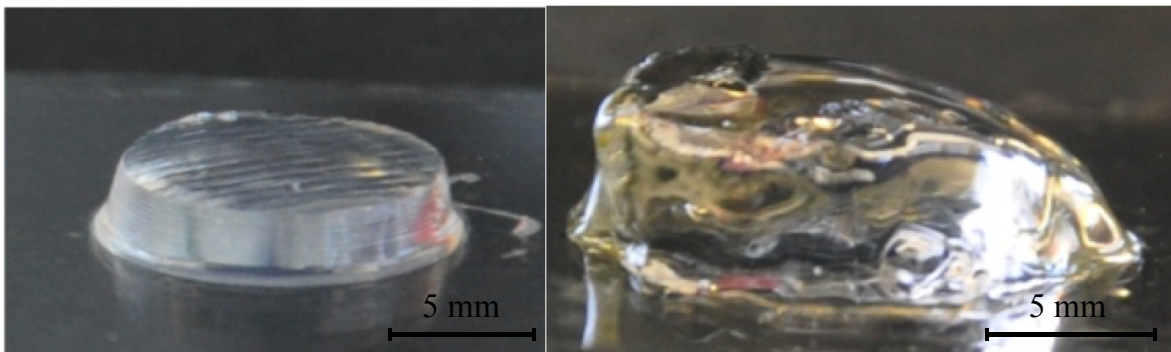


**Figure 36:** Images of hydrogels ( $V = 250 \mu\text{L}$ ;  $M_n(\text{HA}) = 60$  kDa;  $\beta(\text{HA}) = 15$  mg/ml;  $\text{TG} = 0.18$ ; hydrogels formed in TRIS/BSS ( $c(\text{TRIS}) = 0.4$  mol/l;  $\text{pH} = 8.5$ )) prepared with MBAA (a) after 24 hours incubation at 37°C and PEGDAA (b) after five minutes at room temperature.

When hydrogel synthesis was performed with MBAA and different sizes of hyaluronan it turned out, that not all three of the available HS-HA sizes were utilizable for the hydrogel creation: While at  $M_n = 60$  kDa and 100 kDa, HS-HA/MBAA mixtures readily formed gels (Figure 37), no gel formation was observed when using  $M_n = 10$  kDa HS-HA. Therefore, further experiments were performed with the other two size fractions.

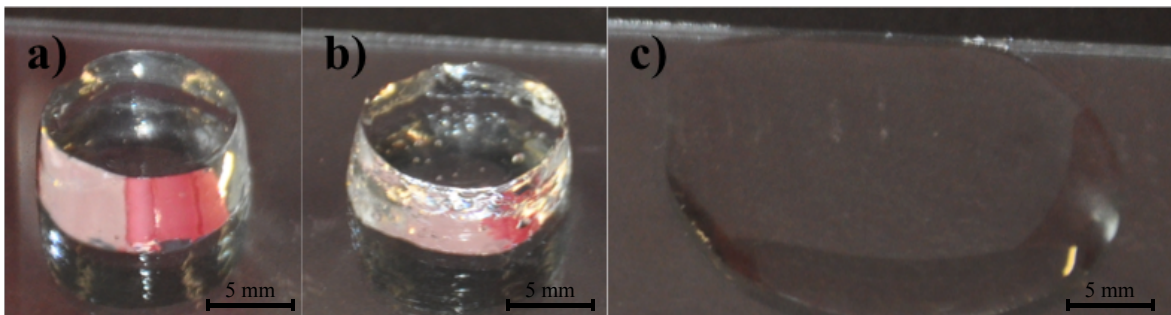


**Figure 37:** Images of HS-HA/MBAA mixtures ( $V = 500 \mu\text{l}$ ;  $\beta(\text{HA}) = 15$  mg/ml;  $\text{TG} = 0.57$ , dissolved in TRIS/BSS ( $c(\text{TRIS}) = 0.4$  mol/l;  $\text{pH} = 8.5$ )) after 24 hours incubation at 37° C with sizes of  $M_n = 100$  kDa (a),  $M_n = 60$  kDa (b) and  $M_n = 10$  kDa (c). 100 kDa and 60 kDa mixtures formed hydrogels while 10 kDa remained a liquid mixture.

## 2. Results & Discussion

Also, by mixing HS-FA-HA with MBAA hydrogels with fluorescent properties were obtained (Figure 38). These gels had an inherent yellow-orange color (Figure 38a) and showed a visible fluorescence (Figure 38b). It illustrated, that the concept of labeling the hyaluronan with FA to yield hydrogels with fluorescent properties was successful and didn't interfere with gelation. Fluorescent hydrogels were useful for the examination of their covalent immobilization to the surfaces of model implants (Section 2.3.2) and the investigation of their ability to regulate external pressures (Section 2.5.1).

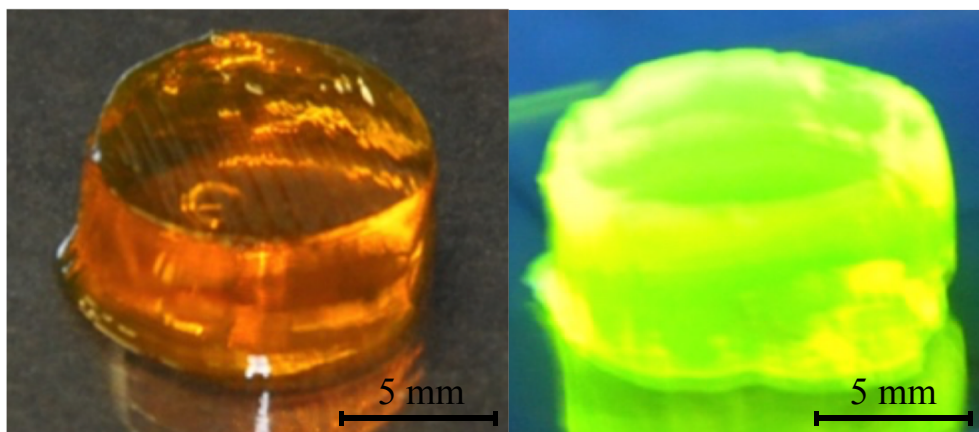


**Figure 38:** (a) Hydrogel ( $V = 500$  ml;  $M_n(\text{HA}) = 60$  kDa;  $\beta(\text{HA}) = 15$  mg/ml;  $\text{TG} = 0.18$ ; hydrogels formed in TRIS/BSS ( $c(\text{TRIS}) = 0.4$  mol/l;  $\text{pH} = 8.5$ )) using MBAA and fluorescently labeled hyaluronan. (b) The same hydrogel under UV illumination, showing its fluorescent properties.

## 2. Results & Discussion

### 2.3.2. Immobilizing hyaluronan hydrogels to epoxide modified surfaces

For achieving long-term performance of the intraocular implants it was necessary to immobilize the hydrogels to their surfaces, preventing their removal if exposed to an external force such as the elevated intraocular pressure. To that end, a concept of covalently linking HS-HA to surface-bound epoxides was proposed (Section 1.6). The general applicability of this concept was already verified for non-crosslinked hyaluronan (Section 2.2). Also generating hyaluronan hydrogels without immobilization was established by mixing HS-HA with suitable crosslinkers carrying multiple acrylamide groups (Section 2.3.1). As a next step, both methods were combined for simultaneously forming and immobilizing HA hydrogels to solid surfaces. This combination was tested first on a macroscopic scale by creating immobilized hydrogels on silanized flat glass and titanium slides. For this, the same 3D-printed molds introduced in Section 2.3.1 were used. They were filled with a HS-HA/MBAA mixture, the top of the wells were sealed with a silanized or non-silanized substrate and finally turned upside down (Figure 39). That way HS-HA/MBAA solutions were in contact with silanized titanium or glass surfaces to enable simultaneous crosslinking and immobilization. HS-HA/MBAA mixtures contact with silanized slides formed gels adhering to their surfaces and even exposing them to small external forces did not remove the gels (Figure 39b-c). For non-silanized surfaces, hydrogels either remained within the wells where they were formed after removing the slides or were displaced easily by the exposure to small external forces. This demonstrated that the proposed concept for the one-step gel formation and immobilization to the silanized surfaces (See Section 1.6) was successful.

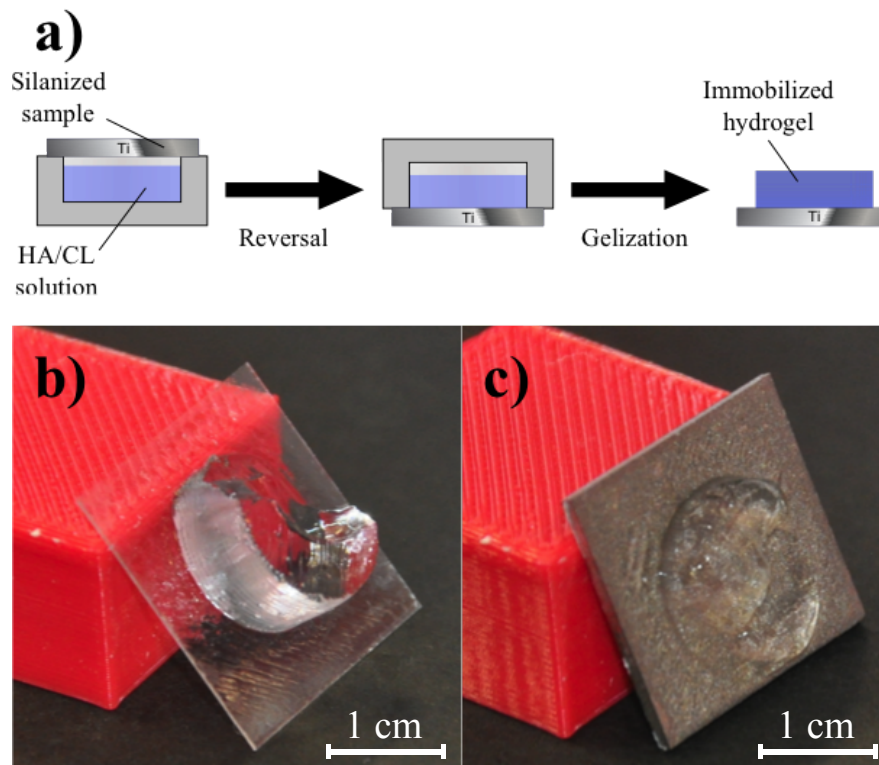


**Figure 39:** (a): Setup used for the one-step formation and immobilization of hyaluronan hydrogels ( $M_n(\text{HA})= 100$  kDa;  $\beta(\text{HA})= 15$  mg/ml;  $\text{TG} = 0.57$ ; hydrogels formed in TRIS/BSS ( $c(\text{TRIS}) = 0.4$  mol/l;  $\text{pH} = 8.5$ )) to flat titanium and glass surfaces. Hydrogels immobilized on flat glass (b) and titanium (c) surfaces using this method resisted a removal by the application of small gravitational forces.

## 2. Results & Discussion

In the next step, transferring this concept to small glass tubes was demonstrated. The setup that was already utilized for non-crosslinked hyaluronan was used (Section 2.2.3, Figure 32) for selectively immobilizing HA gels instead. For better visualizing these hydrogels HS-FA-HA was deployed to allow fluorescence microscopy (Figure 38). Similar to the immobilization of hyaluronan without crosslinking (Section 2.2), glass tubes were employed first instead of titanium for better visualizing them using bright-field and fluorescence microscopy (Figure 40).

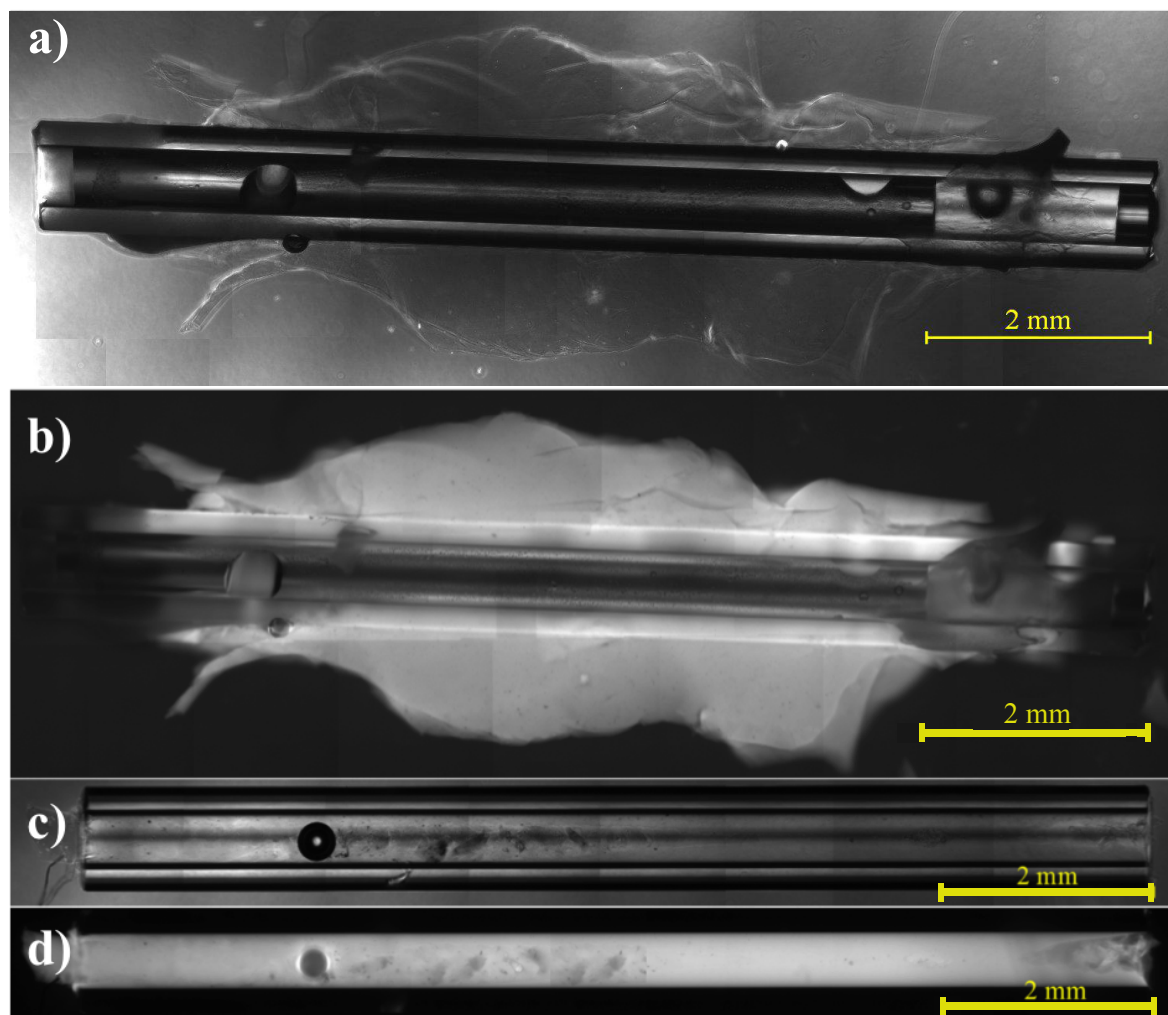


**Figure 40:** Brightfield and fluorescence images of silanized tubes modified with FA labeled HA hydrogels ( $M_n(\text{HA})= 60$  kDa;  $\beta(\text{HA})= 15$  mg/ml;  $\text{TG} = 0.18$ ; hydrogels formed in TRIS/BSS ( $c(\text{TRIS}) = 0.4$  mol/l;  $\text{pH} = 8.5$ )) on their outer surface ((a): Brightfield (b): Fluorescence) and interiors ((c): Brightfield (d): Fluorescence).

The pictures of the sample modified on the outer surface (Figure 40a-b) showed a layer of fluorescent hydrogel, which remained there even after exposure to small external forces (See Section 2.4.2). The same experiment with non-silanized tubes resulted in either no hydrogels adhering to their surface after removal from the incubationary solution or a quick detachment when applying external forces. The thickness of the layer on the outer surface varied because tubes were manually removed from a much larger hydrogel (see Section 4.2.4) causing an uneven breaking of the parts remaining on the surfaces.

## 2. Results & Discussion

The results further showed (Figure 40c-d), that filling the interiors of small tubes with hydrogels was possible. Covalent immobilization working as intended, since noticeable external forces were required for their removal (for further elaboration see Section 2.5.1). Hydrogels synthesized within non-silanized glass tubes instead were easily removed, which further illustrated the necessity and applicability of the covalent immobilization strategy proposed in Section 1.6.

Since the intraocular stents would be made from titanium the same experiment was repeated with small titanium tubes as models (ID: 0.3 mm; OD: 0.5 mm; L: 10 mm; Figure 44a). HS-FA-HA/MBAA hydrogels were grafted to the outer and inner surfaces with the same protocol already employed for glass samples. The successful one-step gelation/immobilization on the outside was confirmed using bright-field and fluorescence microscopy (Figure 41b-c).

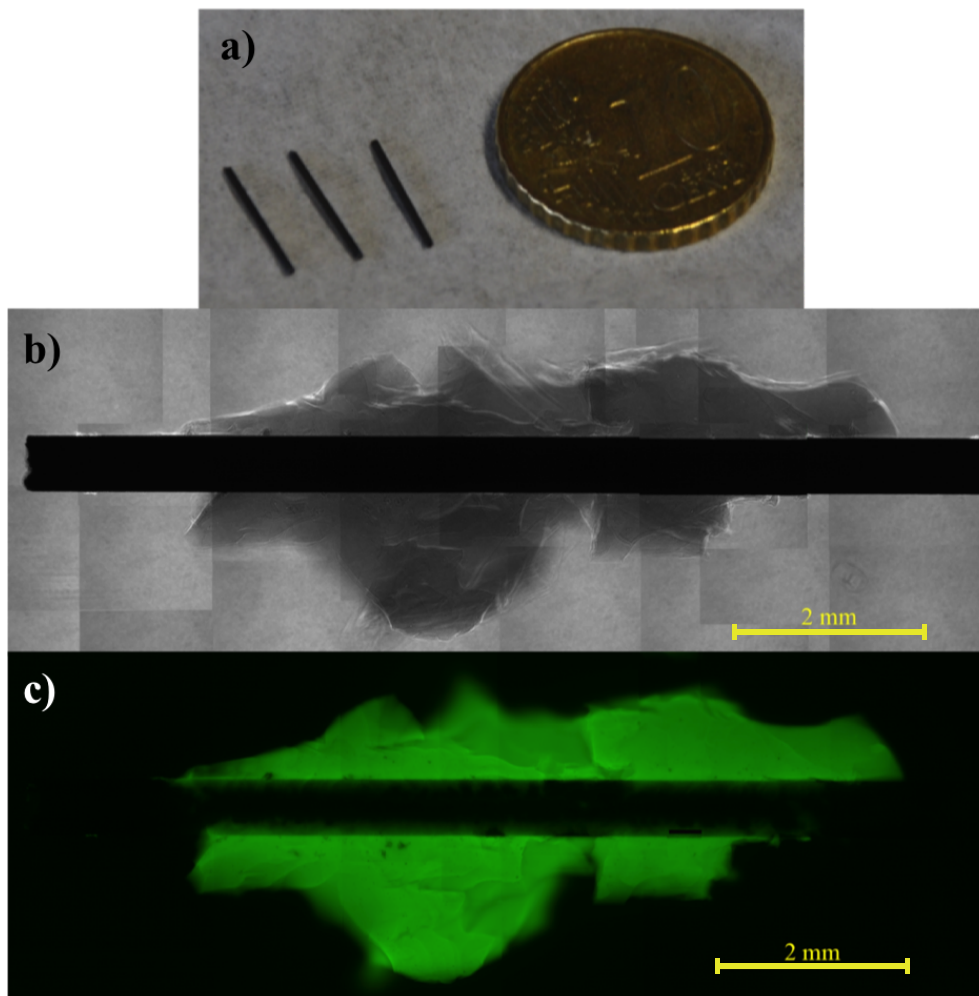


**Figure 41:** (a): Picture of titanium tubes used for the gel immobilization ( $M_n(\text{HA}) = 60$  kDa;  $\beta(\text{HA}) = 15$  mg/ml; TG = 0.18; hydrogels formed in TRIS/BSS (c(TRIS) = 0.4 mol/l; pH = 8.5)) experiments. (b-c): Brightfield (b) and fluorescence (c) images of a titanium tube (L = 10 mm; ID = 0.3 mm) with a fluorescent hydrogel immobilized on its outer surface.

The hydrogels shown in Figure 41 resisted detachment from the surfaces by small forces, as opposed to non-silanized tubes. Those results were in accordance with the experiments conducted on flat titanium surfaces (Figure 39) and the small glass tubes (Figure 41). Monitoring hydrogel immobilization titanium tubes' interiors by microscopy was not possible at that point due to their non-transparency.

## 2. Results & Discussion

---

However, an indirect method devised to measure the resistance of the hydrogels to external pressures (Section 2.4.2) was used for verifying the existence of stable hydrogels there as well (Figure 51). The results shown in this section were a final proof that the concept devised in Section 1.6 was, at least on the outer surfaces, applicable for generating intraocular titanium stents modified with hyaluronan hydrogels.

### 2.3.3. Summary and conclusion

In this section the synthesis of hyaluronan hydrogels (Section 2.3.1) and their subsequent immobilization to flat glass and titanium surfaces (Section 2.2.2) as well as small tubes (Section 2.3.2) was established. MBAA and PEGDAA were selected as model crosslinkers since they promised to form hydrogels with long-term stability opposed to acrylates. MBAA was used further since the relatively longer gelation time of HS-HA/MBAA opposed to HS-HA/PEGDAA mixtures allowed for easier handling when modifying glass tubes. Furthermore, three sizes ( $M_n = 10$  kDa; 60 kDa; 100 kDa) of HS-HA were investigated for the formation of hydrogel. Only 60 kDa and 100 kDa HS-HA formed hydrogels (Figure 37) and were used for further experiments. In addition fluorescent hydrogels were prepared by using mixtures of HS-FA-HA and MBAA (Figure 38). They were subsequently used for better visualizing covalent hydrogel immobilization on a small scale (Section 2.3.2, Section 2.5.1).

One-step hydrogel formation and immobilization was successfully demonstrated on flat glass and titanium surfaces (Figure 39), as well as on outer and inner surfaces of small tubes (Figure 40, Figure 41). No statement at this point was made for the strength of the immobilization. Specifically, whether hydrogels would resist external forces, such as intraocular pressures, without removing themselves from the implants. This was further examined in Section 2.4.2. However, the results shown in this chapter were a proof of principle that the concept proposed originally (Section 1.6) for the one-step grafting of hydrogels from HS-HA to epoxide-modified surfaces can potentially be employed for manufacturing hydrogel-enhanced glaucoma implants.

### 2.4. Development of analytical tools for determining the pressure resistance of hyaluronan hydrogel-modified tubes

#### 2.4.1. Constrained swelling of hydrogels in small tubes

As already outlined hydrogels have the ability to take in water in a large excess to their own weight, which causes a swelling of the polymer network.<sup>108</sup> The general mechanics of this swelling are already well established<sup>108</sup> and data has already been published on the swelling behavior of hyaluronan hydrogels for different crosslinkers and crosslinking densities.<sup>101,176</sup> The aim of the experiments presented in this section was to compare the swelling of hydrogels that were immobilized on the interior of small tubes (“constrained gels”) with non-immobilized (“unobstructed”) gels. This was necessary since a further evaluation of implants (pressure regulation etc.) or their application into a glaucomatous eye should be performed only when the gels’ properties would be stable.

Since hydrogel swelling causes an expansion of volume<sup>108</sup>, it was expected that them forming within tubes would lead to a reduction of swelling capabilities compared to unobstructed samples. Furthermore, swelling of hydrogels was dependent on the composition of the surrounding medium due to an influence of osmotic forces on the process.<sup>109</sup> In order to mimic the physical environment within the human eye the experiments were performed in BSS which is commonly used in eye surgery.<sup>203</sup> For generating distinguishable mass changes during swelling, larger glass tubes (L = 10 mm; ID = 5 mm; OD = 1 mm) were used generating constrained hydrogels. For minimizing the variance of samples they were prepared using the same HS-HA/MBAA mixture ( $M_n(\text{HA}) = 100$  kDa;  $\beta(\text{HA}) = 15$  mg/ml; TG = 0.57). Each hydrogel was incubated separately in BSS with frequent buffer replacements and weights were measured on regular intervals with. For comparing swelling rates among gels with slightly varying starting masses, their relative gains were calculated from these starting values. The more common way of relating the swelling to masses of non-hydrated (= “dry”) hydrogels<sup>101</sup> was not pursued because the ions from BSS would form crusts during lyophilization and create additional weight. The option of extensively washing hydrogels in ddH<sub>2</sub>O to remove ions from the hydrophilic networks<sup>101</sup> was also not taken, since no data on the amount of washing for the HS-HA/MBAA systems were available necessitating additional optimizations. Also, preliminary experiments of incubating hydrogels in ddH<sub>2</sub>O showed a tendency of them to break into fragments causing further random errors by losses of mass. Instead relative mass gains were based on the starting weights of hydrogels before swelling to compare constrained with unobstructed samples. Also, since the HS-HA/MBAA hydrogels only acted as model systems, in-depth swelling experiments were not necessary until a crosslinker for manipulating cell adhesion would be selected. Only a theoretical relation on dry masses was established from calculations using the starting materials were used for comparing the data with literature (See Section 4.4.2 for further elaboration). However, as explained, they were only partially backed by experimental data since no real dry masses were reliably obtained.

## 2. Results & Discussion

The results of these comparative measurements between constrained and unobstructed hydrogels are summarized in Figure 42.

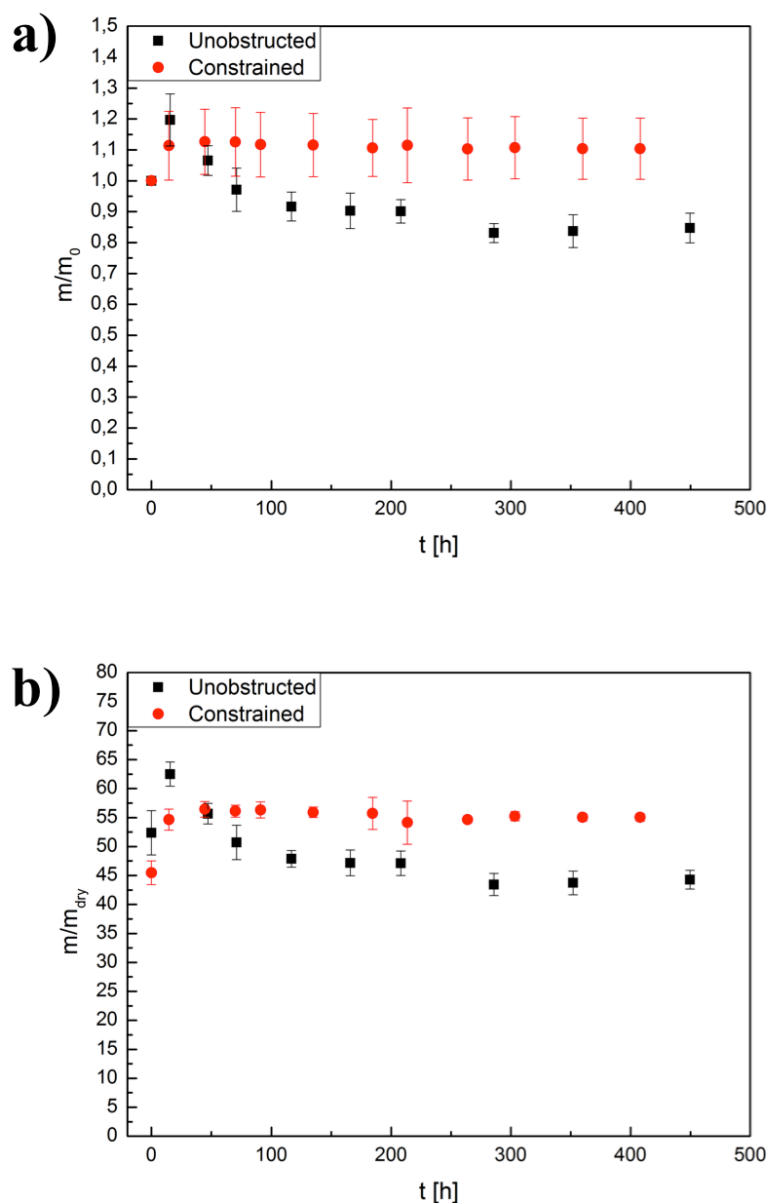


**Figure 42:** Average relative mass gains ( $m/m_0$ ) for constrained and unobstructed hydrogels ( $M_n(\text{HA}) = 100$  kDa;  $\beta(\text{HA}) = 15$  mg/ml;  $\text{TG} = 0.57$  (n/n)). Hydrogels were formed in TRIS/BSS ( $c(\text{TRIS}) = 0.4$  mol/l;  $\text{pH} = 8.5$ ) with constrained samples immobilized on the inner surfaces of glass tubes ( $L = 10$  mm;  $\text{ID} = 5$  mm;  $\text{OD} = 1$  mm). Averages taken from three individual samples with the standard deviations as error bars. **(a):** Mass gains relative to the pre-swollen starting masses after the hydrogels were formed. **(b):** Mass gains relative to the theoretical dry masses calculated from the amounts of starting materials.

The results showed a number of differences between both types of hydrogels. Unobstructed samples had a more rapid initial mass gain than constrained ones before declining into a steady state lower than their own starting masses. This was explained by the presence of TRIS within the hydrophilic networks, which initially caused an increased osmotic force from the surrounding medium. Due to pore-size dependent diffusion through the hydrogel<sup>90</sup>, TRIS left the system over time decreasing the overall molecule concentration within the network.

## 2. Results & Discussion

This resulted in reducing osmotic forces on the hydrogel, which shrunk to a new steady state with a new balance of osmotic and retaining forces.<sup>109</sup> This was verified by a comparative swelling experiment where hydrogels with the same parameters were formed and incubated either in BSS (pH = 7.4) or TRIS/BSS ( $c(\text{TRIS}) = 0.4 \text{ mol/l}$ ; pH = 7.4) (Figure 43). After 811 hours the gels incubated in TRIS/BSS were also placed BSS and further changes recorded. As a result their masses were reduced to the same amounts than the gels swollen in BSS from the beginning. Since the removal of TRIS was the only change made to the system, these results validated the originally proposed mechanism.

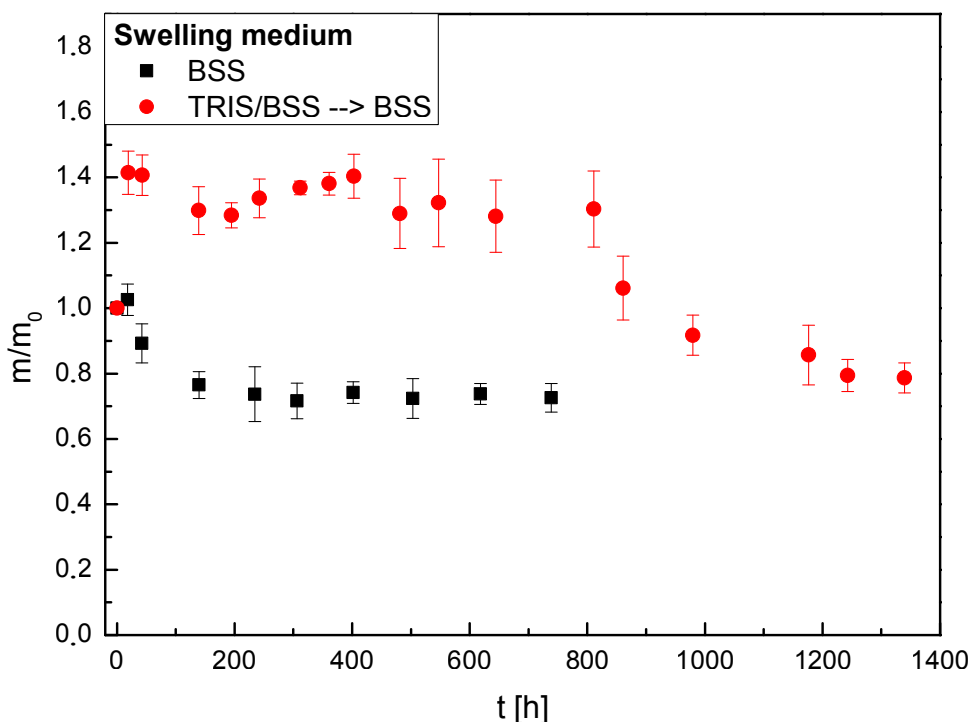


**Figure 43:** Comparison between the swelling rates of hydrogels ( $M_n(\text{HA}) = 100 \text{ kDa}$ ;  $\beta(\text{HA}) = 15 \text{ mg/ml}$ ;  $\text{TG} = 0.57$ ) relative to their starting masses either in BSS or TRIS/BSS ( $c(\text{TRIS}) = 0.4 \text{ mol/l}$ ). For the TRIS/BSS fraction the buffer was replaced by BSS at  $t = 811$  hours causing a reduction of the relative mass similar to the BSS fraction. Four samples were incubated in each medium and the average calculated from all samples with the standard deviation as the error bars.

The differences between swelling of unobstructed and constrained hydrogels (Figure 42) were related to covalent immobilization into glass tubes. The physical barriers of their walls blocked possible expansions while volume reduction was inhibited by the covalent bonds between hydrogels and glass surfaces. As a result the pore size of these samples, which is related to the amount of water in the network<sup>90</sup>, was smaller during the first 45-50 hours where the unobstructed gels showed a higher mass gain. This reduced size of the pores in turn led to more limited diffusion<sup>90</sup> of TRIS molecules within the constrained gels and slowed down their removal from the system. The physical barriers of the tubes' walls further limited molecule exchange with the only hydrogel/medium interfaces located at the ends of the tubes. These effects combined were considered to be responsible for the higher swelling level of the hydrogels immobilized within the tubes compared to the unbound sample. Especially the covalent immobilization serves also for a possible explanation for the formation of channels in samples where a pressure-induced liquid flow was observed (further discussed in Section 2.5.1).

## 2. Results & Discussion

From the results of these comparative swelling experiments it was decided to incubate hydrogel-modified tubes at least 48 hours before conducting any further measurements since no significant changes in mass were observed from the data after this time. Long-term swelling, might reveal further changes in the constrained hydrogels' masses. But for further evaluations of these samples' properties (pressure resistance etc., see the following sections) the selected incubation time was sufficient to ensure an optimal reproducibility.

As already mentioned, the relative swelling rates depending on the dry masses (Figure 42) were not completely accurate due to being calculated from an estimated value, they were still comparable to previously published results. The final mass gain in steady state of the unobstructed gels was higher than the results gained from the groups of Shu et al.<sup>101</sup> and Hagel et al.<sup>176</sup>, which was attributed to different parameters used (Table 1).

**Table 1:** Comparison between synthesis parameters and measured swelling ratios of HA hydrogels used in this thesis and in literature. \*CL/SH denotes the ratio of acrylic groups of crosslinkers and thiols of HA. \*\*Two different swelling ratios were given for two desmosine-inspired crosslinkers one charged (first number) one uncharged (second number). \*\*\*Average swelling value calculated from the last four datapoints taken from swelling experiments with unobstructed hydrogels (Figure 42). Error = standard deviation.

	<b>M<sub>n</sub>(HA) [kDa]</b>	<b>β(HA) [mg/ml]</b>	<b>TG (n/n)</b>	<b>Crosslinker</b>	<b>CL/SH*</b>	<b>Swelling Ratio</b>
Shu et al. <sup>101</sup>	120	10	0.42	PEGDAA	1	39.41
Hagel et al. <sup>176</sup>	450	28	0.49	Desmosine inspired	1	27/30**
Thesis	100	15	0.57	MBAA	1	43.7 +/- 0.4***

As previously mentioned, the accuracy of the determined swelling ratio was not verified since the dry mass was only calculated theoretically. However, it was still comparable to the results published by Shu et al. and Hagel et al. and only support the findings from these groups. When a crosslinker for the generation of hydrogels capable of reliably manipulating cell adhesion is chosen, more in-depth characterization of the swelling will be necessary. As mentioned before, the desmosine-inspired linkers from Hagel et al. are potential candidates for these. Therefore the data already published by this group will be useful for future optimizations of the implants.

### 2.4.2. Continuous pressure application

In the previous sections it was demonstrated that the basic concept for fabricating hydrogel-modified intraocular implants proposed in Section 1.6 was applicable to fabricate small glass and titanium tubes (Section 2.3). For applying them in glaucoma treatment they need to have properties for regulating intraocular pressures<sup>3</sup>. Their covalent immobilization had to be strong enough for resisting the pressures occurring in the glaucomatous eye without them fracturing and leaving the implants. Furthermore they had to allow liquid flow through the tubes for draining excess intraocular fluid. Additionally they had to perform as a valve and prevent pressure in the eye from dropping too low due to extensive drainage. Therefore it was necessary to determine, whether these properties were present in the model systems established in this thesis and how to possibly optimize parameters for an effective pressure regulation. To that end, two analytical methods were developed to apply liquid pressure on hydrogel-filled tubes, referred to as the “Continuous Pressure Application” (CPA), and “Hydrostatic Pressure Application” (HPA, see Section 2.4.3) methods. Both were used to evaluate different aspects of the aforementioned pressure related properties.

The CPA was designed to apply and continuously increase an external force on a liquid column in a closed system. This subsequently influenced pressures of that column on the HA-modified test tubes. Reactions of these samples to those pressures were monitored indirectly by a force sensor of a BOSE Electroforce device (Figure 44).<sup>204</sup> For analyzing reactions of hydrogel-filled tubes to liquid pressures, they were connected to the syringe and the displacement head was moved down at a constant rate, exerting a constantly increasing force on the plunger (Figure 44b). This resulted in a force being exerted on the liquid within the syringe translating into linearly increasing pressures on connected samples. Their reactions would translate into deviations from this linear increase and was monitored in real time by analyzing the forces measured by the force sensor located at the bottom of the setup.

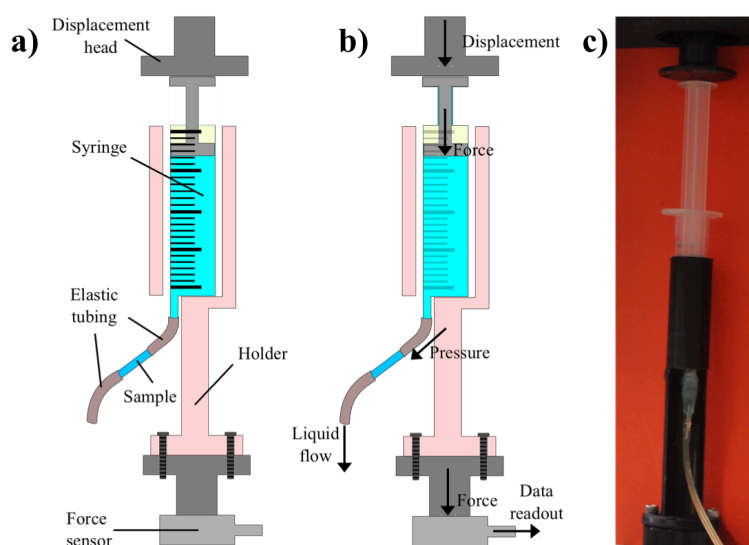


**Figure 44:** (a): Schematic illustration of the experimental setup used for CPA measurements consisting of a plastic syringe inside a sample holder connected to elastic tubing. A displacement head above the setup was able to move at predetermined velocities. (b): Basic principle of the CPA measurement. By moving the displacement head a constant force is exerted on the plunger. This subsequently increases the liquid pressure on the sample until a reaction (e.g. gel expelled, liquid flow) occurs. Forces were recorded by the sensor at the bottom of the device (c): Picture of a real-life CPA setup.

## 2. Results & Discussion

---

Pressures were determined from the force values recorded by the sensor and knowledge of the plunger's surface area according to the following equation:

$$P = \frac{F}{A} \quad \text{Equation 2:2}$$

with “P” being the pressure, “F” being the measured force and “A” being the surface area of the plunger pressing on the liquid in the syringe. For data analysis pressures were plotted against the displacement of the plunger. Total values for displacement were transformed into “relative displacement”, an artificial value used to standardize curves that were recorded from experiments of varying lengths. It was calculated according to

$$\text{Relative displacement} = \frac{\text{Current displacement}}{\text{Maximum displacement}} \quad \text{Equation 2:3}$$

with “Current displacement” being the currently recorded displacement and “Maximum displacement” the maximum value the plunger was displaced during a complete measurement. Relative displacement was calculated since for these measurements only the pressure values in general, e.g. maximum pressures, plateau pressure, were important for an analysis of the pressure behavior. The actual displacement values were of little interest at that point and normalizing them to relative values simplified comparisons between measurements of differing lengths.

Depending on the type of sample, different kinds of curves were attained:

### 1. System characterisation with empty tubes

To begin with, it was necessary to characterize the basic properties of the setup such as the forms of the curves obtained from measurements and their dependency on different parameters of the system. For this, empty tubes were subjected to CPA measurements and the resulting pressure-displacement curves analyzed.

In a first step, the basic shape of curves gained from the experiments was analyzed (Figure 45). It showed three distinct sections. In the first section (relative displacement = 0.0-0.07), the displacement head had no contact to the plunger yet, no force was exerted on the system and the recorded pressure did not change. After both parts made contact with each other, the pressure increased relatively fast (relative displacement = 0.07-0.19) and a water flow was initiated. At a relative displacement of 0.19 a plateau was achieved where the water flow through the tube was in balance with the forces exerted on the system through movement of the displacement head.

## 2. Results & Discussion

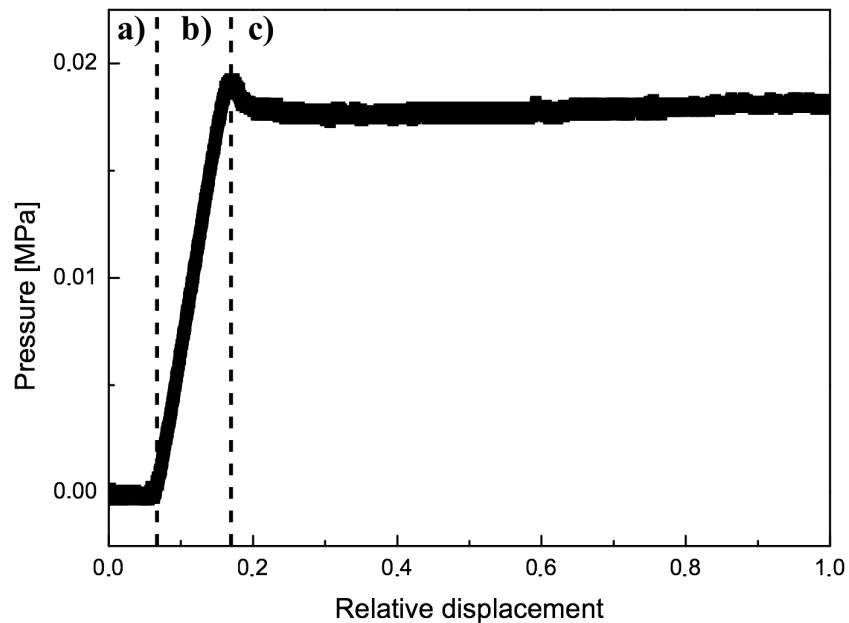


**Figure 45:** Exemplary CPA pressure/displacement curve of a non-modified tube ( $L = 10$  mm;  $ID = 0.5$  mm), showing the three distinct sections of a curve. **(a)** The displacement head was not in contact with the plunger and no force was exerted on the system. **(b)** The displacement head came in contact with the plunger, exerting a force on the liquid within the syringe. **(c):** Plateau/equilibrium area where the water flow was in balance with the force applied from the plunger.

For determining possible size dependencies these measurements were performed on empty tubes with different lengths. However no significant differences were observed for the values of the plateau pressures (Figure 46). The figure showed, that the variation of the equilibrium pressures of empty glass tubes with different lengths was only minimal. This illustrated minimal influence of the empty glass tubes on the pressure development and future differences of hydrogel-filled samples were attributed to the presence of the gels.

## 2. Results & Discussion

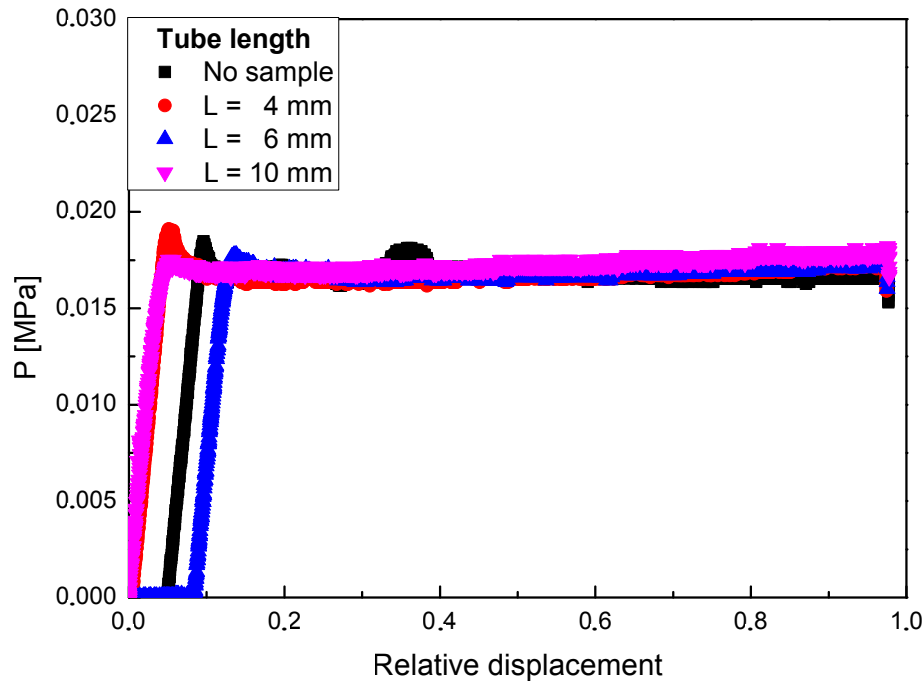


**Figure 46:** Comparison of pressure-displacement curves of non-modified tubes (ID = 0.5 mm; L = 4-10 mm) at a displacement velocity of 0.01 mm/s. The values of the plateaus pressure almost the same for all lengths with only minimal differences.

In a next step, the basic relation between displacement velocity and pressure values was determined (Figure 47). The graph showed, that an increase of the velocity of the displacement head directly lead to an increase of the plateau pressure. These results illustrated the importance for using the same displacement velocity between experiments in order to attain comparable results.

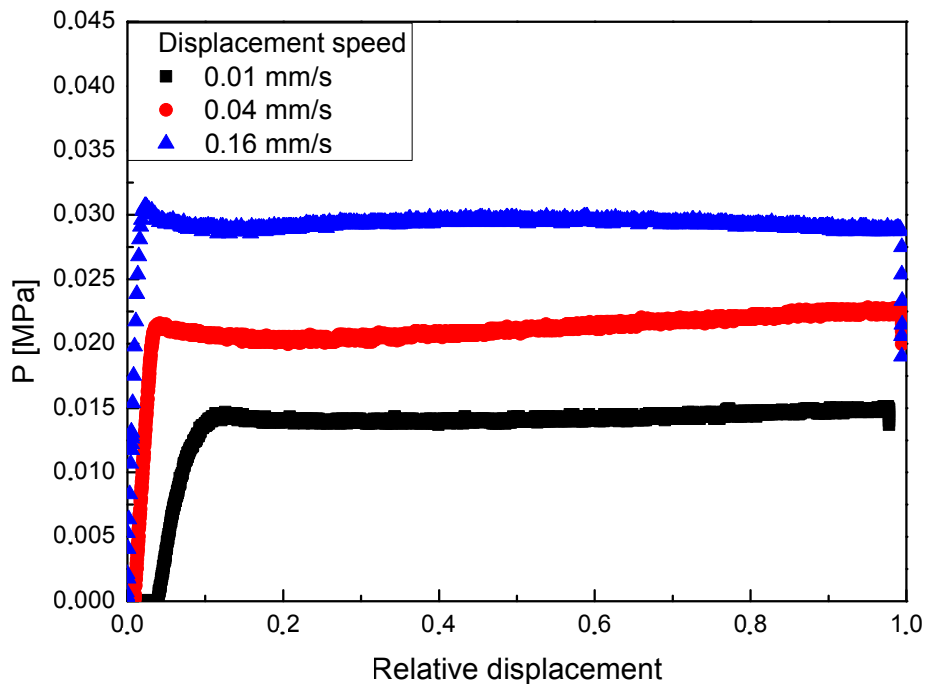


**Figure 47:** Pressure displacement curves of CPA measurements on a empty glass tube (L = 10 mm; ID = 0.5 mm) with different velocities of the displacement head. An increase of the velocity led to higher values of EP.

## 2. Results & Discussion

### 2. Non-silanized tubes filled with hydrogels

In a next step non-silanized, hydrogel-filled tubes were analyzed with CPA measurements to further verify the effectiveness of the incepted covalent immobilization concept (Section 1.6). During sample preparation, hydrogels were usually easily removed already from the containing glass tubes when the tubing connecting the samples was removed (See 4.3.2). These low forces for the removal of the HA hydrogels were further quantified by subjecting non-silanized gel-filled tubes, that were successfully retrieved with hydrogels still inside, to CPA measurements (Figure 48). It was observed that after the start of the measurements the hydrogels were pushed out and the resulting curves. By analyzing the resulting pressure-displacement curves it was shown, that the plateau areas were similar to the results gained from empty tubes (Figure 46). This illustrated, that an immobilization of the hydrogels was necessary to ensure the function and the longevity of potential glaucoma implants.

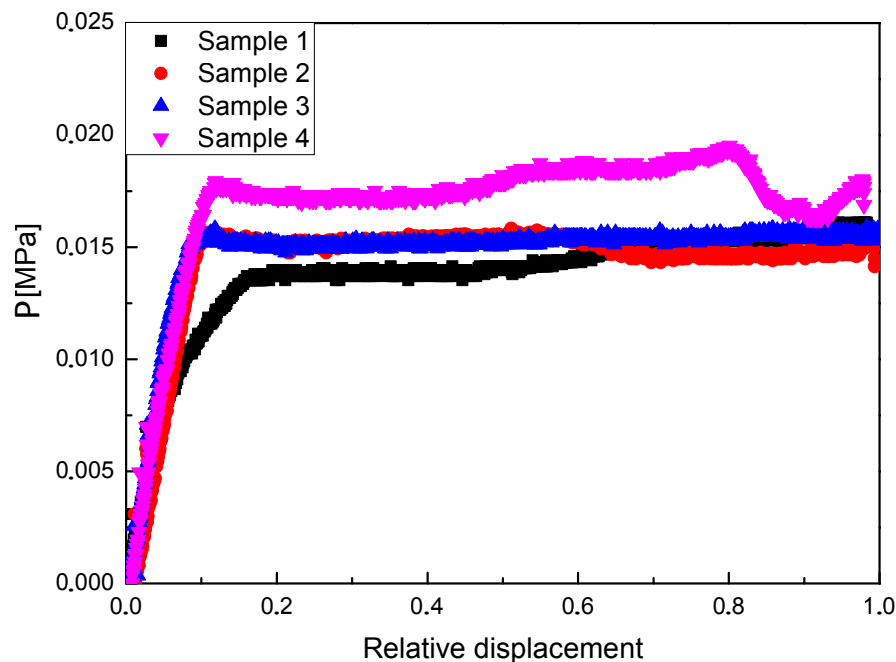


**Figure 48:** CPA measurements (Displacement velocity = 0.01 mm/s) on hydrogel-filled non-silanized tubes (ID = 0.5 mm; L = 10 mm;  $M_n(\text{HA}) = 100$  kDa;  $\beta(\text{HA}) = 15$  mg/ml; TG = 0.57). No big differences to the curves of empty tubes (Figure 46) were observed.

## 2. Results & Discussion

### 3. Silanized and Hydrogel-filled tubes without liquid flow

When performing CPA measurements on hydrogel-filled tubes, two different reactions of the sample to the external pressure were observed. Either a liquid flow was established which lead to a decreased pressure (discussed later) or the hydrogels within the tubes completely resisted any pressure-induced liquid flow. Instead the pressure increased linearly with the movement of the displacement head until the gels were forcefully ejected from the tubes resulting in a sharp drop of the measured force values (Figure 49).

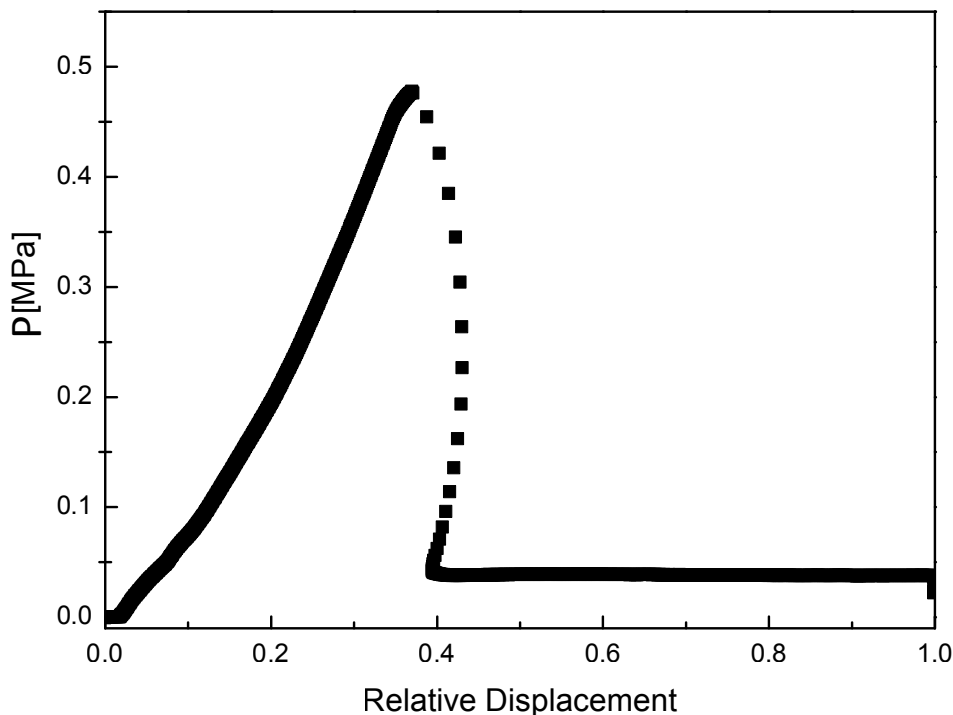


**Figure 49:** Pressure-displacement curve of a silanized and hydrogel-filled tube ( $M_n(\text{HA})= 60$  kDa;  $\beta(\text{HA})= 15$  mg/ml;  $\text{TG} = 0.18$ ; hydrogels formed in TRIS/BSS ( $c(\text{TRIS}) = 0.4$  mol/l)) that blocked a liquid flow through it's interior. At a relative displacement of 0.38-0.4 the gel was forcefully ejected from the tube and the pressure dropped to similar levels than an unmodified sample (Figure 46).

The graph showed, that the pressure increased to relatively high levels, compared to non-modified tubes (Figure 46) or samples that allowed the passage of fluid (Figure 52). At the peak pressure, the hydrogels were forcefully ejected from the tubes (= “breaking point”) and the pressure dropped down to levels similar to empty tubes (Figure 45). At this time of the project, the majority of samples showed this behavior when exposed to an external pressure. While undesirable in respect to the model implant’s ability to regulate external pressures, it was utilized for analyzing the stability of the immobilization by quantifying breaking points. To that end a number of samples was prepared with different hydrogel parameters ( $\beta(\text{HA})$ ;  $M_n(\text{HA})$ ;  $\text{TG}$ ) as summarized in Table 2 and breaking points determined with CPA (Figure 50).

## 2. Results & Discussion

**Table 2:** Overview over the gel-filled tubes with different parameters used for breaking point experiments. All hydrogels were formed in TRIS/BSS ( $c(\text{TRIS}) = 0.4 \text{ mol/L}$ )

Series	TG	$\beta$ [mg/ml]	$M_n$ [kDa]
1	0.57	15	100
2	0.57	10	100
3	0.57	15	60
4	0.57	10	60
5	0.19	15	60
6	0.23	15	100
7	0.39	15	60
8	0.42	15	100

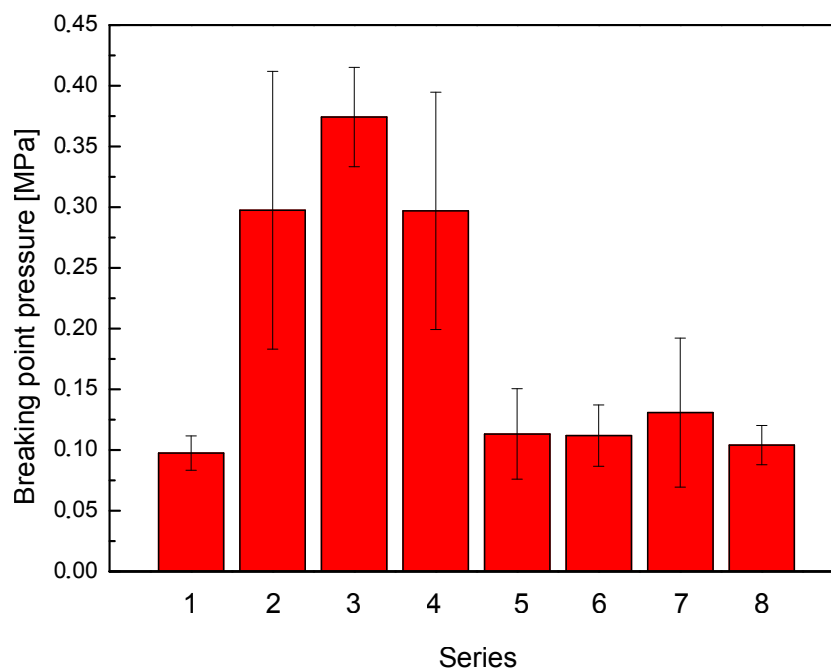


**Figure 50:** Overview over the average median values for breaking points of at least four hydrogel-filled tubes (tube:  $L = 10 \text{ mm}$ ;  $ID = 0.5 \text{ mm}$ ; hydrogels prepared in TRIS/BSS ( $c(\text{TRIS}) = 0.4 \text{ mol/l}$ ;  $\text{pH} = 8.5$ )) modified with the parameters as listed under (Table 2). Average breaking point values were constantly above  $100000 \text{ Pa}$  for all series. Error bars were the standard deviations between samples.

The variation within one series of samples sometimes was relatively high, with some hydrogels breaking out of the tubes much earlier than others. The exact reason for this as of yet was unexplained. However, since all glass tubes were silanized in the same solution, it was attributed to random errors during hydrogel formation. The data further showed a tendency of gels within tubes with a higher degree of crosslinking to also possess a higher breaking point, with series #1 ( $M_n(\text{HA}) = 100 \text{ kDa}$ ;  $\beta(\text{HA}) = 15 \text{ mg/ml}$ ;  $\text{TG} = 0.57$ ) being an exception. The data acquired within this thesis was not enough to make a conclusive statement on the relation between these gel parameters and the pressure values of the breaking points. However, and more importantly, they all showed breaking points of more than  $100 \text{ kPa}$ , which is sufficient to resist a removal from pressures encountered within the glaucomatous eye ( $<10 \text{ kPa}$ )<sup>3</sup>.

## 2. Results & Discussion

As mentioned in Section 2.3.2, it was not possible to verify the presence of hyaluronan hydrogels on the interiors of titanium tubes due to them being non-light-transmissive. Therefore CPA measurements were conducted on hydrogel-filled titanium tubes to confirm the presence of hydrogels by determining the breaking points (Figure 51).

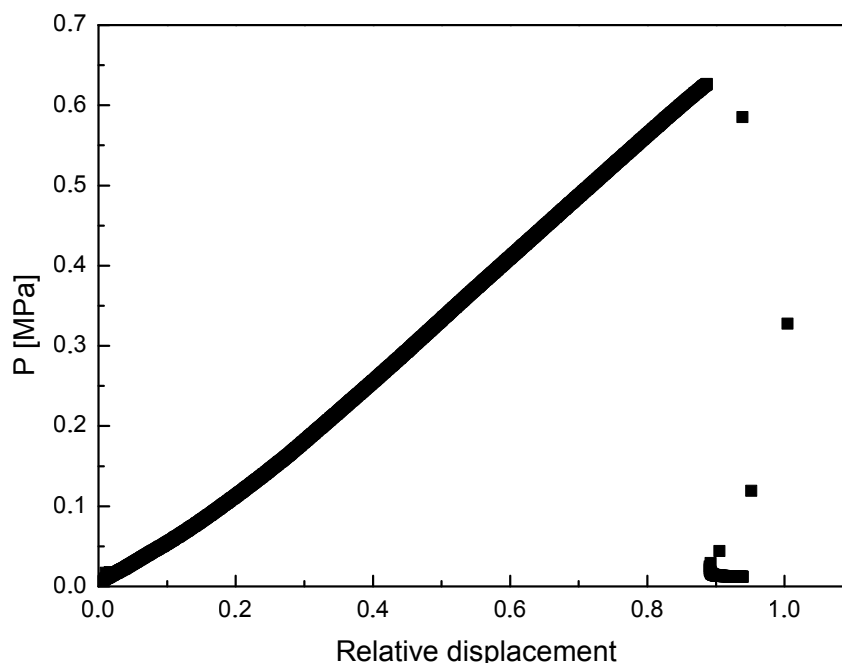


**Figure 51:** Curve of a breaking point CPA measurement of a hydrogel-modified ( $M_n(\text{HA})= 100$  kDa;  $\beta(\text{HA})= 15$  mg/ml;  $\text{TG} = 0.57$ ; hydrogels formed in TRIS/BSS ( $c(\text{TRIS}) = 0.4$  mol/l;  $\text{pH} = 8.5$ )) titanium tube ( $L = 15$  mm;  $\text{ID} = 0.3$  mm). The existence of a breaking point verified the presence of an immobilized hydrogel on the tube's interior.

These results verified, in addition to previously conducted immobilization experiments (Sections 2.2 and 2.3.2), that immobilizing hydrogels on the inside of small titanium tubes was also possible. Furthermore, the breaking point was much higher than the values gained for glass tubes (Figure 50). This verified the ability for the hydrogels in titanium tubes for withstanding pressures encountered in the glaucomatous eye. It was seen as final proof, that the concept for the covalent immobilization of hydrogels to titanium tubes established in Section 1.6 was applicable. The reason for the relatively higher breaking point compared to glass tubes (Figure 50) modified with hydrogels using similar parameters was attributed to the smaller diameter used for the titanium tube and is further discussed in Section 2.5.2.

## 2. Results & Discussion

### 4. Silanized Hydrogel modified tubes with liquid flow

In some cases the silanized hydrogel-filled tubes established a liquid flow when exposed to external pressure and the pressure-displacement curve from a CPA measurement (Figure 52).

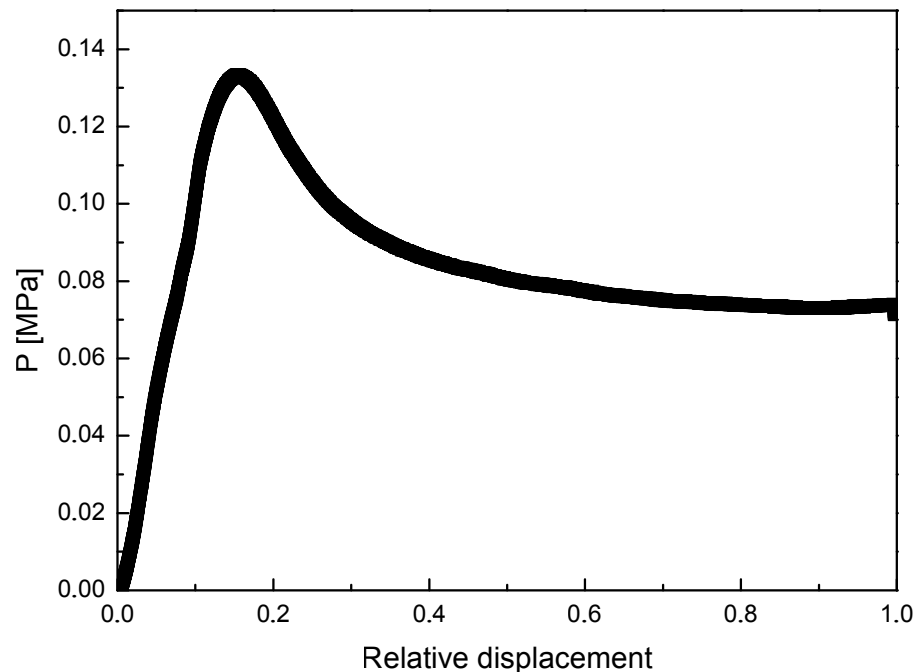


**Figure 52:** Exemplary CPA curve of a gel modified tube ( $M_n(\text{HA}) = 60$  kDa;  $\beta(\text{HA}) = 15$  mg/ml;  $\text{TG} = 0.18$ ; hydrogels formed in TRIS/BSS ( $c(\text{TRIS}) = 0.4$  mol/l,  $\text{pH} = 8.5$ )) where a passage of fluids through its interior was established. At the beginning the pressure increased linearly with the movement of the displacement head. At the peak pressure (here at 0.18 rel. displacement) a liquid flow through the tube was observed, causing it to decline into an equilibrium pressure (EP) at which the forces exerted by the constantly moving displacement head and the liquid flow were in balance.

The graph showed a linear increase of the pressure with the movement of the displacement head while no liquid flow was observed. At the peak pressure, in this example at a relative displacement of 0.18, a liquid flow was observed through the gel-filled stents. The pressure started to decline before going into an equilibrium (equilibrium pressure, EP) where the forces exerted by the movement of the plunger were in balance with the outflow rate of the liquid through the tube.

Furthermore, the EP for gel-filled samples was higher than plateaus of non-modified tubes measured using the same displacement velocity (Figure 53). The equilibrium pressure of the tube containing a hyaluronan hydrogel was noticeably higher than of the non-modified sample. This proved, that the hydrogels within influenced passage of liquids through the tube's interiors, requiring a higher pressure to maintain a steady flow compared to non-modified samples. The mechanism of the hydrogel-controlled liquid flow was further discussed in Section 2.5.1.

## 2. Results & Discussion

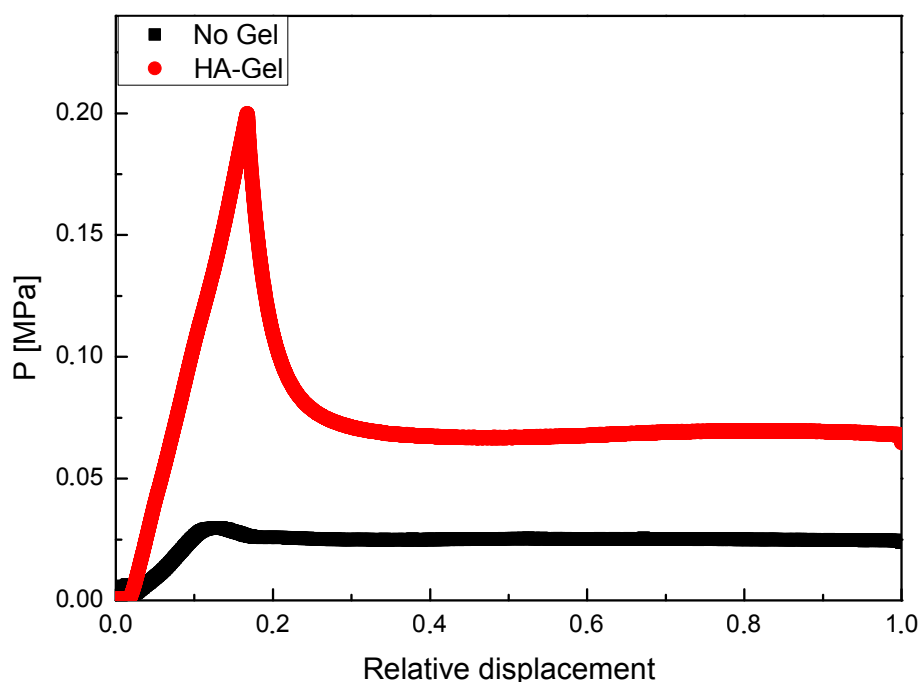


**Figure 53:** Comparison of the pressure-displacement curves between a hydrogel-filled ( $M_n(\text{HA})= 60$  kDa;  $\beta(\text{HA})= 15$  mg/ml;  $\text{TG} = 0.18$ , hydrogels formed in TRIS/BSS ( $c(\text{TRIS}) = 0.4$  mol/l,  $\text{pH} = 8.5$ )) tube with an unmodified sample ( $L = 10$  mm,  $\text{ID} = 0.5$  mm) using a displacement velocity of  $0.025$  mm/s.

In order to be viable for comparative measurements it was necessary for the method to have a good reproducibility. Furthermore, it was important, that the properties of the samples would not change when repeatedly exposed to external pressures, for example by degradation of the hydrogels. In order to evaluate these properties of the setup and the hydrogels, a series of repeated CPA measurements was conducted on the same sample to see, whether any changes in the pressure-displacement curves would occur (Figure 54a) with a repetition 24 hours later (Figure 54b). The results showed repeated runs always resulting in similar values of EP, which could be repeated 24 hours later. This demonstrated the reproducibility of the method necessary for comparative measurements between different samples. The results also indicated short-term stability of the hydrogels since changes in the curves, for example by gel deterioration, would have been observed.

## 2. Results & Discussion

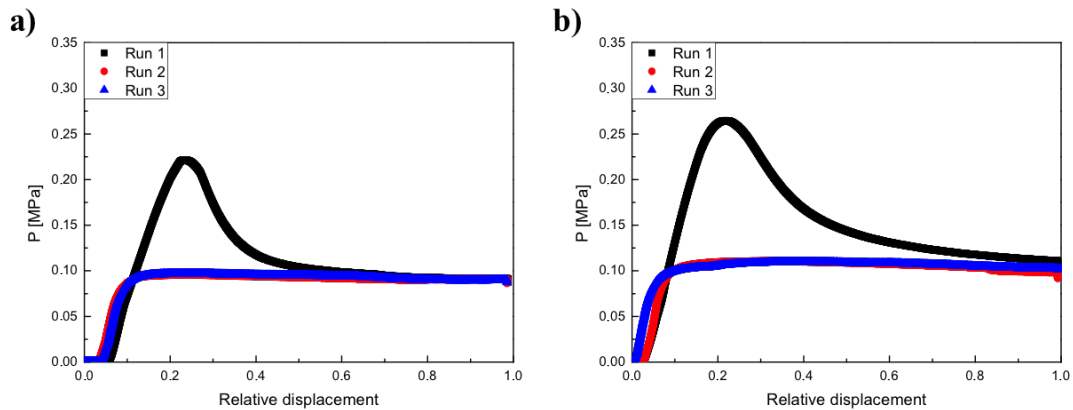


**Figure 54:** (a): Pressure-displacement curves of repeated CPA measurements on the same hydrogel-filled tube ( $L = 10$  mm;  $ID = 0.5$  mm;  $M_n(\text{HA}) = 60$  kDa;  $\beta(\text{HA}) = 15$  mg/ml;  $TG = 0.18$ ; hydrogel formed in TRIS/BSS ( $c(\text{TRIS}) = 0.4$  mol/l;  $\text{pH} = 8.5$ )). (b): Pressure-displacement curves of the same sample 24 hours later. The EP's were similar for all experiments. Noticeable was a different shape of the pressure-displacement curve of the first round of a series compared to subsequent measurements. The displacement velocity was  $0.025$  mm/s.

One noticeable difference was the shape of the curves between the first and subsequent CPA measurements of one series of experiments. Pressure on the first round increased to values around twice the EP before hitting a peak where a liquid flow through the gel-filled tube was induced. However in subsequent rounds no peak pressures were observed and the equilibrium liquid flow was established directly instead. It indicated that an “activation” of the hydrogels within the tubes was necessary the first time they were exposed to external pressures in for inducing flow. On subsequent runs this “activation” was not necessary anymore. The same behavior was observed when the experimental series was repeated 24 hours later on the same sample (Figure 54b), therefore this activation was not related to irreversible changes of samples. Rather a reversible process that “deactivated” the samples when not exposed to heightened pressures over a longer period of time was proposed and the nature of this effect was further explored in Section 2.5.1. Nonetheless, the results in Figure 54 showed that the pressure of the equilibrium flow was constant between different runs, illustrating the reproducibility of the method and its applicability for conducting comparative measurements on samples prepared with different parameters.

The EP dependence on displacement head velocity was demonstrated already for empty tubes. Similar variations EPs with an accelerated speed of the displacement head (Figure 55) was also shown with hydrogel filled tubes (Figure 47). The measurements illustrated, that not only the equilibrium pressure increased with displacement velocity. Also the time-span required to achieve equilibrium was significantly higher at faster displacement rates. For that reason it was necessary to perform CPA measurements at relatively low velocities ( $0.005$ - $0.02$  mm/s). These results also further reinforced the requirement to perform comparative measurements with the same displacement velocities.

## 2. Results & Discussion

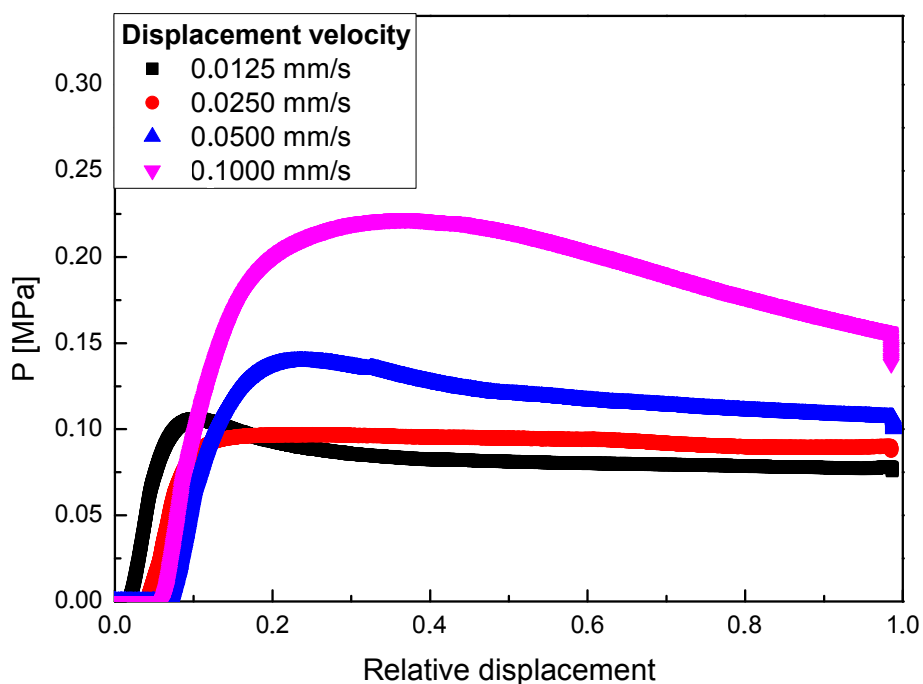


**Figure 55:** Pressure-displacement curves of CPA measurements of a gel-modified ( $M_n(\text{HA}) = 60$  kDa;  $\beta(\text{HA}) = 15$  mg/ml; TG = 0.18; hydrogels formed in TRIS/BSS ( $c(\text{TRIS}) = 0.4$  mol/l, pH = 8.5)) glass tube (L = 10 mm, ID = 0.5 mm) at different displacement velocities. They illustrate the dependency of their shape on the displacement velocity.

The main aspect of the glaucoma therapy was reducing intraocular pressures to “normal” levels less than 21 mmHg (ca. 2100 Pa).<sup>3</sup> Optimizing the parameters of implants and hydrogels was necessary for achieving these target values. Therefore it was necessary to gain insight on how a variation of these parameters would influence the liquid flow. CPA was ideal for this task, since individual measurements were done quickly to evaluate a large number of samples.

The yield of tubes allowing passage of fluids was low and the main focus at that point was optimizing sample preparation (see Section 2.5). Therefore some preliminary measurements were performed for evaluating the sensitivity of the method. To that end samples with varying parameters were prepared and analyzed with CPA. Due to a constantly low number of samples allowing liquid flow at that point, the amount of data was not exhaustive and more extensive series of measurements will have to be performed in the future. Still, although not conclusive, general parameter-dependent differences were observed. First, the lengths of glass tubes were varied (Figure 56) resulting in higher EP's when length was increased. This was related to a higher amount of hydrogel within tubes, since unmodified samples did not show a similar relation.

## 2. Results & Discussion

---

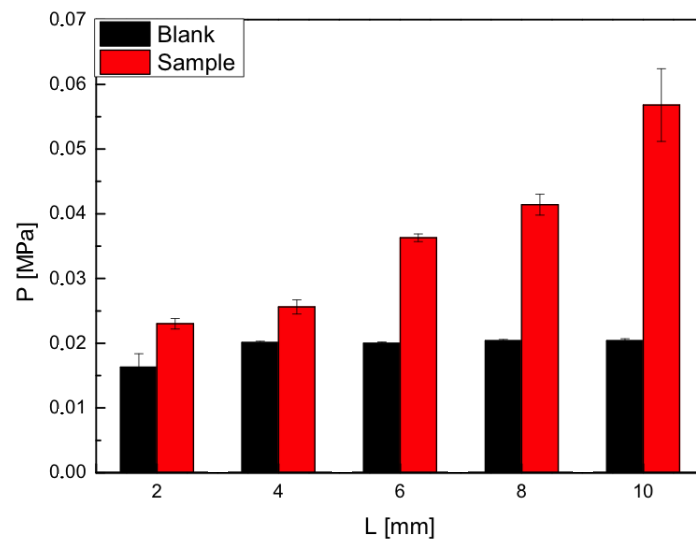


**Figure 56:** Average equilibrium pressures determined by CPA measurements of glass tubes modified with hyaluronan hydrogels ( $M_n(\text{HA}) = 60$  kDa;  $\beta(\text{HA}) = 15$  mg/ml;  $\text{TG} = 0.18$ , gels synthesized in TRIS/BSS ( $c(\text{TRIS}) = 0.4$  mol/l;  $\text{pH} = 8.5$ )), with different tube lengths ( $L = 2$  mm – 10 mm;  $\text{ID} = 0.5$  mm). Error bars were standard deviations. Due to a low amount of samples (2-3), significance was not established. A general relation between tube length and EP was still visible.

## 2. Results & Discussion

Furthermore EP dependencies on hydrogel concentrations were evaluated. To that end, HS-HA/MBAA with different HA mass concentrations were prepared and a number of glass tubes with the same length modified (Figure 58). The results showed, that an increase of the hyaluronan concentrations required increasing pressures to get a liquid flow through the tubes and to reach equilibrium. A further analysis on the mechanism of the dependence of the liquid flow through the stents can be found in Section 2.5.1. Still, these results illustrated the applicability of the CPA measurements for the comparison of the pressure resistance of model implants created with different parameters.

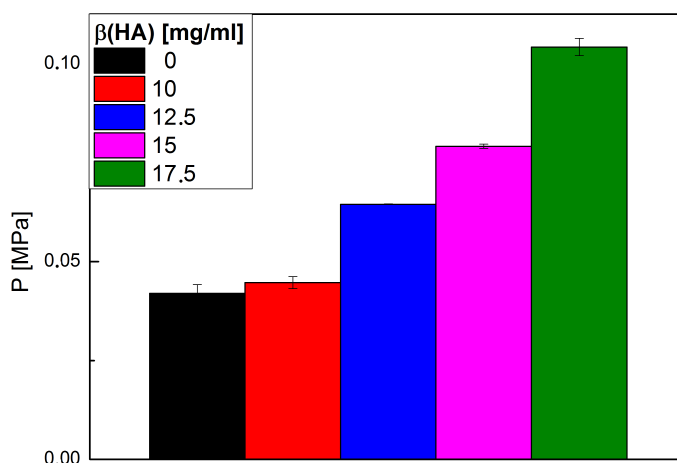


**Figure 57:** Average equilibrium pressures of CPA measurements of HA-hydrogel modified glass tubes ( $L = 10$  mm;  $ID = 0.5$  mm) using different mass concentrations of hyaluronan ( $M_n(\text{HA}) = 60$  kDa;  $\beta = 10$ -17.5 mg/ml;  $TG = 0.18$ ; gels synthesized in BSS/TRIS ( $c(\text{TRIS}) = 0.4$  mol/l;  $\text{pH} = 8.5$ )). Due to a low amount of samples (2-3), significance was not established. A general relation between tube length and EP was still visible.

As mentioned before, a “normal” intraocular pressure is considered to be at a daily average of 21 mmHg (ca. 2100 Pa).<sup>3</sup> Therefore it was then necessary to optimize the stents’ parameters in a way that the tubes would only allow a liquid passage while exposed to pressure values above 2100 Pa. It was attempted to measure potential flow barrier properties of the model implants using the CPA setup. First, an artificially high pressure value by pushing the plunger into the syringe at a constant rate with the displacement head was created. Next the displacement head was set to remain in a fixed position. As a result, forces exerted upon the system remained constant and changes to the pressure were dependent only on the sample reactions. However, a number of complications were encountered, which rendered the CPA setup unsuitable for this kind of measurement (Figure 58).

## 2. Results & Discussion

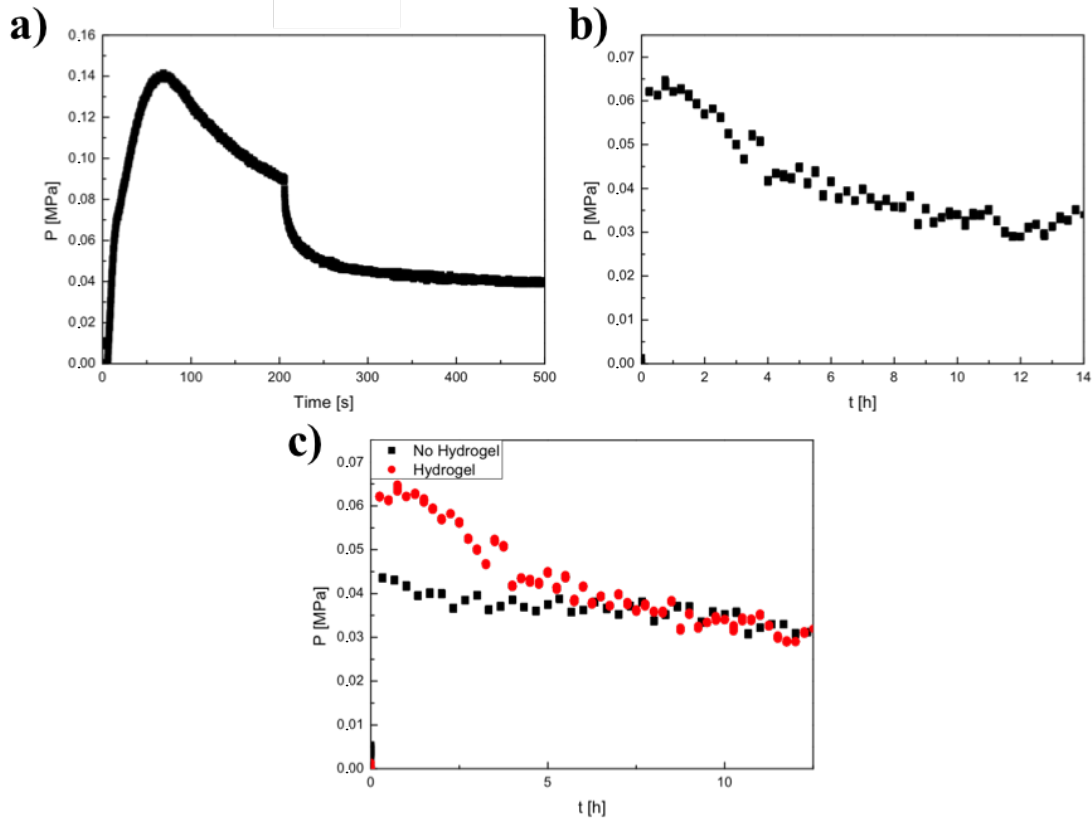


**Figure 58:** (a): The first 500 seconds of a pressure-displacement curve of a CPA measurement on a gel-filled tube ( $M_n(\text{HA}) = 60$  kDa;  $\beta = 10$  mg/ml – 17.5 mg/ml; TG = 0.18; gels synthesized in BSS/TRIS (c(TRIS) = 0.4 mol/l; pH = 8.5)) with a stop of movement of the displacement head at 200 s. (b): The pressure-displacement curve of the whole CPA measurement. (c): Comparison of the long-term development of a gel-filled and an empty glass tube (10 mm, ID: 0.5 mm) after the displacement head stopped moving.

After stopping the displacement head, the pressure immediately dropped (Figure 58a). However a relatively strong noise influenced the course of the curve and reducing accuracy (Figure 58b). The reasons for this were unclear and potentially related to room pressures affecting the force sensor. Due to these variations, the CPA was too inaccurate for these kinds of measurements to a point where curves of hydrogel-modified and blank tubes aligned (Figure 58c).

As a result the CPA method was not used for determining and optimizing the flow barriers of the model implants and another method was developed to conduct further measurements (Section 2.4.3). Still, it's applicability for quickly evaluating general parameter dependencies and breaking of gel-modified tubes was demonstrated. Specifically the ability for quickly performing measurements on large amounts of samples in relatively short times makes it useful for future optimizations of implant parameters.

## 2. Results & Discussion

### 2.4.3. Hydrostatic pressure measurements

As outlined in 2.4.2, the CPA method was very useful in quickly determining the behavior of hydrogel-modified tubes to external pressure, whether they permitted or resisted a liquid flow or broke when exposed to different levels of pressure. By using CPA measurements it was also possible to quickly compare the pressure resistance of samples created with different parameters. However the method was unsuitable for a determination of the pressure-barrier levels of the stents, especially for values less than 5000 Pa (Figure 58). The target pressure for the glaucoma treatment was at 2100 Pa<sup>3</sup>. For that reason second method was developed for specifically measuring the pressure-barrier values at lower levels. To that end, an experimental setup utilizing the hydrostatic pressure within a long glass capillary, further referred to as “Hydrostatic Pressure Application” (HPA), was utilized (Figure 59). It consisted of a glass capillary with an outlet that was placed on a commercially available balance and a sample connected to the outlet by elastic tubing. By filling the capillary with watery solutions (e.g. BSS) hydrogels within the tubes were subjected to hydrostatic pressures exerted from the liquid column. Mass changes were recorded by the balance and subsequently used to analyze the tubes’ reactions to the hydrostatic pressure.

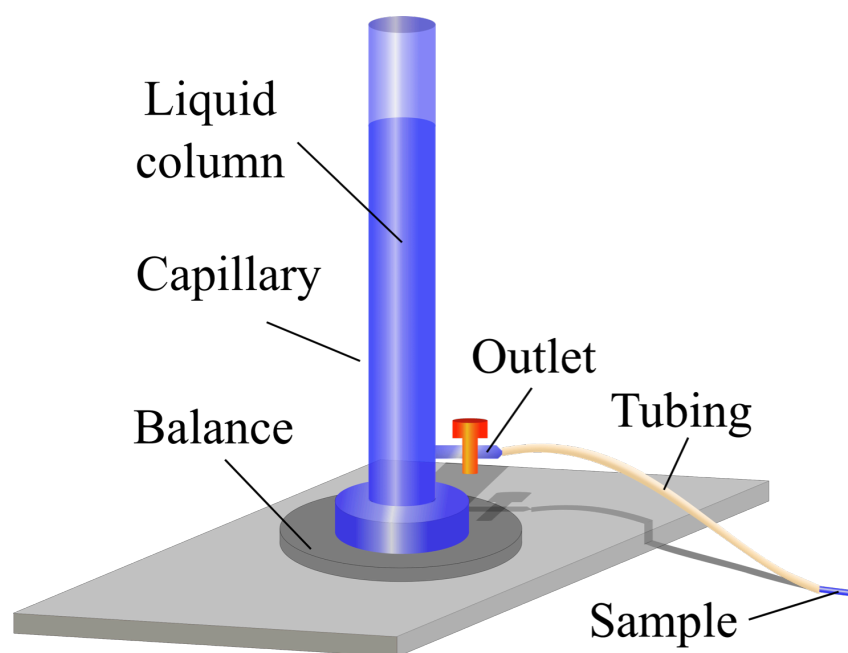


**Figure 59:** Experimental setup for the HPA measurements: A glass capillary with an outlet was placed on top of a balance and a hydrogel-filled tube was connected to the outlet. Hydrostatic pressure was applied on the sample by filling the capillary with liquid. Reactions of samples to hydrostatic pressures were analyzed by mass changes recorded from the balance.

## 2. Results & Discussion

---

For calculating hydrostatic pressure values affecting the samples from the masses recorded by the balance, a conversion constant  $K_p$  was defined:

$$K_p = \frac{P}{m} \quad \text{Equation 2:4}$$

with “P” being the hydrostatic pressure and “m” the mass of the liquid column within the capillary. The hydrostatic pressure was calculated with the common formula

$$P = \rho * g * h \quad \text{Equation 2:5}$$

with “ $\rho$ ” as the density of the liquid, “g” as the gravity acceleration and “h” the height of the liquid column.

Using the basic definition for density after the formula

$$\rho = \frac{m}{V} \quad \text{Equation 2:6}$$

with “m” as the mass and V as the volume of the liquid column and the height being calculated from

$$h = \frac{V}{A} \quad \text{Equation 2:7}$$

with “A” being the ground area and “V” being the volume of the liquid column and inserting them into Equation 2:5  $K_p$  is then defined as

$$K_p = \frac{P}{m} = \frac{m * g * V}{m * V * A} = \frac{g}{A} \quad \text{Equation 2:8}$$

and therefore only dependent on the gravity acceleration and the ground area of the liquid column. The use of  $K_p$  allowed for a direct translation of the masses recorded by the balance into hydrostatic pressures affecting the hydrogel-filled tubes during HPA measurements.

Due to the low amount of hydrogel-filled tubes available for passaging of liquids through their interior, similar to the CPA measurements (Section 2.4.2) only a few experiments were conducted. However, samples that did enable a controlled liquid flow and were measured with the HPA method illustrated the general applicability of the method for future experiments (Figure 60).

## 2. Results & Discussion

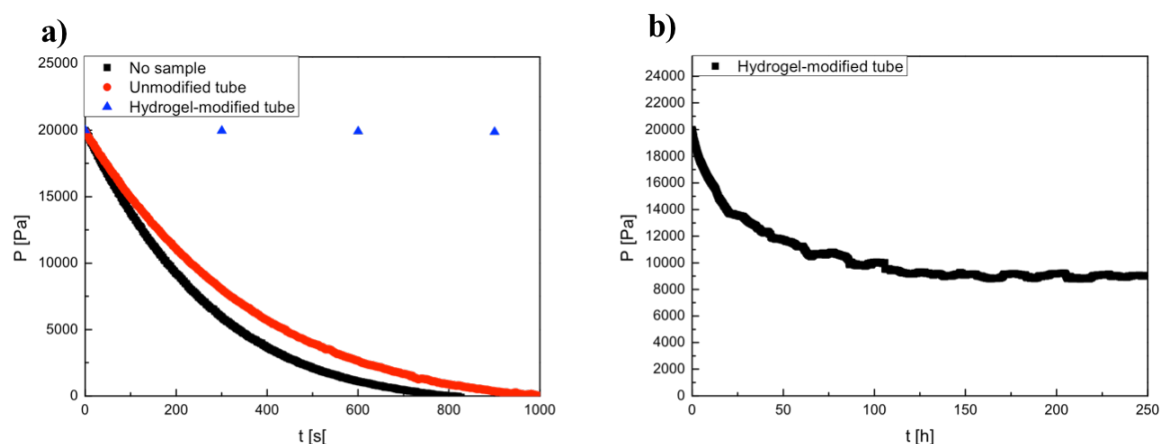


**Figure 60: (a):** Comparison pressure developments of HPA measurements without a sample, with an unmodified sample ( $L = 10$  mm;  $ID = 0.5$  mm) and a gel-modified tube ( $L = 6$  mm;  $M_n(\text{HA}) = 60$  kDa;  $\beta(\text{HA}) = 15$  mg/ml;  $TG = 0.18$ ; gels synthesized in BSS/TRIS ( $c(\text{TRIS}) = 0.4$  mol/l;  $\text{pH} = 8.5$ )) of the first 1000 seconds. **(b):** Pressure development of the same measurement over the next 250 h. The graphs illustrate the ability of some hydrogel-modified tubes to control the hydrostatic pressure by draining liquid more slowly from the capillary than empty tubes **(a)** and that this drainage was stopped at pressure levels  $>0$ , in this case at 9000-10000 Pascal, effectively performing as a valve. Only four data points were shown for the hydrogel-filled tube in **(a)**, since that measurement was performed long-term (the data points and the curve in **(b)** belong to the same measurement) and the intervals were longer in order to reduce the amount of data.

Curves for unmodified and gel-modified tubes varied noticeably from each other, with the former dropping from a pressure of  $>20000$  Pascal to zero Pascal within less than 17 minutes (Figure 60a) while the later lowered the pressure to a level of 9000-10000 Pa, where the outflow of liquid from the capillary stopped (Figure 60b). This demonstrated the ability of HPA setups to determine pressure barriers of gel-filled tubes with less noise, compared to the CPA measurements (Section 2.4.2). More importantly it gave a clear proof-of-principle, that small tubes filled with hydrogels were able to act as pressure sensitive valves by allowing a passage of liquid only at pressure levels at certain thresholds. The HPA setup was also more similar as a model system to the human eye. An implant inserted for glaucoma therapy would encounter a “constant” starting pressure similar to the HPA setup instead of a rapidly and constantly increasing pressure as encountered in the CPA measurements. Therefore HPA was a valuable tool for analyzing valve functions of gel-filled tubes and was later used for determining further optimizations (Section 2.5.2).

### 2.4.4. Summary and conclusion

In this chapter, several methods were used for characterizing hydrogel-filled tubes that acted as model glaucoma implants. In a first step, a few basic experiments were conducted to compare swelling of hydrogels immobilized to the inside of glass tubes (constrained gels) with non-immobilized samples (unobstructed gels). The aim was to see differences in swelling behaviors due to covalent immobilizations in tubes for establishing an incubation protocol before conducting further experiments. The results showed a stronger initial swelling of unobstructed gels before declining into a steady state lower than the constrained gels (Figure 42). This was related to TRIS residues within the hydrophilic networks from the gel synthesis (See Figure 43). Their presence caused an elevated initial osmotic pressure and water infiltration before diffusing themselves out of the hydrogels leading to their shrinking, again due a change of osmotic forces.<sup>109</sup> Constrained hydrogels directly achieved a steady state that was higher than unobstructed samples. One probable cause was an inhibition of initial swelling and volume expansion due to physical barriers posed by the walls leading to decreased pore sizes and limited diffusion of TRIS. This was further enhanced by general limited molecule exchanged due to hydrogel/medium interfaces present only at the tubes ends. A further explanation for the lower reduction of masses and volumes of constrained gels were the physical limitations through the covalent immobilization preventing gels from expanding or contracting. Future experiments, for example by determining pore sizes of the networks with fluorescent probes<sup>90</sup>, or using constrained but non-immobilized hydrogels, can aid in a more in-depth understanding of this mechanism.

Furthermore, two methods were established for allowing characterization of gel-modified tubes reactions to liquid pressures: The CPA (Section 2.4.2) was based on the continuous application of an external force to the plunger of a syringe connected to gel-filled tubes (Figure 44) and was employed for quick evaluations of basic properties of a large number of samples. These basic properties were, whether the gel would allow a liquid flow through the interior of the containing tube (Figure 52) or whether it would block any drainage through the sample destroying the hydrogels when certain pressure thresholds were reached (Figure 49). It was demonstrated that the immobilization of the hydrogels (See Section 2.3.2) was enough to withstand any potential pressures encountered in glaucomatous eyes (Figure 50). Furthermore, some samples used in CPA measurements showed passage of liquid when certain levels of pressure within the system were achieved (Figure 52, Figure 53). The method was further used to determine variations of the pressure resistance depending on different parameters such as tube length (Figure 56)) or hyaluronan concentrations within the hydrogels (Figure 54). The big advantage of this method was the low time-requirement to conduct measurements.

## 2. Results & Discussion

---

HPA (Section 2.4.3) was developed as a complementary method to the CPA and used the hydrostatic pressure generated by a water column (Figure 59) for evaluating the potential of hydrogel-modified model implants to act as a pressure sensitive valve (Figure 60b). CPA could not provide this kind of data since it only gave pressure values relative to the movement speed of the syringe's plunger (Figure 55). CPA was also not sensitive enough for detecting smaller variations in the pressure (Figure 58), which was required for determining the absolute pressure threshold where a liquid flow was enabled. HPA also mimicked the conditions within the aqueous humor better, where pressure did not continuously and relatively rapidly increase. The disadvantage of the HPA compared to CPA measurements was the relatively long time required to perform an individual evaluation of a sample which was days (Figure 60b), as opposed to the CPA, where measurements were performed within minutes. Nonetheless, both methods were very useful for evaluating different properties of the model implants and can be used for further optimizations in the future.

However, one issue became apparent during measurements with these systems: The majority of samples did not perform as intended when exposed to liquid pressures. Instead they completely resisted any passage of liquid through their interiors with low yields of samples performing correctly (< 10%). An improvements of the yields by varying different parameters ( $\beta(\text{HA})$ , crosslinking density, etc.) was not possible and samples capable of pressure regulation were obtained at random. This made it difficult to acquire larger datasets for a more statistically significant characterization of the model tubes. Therefore respective measurements were set aside in favor of exploring the mechanism behind the liquid flow (See Section 2.5).

Nonetheless, the general usefulness of CPA and HPA measurements for a characterization of hydrogel-filled model implants was successfully established. More importantly, the general ability of hydrogel-filled stents for regulating intraocular pressures was demonstrated. Therefore the focus in subsequent chapters lay on explaining the mechanism of the liquid flow and finding ways for improving the yield of functional samples.

### 2.5. Optimization of the concept for creating intraocular stents

#### 2.5.1. The mechanism of liquid flow through gel-filled tubes

It was already shown, that small glass and titanium tubes were successfully modified with hyaluronan hydrogels immobilized on their outer and inner surfaces (Section 2.3). Furthermore, two analytical methods were developed for analyzing reactions of hydrogel-filled tubes to external liquid pressures (Section 2.4). Pressure induced liquid flow through these samples was successfully confirmed (Figure 52, Figure 53). Moreover the principal ability of these samples to act as pressure-sensitive valves by allowing a liquid flow until pressure dropped to certain thresholds (10000 Pa) were reached, was demonstrated (Figure 60). These data sets already showed that the concepts for generating intraocular stents modified with hyaluronan outlined in Section 1.6 is possible. However, two problems remained:

It was not possible to optimize the parameters required for generating a stent suitable for the reduction of liquid pressures to normal levels of bellow 21 mmHg (ca. 2100 Pa)<sup>205</sup> yet. Therefore further testing and optimizing the model implant's parameters was required. Secondly, and at that point more importantly, yields of functional model stents gained from established methods presented in previous chapters were too low. Many hydrogel-modified tubes did not enable for any drainage of liquid. Instead gels immobilized within the tubes completely resisted any liquid flow during CPA measurements and pressure levels increased until they were destroyed and ejected from the tubes (Figure 49). As a result, it was not possible to gain large datasets for statistically significant characterizations of the tubes' pressure resistances. Furthermore, for a potential industrial manufacture, the process of stent production needed to be reproducible and reliable otherwise the amount of deficient products would create undesirable extra costs. Therefore the further focus of the thesis, presented in this chapter, was finding a way for improving reliability and reproducibility of the production process.

The first step towards this goal was to gain understanding of pressure induced liquid flow's mechanisms. To that end, an experimental setup was devised, where hydrogel filled glass tubes were connected on both ends to elastic tubing and placed on a small glass plate within a fluorescence microscope (Figure 61). A syringe containing solutions of fluorescein or BSS was connected to the setup. Pressure was created by pushing the solution manually with the syringe at the gel-filled tube while recording fluorescent signals of the tubes inside with a microscope (Figure 62).

## 2. Results & Discussion

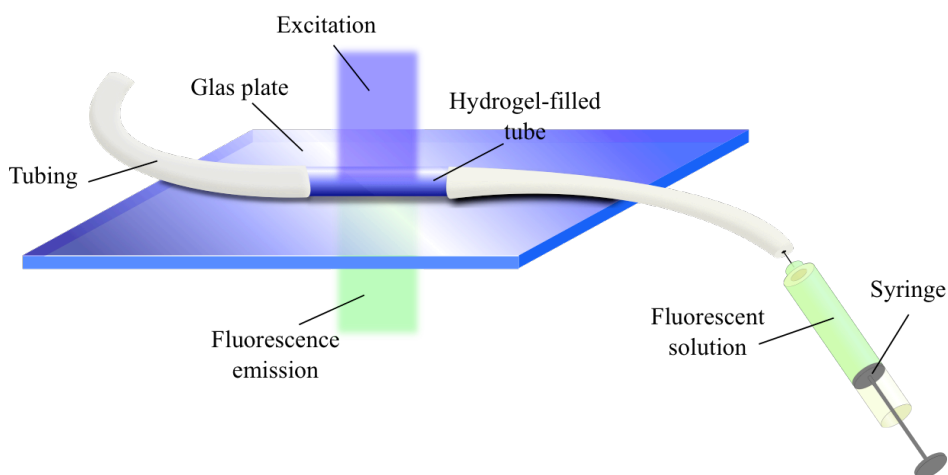


**Figure 61:** Experimental setup for observing the mechanism of pressure induced liquid flow within hydrogel-filled tubes on a microscopic level. Samples were placed on a glass plate in the focus region of a fluorescence microscope. Fluorescent solutions or BSS were manually pressed into the tube and reactions of the hydrogels monitored.

Figure 62a showed the beginning of a fluorescent pressure resistance (FPR) measurement before any external pressure was applied to the system. The observed location was the interface between the tubing containing the fluorescent solution and the examined sample. In Figure 62b, pressure was manually applied on the system and slowly increased. No liquid flow was detected at that point. The only change within the tube was a small bulge of the fluorescein solution, indicating slight compression of the hydrogel. This bulge increased gradually in small steps when pressure was further increased. When pressure was high enough to initiate liquid flow a channel formed at the side of the tube (Figure 62c). Figure 62d is a merge of several pictures recorded right after the gel flow started to show an extended section of the tube. The channel wandered to the center of the glass tube.

## 2. Results & Discussion

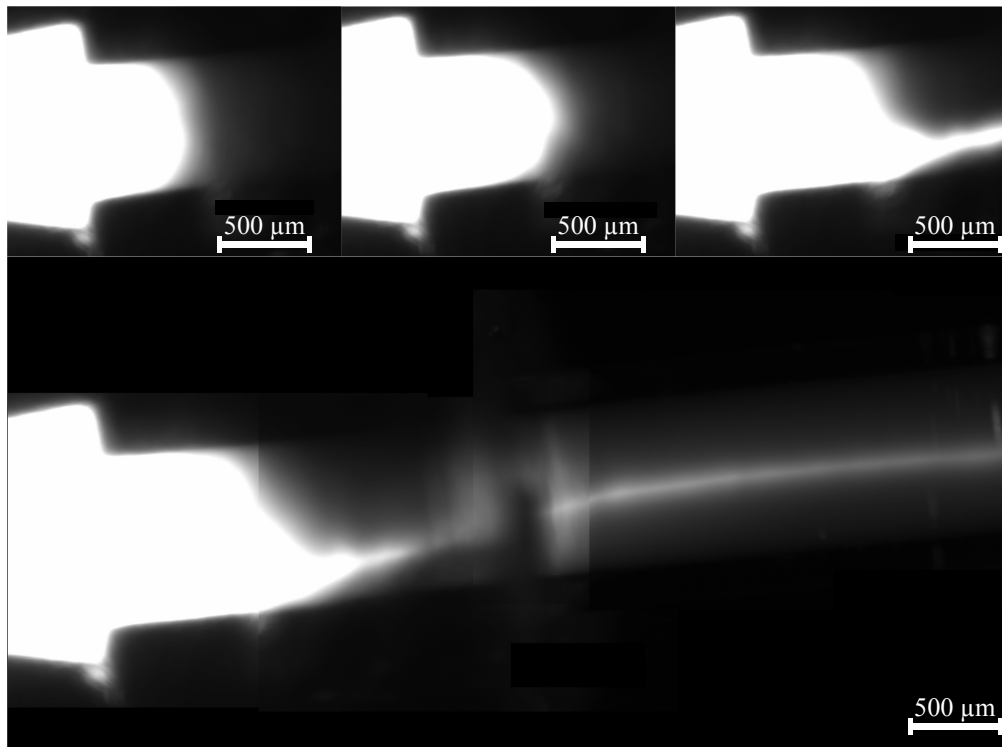


**Figure 62:** (a-c): Fluorescence images at different time-points of a fluorescent pressure resistance measurement. The location was at the interface between the gel-filled sample ( $L = 10$  mm;  $ID = 0.5$  mm;  $M_n(\text{HA}) = 60$  kDa;  $\beta(\text{HA}) = 15$  mg/mL;  $TG = 0.18$ ; gels synthesized in TRIS/BSS ( $c(\text{TRIS}) = 0.4$  mol/l;  $\text{pH} = 8.5$ )) and the tubing. (a): Image taken before pressure was applied. (b): Pressure was applied on the fluorescent solution but no liquid flow was observed. (c): Picture from a time-point when the pressure just induced a liquid flow through the tube. (d): Combination of several images taken at almost the same time from the connection point and farther into the sample.

Subsequently the time after channel formation, when a steady flow was established, was monitored further. To that end tubes modified with fluorescent hydrogels made from HS-FA-HA were used and the tubes' central parts were observed (Figure 63). Background fluorescence (Figure 63a) originated from the hydrogel itself since HS-FA-HA was used to create it. Figure 63b-f shows small amounts of liquid infiltrating the sample on a distinct path along the central axis. Figure 63g shows more liquid entering the channel, broadening it and fluorescein starting to infiltrate the polymeric network (Figure 63h-k) until it was distributed evenly in the whole tube (Figure 63l).

## 2. Results & Discussion

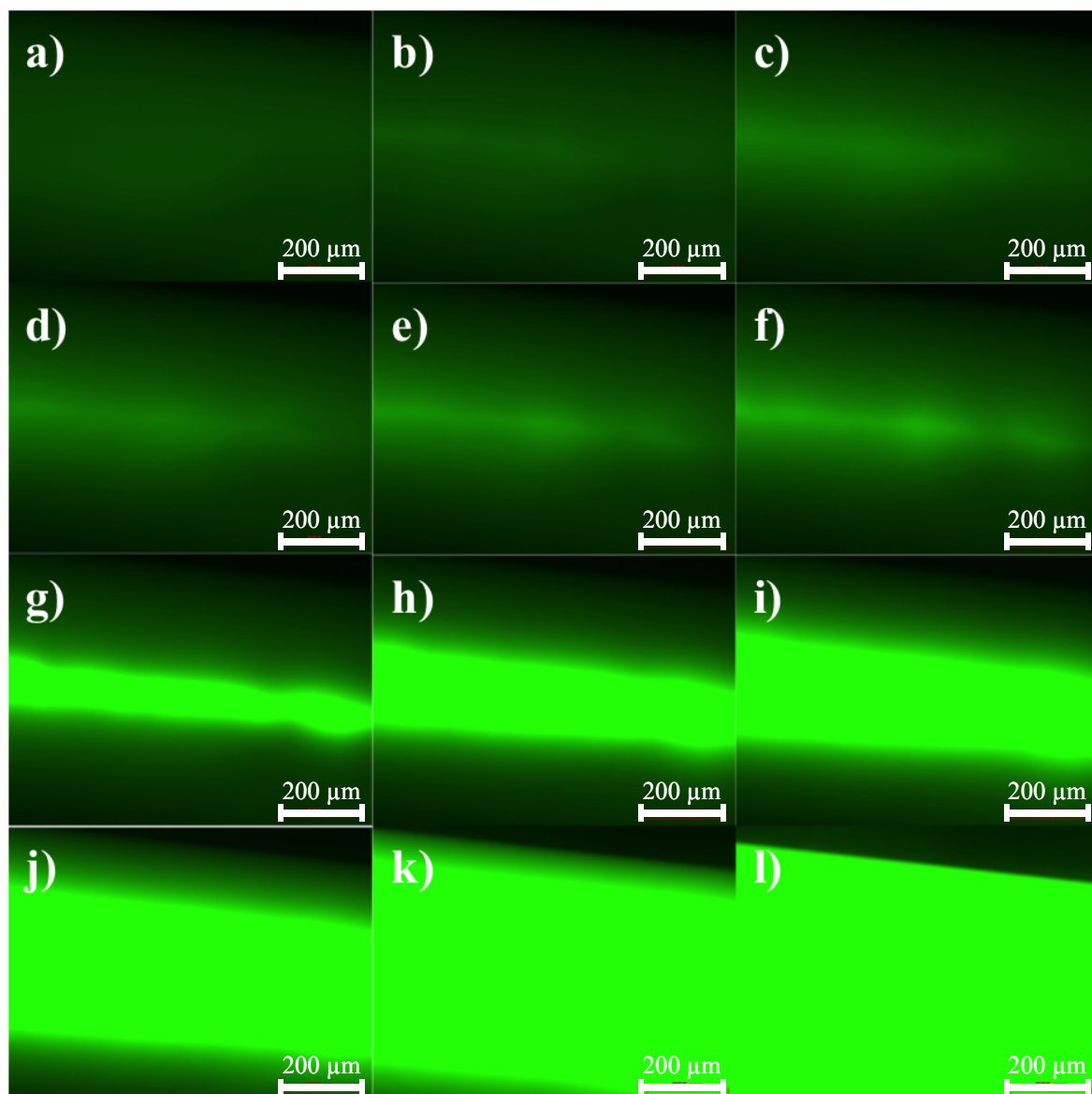


**Figure 63: (a-l):** Fluorescence images of an FPR measurement using fluorescein on a hydrogel-modified tube ( $L = 10$  mm;  $ID = 0.5$  mm;  $M_n(\text{HA}) = 60$  kDa;  $\beta(\text{HA}) = 15$  mg/mL;  $TG = 0.18$ ; gels synthesized in TRIS/BSS ( $c(\text{TRIS}) = 0.4$  mol/l;  $\text{pH} = 8.5$ )) at different time-points. Fluorescent liquid was observed to slowly infiltrate the tube along the center before opening to a channel. Subsequently the dye spread among the whole hydrogel.

Subsequently the tube was rinsed with BSS (Figure 64) and the distribution of fluorophores monitored, which were flushed from the hydrogel. Instead of being removed evenly across the whole network, fluorophore concentration declined from the outer areas to the center axis of the tube. This indicated the main flow of liquid through the hydrogel concentrated there with the outer areas only slightly contributing to the passage of fluid. After complete removal, a darker streak in the middle of the gel was visible (Figure 64h-i). It hinted at a lower concentration of the fluorescent hydrogel at this position due to the presence of a channel.

## 2. Results & Discussion

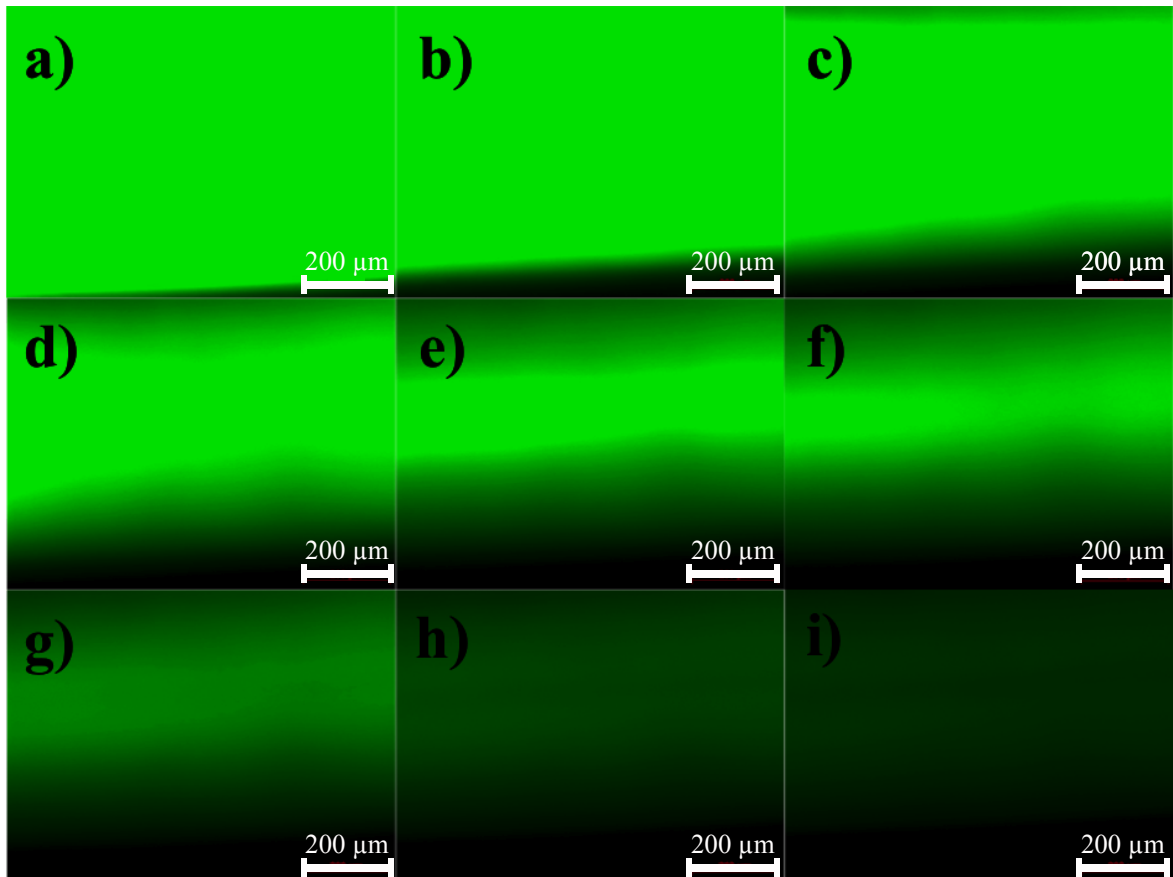


**Figure 64: (a-i):** Fluorescence images of a hydrogel-modified stent ( $L = 10$  mm;  $ID = 0.5$  mm;  $M_n(\text{HA}) = 60$  kDa;  $\beta(\text{HA}) = 15$  mg/mL;  $TG = 0.18$  gels synthesized in TRIS/BSS ( $c(\text{TRIS}) = 0.4$  mol/l;  $\text{pH} = 8.5$ )), saturated with fluorescein from a previous FPR measurement and rinsed with non-fluorescent BSS. The fluorophores were not washed out evenly among the whole tube and were concentrated in the middle, indicating the presence enhanced liquid flow at that point. This channel becomes slightly visible in image (h) and (i).

For further investigating the presence of these channels, BSS solutions were pressed through samples with fluorescent hydrogels repeatedly. The darker areas were only observed when an external liquid pressure with BSS was applied on the tube initiating liquid flow (Figure 65) and were determined to be channels conducting the liquid flow. After pressure was removed they vanished (Figure 65c) and reformed at subsequent re-applications of the external pressure (Figure 65d). This showed the formation of channels being directly related to pressure-induced liquid flow.

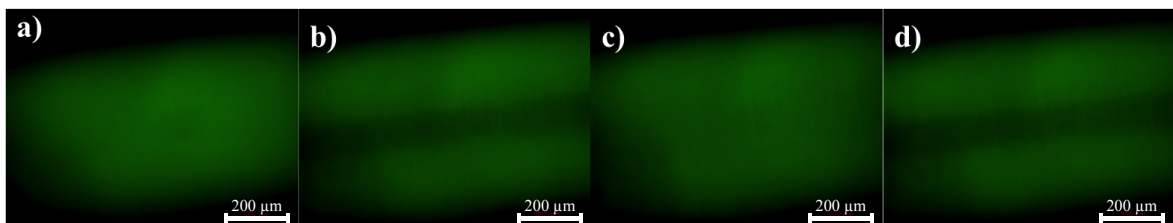


**Figure 65:** Fluorescence pictures of a set of repeated pressure applications of BSS on a tube filled with fluorescent hydrogels ( $L = 10$  mm;  $ID = 0.5$  mm;  $M_n(\text{HA}) = 60$  kDa;  $\beta(\text{HA}) = 15$  mg/mL;  $TG = 0.18$  gels synthesized in TRIS/BSS ( $c(\text{TRIS}) = 0.4$  mol/l;  $\text{pH} = 8.5$ )): (a): Time-point before the first application of pressure. The gel was uniform within the tube. (b): Image from a time-frame where pressure was applied for the first time and a channel was visible running through the center of the gel. (c): Time-point after the first and before the second pressure application. The channel closed again. (d): Image from the second interval for a pressure application where the channel was visible again.

## 2. Results & Discussion

The presence of these channels was confirmed in all observed samples that allowed a liquid flow during CPA measurements. This indicated them being a necessary feature of the hydrogels to enable any pressure regulation. From these collected results a mechanism was proposed on the mechanism of channel regulated liquid flow (Figure 66).

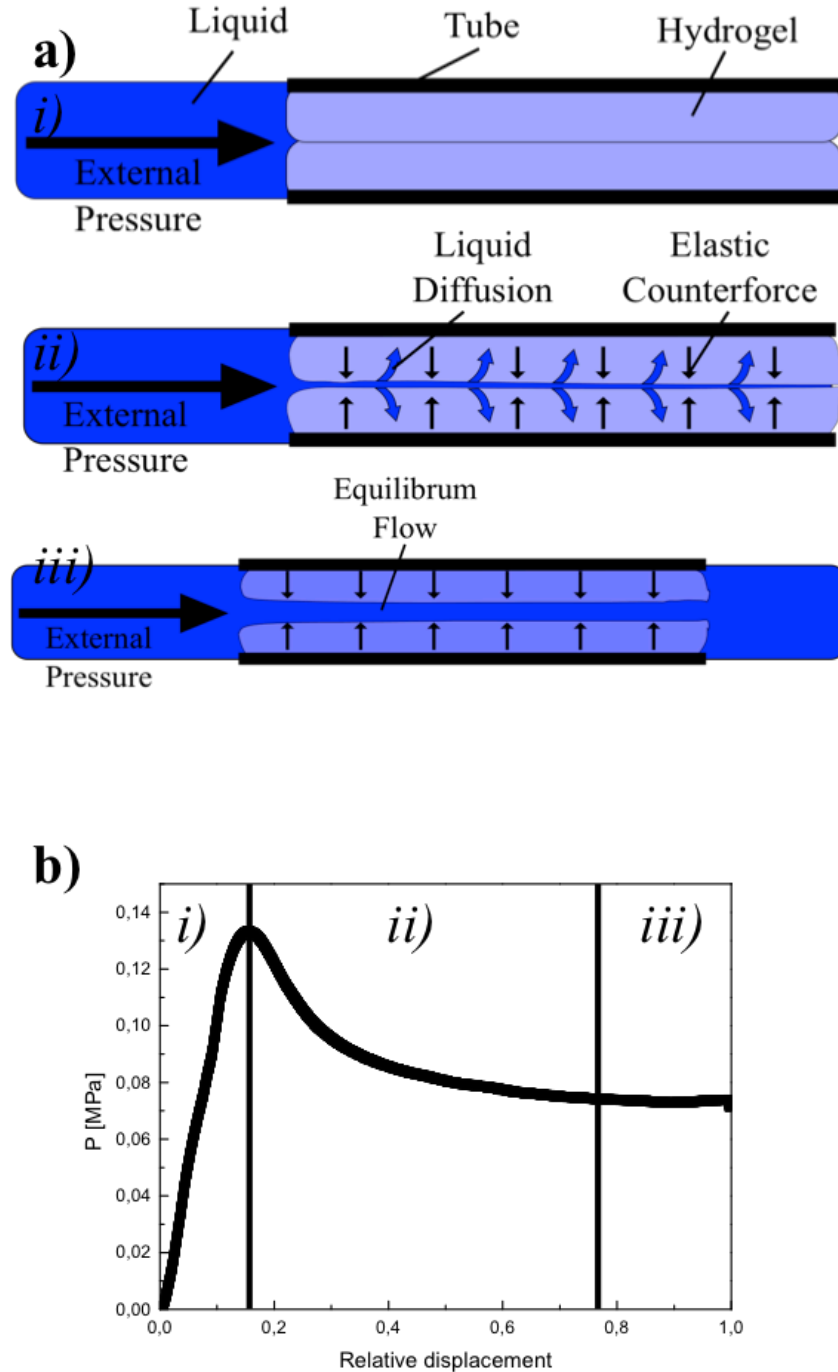


**Figure 66:** Proposed mechanism (a) and correlation with CPA measurements (b) for pressure-induced liquid flow through hydrogel-filled tubes. A “flaw” in the form of a small channel is located within the hydrogels. **i)** As long as the external pressure is below a certain threshold, the channel is “closed” due to a combination of elastic forces and hydrophilic interactions between the interfaces of hydrogels. No water flow is established. **ii)** When the pressure is more than that threshold, water infiltrates the system, overcoming the hydrophilic forces and enacting compressive forces upon the hydrogels, which causes the channel to “open”. **iii)** These compressive forces of the external pressure and the elastic counter-forces are in balance, which establishes a constant channel size and enables liquid flow.

## 2. Results & Discussion

---

The proposed mechanism is based on the existence of a “flaw” within the hydrogel filling the interior of the tube. Due to their nature of consisting of hydrophilic networks<sup>70</sup> their interfaces can interact with each other (H-bonds, etc.). Hydrogel also possess viscoelastic properties, which means the hydrogels within the tubes are able to be reversibly compressed.<sup>206,207</sup> As long as external liquid pressures affecting the implant are below certain thresholds (“pressure barrier”) the channel remains “closed” due to a combination of hydrophilic interactions and elastic forces between HA molecules at the hydrogel’s interfaces (Figure 66*i*). When external pressures exceed that pressure barrier, the forces exerted on the hydrogel overcome the hydrophilic interactions and slightly compress the hydrogel, thereby “opening” the channel (Figure 66*ii*). As a result a water flow is established reducing the external liquid pressure. Since the hydrophilic interactions cannot re-form as long as the channel is open, the only forces influencing the liquid flow stemming from the pressurized liquid exerted on the hydrogel and the elastic counterforce originating from the compression of these hydrogels. Therefore the peak pressure observed in CPA measurements (Figure 66*b*) is only necessary for initial channel opening. When both forces are in balance, the channel gains a constant size and the external pressure is in balance with the liquid flow (Figure 66*iii*).

The proposed mechanism is in good agreement with results obtained from the CPA measurements (Section 2.4.2, Figure 66). External forces were constantly affecting the liquid in the syringe causing a constant water flow during the duration of the measurements. For HPA measurement, where no additional external forces influenced the hydrostatic pressure of the liquid column, water-flow stopped when the pressure dropped to certain levels (Figure 60*b*). This was explained, according to this proposed mechanism, by the elastic counterforces overcoming the forces exerted from the hydrostatic pressure, thereby causing a relaxation of the hydrogel within the tube and channel closure. Further confirmation was found by the results of the FPR measurements with BSS (Figure 65), where the channel opened only during the application of an external pressure. The findings from the CPA measurements, where the curve on repeated measurements only showed a peak pressure on the first run (Figure 54), could be explained in a similar fashion. The remaining pressure within the closed chamber of the CPA after movement of the displacement head stopped prevented hydrogels from fully relaxing and fully closing the channels. As a result no extra forces were necessary on subsequent measurements performed immediately afterwards.

However this theory was only speculation at that point and required further verification by future research. At that point it was sufficient however for explaining the experimental findings of CPA, HPA and FPR measurements. It also helped establishing protocols for physically creating such channels to induce the pressure regulatory effect (Section 2.5.2).

The reasons of the channel’s origin within the hydrogels are also currently unexplained. Several potential reasons were considered. One possibility is the formation of hydrogels in the tubes not being uniform over the whole volume of their interiors. Instead the crosslinking between the HS-HA chains occurred predominantly at the surfaces of the substrates due to an increased HS-HA concentration from the simultaneously occurring immobilization reaction. This may have resulted in the hydrogels growing from the surfaces of the tube into the rest of the interior.

## *2. Results & Discussion*

---

At the center axis not enough material was left to ensure tight crosslinking, which resulting in the formation the channel. Also it was demonstrated during swelling experiments with BSS (2.4.1), that hydrogels used in this thesis showed an initial volume gain followed by a reduction of masses due to the presence of TRIS within the hydrophilic networks. Comparing unobstructed gels with constrained samples also revealed that the mass (and volume) reduction did not occur in hydrogels within glass tubes. The covalent immobilization to the tubes' walls preventing a gel contraction was seen as a possible reason for this. Concerning the channel formation, this inability of reducing its volume could lead to an osmotic force induced strain on the hydrogels and causing a tear within its body. However, these are only speculations and the mechanism for natural channel formation has not been further explored, especially since their presence within these hydrogel-filled model implants was completely random after sample preparation. Instead, other more reproducible possibilities to create these channels artificially have been explored (See 2.5.2).

## 2. Results & Discussion

### 2.5.2. Exploration of physical methods for creating small channels in hyaluronan hydrogels

In the previous section it was demonstrated that the observed pressure-dependent liquid flow through hydrogel-filled tubes (Sections 2.4.2 and 2.4.3) was linked to the presence of small channels within the hydrogels (Section 2.5.1). Up to that point all attempts at optimizing the chemical parameters (crosslinking density of HS-HA,  $\beta$ (HS-HA), ratio of thiols to crosslinkers etc.) for more reproducibly creating hydrogel-filled tubes with these channels failed. Therefore creating these channels by the use of physical methods was attempted instead. Two concepts were further explored and the results are presented in this Section (Figure 67).

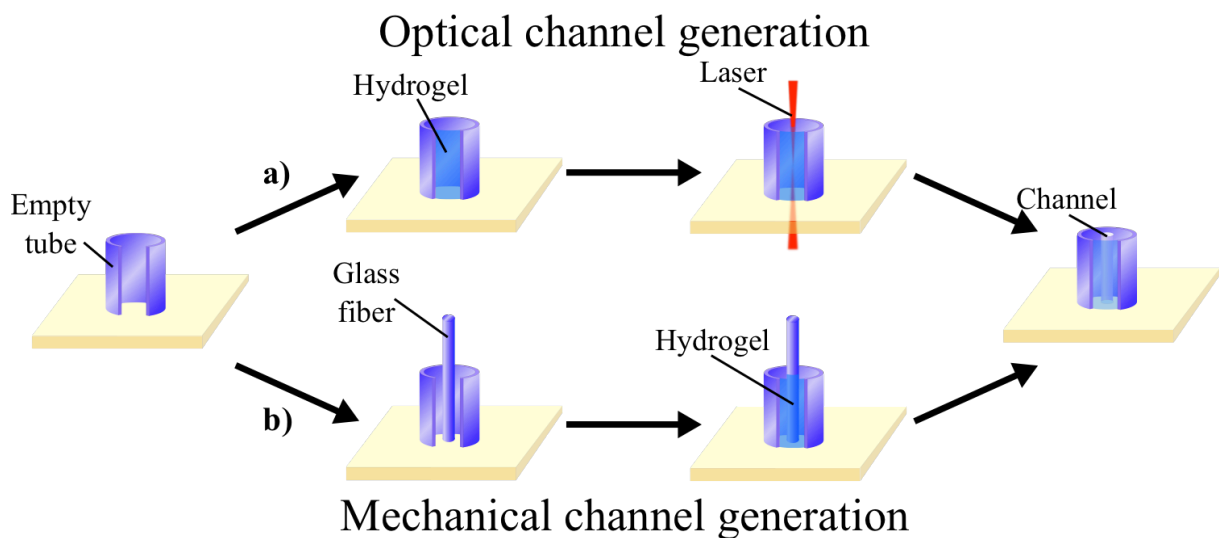


**Figure 67:** Concepts for physically creating channels within hydrogel-filled tubes for artificially inducing the ability for liquid pressure regulation. **(a):** In the optical method covalently immobilized hydrogels were first prepared within tubes and a laser applied to “burn” the channel into the gel. **(b):** In the mechanical method a small fiber into was placed coaxially into the empty tube. After the gel formation the fiber was removed leaving behind the channel.

An “optical” concept included the use of a CO<sub>2</sub> laser for creating the channels (Figure 67a). First, covalently immobilized hydrogels were formed within silanized tubes followed by the application of a laser strong enough to “burn” away the hydrogels in its path. This idea was inspired by the work of A. Holle who similarly generated artificial channels in PDMS.<sup>208</sup>

The other “mechanical” method involved using small glass fibers placed coaxially within the tubes (Figure 67b). After hydrogel formation the fibers were removed and left behind channels in their previously occupied volume. In both methods subsequently swelling gels “closes” the channel after 48 hours as described in Section 2.5.2. Both methods allowed in theory to create channels with different widths. This would potentially allow, together with varying other gel properties (e.g. elasticity) adjusting the pressure regulatory levels of intraocular implants.

One issue that came up early when designing the experimental setups was the size of the glass tubes. In previous sections mostly relatively small samples were used (L = 10 mm, ID = 0.5 mm) for creating and analyzing hydrogel-modified model implants.

## 2. Results & Discussion

According to the observations in Section 2.5.1 the original channel had to be relatively small in relation to the hydrogels. Otherwise blocking liquid flow at low pressures would not have been possible for a lack of “closed state”. Sizes of “open” channels in FPR measurements were estimated to be ca. 100 $\mu\text{m}$  (Figure 65) with “closed” states being even smaller. This created the problem, that among the available equipment no laser was small enough to create channels of the required size. Properly aligning laser and sample on that scale was also not possible without the use of computer-controlled movable sample holders. Also, producing and handling small glass fibers on that scale for the mechanical method would have required more elaborate methods than what was readily available. Instead of obtaining such equipment it was decided, for the pre-emptive experiments presented in this thesis, to scale up the size of the samples instead. If the concept proposed in this section could be verified to be applicable, more elaborate setups for a re-miniaturization on sizes required for manufacturing glaucoma implants can be devised in the future. For these reasons larger glass tubes ( $L = 10\text{ mm}$ ,  $ID = 5\text{ mm}$ ) were obtained and the respective experiments on generating channels within hydrogel-filled tubes using the optical or mechanical method conducted on them instead of the previously used samples.

### Optical method

By using a  $\text{CO}_2$  laser cutter it was possible to create holes within hydrogels of different sizes (Figure 68). However shapes of the channels were often irregular (Figure 68a) and not very reproducible since they heavily depended on the laser parameters such as power, movement speed, frequency, number of applications, etc. The biggest contribution to this irregularity was the focus point of the laser, which was only manually adjustable. Therefore it was not possible to create channels with a reproducible shape with the available setup. Still, the creation of the channels themselves, regardless of shape was possible at all times for most widths (Figure 68a/c).

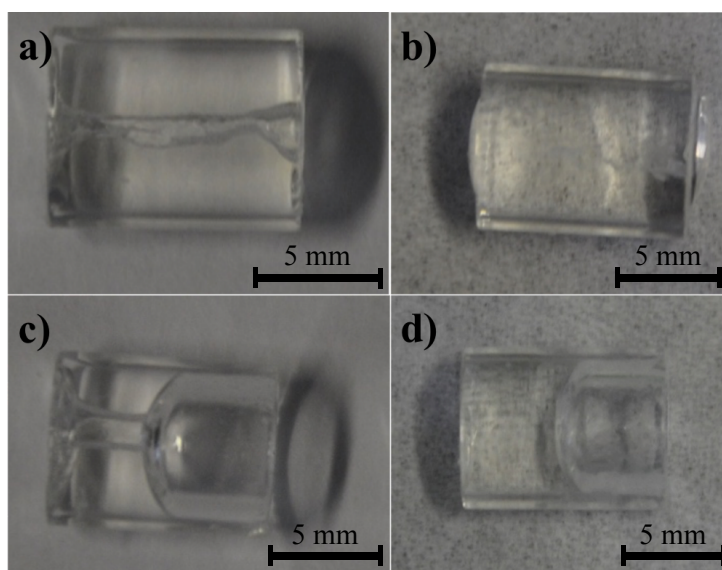


**Figure 68:** Two examples of hydrogel-filled tubes ( $L = 10\text{ mm}$ ;  $ID = 5\text{ mm}$ ;  $M_n(\text{HA}) = 100\text{ kDa}$ ;  $\beta(\text{HA}) = 15\text{ mg/mL}$ ;  $\text{TG} = 0.57$ ; gels synthesized in TRIS/BSS ( $c(\text{TRIS}) = 0.4\text{ mol/l}$ ;  $\text{pH} = 8.5$ )) with channels created by the application of a laser before (a/c) and after (b/d) swelling them in BSS. The channels were burned through hydrogels with 0.5 mm (a) and 1 mm (c) width. However, channel shapes often were irregular (a) and heavily dependent on the laser parameters. In both cases the channels were not seen visually after swelling for 48h in BSS (b/d).

## 2. Results & Discussion

Despite these issues during their formation a number of tubes with differently sized channels were subjected to HPA measurements (See Section 2.4.3). At this point it should be noted, that due to the irregular shapes of the channels generated by the laser application the “sizes” given for the channels were the channel widths the laser was programmed to produce (See Section 4.8.2) and did not necessarily represent their actual widths.

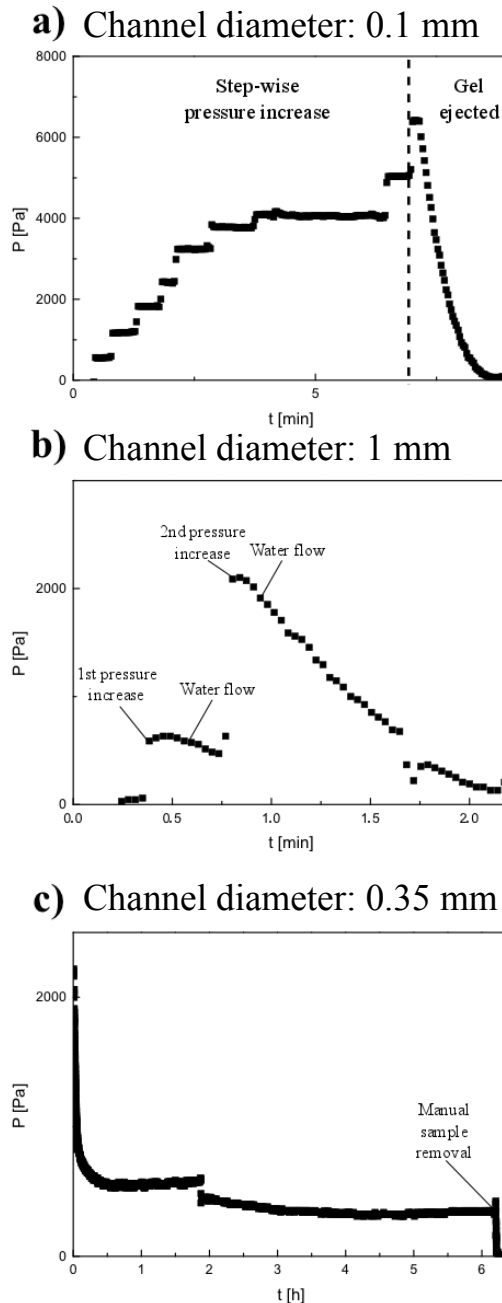


**Figure 69:** HPA measurements of hydrogel-filled tubes ( $L = 10$  mm;  $ID = 5$  mm;  $M_n(\text{HA}) = 100$  kDa;  $\beta(\text{HA}) = 15$  mg/mL;  $TG = 0.57$ ; gels synthesized in TRIS/BSS ( $c(\text{TRIS}) = 0.4$  mol/l;  $\text{pH} = 8.5$ )) with channels of different sizes created by the optical method. **(a)** Curve of a HPA measurement where no channel was formed (Laser setting: 0.1 mm). The pressure was increased manually step by step until the breaking point was reached ( $t = 7.25$  min) and the water flowed out freely. **(b):** HPA measurement curve of a sample with a too large channel (Laser setting: 1 mm). Even after the first pressure increase liquid freely passed through the tube. **(c):** Curve of a HPA measurement, where the sample created by laser application was able to regulate the liquid flow (Laser setting: 0.35 mm), albeit on a lower level as required for intraocular pressure regulation.

## 2. Results & Discussion

---

The results of the measurements were dependent on channel sizes and yielded different informations. At width settings too small for the laser (Figure 69a), it was often not possible to create a proper channel. As a result no liquid flow was detected when increasing hydrostatic pressures. Instead the curve showed a breaking point at 6000 Pa, where the whole hydrogel was ejected from the tube leading to an unimpeded liquid flow from the glass capillary. Breaking point values were much lower compared to CPA measurements on smaller tubes (Figure 50). This was explained in a changed ratio of the external forces being exerted on the hydrogel from the liquid and the immobilization forces that keeps the hydrogel inside. The basic formula

$$P = \frac{F}{A} \quad \text{Equation 2:9}$$

with “P” as the pressure, “F” the force exerted and “A” being the targeted surface illustrates, that the hydrogel in the tube experienced a larger force from the liquid pressure due to the bigger diameter of the tube. In contrast the immobilization is related to the number covalent links between hydrogel and the inner surface. The immobilizing force of these bonds keeping the hydrogels inside of the tubes therefore also increased with the diameter of the tubes. However, the surface are of the hydrogels at the tubes ends, that is exposed to the hydrostatic pressure from the liquid column, increased according to the formula for a circular area. The formula is

$$A_E = r^2 * \pi \quad \text{Equation 2:10}$$

with  $A_E$  being the surface area of the tubes entrance,  $r$  being the radius of the cylindrical tube, The inner surface ascends according to the formula for the inner surface of a cylinder according to

$$A_{IS} = 2 * \pi * r * h \quad \text{Equation 2:11}$$

with  $A_{IS}$  being the area of the inner surfaces of the tubes  $r$  being their radius and  $h$  their height of the cylinder. A comparison between both formulas shows a larger growth of  $A_E$ , which is exposed to dependent on the tube’s radius than the area of the inner surfaces of the tube  $A_{IS}$  the hydrogel is immobilized to. This growth can roughly be quantified, with

$$\frac{A_E}{A_{IS}} = \frac{r}{2 * h} \quad \text{Equation 2:12}$$

When the radius was increased from 0.5 mm to 5 mm the force exerted from external pressures on the hydrogels grew five times more than the immobilizing forces between the hydrogel and the inner surfaces of the tube. This resulted in the immobilization failing at lower pressures than observed during CPA measurements on smaller samples (Figure 50).

## 2. Results & Discussion

---

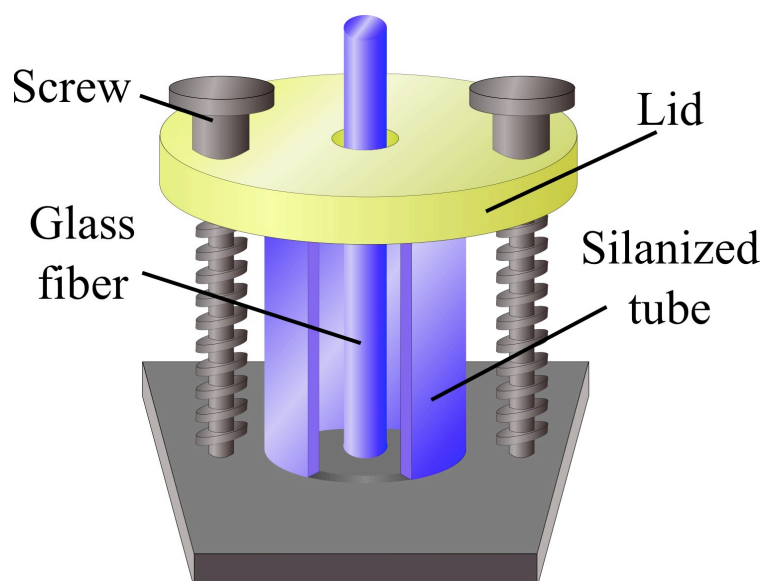
In this simplified model, other possible influences like the hydrogel's own weight also increasing with the size or the channels created with the laser destabilizing the hydrogel's integrity were excluded. A comparison between the CPA measurements of the breaking points of the smaller tubes (ID = 0.5 mm, see Figure 50) were much more than five times of the breaking points gained from the HPA measurements of the larger tubes (ID = 5 mm, Figure 69a). Still it was a sufficient explanation of the visible differences in breaking point values.

Figure 69b showed the HPA measurement with a sample where the laser was set to create a channel with an ID = 1 mm. After initial pressure increase, liquid flow started immediately (0.4 – 0.75 min) with no pressure resistance observed. The width of the channel being too large for being properly “closed” by swelling was the most probable reason for this result. On a sample with the settings for an ID = 0.35 mm, however, it was possible to create pressure regulation, albeit for comparatively low level. This demonstrated, although a lot of optimization would be necessary in the future, that artificially creating channels using lasers for pressure regulation was possible.

## 2. Results & Discussion

### Mechanical method

A reaction chamber was designed for testing the mechanical method. The setup consisted of a sample holder with a circular incision and a small hole in the center of that incision (Figure 70). Silanized glass tubes (ID = 5 mm, OD = 7 mm, L = 10 mm) were placed into the holder. A lid with a similar incision and a hole in the center was placed on top of the sample and fastened with screws. Through the hole in the lid, a small glass fiber was inserted coaxially to the tube prior to hydrogel formation. After gelation the fiber was removed resulting in a physically created channel with the potential ability to regulate external liquid pressures.



**Figure 70:** Concept of the experimental setup for artificially creating channels using the mechanical method. By inserting a glass fiber coaxially to the tube followed by hydrogel formation channels were formed after the fibers' removal.

Glass fibers with a thickness of 0.1-0.2 mm were obtained and successfully used with the aforementioned experimental setup for creating hydrogel-filled tubes (L = 10 mm, ID = 5 mm) containing small channels (Figure 71a).

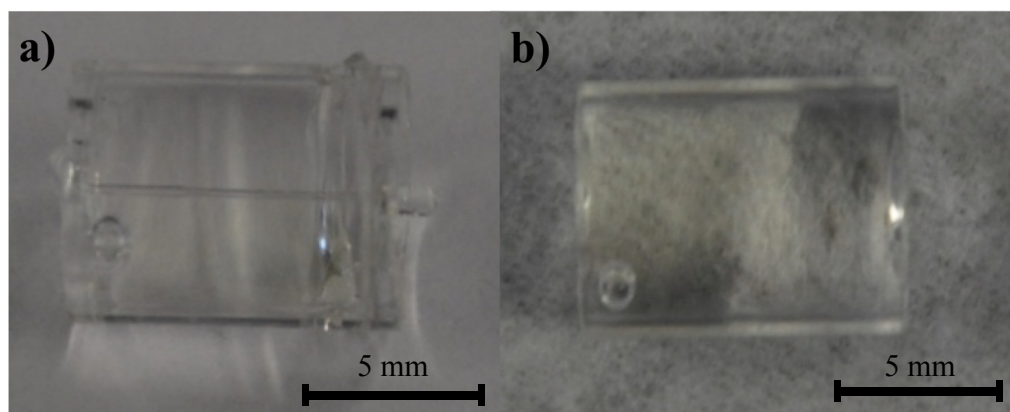


**Figure 71:** Hydrogel-filled tube (L = 10 mm; ID = 5 mm;  $M_n(\text{HA}) = 100$  kDa;  $\beta(\text{HA}) = 15$  mg/mL; TG = 0.57; gels synthesized in TRIS/BSS ( $c(\text{TRIS}) = 0.4$  mol/l; pH = 8.5)) with a channel created by the mechanical method directly after sample preparation was finished (a) and after 48 hours of incubation in BSS (b). There was no visual indication of the presence of the channel after the swelling in BSS.

## 2. Results & Discussion

Samples made with this method were subjected to HPA measurements. There was still the issue of hydrogels being ejected from the tubes at relatively low pressures (See Figure 69a). Nonetheless, pressure regulation of hydrogel-filled tubes with channels made by the physical method could be demonstrated by HPA (Figure 72).

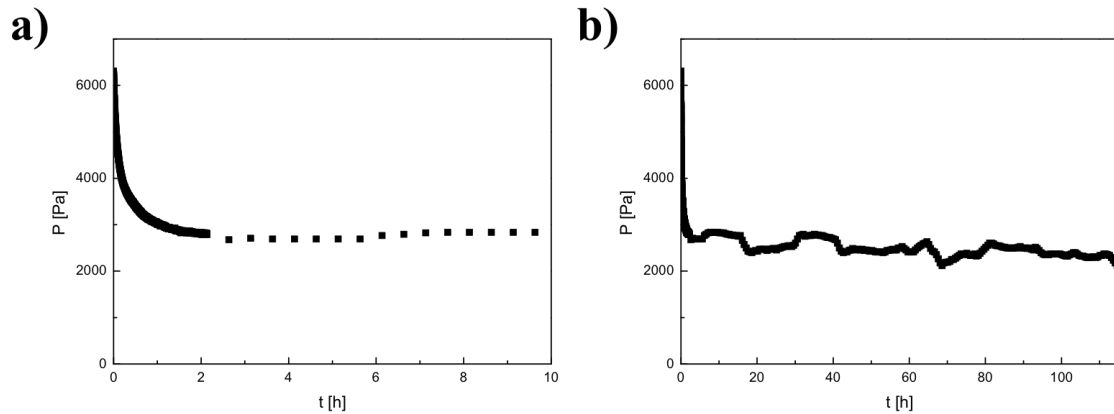


**Figure 72:** HPA measurement of a hydrogel-filled tube (ID = 5 mm) with channels formed using the small glass fibers (diameter = 0.1 mm). The pressure dropped to an average level of 2500 +/- 200 Pa after 2 hours (a) with long-term variations (b) mostly originating from pressure fluctuations within the lab.

At a hydrostatic pressure of >6000 Pa, a slow liquid flow was detected that reduced the pressure to 2500 +/- 200 Pa, where it remained constant over the next 10 hours (Figure 72a). Long-term measurements (Figure 72b) showed fluctuations of the pressure, which was attributed to changes in the air pressure within the lab affecting the balance. Future improvements therefore might be to conduct these measurements in an environment without environmental pressure fluctuations. Nonetheless, the results demonstrated a general ability of hydrogel-filled tubes created with the physical method for regulating external pressures.

### 2.5.3. Summary and conclusion

In this section, the mechanism of the ability of hydrogel-filled tubes for pressure regulation was investigated (Section 2.5.1). Reactions of glass tubes filled with fluorescent hydrogels made from HS-FA-HA when exposed to elevated pressures of fluorescent solutions (Figure 63) and BSS (Figure 65) were observed. Water flow through the samples was enabled by the presence of small channels running coaxially through the tubes. Furthermore the presence of these channels only when samples were subjected to elevated pressures was demonstrated (Figure 65). From these findings, a theory for the mechanism of the pressure-regulatory properties of the gel-filled tubes was proposed (Figure 66). Hydrogels within tubes possess a flaw in the form of a channel, which in its natural state is closed due to hydrophilic interactions of the hydrogels. When a certain threshold for an external liquid pressure is reached forces exerted on the hydrogel open the channel, allowing for passage of liquid. The process is reversible and the channel closes when the elastic counterforces of the hydrogel surpass the external forces enacted by the pressurized liquid.

Furthermore, a few basic experiments were conducted for artificially creating these channels within the hydrogels (Section 2.5.2). Two potential methods have been explored to achieve this goal. The optical method used a laser to “burn” channels into hydrogel-filled tubes and the physical method inserted small glass fibers coaxially into the tubes prior to gel formation (Figure 67). Creating channels within gel-filled tubes (Figure 68 and Figure 71) and enabling them to regulate external liquid pressures was successfully demonstrated using HPA measurements (Figure 69 and Figure 72). The results in this chapter show, that it is generally possible to create HA hydrogel filled tubes with the potential to regulate the intraocular pressures with these methods. The concept for creating implants with the ability for treating glaucoma by regulating intraocular pressures was thereby proven.

### 3. Summary and Outlook

#### 3.1.1. Summary and Discussion

The aim of this thesis was the development of a new type of medical implant for glaucoma therapy by grafting hyaluronan hydrogels on outer and inner surfaces of titanium tubes. The main idea was, that a hydrogel on outer surfaces, with a proper selection of parameters, would be able to facilitate cell adhesion and improve biocompatibility. Hydrogels on implant's interiors would be able to prevent migration of cells to their insides and clogging of the implant. Furthermore they act as valves to regulate intraocular pressure, which is the main aspect of a successful glaucoma therapy.<sup>1</sup> In order to fulfill these goals a number of steps have been undertaken for developing methods to create small tubes with their outer surfaces and interiors modified by hyaluronan hydrogels. They performed as model implants for future research. All methods have been developed in respect to a potential industrial manufacturing process of these implants, where further requirements concerning a possible simplicity, low costs and low hazardousness of the production steps have to be taken into account. .

#### Synthesis of starting materials

The first part of this thesis was concerned with synthesizing starting materials for creating hydrogels made from hyaluronic acid (Section 2.1). Modification of HA with thiols (HS-HA) by a peptide coupling reaction was adapted from Shu et al.<sup>101</sup> and successfully implemented. Degrees of substitution with thiols (thiolation grade) between 0.2 to 0.6 (n/n) were achieved by varying reaction times (10 min – 2 h). Furthermore, by examining HA with different molecular masses ( $M_n = 10$  kDa, 60 kDa and 100 kDa), a size dependency of thiolation grades was revealed (Figure 21) with smaller size HA resulting in smaller amounts of active thiols. There are some speculations about reasons for these findings. It was expected, assuming a diffusion-limited reaction<sup>209</sup>, that saccharide chains of a smaller size would be more mobile and therefore react quicker than larger size counterparts. But since secondary and tertiary structures of hyaluronan in watery solutions are diverse, complex and not fully understood<sup>121</sup> a possible reason might be a higher amount of intramolecular interactions of smaller-size HA. This may have resulted in a tighter structure (random coil etc.) and blocking access to reaction sites. Larger size hyaluronan on the other hand might form more intermolecular interactions, thereby creating more loose and mobile tertiary structures with more access to its reaction sites. But as already mentioned, this is so far speculation and with deeper understanding of hyaluronan structures in solutions, an answer might be found in the future. Still, thiolation grades were comparable to results published by Shu et al.<sup>102</sup>, where modification of larger HA ( $M_n = 120$  kDa) resulted in higher values for thiolation grades compared to polysaccharides examined in this thesis.

In addition to the modification with thiol groups, fluorescent labeling of hyaluronan with fluoresceinamine (FA) was established (Section 2.1.1). This was achieved by adapting a NHS/EDC mediated peptide coupling reaction between amines of FA and carboxyl functions of hyaluronan similar as described in by Ogamo et al. and Belder et al.<sup>186,210</sup>

### 3. Summary and Outlook

---

However the method was modified with an exclusion of organic solvents and only performed in watery solutions with parameters adapted from Sehgal et al.<sup>189</sup> to improve the adaptability for potential industrial applications. In order to change hydrogel properties ( $M_n$ , hydrophilicity etc.) as little as possible synthesis parameters of FA-HA were selected for achieving low degrees of substitution (0.006 – 0.012 (n/n)). These numbers were comparable to the commonly used method developed by Ogamo et al.<sup>186</sup> but without using organic solvents.

In a next step, both methods for modifying hyaluronan with thiols and fluorescent labels were combined to create hyaluronan that simultaneously formed hydrogels and had fluorescent properties (Section 2.1.3). Since both reactions were competing for the same active sites of hyaluronan, the sequence was developed in a way to allow reproducing the grade of modification with thiols (thiolation grade, TG) (Figure 22). It was shown that the additional modification with FA did not have an impact on thiolation grades when using this sequence (Figure 25). Thiolated and fluorescently labeled hyaluronan (HS-FA-HA) was subsequently used to analyze their immobilization to glass and titanium surfaces (Section 2.2.3). Furthermore, hydrogels made from HS-FA-HA had fluorescent properties (Figure 38), which were used for analyzing an immobilization of these hydrogels into small tubes (Section 2.2.3) and their reaction to external liquid pressures (Section 2.5.1). These fluorescent HA hydrogels were already very useful for the experiments conducted in this thesis. In the future they may also find alternative uses in other areas of research, for example analyzing enzymatic degradation<sup>190</sup>, cellular uptake<sup>188</sup> and other applications of hyaluronan hydrogels as biomaterials<sup>211</sup>. Especially their non-toxicity in addition to their inexpensiveness makes them a more probable candidate than for example quantum nanodots.<sup>212</sup>

In conclusion, the methods for the synthesis of starting materials to create (fluorescent) hydrogels have been well established and should also be sufficient for an industrial production because of inexpensive starting materials, scalability of the involved reactions and minimal use of harmful materials. By using different reactions times it was easily possible to modulate thiolation grades for potentially creating hydrogels with different crosslinking densities and properties<sup>176</sup> and manufacturing hydrogel-modified implants with the required abilities for glaucoma treatment.

#### **Immobilization of hyaluronan hydrogels on glass and titanium surfaces**

The next step, after synthesizing starting materials, was developing protocols to crosslink HS-HA into hydrogels and immobilize them on surfaces of model glaucoma implants. As outlined before (Section 1.6), a Thiol-Michael Addition between HS-HA and acrylamides was adapted from literature (Section 2.3.1).<sup>101,176</sup> The main modification was implementing a buffer to enable a better control of the pH in small volumes. N,N'-Methylenebisacrylamide (MBAA) was used as model crosslinker to allow longer handling times for modifying tubes with hydrogels (Section 2.2.3). The other crosslinker tested was poly(ethyleneglycol) bis(acrylamide) (PEGDA), which was not suitable since crosslinking occurred too quickly (< 5 min) (Figure 36).

### 3. Summary and Outlook

---

For immobilizing hydrogels, the proposed method (Section 1.6) of grafting epoxide groups to glass and titanium surfaces with subsequent hydrogel formation and immobilization in one step was successfully implemented. In order to modify test surfaces with these reactive groups a reaction between surface-bound hydroxides with silanes was selected.<sup>173</sup>

To that end protocols involving the surface hydroxylation/cleaning with a commercially available basic cleaning solution (Extran MA01) followed by incubation in silane/toluene solutions using (3-Glycidyloxypropyl)tri-methoxysilane (GPS) (Section 2.2.1) was implemented. Other surface activations, such as plasma<sup>173</sup> or piranha solution<sup>197</sup>, had the disadvantages that they were potentially dangerous (piranha solution) or required a more expensive setup (plasma). Additionally they did not guarantee homogeneous surface modification for small tubes due to either a partial shielding of the tube's interiors against reactive species (plasma) or bubble formation (piranha solution). Applying Extran probably resulted in a lower amount of hydroxyl groups on the surfaces, a lower number of epoxides attached and a less powerful immobilization. However, it was an inexpensive and almost non-hazardous method to activate samples and lowered the risk of accidents as well as production costs. Furthermore subsequent measurements showed hydrogels immobilized within model implants were able to resist pressures usually encountered within the glaucomatous eye ( $< 10000 \text{ Pa}$ )<sup>3</sup> (Figure 50 and Figure 51), thereby validating the use of Extra. In the same manner using toluene/silane solutions for silanization guaranteed homogeneous exposure of all surfaces of the small tubes to the silanes. While toluene is an organic solvent replacing it by water was not possible for further improving the non-hazardousness of the method, since silanes, as well as the epoxide would be hydrolyzed in such an environment. Nonetheless, it was shown, that the methods established in this thesis to form and covalently immobilize hyaluronan hydrogels selectively on the outer and inner surfaces of small glass and titanium tubes in one step was possible (Section 2.2.3 and Section 2.4.2 for the interior of titanium tubes). This provided a cheap and efficient way for selectively grafting hydrogels to different parts of potential glaucoma stents opposed to other methods that would require multiple steps (Section 1.6). The concept allows creating the hydrogels on the inside and the outside of the stents with different properties to manipulate cell adhesion (See Section 1.1) on an industrial scale.

#### **The pressure behavior of HA hydrogel filled tubes**

The main feature of using implants for glaucoma therapy is their ability to regulate elevated intraocular pressures<sup>9,19</sup>. One goal of this thesis was using hyaluronan hydrogels to act as pressure-sensitive valves for reducing pressures within a glaucomatous eye without draining too much liquid, thereby preventing hypotony<sup>32</sup>. For evaluating the capabilities of hydrogel-filled model implants to perform this function it was necessary to see how they would react when exposed to external liquid pressures.

Before performing experiments concerning this issue, a number of basic swelling measurements were conducted for comparing hydrogels immobilized within glass tubes to non-immobilized "unobstructed" gels (Section 2.4.1).

### 3. Summary and Outlook

---

Both types showed differing swelling rates with unobstructed gels initially absorbing water at a higher rate up to 62 times their calculated dry masses in the first 16 hours. Over the following 270 hours they contracted to a steady state with only 45 times their calculated dry masses (Figure 42). This initial volume expansion followed by deswelling was linked to the presence of TRIS residues from the sample preparation. Their presence in and subsequent diffusion out of the hydrogels during swelling influenced the osmotic forces<sup>109</sup> over time (Figure 43).

This caused initial swelling followed by deswelling of unobstructed hydrogels. Instead of following the same behavior, constrained gels swelled to 55 times their calculated dry masses within 45 hours where they remained without significant changes for the rest of the observed duration. Limited initial swelling was inhibited by the physical barriers of the glass walls. Also covalent immobilization of hydrogels to these surfaces prevented hydrogel contraction afterwards. As a result deswelling of constrained gels was not possible, retaining higher volumes and amounts of liquid compared to the unobstructed samples. The mechanism was not fully explained though and further experiments, potentially using fluorescent probes to evaluate the pore size and diffusion rates within unobstructed and constrained hydrogels<sup>92</sup>, are necessary in the future. The in-depth analysis of this behavior was beyond the scope of this thesis and the HS-HA/MBAA hydrogels were only model systems. Therefore any such attempts were foregone until a proper crosslinker for influencing cell adhesion would be selected.

For evaluating hydrogel-filled model stent's reactions to external liquid pressures, two experimental setups were designed (Sections 2.4.2 and 2.4.3). In the "Continuous pressure application" (CPA) method, hydrogels were subjected to steadily increasing forces from liquid within a syringe (Figure 44). This method allowed determining the pressure levels where covalent immobilization of the hydrogels within the tubes failed, resulting in their removal (= breaking point) (Figure 49). Breaking points of immobilized hydrogels in small tubes (ID = 0.5 mm; L = 10 mm) ( $> 100000$  Pa; (Figure 50)) were far above levels encountered in the glaucomatous eye ( $< 10000$  Pa)<sup>3</sup>, verifying the potential applicability for manufacturing glaucoma implants. Also a number of hydrogel-filled tubes enabled controlled liquid flow when forces from the liquid exceeded certain thresholds (0.12 MPa up to 0.25 MPa depending on sample parameters) (Figure 53). Preliminary experiments further illustrated, that the resistance of the model implants was dependent on their parameters such as length (Figure 53) and the concentration of hyaluronan used to synthesize the hydrogels (Figure 54). An interesting effect was observed when several repeated CPA measurements were performed on a single sample. Similar to previous measurements the pressure first rose to a peak value (0.23 – 0.27 MPa) before declining into a steady state (0.1 MPa), while on subsequent measurements it was achieved directly (Figure 54a). This effect was recreated 24h later (Figure 54b), hinting at a reversible change within the hydrogel. At first unexplained its mechanism was later related to the presence of small channels within the hydrogel-filled tubes (Section 2.5.1) discussed further down.

### 3. Summary and Outlook

---

Additionally the “hydrostatic pressure application” (HPA) method was established, which used a setup to expose hydrogel-filled tubes to hydrostatic pressures (Figure 59), which reflected the eye’s environment in a more realistic way than the closed systems of the CPA setup. HPA was successfully used for showing the potential ability of HA gel modified tubes acting as pressure-sensitive valves. A flow of liquid through these samples was only observed when pressure levels were above certain thresholds (Figure 60). However, pressures where liquid flow stopped (ca. 10000 Pa) were too high for target values in glaucoma therapy (2100<sup>3</sup>). Therefore, further optimizations were required to adjust the implant’s pressure regulation accordingly with HPA being an effective method for achieving these optimizations in the future. The method was further utilized later for examining the applicability of processes for reproducibly generating this pressure regulatory effect (Section 2.5.2).

CPA and HPA confirmed the general functionality of the model-implants for potentially regulating pressure of glaucomatous eyes. More research will be required in the future to optimize the implants’ parameters including tube size and gel properties until the required intraocular pressure of 2100 Pa can be achieved. The CPA and HPA methods developed in this thesis are complementary methods that can be used for the necessary follow up studies. However, to also provide enough samples for such optimization the reproducibility of stents had to be improved first. A first step in this direction was understanding the underlying mechanism of liquid flow, which was the main focus of the rest of this thesis.

#### **Exploration of the liquid flow mechanism through hydrogel-filled tubes and physical creation of channels**

While the general potential for generating pressure-induced liquid flow with hydrogel-filled tubes was shown, further understanding the mechanisms of this process was required. Optimizing the yields of functional samples for a more efficient data collection and potential mass production was also necessary before further characterizations were feasible. To that end, an experimental setup was created for monitoring liquid flow through hydrogel-filled tubes on a microscopic level. It utilized the fluorescent properties of hydrogels created from HS-FA-HA by monitoring their behavior within small glass tubes with a microscope (Section 2.5.1, Figure 59). Measurements with fluorescent solutions (Figure 63) and BSS (Figure 65) exposed the existence of small channels conducting liquid flow observed during CPA and HPA previously. These channels were only present when pressure was applied to the samples (Figure 65b/d) and were confirmed for all HA-modified tubes allowing pressure-induced liquid flow. A theory was proposed, that these channels naturally exist in a closed state due to interactions between and elastic forces of the hydrogel interfaces on their inside (Figure 66a). The channels opened when the external pressure exceeded a certain threshold to overcome these forces, enabling passage of liquid. A steady state was achieved when the forces from external pressures were in balance with the elastic counterforces from the hydrogels (Figure 66c). When pressure dropped low enough due to gels relaxing and their elastic counterforces closed the channels, thereby stopping liquid flow.

### 3. Summary and Outlook

---

This theory was supported by iterative opening and closing of these channels (Figure 65) via application and removal of external pressures. Those results hint at a reversible mechanism, most probably due to the viscoelastic properties of hydrogels<sup>113,207</sup> allowing for repeated opening and closing. This mechanism also explained the findings from CPA and HPA experiments. During CPA measurements, as mentioned before, pressures initially rose to a peak value (0.23-0.27 MPa) initiating liquid flow and subsequently declined to a steady state (ca. 0.1 MPa) (Figure 54). On subsequent rounds this peak was not observed and steady state was achieved immediately. This was explained by a residual pressure remaining in the closed system of the CPA setup preventing the hydrogels from fully relaxing and closing the channels. As a result subsequent measurements did not require additional forces to re-open the channels and induce flow, ultimately leading to the results shown in Figure 53. Similarly, the stop of liquid flow when pressures dropped to certain thresholds during HPA measurements on some samples (Figure 60) was explained by elastic counterforces of the hydrogels closing the channel.

In conclusion this theory supported all experimental results of the CPA and HPA measurements as well as the channels observed on a microscopic level. Future experiments on a macroscopic scale should be able to further confirm this theory. Alternatively distributing additional dyes, fluorescent micro-beads e.g. within the hydrogels or only in the channels to illustrate possible deformations should be possible as well.

Following this theory possibilities have been explored for creating these channels artificially and reproducibly (Section 2.5.2). Two concepts were tested: An optical method applied a CO<sub>2</sub> laser for burning channels into crosslinked hydrogels within tubes was designed (Figure 67a). And a mechanical method, where a small fiber was inserted coaxially into tube prior to gel formation (Figure 67b) was tested. Performing these modifications on previously small tubes (ID = 0.5 mm) would have required a more elaborate setup to align samples with the laser or fibers. Therefore both methods were tested on larger tubes (ID = 5 mm), where it was possible to perform the necessary experiments manually and with standard lab equipment.

For both setups, channels were generated within hydrogel-filled tubes (Figure 68, Figure 71). Subsequent HPA measurements showed their ability for regulating hydrostatic pressures of the water column in the capillary with final pressure levels at 2500-3000 Pa (Figure 69, Figure 72). Concluding from these results it was decided that these methods were good candidates for creating hydrogel-enhanced glaucoma stents with the ability to regulate intraocular pressure of glaucomatous eyes. More research is required in the future however, since experiments regarding an artificial channel creation in this thesis were only conducted with "large" (ID = 5 mm) tubes. Therefore, in a next step, possibilities for miniaturization have to be explored, since glaucoma implants are usually of a much smaller size (<1 mm OD).<sup>35,213</sup>

To that end both designs show a number of advantages and potential problems. The optical method is probably very suitable for the miniaturization itself, since these days lasers of nanoscale sizes exist<sup>214</sup> that could be adapted for creating smaller implants.

### 3. Summary and Outlook

---

However, preliminary results in this thesis illustrated, that channels would often not form homogeneously (Figure 68a). As a result many parameters (Laser type, laser power, placement of focus area, movement speed, etc.) influencing this process have to be optimized for reproducing samples with the same properties. The physical method would be easier in terms of parameter optimization since channel sizes only depend on the thickness of utilized fibers. The downside is a dependency on using small-scale materials and their handling. Fibers smaller than  $< 0.1$  mm in diameter have to be aligned coaxially within small tubes (OD = 0.6 mm and less)<sup>213</sup> For this, utilizing robotics is the most probable solution. Both methods, however, might simplify optimizing the pressure regulatory abilities of the implants, without overly adjusting hydrogel parameters. Instead varying the channels' diameters might be sufficient to adjust implants for lowering intraocular pressure to normal levels (2100 Pa)<sup>3</sup>. Still, more research is necessary to examine, which of these methods is more reliable and cost-effective for a mass production of implants and how to conduct an optimal miniaturization.

#### 3.2. Outlook

The results of this thesis, comprising most importantly starting material synthesis, the immobilization of HA hydrogels to glass and titanium tubes and pressure related experiments on these model implants, are fundamental steps towards a new type of implant for glaucoma treatment. Further research has to be conducted for designing and optimizing hydrogel-modified model stents to employ them in medical applications and production in an industrial scale. First crosslinkers for HA-hydrogel polymerization with the desired cell attachment regulating properties as described in Section 1.6 have to be found and tested. Promising candidates could be the desmosine-inspired crosslinkers developed by Hagel et al.<sup>176</sup> HA hydrogels created with these crosslinkers have to be further characterized concerning swelling behavior, elastic modulus, cell attachment and long-term stability. Some basic data concerning swelling has already been shown in this thesis. Still, a more thorough exploration of the swelling behavior in respect to the finally used crosslinker, crosslinking density, hyaluronan size and HA concentrations prior to crosslinking have to be conducted for a better understanding of the system. Closely related to this topic is the elastic modulus of the crosslinked networks depending on the same parameters than the swelling.<sup>176</sup> Elasticity is of importance since cell adhesion behavior is dependent on the target surfaces stiffness.<sup>215</sup> It is also of interest to investigate a correlation between swelling, elastic modulus and the pressure resistance behaviors presented in Sections 2.4 and 2.5. Even more interesting is the influence of elastic modulus on the channel opening and closing mechanism described in Section 2.5.1. More specifically, how changes of the hydrogel parameters impact swelling, elasticity and in turn pressure resistance. In addition cell experiments have to be performed with the HA hydrogels for finding compositions with cell adhesive properties on the outside of the tubes and cell repellent properties on the inside. Gels in the tubes' interiors are the challenging part since they have to perform as valve and as cell repellent at the same time.

### 3. Summary and Outlook

---

Furthermore long-term stability experiments with model-implants modified with HA gels fulfilling the said requirements need to be conducted. Specifically, whether the hydrogels would be enzymatically degraded, which was something the fluorescent hydrogels established in this thesis could be used for. It would also be important to examine, if the immobilization of the gels to the tubes' surfaces deteriorates and whether their pressure regulatory abilities change over time. Since glaucoma implants need to be in use for an extended period of time, the long-term stability has to be tested probably over the course of several years.

Another very important area for future research is optimizing the methods established here for generating smaller-size implants. Their general applicability, as presented in this thesis, for creating the envisioned glaucoma implants (See Section 1.6) has been verified. However, they were so far only performed on model systems, which were too large for the actual implantation into the human eye. Especially the physical insertion of channels within hydrogels discussed in Section 2.5.2 requires further optimization of the methods for applying them to smaller tubes. For "burning" channels into hydrogels a thinner laser-beam has to be selected and systems to exactly align laser and sample need to be established, probably by utilizing robotics. Afterwards optimizing parameters (laser power, etc.) is necessary for reliably creating channels with defined sizes and properties. The setup for creating these channels with a microfiber also needs to be improved for exactly aligning them coaxially within tubes.

A solution will probably be found again in the field of robotics, where manipulations on such small scales are not an issue. In addition, setups need to be developed for establishing large-scale industrial manufacturing processes.

The *in vivo* performance of the new implants also needs to be explored. To that end animal tests will be necessary for confirming a potential non-hazardousness of the new implants *in vivo*. Furthermore the properties of implants concerning an improved biocompatibility as well as the pressure regulation envisioned in Section 1.1 need to be examined, especially concerning inflammatory responses. Finally clinical trials have to be conducted for showing an improvement of the glaucoma therapy with HA gel modified implants compared to other established designs<sup>43</sup> and treatments.<sup>9,24,28</sup> Specifically whether occurrence of bleb fibrosis is reduced by using these new types of hydrogel-modified implants.

Although much more research will have to be done in the future before a commercial product can be realized, the fundamental methods and steps for the final objective, a new superior implant for the treatment of glaucoma, have been established in this thesis. This brought the vision of an improved glaucoma therapy for millions of affected people worldwide one step closer to reality.

### 4. Materials and Methods

#### 4.1. Modification of Hyaluronan

Hyaluronic acid was functionalized with thiol groups for immobilization and crosslinking as well as with fluorescein for visualization.

##### 4.1.1. Materials

Hyaluronic acid of different sizes ( $M_n = 10$  kDa; 60 kDa; 100 kDa) was bought from Lifecore Biomedical (Chaska, U.S.A.). N-(3-Dimethylaminopropyl)-N'-ethylcarbodiimide hydrochloride (EDC; CAS: 25952-53-8), deuterium dioxide ( $D_2O$ ; "100%"; CAS: 7789-20-0), N-Hydroxysuccinimide (NHS; CAS: 6066-82-6), 3,3'-Dithiodipropionic acid (DTPA; CAS: 25952-53-8), (4-(2-hydroxyethyl)-1-piperazineethanesulfonic acid) (HEPES; CAS: 7365-45-9) and fluoresceinamine, isomer I (FA; CAS: 3326-34-9) were bought from Sigma Aldrich (St. Louis, U.S.A.). Ethanol (EtOH; p.a.; CAS: 64-17-5), sulfuric acid ( $H_2SO_4$ ; 95-98%, CAS: 7664-93-9), sodium chloride (NaCl; p.a.; CAS: 7647-14-5), magnesium sulfate ( $MgSO_4$ ; p.a.; CAS: 7487-88-9) and hydrochloric acid (HCl; 37%; CAS: 7647-01-0) were purchased from Carl Roth (Karlsruhe, Germany). Sodium hydroxide solution (NaOH; 6 mol/L; CAS: 1310-73-2) was obtained from Merck (Schwalbach, Germany). Low size, low polydispersity HA ( $M_n = 60$  kDa) was purchased from Lifecore Biomedical (Chaska, U.S.A.). 5,5'-Dithiobis(2-nitro-benzoic acid) (DTNB) was purchased from Serva Electrophoresis GmbH (Heidelberg, Germany). 1,4-dithiothreitol (DTT; CAS: 3483-12-3) was purchased from biomol (Hamburg, Germany). For lyophilization, a freeze dryer (model: P8K-E-85-4) from Dieter Piatkowski Forschungsgeräte (Munich, Germany) was used.  $^1H$ -NMR spectra were obtained using a Bruker Spectrospin 300 Ultrashield (Bruker, Billerica, U.S.A.). Absorbance measurements were performed with a Tecan infinite M200 (Tecan, Männedorf, Switzerland). The ultrasonicator (Bandelin Sonorex; 60/240 W; 35 kHz) was obtained from Bandelin electronic (Berlin, Germany).

##### 4.1.2. Modification of hyaluronan with thiol groups

###### *Synthesis of 3,3'-dithiobis(propanoic hydrazide)*

The protocol was adapted and modified according to a publication of Vercruyssen.<sup>190</sup> 10 g (48 mmol) of 3,3'-dithiobis(propanoic acid) (DTPS) were dissolved in 100 mL of EtOH, a few drops of concentrated  $H_2SO_4$  were added, and the mixture heated under reflux and oxygen exclusion. The solution was concentrated to 40 ml under reduced pressure (40° C; 100-150 mbar) and transferred to a separatory funnel by the addition of 120 ml ethyl acetate. Two washing steps of the organic phase were conducted using first 60 ml ddH<sub>2</sub>O followed by 60 mL of a saturated NaCl solution. After a drying step using  $MgSO_4$ , the solvent was removed under reduced pressure (40° C; 240 mbar) yielding the oily propanoic ester intermediate product. The ester was re-dissolved in 30 ml EtOH and added drop-wise to a stirred solution of 30 ml hydrazide hydrate in 20 ml EtOH.

## 4. Materials and Methods

---

The mixture was heated under reflux for 6 hours, after which the propanoic ester was fully consumed, as determined by thin-layer chromatography. A crystallization of 3,3'-dithiobis(propanoic hydrazide) DTPH started at room temperature and was completed at 4° C over night. The solvent was drained and the raw product was washed with hexane and dried under vacuum at 50° C for several days, yielding a white crystalline solid. Success of the reaction was determined via <sup>1</sup>H-NMR (D<sub>2</sub>O) (see Section 6.2).

### *Modification of hyaluronan with 3,3'-dithiobis(propanoic hydrazide)*

The protocol was adapted and modified according to a publication of Shu et al.<sup>101</sup> 1 g (2.5 mmol) HA was dissolved in 100 ml ddH<sub>2</sub>O ( $\beta = 10$  mg/ml) and the pH adjusted to 4.75. 1.33 g DTPH were added and, after complete dissolution was achieved by prolonged stirring, the reaction was initiated by the addition of 960 mg EDC. The reaction was kept at room temperature for 10 min to 2 h depending on the desired thiolation grade while the pH was constantly re-adjusted to 4.75 with HCl (1 mol/l). After the required time the reaction was stopped by elevating the pH to 7.0. The mixture was O<sub>2</sub>-purged with Argon (30 min) and 5 g DTT were added before adjusting the pH to 8.5, followed by stirring for 24 h at room temperature in sealed round-bottomed flasks. The pH was lowered to 3.5 and the solution dialyzed with HCl (pH = 3.5) until a sample of the dialysis buffer remained colorless after the addition of 1 mL to 3 mL of a basic (pH = 8.5) DTNB solution ( $\beta = 1$  mg/ml). The purified product was frozen and lyophilized, yielding thiolated hyaluronan (HS-HA) with a colorless solid foam-like appearance. Products were stored at -20° C in parafilm-sealed falcon tubes.

### *Evaluation of the reaction time dependency of the thiolation grade*

These experiments were conducted to gain information on the thiolation grade in relation to different reaction times. 1 g (2.5 mmol) HA was dissolved in 100 ml ddH<sub>2</sub>O ( $\beta = 10$  mg/ml) and the pH was adjusted to 4.75. 1.33 g DTPH were added and, after complete dissolution was achieved by prolonged stirring, the reaction was initiated by the addition of 960 mg EDC. The pH was constantly re-adjusted to 4.75 with HCl (1 mol/l). At set time intervals (10 min; 30 min; 60 min), 25 mL samples were drawn from the mixture and transferred into 50 mL round-bottomed flasks where the reaction was stopped by an increase of the pH to 7.0 using NaOH (6 mol/l). The reaction of the remaining fraction was stopped after 120 min by raising the pH 7.0 using NaOH (6 mol/l). All fractions were oxygen purged for 30 min with argon before 1.25 g DTT were added and the pH adjusted to 8.5. Disulfide reduction commenced for 24 hours at room temperature in sealed round-bottomed flasks. The pH was lowered to 3.5 and the solution dialyzed with HCl (pH = 3.5) until a sample of the dialysis buffer remained colorless after the addition of 1 mL to 3 mL of a basic (pH = 8.5) DTNB solution ( $\beta(\text{DTNB}) = 1$  mg/ml). The products were four HS-HA fractions with different grades of thiolation.

## 4. Materials and Methods

---

### *Analytical methods*

General success of the HA modification with thiols was determined with  $^1\text{H-NMR}$  while the grade of thiolation was determined with a modified Ellman's test. For the NMR measurements, 3-5 mg of the thiolated HA were dissolved in  $\text{D}_2\text{O}$  and spectra recorded at 300 MHz.

For the Ellman's test, a serial dilution of cysteine in HCl ( $\beta(\text{Cysteine}) = 0.015 \text{ mg/mL}$ - $0.15 \text{ mg/mL}$ ;  $\text{pH} = 3.5$ ) and a sample solution of HS-HA in HCl ( $\beta(\text{HA}) = 5\text{-}10 \text{ mg/mL}$ ;  $\text{pH} = 3.5$ ) were prepared.  $50 \mu\text{L}$  of the sample and serial dilution were distributed in a 96-well plate (8 wells for each dilution and sample) and  $150 \mu\text{L}$  of a mixture consisting of 3 mL DTNB in a basic solution ( $\beta(\text{DTNB}) = 1 \text{ mg/mL}$ ;  $\text{pH} = 8\text{-}10$ ), 15 ml  $\text{ddH}_2\text{O}$  and 2 ml TRIS solution ( $c(\text{TRIS}) = 1 \text{ mol/L}$ ;  $\text{pH} = 8.5$ ) were added. After a 10 min incubation at room temperature, the absorbance in each well at  $\lambda = 412 \text{ nm}$  was measured. The absorption of the serial dilution was plotted against the cysteine concentrations (= concentrations of  $-\text{SH}$  groups). A linear fit was performed using the commercially available "Origin" software and a linear equation calculated, which was subsequently used to calculate the amount of thiol groups in the sample solutions. These values were subsequently used to calculate the total mass of thiopropionic hydrazide groups attached to the HS-HA using the formula

$$m_{\text{TPH}} = n_{\text{TPH}} * M_{\text{TPH}} = n_{\text{SH}} * M_{\text{TPH}} \quad \text{Equation 4:1}$$

with  $m_{\text{TPH}}$  as the total mass of TPH,  $n_{\text{TPH}}$  the amount of TPH,  $M_{\text{TPH}}$  the molar mass of TPH and  $n_{\text{SH}}$  the amount of thiols in the sample. The total mass of HA was calculated after the formula

$$m_{\text{HA}} = m_0 - m_{\text{TPH}} \quad \text{Equation 4:2}$$

with  $m_{\text{HA}}$  as the mass of the hyaluronan fraction and  $m_0$  the total masses of the HS-HA sample. From  $m_{\text{HA}}$  the amount of HA in the sample ( $n_{\text{HA}}$ ) was calculated. Finally the thiolation grade (TG) was determined with

$$\text{TG} = \frac{n_{\text{SH}}}{n_{\text{HA}}} \quad \text{Equation 4:3}$$

The Ellman's test was performed at least three times on each sample to determine the average thiolation grade with the standard deviation forming the error bars.

### 4.1.3. Modification of hyaluronan with fluorescent markers

#### *Binding of Fluoresceinamine to HA*

640 mg (1.8 mmol) of FA was dissolved in 40-50 ml of ddH<sub>2</sub>O by the drop-wise addition of NaOH (6 mol/l) followed by alternating ultrasonication (240 W; 35 kHz) and manual shaking until it fully dissolved. The mixture was added to a solution of 500 mg HA (1.3 mmol) in 100 ml HEPES buffer (c(HEPES) = 0.1 mol/l; pH = 7.0). After stirring for 30 min, the reaction was initiated by the addition of 656 mg (4.2 mmol) EDC and 1 g NHS (8.7 mM) and maintained for 5 hours. NaOH (6 mol/L) was added drop-wise to the resulting viscous and cloudy solution until it cleared. Dialysis was performed against diluted NaOH (pH = 10.0), with frequent changes of the dialysis medium until it remained colorless for an extended period of time. The product solution was frozen and lyophilized to yield a solid yellow foam-like substance of fluorescein-marked hyaluronan (FA-HA).

#### *Analytical methods*

Reaction success was determined visually by confirming the yellow color of the product. In order to determine the degree of substitution (n(FA)/n(disaccharide units)) a serial dilution of FA ( $\beta(\text{FA}) = 0.007\text{-}0.07$  mg/ml) in borate buffer (c(borate) = 0.1 M; pH = 8.5) and a sample solution of FA-HA ( $\beta(\text{FA-HA}) = 2.5$  mg/ml) were distributed in a 96-well plate (8 wells each). The absorbances of the serial dilution and samples were measured at  $\lambda = 440$  nm, and the values of the serial dilution plotted against their concentrations using the commercially available “Origin” software. The linear fit was obtained and the linear equation calculated using the same software, which was subsequently used to gain the total amount of FA and their respective total masses in the sample by using their measured absorptions. The total masses of HA and amounts were gained using the formula

$$n_{\text{HA}} = \frac{m_0 - m_{\text{FA}}}{M_{\text{HA}}} \quad \text{Equation 4:4}$$

with  $n_{\text{HA}}$  the total amount of HA,  $m_{\text{FA}}$  the total mass of FA and  $m_0$  the total combined masses in the sample and  $M_{\text{HA}}$  the molar mass of HA. Subsequently the degree of substitution was determined by

$$\text{d. s.} = \frac{n_{\text{FA}}}{n_{\text{HA}}} \quad \text{Equation 4:5}$$

with d.s. as the degree of substitution,  $n_{\text{FA}}$  the total amount of FA gained from the experimental values and the linear equation and  $n_{\text{HA}}$  the total amount of HA obtained from Equation 4:4.

### 4.1.4. Combined modification of hyaluronan with fluorescein and thiol groups

1 g (2.5 mmol) HA were dissolved in 100 ml MilliQ water ( $\beta = 10$  mg/ml) and the pH adjusted to 4.75. 1.33 g DTPH were then added, and after complete dissolution by prolonged stirring, the reaction was initiated by the addition of 960 mg (5 mmol) EDC. It was kept at room temperature for 10 min to 2 hours depending on the desired thiolation grade while constantly re-adjusting the pH to 4.75 with HCl (1 mol/l). Afterwards, the reaction was stopped by raising the pH to 7.0 and the solution was dialyzed against distilled water. 2.38 g HEPES (10 mmol) were added, the pH re-adjusted to 7.0. 640 mg (1.8 mmol) FA were dissolved in 40-50 ml water by the drop-wise addition of NaOH (6 mol/l), ultra-sonication (240 W; 35 kHz) and manual shaking followed by addition to the HA solution. After stirring for 30 min, the reaction was started by the addition of 656 mg (4.2 mM) EDC and 1 g NHS (8.7 mM) and maintained for 5 hours. Concentrated NaOH (6 mol/l) was added drop wise to the resulting viscous and cloudy solution until it became clear (pH = 10-11). Dialysis was performed against NaOH (pH = 10), with frequent changes of the dialysis medium until it medium remained colorless for an extended period of time. The mixture was O<sub>2</sub>-purged with Argon (30 min) and 5 g DTT were added before adjusting the pH to 8.5, followed by stirring for 24 h at room temperature. The pH was then lowered to 3.5 and the solution dialyzed with diluted HCl (pH = 3.5) until a sample of the dialysis buffer remained colorless after the addition of a basic (pH = 8.5) DTNB solution ( $\beta(\text{DTNB}) = 1$  mg/ml). The purified product solution was frozen and lyophilized, resulting in the thiolated, fluorescently labeled hyaluronan (HS-FA-HA) with a solid yellow foam-like appearance. Products were stored at -20° C in parafilm-sealed falcon tubes.

For a comparison of the thiolation grade between HS-HA and HS-FA-HA the HA/DTPH mixture was split into two fractions. One fraction was further modified with FA following the protocol established in Section 4.1.3 to produce HS-FA-HA. The other fraction was further processed to HS-HA following the protocol established in Section 4.1.2. The protocols were scaled appropriately to accommodate the reduced amount of HA due to the fractioning.

#### *Analytical methods*

The methods described in sections 4.1.2 and 4.1.3 were applied to determine the thiolation grade and the degree of substitution of FA.

### 4.2. Immobilization of hyaluronan to glass and titanium surfaces

Surfaces of glass and titanium were silanized and fluorescently labeled hyaluronan covalently immobilized.

#### 4.2.1. Materials

Glass slides (18 x 18 mm) (Article number: 0657), were obtained from Carl Roth (Karlsruhe, Germany). Glass tubes (borosilicate, OD: 1 mm; ID: 0.5 mm; length: (2-20 mm) were manufactured at the glass workshop of the Max Planck Institute for Intelligent Systems, Stuttgart. Titanium tubes (ID: 0.3 mm; OD: 0.5 mm) were obtained from Euroflex GmbH (Pforzheim, Germany) and cut to 10 mm length by the workshop of the Max Planck Institute for Intelligent Systems, Stuttgart. The setup for the partial silanization of flat surfaces was manufactured by the precision mechanics workshop from the Max Planck Institute for Intelligent Systems in Stuttgart. Extran<sup>®</sup>MA 01 (Extran) alkaline solution was obtained from Merck (Schwalbach, Germany) as well as (3-Glycidyloxypropyl)trimethoxysilane (GPS), 3-(Aminopropyl)triethoxysilane (APTES) were bought from Sigma Aldrich (St. Louis, Germany). 1H,1H,2H,2H-Perfluorotrichlorosilane (PFS) obtained from abcr GmbH & Co. KG (Karlsruhe). A two-component dental glue (Picodent twinsil<sup>®</sup> speed 22) was obtained from Picodent (Wipperfurth, Germany). For contact angle measurements a Contact Angle System (OCA) from Dataphysics (Filderstadt, Germany) was used. The fluorescence measurements were performed on an Axiovert 200M with a 38 HE eGFP (Ex: 470/40 Em: 525/50) filterblock (Zeiss, Oberkochen, Germany). The ultrasonicator (Bandelin Sonorex; 60/240 W; 35 kHz) was obtained from Bandelin electronic (Berlin, Germany).

#### 4.2.2. Basic silanization protocol

Glass slides or titanium sheets were immersed in Extran for >2 h, rinsed in MilliQ water, dried in an N<sub>2</sub> stream and immersed in a 2% (v/v) solution of silane in toluene (99.9%) for 24 hours. The silanized samples were cleaned with two sonication steps (240 W, 35 kHz), toluene followed by EtOH, for 15 min each. The same protocol was applied for the silanization small (ID = 0.5 mm) and large (ID = 5 mm) tubes in the following sections. The only addition to this protocol was to avoid the formation of air bubbles on the tubes' interiors.

#### *Analytical methods*

Success of the silanization was determined by comparing the surface energies of unmodified and silane-modified samples. A serial dilution with different amounts of volume fractions  $\Phi_i$  of ethyleneglycol and ddH<sub>2</sub>O was prepared according to (Table 3).

## 4. Materials and Methods

**Table 3:** Serial dilution used for the determination of the surface energies of silanized surfaces.  $\Phi_W$  and  $\Phi_E$  denoted the volume fractions of water and ethyleneglycol respectively and  $\gamma_{LV}$  the liquid/surface tension according to Tsierkezos et al.<sup>200</sup>

$\Phi_W$	$\Phi_E$	$\gamma_{LV}$
0	1	49.15
0.6	0.4	54.97
0.9	0.1	60.69
1	0	72.58

The average contact angles of the water/ethyleneglycol mixtures were recorded on 10 different points of the surface of a silanized glass or titanium slide. This was achieved by manually placing a small drop on the surface with a syringe. Using the built-in camera an image of the drop's silhouette was taken and the contact angles on both sides of the drop determined by the accompanying program. From these two contact angles the median contact angle was calculated. For each sample ten drops were analyzed and the average median contact angle from all drops was determined. This process was repeated with all sample solutions of the serial dilution, with extensive rinsing first with EtOH (99%) and ddH<sub>2</sub>O to clean the sample surfaces in-between the measurements.

Data analysis was conducted after the simplified formula established from Balkenende et al.<sup>198</sup>

$$\cos\theta = -1 + \Phi 2 \sqrt{\frac{\gamma_{SV}}{\gamma_{LV}}} e^{-0,0001247(\gamma_{LV}-\gamma_{SV})^2} \quad \text{Equation 4:6}$$

with  $\theta$  being the contact angle,  $\gamma_{SV}$  the surface-vapor and  $\gamma_{LV}$  the liquid-vapor tensions. The exponential term was treated as being a constant 1 for simplification. By plotting  $\cos\theta$  against  $(\gamma_{LV})^{-0.5}$  using the "Origin" software followed by a linear fit with the y-axis intersection at -1 it was possible to calculate  $\gamma_{SV}$  from the slope. The absolute error of the slope was calculated by Origin from the fitting of the slope including the individual standard deviations of each data point.

## 4. Materials and Methods

### 4.2.3. Immobilization of hyaluronan on partially silanized flat surfaces

#### *Immobilization of HA*

HS-FA-HA was prepared as described in Section 4.1.4. Flat glass and titanium slides silanized with GPS were prepared following the basic protocol in Section 4.2.2. Partial silanization was achieved by the use of a “silanization chamber” that was constructed to modify 18mm x18 mm glass or titanium slides (Figure 73).

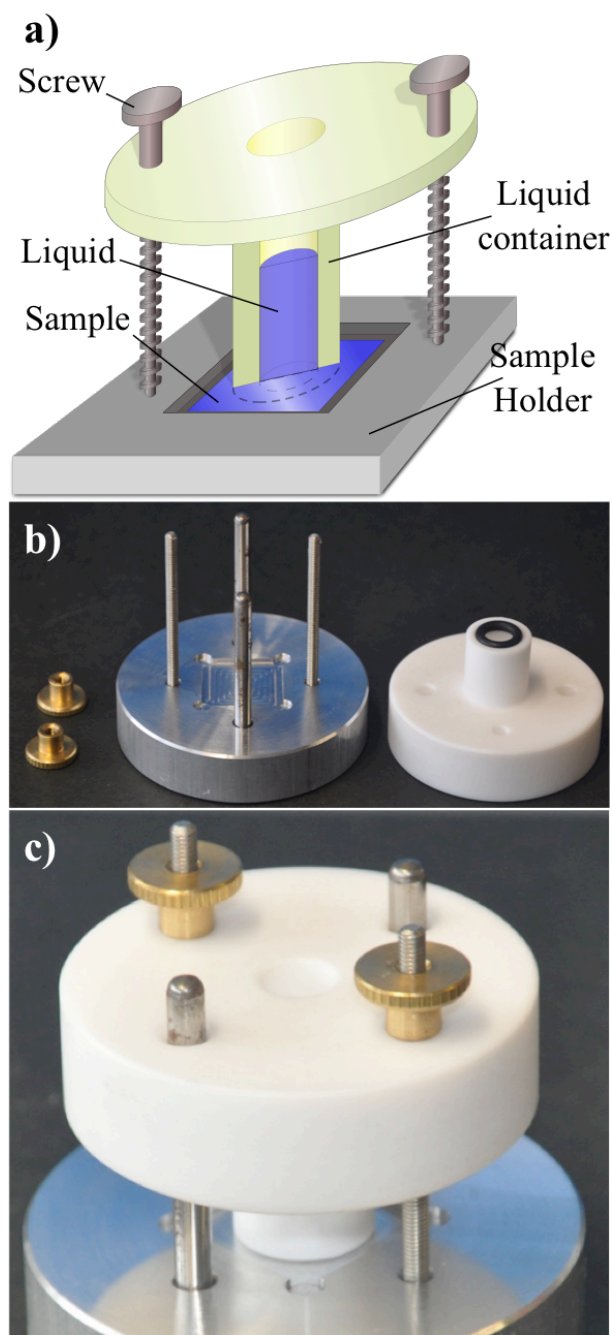


**Figure 73:** (a): Schematic drawing of the setup used for a partial silanization of flat samples with GPS. By placing the liquid container on top of the flat glass or titanium sheet in the sample holder and filling it with a silane/GPS mixture, only the part of the sheet's surface in contact with the silane solution was silanized. (b): The picture shows a disassembled and (c) a fully assembled setup.

## 4. Materials and Methods

The Extran treated and H<sub>2</sub>O rinsed substrates were placed in the sample holder and the liquid container placed on top, guided by the metallic pillars. Pressure was applied to the liquid container by placing and tightening the screws along the threads to prevent a leakage of liquid between the interfaces of substrate and container. See Figure 73c for an assembled setup. 1 mL of GPS/toluene solution (2% v/v) was injected into the liquid container with a syringe and the entrance sealed with a small glass plate (18 mm x 18 mm) to prevent an evaporation of toluene. Silanization commenced at room temperature for 24h. Afterwards, the samples were removed and cleaned by ultra sonication (240 W; 35 kHz) first in toluene followed by EtOH for 15 min each.

Directly after cleaning the samples were immersed in a 10 mg/ml HS-FA-HA solution (TG = 0.32) for 24 h at 37°C resulting in the formation of a layer of disulfide-crosslinked gel. The plates were washed manually, first by immersing them in water and careful shaking followed by rinsing in a water jet (low pressure). If the immobilization was successful, residual HS-FA-HA gel remained only on silanized parts. The samples were dried in air and the residues were further analyzed using fluorescence microscopy. Images of the whole area with the gel residues were taken with the Axiovert and put together into a combined picture manually using the freeware “Inkscape” ([www.inkscape.com](http://www.inkscape.com)) program.

### 4.2.4. Selective hyaluronan immobilization on the outer and inner surfaces of small glass and titanium tubes

#### *Immobilization of HA*

Glass and titanium tubes were silanized with GPS following the protocol in Section 4.2.2. Special care was taken to avoid air bubbles during the immersion in either Extran or the silane/toluene solutions.

For a modification of the inner surfaces of tubes with fluorescent HA, they were connected to each other in series with short pieces of plastic tubing (see Figure 74a). FA-HA solution in PBS ( $\beta(\text{FA-HA}) = 3 \text{ mg/ml}$ ; pH = 7.4) was injected into the setup using a syringe. In order to modify the outer surface of the tubes, both ends were sealed with dental glue immediately after silanization (see Figure 74b) and immersed in an HS-HA solution in PBS ( $\beta(\text{FA-HA}) = 3 \text{ mg/ml}$ ) for 24 h. After an incubation period of 24 h at 37° C in a cell incubator, the samples were rinsed manually with ddH<sub>2</sub>O using a syringe (modification on the inside) or by a full immersion (modification outside), and then further washed by placing them in a PBS-Tween solution ( $\beta(\text{Tween}) = 1 \text{ mg/ml}$ ; pH = 7.4) on a vibrating plate (~60 rpm) for 7 days at room temperature.

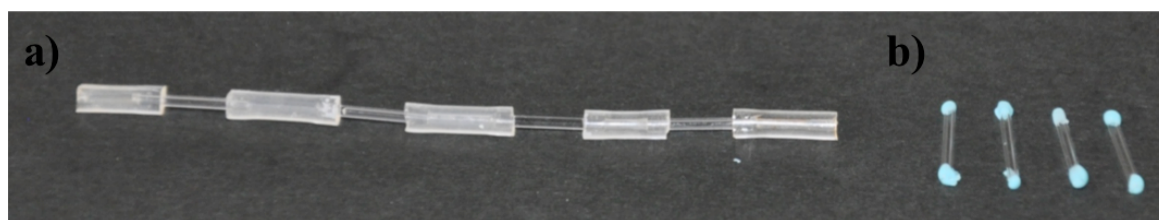


**Figure 74:** (a): Experimental setups used for the selective immobilization of FA-HA to the inner (a) or outer (b) surfaces of small glass tubes silanized with GPS. (a): The samples were connected with small pieces of elastic tubing. (b): A watertight polymer (dental glue) was grafted to the entrances of each individual tube.

### *Analytical methods*

The quality of the hyaluronan immobilization was assessed by fluorescence microscopy. For comparison, a non-silanized sample, which was subjected to the same FA-HA modification and washing protocols except the silanization, was placed alongside the test sample. Bright-field and fluorescence images were made manually and the signals between silanized and non-silanized samples were compared.

### **4.3. Creation and immobilization of hyaluronan hydrogels**

Hydrogels were formed by a reaction between thiolated hyaluronan and bi-functional acrylamides. Also hydrogels were immobilized on silanized surfaces.

#### **4.3.1. Materials**

N,N'-Methylenebis(acrylamide) (MBAA) was obtained from Carl Roth (Karlsruhe, Germany). Poly(ethylene glycol) dicrylamide (PEGDA) was obtained from Sigma Aldrich (Schnelldorf, Germany). Tris(hydroxymethyl)-aminomethan (TRIS) was obtained from Serva (Heidelberg, Germany) and "Balanced Saline Solution" (BSS) was obtained from Beaver Visitec (Waltham, U.S.A.). Molds for the creation of macroscopic gels (See Figure 84) were designed using the Autodesk Inventor Professional 2014 (64-Bit Edition) software from Autodesk (San Rafael, U.S.A.) and the "Replicator 2" software from Makerbot (New York City, U.S.A.). They were 3D-printed using the Makerbot Replicator 2 and polylactide (PLA), both obtained from Makerbot. Simultaneously, molds made from PTFE were manufactured by the precision mechanics workshop of the Max-Planck-Institute for Intelligent Systems in Stuttgart. QCMD tubing (Tygon® ST R-3607; ID = 0.64 mm) was obtained from Ismatec (Wertheim, Germany) and TPP tubing (ID = 0.51 mm) was obtained from Helix Medical (Kaiserslautern, Germany). 2-component dental glue (Picodent twinsil® speed 22) was purchased from Picodent (Wipperfürth, Germany). For fluorescence measurements, an Axiovert 200M with a 38 HE eGFP (Ex: 470/40; Em: 525/50) (Zeiss, Oberkochen, Germany) was used.

#### **4.3.2. Formation of hydrogels**

##### *General procedure*

Hyaluronan hydrogels were synthesized by mixing HS-HA or HS-FA-HA solutions with MBAA or PEGDAA solutions. To that end, modified HA and crosslinker (CL) were dissolved separately in a solution of TRIS in BSS (0.4 mol/l; pH = 8.5), which was O<sub>2</sub> purged using Argon gas before use. The total masses of HA and CL, and the required volumes of the solvents for the HA and CL solutions, depended on the desired final mass concentration of HA after mixing, the target ratio of the crosslinkers' acrylamide groups to the number of active thiols, and the total required volume of the HA/CL mixture for each individual experiment. The HA and the CL solutions were mixed in a ratio of  $V(\text{HA})/V(\text{CL}) = 7:3$  and individual concentrations of starting materials in the individual solutions calculated based on that ratio (See Table 4).

## 4. Materials and Methods

**Table 4:** MBAA concentrations in [mg/ml] for creation of hydrogels depending on thiolation grades (TG) and HA concentrations

		$\beta$ (HA) [mg/ml]			
		10.0	12.5	15.0	17.5
TG	0.19	1.20	1.50	1.80	2.10
	0.23	1.44	1.80	2.16	2.52
	0.39	2.35	2.93	3.52	4.11
	0.42	3.51	3.14	3.76	4.39
	0.57	3.29	4.11	4.93	5.75

For the PEGDA crosslinker gelation started within 30 s at room temperature, and within 5-8 min when both solutions were cooled to 0 °C in an ice bath, resulting in a sharp increase of viscosity. Full gel formation was achieved in under <5 min (RT) or >15 min (0°C). HS-HA/MBAA solutions formed gels after an incubation over night at 37 °C, under oxygen exclusion in order to minimize disulfide formation. If not immediately used afterwards, the resulting hydrogels were immersed in BSS for long-term storage.

### *Generation of macroscopic non-immobilized and immobilized gels*

For the synthesis of macroscopic gels, 450  $\mu$ L of the HA/CL mixture was poured into the molds. Small glass or titanium slides were placed on top and secured with adhesive tape and the molds turned upside down. This resulted in the mixtures resting on top of the silanized samples, allowing interaction between the thiol groups and the epoxides (See Figure 75). All samples were placed into a petri dish, which was flushed with argon for 30 s and sealed with Parafilm followed by an incubation at 37 °C for 24 hours. For immobilized hydrogels slides silanized with GPS were used. Non-immobilized hydrogels were created by using non-silanized slides.

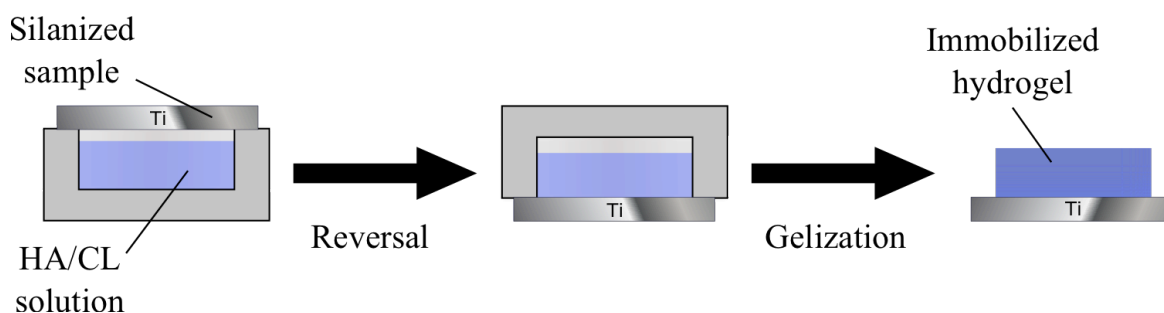


**Figure 75:** Schematic drawing for the formation and immobilization of macroscopic hydrogels on flat silanized samples. (a): The HS-HA/MBAA solution as filled into the mold and the silanized sample was placed on top and secured with adhesive tape (not shown). (b): The setup was turned upside down to bring the HS-HA/MBAA solution in contact with the surface of the sample. (c): After gel formation and immobilization occurred, the hydrogel-modified plate was removed from the mold. The same setup was also used for an immobilization on glass samples. For the creation of non-immobilized gels, unmodified slides were used.

## 4. Materials and Methods

---

### *Modification of small tubes with hydrogels*

In order to modify the inside of the glass tubes, the samples were connected in series using short QCMD tubing (length = 1 - 2 cm) to form a long channel (see Figure 74a), and an HS-HA/MBAA mixture was manually injected using a syringe. The whole setup was placed into a plastic petri dish, which was subsequently flushed with argon and sealed with parafilm. The petri dishes were placed at 37 °C for 24 hours before the QCMD tubing was removed and the glass samples placed in BSS for 48 hours before performing further measurements on them.

For a selective modification of the outer surface, the ends of the tubes were sealed with dental glue (Figure 74b) and immersed in an HS-HA/MBAA solution in a small beaker. After flushing with argon and sealing the beaker with parafilm, it was placed in a cell incubator at 37 °C for 24 hours. Afterwards, the glue was removed and the samples stored in BSS for at least two days prior to further measurements.

### *Modification of large glass tubes (ID = 5 mm) with hydrogels*

The tubes were placed within the special sample holders and the lid fastened on top with the screws. Through the hole in the lid, the HS-HA/MBAA mixtures were injected with a syringe. The hole was sealed with a small glass plate (18 mm x18 mm) and the whole setup placed in a cell incubator at 37° C for 24 hours. Afterwards the lid was removed and the hydrogel-modified sample retrieved. For a picture for the whole setup compare Figure 81c without using a glass fiber.

### *Analytical methods*

The immobilization of macroscopic gels on flat titanium and glass slides was confirmed by rinsing the samples in water manually. To that end, the slides were first inserted into ddH<sub>2</sub>O and shaken by hand, then carefully subjected to a low to medium strength water flow. Immobilization was deemed a success when the gel remained on the slides throughout and after this procedure.

Immobilizations of hydrogels on glass and the outer surfaces of titanium tubes with hyaluronan were confirmed by using HS-FA-HA for the modification and observing the samples with fluorescence microscopy. For that bright-field and fluorescence images were taken from every part of the tubes and manually put together using the freeware program “Inkscape” ([www.inkscape.com](http://www.inkscape.com)). The covalent immobilization of the hydrogels to the inner surfaces of the Ti tubes was confirmed indirectly during pressure resistance experiments (see section 4.5).

### 4.4. Swelling behavior of hydrogels

Immobilized and non-immobilized hydrogels were incubated in BSS to compare their swelling behavior.

#### 4.4.1. Materials

Molds for the creation of the macroscopic hydrogels were the same as in Section 4.3. Glass tubes (ID = 5 mm; OD = 7 mm; L = 10 mm) were manufactured at the glass workshop of the Max-Planck Institute for Intelligent Systems in Stuttgart, Germany. BSS was obtained from Beaver Visitec (Waltham, U.S.A.) and TRIS was bought from Serva (Heidelberg, Germany). For lyophilization a freeze dryer (model: P8K-E-85-4) from Dieter Piatkowski Forschungsgeräte (Munich, Germany) was used.

#### 4.4.2. Experimental procedure

##### *Data acquisition*

Non-immobilized macroscopic HA-hydrogels were created following the protocol in section 4.3. by filling the HS-HA/MBAA mixtures into custom-made molds (see Figure 84). Hydrogels immobilized to the inner surfaces of large tubes were prepared following the protocol for large tubes in Section 4.3.

For swelling-over-time experiments, the hydrogels' masses were recorded before swelling, and afterwards placed in a TRIS in BSS solution ( $c(\text{TRIS}) = 0.4 \text{ mol/l}$ ). At regular time intervals (ca. 24h, 48h or 72h), the gels' masses were recorded after carefully draining and blotting away excess fluids.

##### *Data analysis*

For each set of experiments, four gels were prepared individually and swollen simultaneously. In order to analyze the swelling of hydrogels immobilized to the inner surfaces of large tubes, the masses of the hydrogels were gained by a determination of the total mass of the hydrogel + tube and subtracting the mass of the empty tube recorded before the modification with hydrogels. The swelling ratios were analyzed by calculating the relative mass gain at the different time-intervals using the formula

$$m_{rel} = \frac{m}{m_0}$$

with  $m_{rel}$  being the relative mass,  $m$  the absolute mass and  $m_0$  the starting mass recorded directly after the gel formation was finished. Theoretical dry masses were calculated from the combined mass concentrations of HS-HA and MBAA and the total volumes.

### 4.5. Pressure resistance measurements of hyaluronan-hydrogel modified tubes

A linearly increasing pressure was applied to hydrogel-filled tubes to evaluate their immobilization stability and potential to allow liquid flow.

#### 4.5.1. Materials

Measurements were performed using a BOSE Electroforce Series 3200 from Bose (Framingham, U.S.A.) connected to a computer using the “WinTest” software. The holder for the pressure chamber was designed using the Autodesk Inventor Professional 2014 (64-Bit Edition) software from Autodesk (San Rafael, U.S.A.) and the “Replicator 2” software from Makerbot (Munich, Germany). The design was 3D-printed with PLA using the Makerbot Replicator 2 from Makerbot. For the manufacture of the pressure chamber, a 5 ml Omnifix<sup>®</sup> syringe with a Sterican<sup>®</sup> metallic needle (0.8 mm x 12 mm) from B.Braun (Melsungen, Germany), QCMD tubing (Tygon<sup>®</sup> ST R-3607, ID = 0.64 mm) from Ismatec (Wertheim, Germany) or TPP tubing (ID = 0.51 mm) from Helix Medical (Kaiserslautern, Germany), and two component quick-setting epoxide glue (UHU Plus 2k-Epoxidkleber) from UHU<sup>®</sup> (Bühl, Germany) were used.

#### 4.5.2. Measurements

##### *Construction of the “pressure chamber”*

The Sterican<sup>®</sup> metallic syringe needle was manually cut down to a length of 1-1.5 cm and attached to the tip of the 5 ml Omnifix<sup>®</sup> syringe. Appropriate tubing (QCMD tubing for glass samples, PPA tubing for titanium samples) was connected to the shortened needle and the joints were sealed off by generously mixing the two component quick-setting glue at a 1:1 ratio and generously spreading it onto the to be sealed parts of the setup with a disposable plastic spatula. This was followed by drying for >2 hours to ensure a full solidification of the glue. See Figure 76 for pictures of the assembled pressure chambers.



**Figure 76:** Images of the assembled pressure chambers used in CPA measurements for glass (a) and titanium (b) tubes. The use of quick-setting glue is illustrated, which was used to seal the syringe-needle and needle-tubing joints for a prevention of leakage during experiments.

## 4. Materials and Methods

### *Assembly of the experimental setup and measurements*

Small hydrogel-filled glass (ID = 0.5 mm) or titanium tubes were created according to the protocol in section 4.3. In order to assemble the setup for CPA measurements the sample holder was mounted to the 225 N load cell. The pressure chamber was then filled with 5 ml BSS, cleared of air bubbles, and placed in the sample holder. A hydrogel-modified glass or titanium tube was connected to the tubing of the pressure chamber and a second short piece of tubing was fastened to the other end. The setup was raised until the syringe's plunger almost touched the displacement head. See Figure 77 for a picture of the assembled setup.

In order to perform a pressure resistance measurement on the above-mentioned samples, the BOSE was programmed to move the displacer down a maximum of 5 mm with a fixed predetermined movement rate (0.005 mm/s-0.1 mm/s). Simultaneously the force readout from the 225 N force sensor was recorded. In order to save time, the measurements were only carried out until the pressure-time relationship had reached equilibrium and were then manually stopped, even when the maximum displacement of 5 mm was not yet achieved.

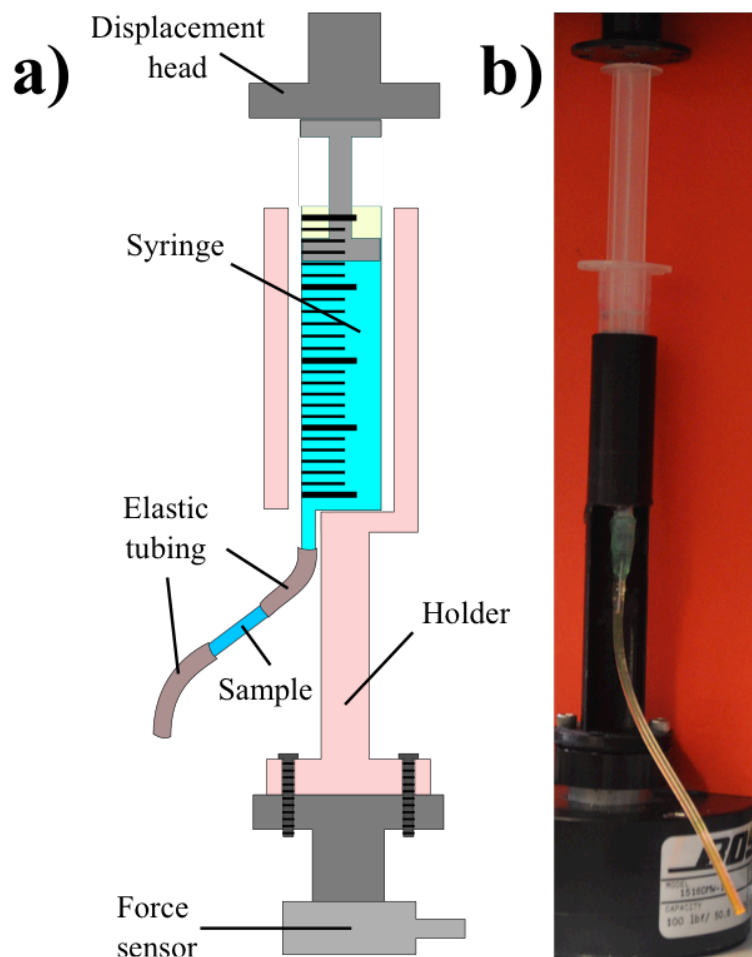


**Figure 77:** Schematic drawing (a) and image (b) of the assembled setup for CPA measurements using a BOSE force-meter.

### *Data Analysis*

The force values were normalized to a starting value of zero and divided by the area of the syringe's plunger to obtain pressure values. The displacement was divided by the maximum displacement achieved during the experiment to get the relative displacement. Pressure was plotted against relative displacement using the commercially available "Origin" software to enable further data analysis:

In order to examine breaking points, the peak pressure was identified where the hydrogels were removed from the tubes.

For a determination of the equilibrium pressure (EP), all data points in the EP region were used to calculate an average equilibrium pressure. The standard deviation of the average pressure was so low (<0.5%), that it was disregarded for further calculations. Each sample was measured three to five times and a mean value of the obtained equilibrium pressures with a standard deviation was calculated. The average pressures of several samples fabricated with the same set of parameters were combined into a weighted average value.

### **4.6. Hydrostatic pressure measurements**

Hydrostatic pressure was applied to hydrogel-filled tubes in order to evaluate their pressure regulation abilities.

#### **4.6.1. Materials**

A glass capillary (height: 2 m, ID: 9,3 mm) with an outlet and a valve was manufactured by the glass workshop of the Max Planck Institute for Intelligent Systems in Stuttgart (See Figure 78). The mass changes within the capillary were recorded with a KERN 572 scale from Kern & Sohn GmbH (Balingen-Frommern, Germany) connected to the COM1 port of a computer. Markus Weiler, a co-worker, wrote the program for reading out the data sent from the balance to the COM1 port at variable time intervals. QCMD tubing (Tygon® ST R-3607, ID = 0.64 mm) was bought from Ismatec (Wertheim, Germany) and TPP tubing (ID = 0.51 mm) was purchased from Helix Medical (Kaiserslautern, Germany).

#### **4.6.2. Measurements**

##### *Experimental setup*

HA hydrogel modified glass or titanium tubes were created according to the protocols established in section 4.3. The glass capillary was placed on the scale, which was connected to the computer and programmed to constantly transmit the current measured mass. The valve of the outlet was closed, the capillary filled with BSS and elastic tubing connected to the outlet. The valve was opened for a short time to remove the air from the setup. See Figure 78 for exemplary pictures of the setups for small and large hydrogel-filled samples.

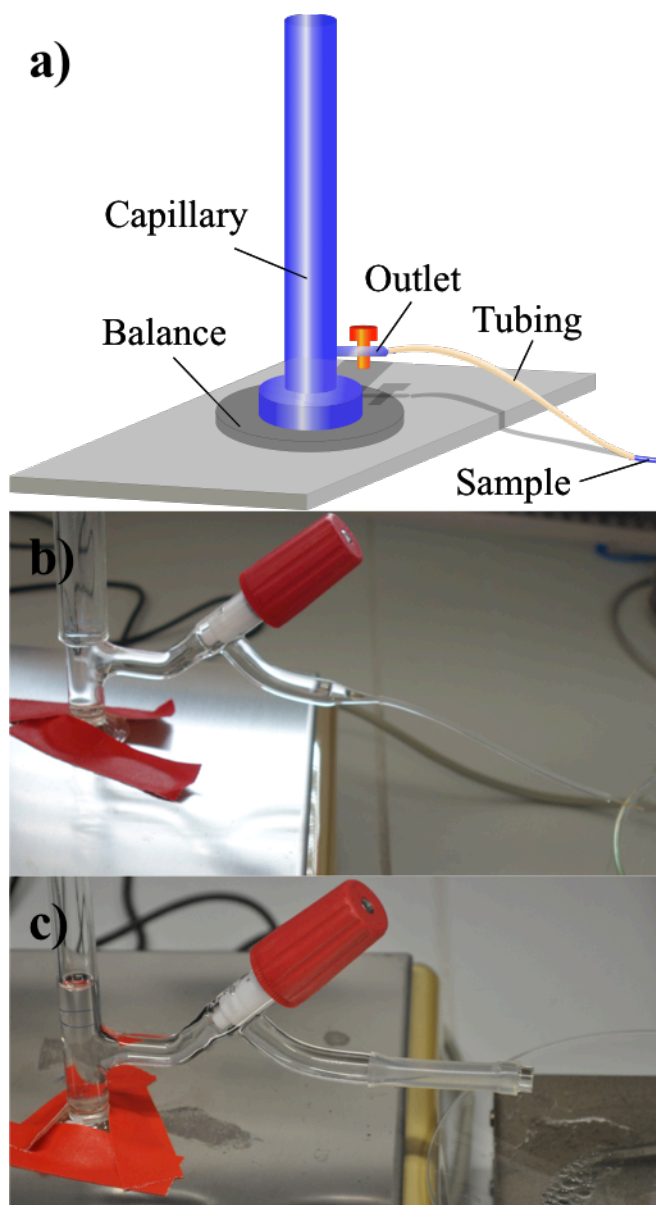


**Figure 78:** (a): Schematic drawing of the setup used for HPA measurements. (b/c): Image of the lower part of the setup used for the HPA measurements on small glass tubes (ID = 0.5 mm) (b) or large glass tubes (ID = 5 mm) (c) using different tubings for the connection to the glass capillary.

A second piece of tubing was connected to the other end of the sample and laced into a beaker to collect outflowing liquid. In order to minimize evaporation during long-term measurements, the top entrances of the capillary and the beaker were sealed with parafilm containing small holes to allow for pressure equalization.

### *Data collection*

The data readout program was started to collect the masses recorded by the balance at regular time intervals (2 sec – 30 min), depending on how quickly the mass changed, and the valve was opened to initiate the experiment. Measurements were conducted until the average mass did not change significantly over an extended period of time.

### *Data analysis*

The zero-point mass was determined to be the height of the liquid column, where no more flow was detected through an empty tube. The recorded masses from the measurements were normalized with this zero-point mass and transformed into pressures according to the conversion constant established in Section 2.4.3. The gained pressure values were plotted versus the measurement time to get the pressure-over-time curves.

## **4.7. Microscopic pressure-flow experiments**

Pressure was applied to hydrogel-filled tubes while observing them in a microscope in order to analyze the mechanism of pressure-induced liquid flow.

### **4.7.1. Materials**

QCMD tubing (Tygon® ST R-3607, ID = 0.64 mm) was bought from Ismatec (Wertheim, Germany) and TPP tubing (ID = 0.51 mm) from Helix Medical (Kaiserslautern, Germany). BSS was obtained from Beaver Visitec (Waltham, U.S.A.). Fluorescein was purchased from Sigma Aldrich (St. Louis, U.S.A.). A 5 ml Omnifix® syringe with a Sterican® metallic needle (0.8 mm x 12 mm) was obtained from B.Braun (Melsungen, Germany). For fluorescence measurements, an Axiovert 200M with a 38 HE eGFP (Ex: 470/40; Em: 525/50) filterblock (Zeiss, Oberkochen, Germany) was used.

### **4.7.2. Measurements**

#### *Experimental setup*

Small hydrogel-filled glass tubes (ID = 0,5 mm; L = 10 mm) were prepared with HS-HA or HS-FA-HA according to the instructions in Section 4.3. Before use, CPA measurements (Section 4.5) were performed to examine, whether establishing a liquid flow through the samples was possible. The tubes were connected on both ends to QCMD tubing, which was then fastened to an object holder with adhesive tape. The setup was placed in the Axiovert microscope and the end of piece of QCMD tubing was connected to the syringe, which was filled either with BSS or fluorescein solution. The needle was shortened manually to a length of 0.5-1.0 cm to allow for a better insertion. The end of the other QCMD tubing was placed into a small beaker to the side of the microscope to collect any fluids pressed through the system (= “outlet”). See Figure 79 for an overview of the experimental setup.

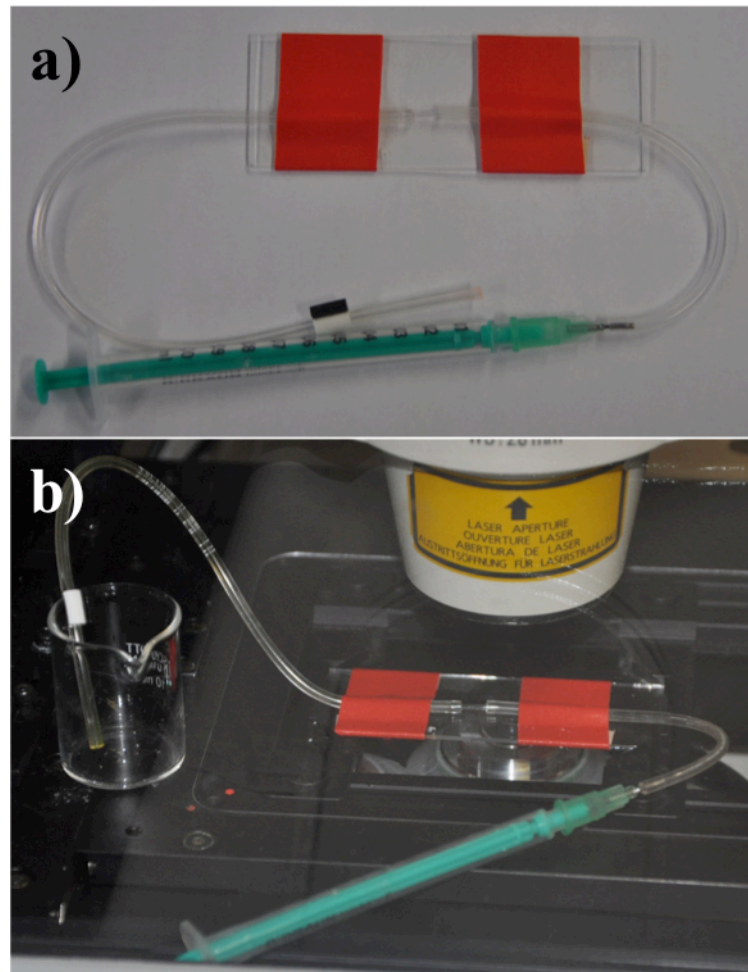


**Figure 79:** (a): Image of the assembled setup to perform microscopic pressure-flow experiments. (b): Picture of the setup placed in the Axiovert microscope prior to flow measurements.

### *Data acquisition*

The Axiovert microscope was programmed to record a time-lapse with intervals of one second and the measurement started. The pressure of the liquid in the syringe, BSS or fluorescein dissolved in NaOH (0.1 mol/l, pH = 12), was slowly increased manually by pressing on the syringe plunger until a liquid flow was detected in the time-lapse. At that point the pressure was kept as constant as possible by hand. If the syringe contained the fluorescence solution, pressure was maintained until the time-lapse showed an equal distribution of fluorescein within the hydrogel. Afterwards, the fluorescein-saturated tube was exposed to the same treatment using a blank BSS solution until the fluorophores were removed. For repeated channel opening and closure experiments, pressure was applied manually to the syringe filled with pure BSS until the channel was visible and maintained for an extended period of time (ca. 30 s). Then application of forces on the plunger was stopped until the channel was closed and this status was then maintained for another 30 s. This sequence was repeated several times.

### *Data Analysis*

The individual frames from the time-lapse were edited using the open-source ImageJ software. First, all images were imported and a stack was created using the “Images to Stack” command. This stack was then saved as a “.avi” video file. The stack was further modified by lowering the brightness and increasing the contrast to better visualize the channels.

### **4.8. Artificial creation of channels in hydrogels**

Two methods were used to artificially generate channels within hydrogels for enabling them to regulate external liquid pressures.

#### **4.8.1. Materials**

For laser cutting an “Epilog Zing 16” CO<sub>2</sub> device from cameo (Stuhr, Germany) was used. For the mechanical creation of channels with small fibers, a sample holder for the modification of large glass tubes (ID = 5 mm) with hydrogels (See Figure 81) was manufactured by the precision mechanics workshop. The glass fibers necessary to create the channels in this setup (diameter = 0.1 mm) were provided by the glass workshop of the Max Planck Institute for Intelligent Systems in Stuttgart.

#### **4.8.2. Channel creation and pressure measurement**

##### *Sample preparation*

Hydrogel-filled large glass tubes (L = 10 mm; ID = 5 mm) were prepared according to the protocols in Section 4.3 using the custom-made reaction chamber without a glass fiber (Figure 81).

For the channel creation with lasers the gel-filled tubes were subsequently placed in the laser cutter with the entrance of the tube facing the direction of the beam (Figure 80). The commercially available “Corel Draw” software was used to draw a circle with the target diameter of the channel with the thickness of the stroke set to “hairline”. The parameters for the laser cutter were set to 50% movement speed, frequency = 5000 Hz (100%) and a 100% laser power. The focus was adjusted manually to a point roughly in the first quarter of the hydrogel facing the laser beam. One to three laser applications were conducted until a channel formed.

## 4. Materials and Methods

---

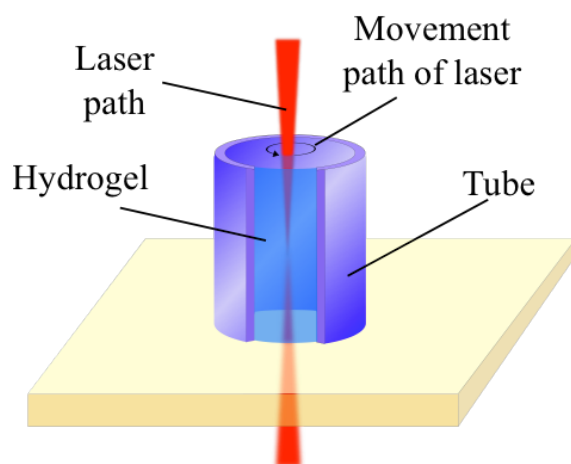


**Figure 80:** Schematic drawing of the experimental setup to create artificial channels in hydrogel-filled tubes using a commercially available laser cutter.

For a channel creation using the mechanical method, a small glass fiber (diameter ca. 0.1 mm) was inserted through the hole of the lid down into the circular incision of the sample holder, displacing the HS-HA/crosslinker mixture in the process. See Figure 81 for a visual representation of the experimental setup. The assembly with the silanized tube containing the HS-HA/MBAA mixture and the glass fiber were then placed into a cell incubator at 37° C for 24 hours. Finally the glass fibers were removed leaving behind a channel in the gel.

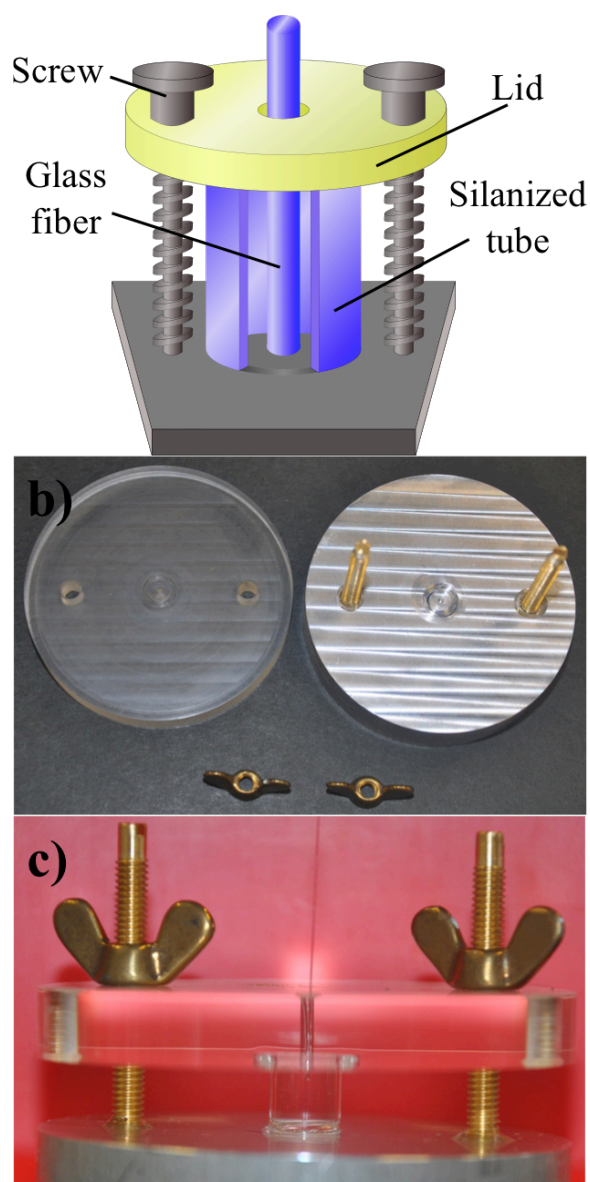


**Figure 81:** (a): Schematic drawing of the experimental setup used for the creation of hydrogels channels in large (ID = 5 mm) hydrogel-filled tubes. (b): Picture of a disassembled setup. (c): Picture of a fully assembled setup containing a silanized sample. The same setup, without the fiber, was also used in general to immobilize hydrogels within these glass tubes.

### *HPA measurements*

Prior to HPA measurements, the samples were incubated in BSS at room temperature for 48 hours to allow for a swelling of the gels within the tubes to close the artificially generated channels. The samples were then connected to the HPA empty glass capillary using a piece of elastic tubing (See Figure 78b). The data-readout program for the balance on the computer was started and BSS was filled into the capillary in intervals until a liquid flow through the tube was detected, resulting in continued measurements until no more changes in masses were detected. The data analysis was conducted similarly to the HPA measurements in Section 4.6.



### 5. Literature

- 1 Weinreb, R. N. & Khaw, P. T. Primary open-angle glaucoma. *The Lancet* **363**, 1711-1720 (2004).
- 2 Casson, R. J., Chidlow, G., Wood, J. P., Crowston, J. G. & Goldberg, I. Definition of glaucoma: clinical and experimental concepts. *Clinical & experimental ophthalmology* **40**, 341-349 (2012).
- 3 Sampaolesi, R., Sampaolesi, J. & Zarate, J. *The glaucomas volume II - Open angle glaucoma and angle closure glaucoma* (Springer Berlin Heidelberg, 2014).
- 4 Tham, Y. *et al.* Global prevalence of glaucoma and projections of glaucoma burden through 2040. *Ophthalmology* **121**, 2081-2090 (2014).
- 5 The collaborative normal-tension glaucoma study group. Comparison of glaucomatous progression between untreated patients with normal-tension glaucoma and patients with therapeutically reduced intraocular pressures. *American Journal of Ophthalmology* **126**, 487-497 (1998).
- 6 Pascolini, D. & Mariotti, S. P. Global estimates of visual impairment: 2010. *The British journal of ophthalmology* **96**, 614-618 (2012).
- 7 Jakobs, T. C., Libby, R. T., Ben, Y., John, S. W. & Masland, R. H. Retinal ganglion cell degeneration is topological but not cell type specific in DBA/2J mice. *The Journal of cell biology* **171**, 313-325 (2005).
- 8 Barde, Y. Trophic factors and neuronal survival. *Neuron* **2**, 1525-1534 (1989).
- 9 Quigley, H. A. Glaucoma. *The Lancet* **377**, 1367-1377 (2011).
- 10 Fechtner, R. D. & Weinreb, R. N. Mechanisms of optic nerve damage in primary open angle glaucoma. *Survey of ophthalmology* **39**, 23-42 (1994).
- 11 Grehn, F. & Stamper, R. *Glaucoma*. (Springer Berlin Heidelberg, 2006).
- 12 Care, N. C. C. f. A. *Glaucoma: Diagnosis and management of chronic open angle glaucoma and ocular hypertension*. (National Collaboration Centre for Acute Care, 2009).
- 13 Bellezza, A. J. *et al.* Deformation of the lamina cribrosa and anterior scleral canal wall in early experimental glaucoma. *Investigative Ophthalmology & Visual Science* **44**, 623-637 (2003).
- 14 Quigley, H., McKinnon, S. & Zack, D. Retrograde axonal transport of BDNF in retinal ganglion cells is blocked by acute IOP elevation in rats. *Investigative Ophthalmology & Visual Science* **41**, 3460-3466 (2000).
- 15 Schwartz, B. Circulatory defects of the optic disk and retinal ocular hypertension and high pressure open-angle glaucoma. *Survey of ophthalmology* **38**, 23-34 (1994).
- 16 Buckingham, B. P. *et al.* Progressive ganglion cell degeneration precedes neuronal loss in a mouse model of glaucoma. *The Journal of neuroscience : the official journal of the Society for Neuroscience* **28**, 2735-2744 (2008).
- 17 Burgoyne, C. F., Downs, J. C., Bellezza, A. J., Suh, J. K. & Hart, R. T. The optic nerve head as a biomechanical structure: a new paradigm for understanding the role of IOP-related stress and strain in the pathophysiology of glaucomatous optic nerve head damage. *Progress in retinal and eye research* **24**, 39-73 (2005).
- 18 Mi, X. S., Yuan, T. F. & So, K. F. The current research status of normal tension glaucoma. *Clinical interventions in aging* **9**, 1563-1571 (2014).
- 19 Kass, M. *et al.* The ocular hypertension treatment study. *Archives of Ophthalmology* **120**, 701-713 (2002).

## 5. Literature

---

- 20 Cracknell, K. P. & Grierson, I. Prostaglandin analogues in the anterior eye: their pressure lowering action and side effects. *Experimental Eye Research* **88**, 786-791 (2009).
- 21 Fiscella, R. G., Green, A., Patuszynski, D. H. & Wilensky, J. Medical therapy cost considerations for glaucoma. *American Journal of Ophthalmology* **136**, 18-25 (2003).
- 22 Wistrand, P., Stjernschantz, J. & Olsson, K. The incidence and time-course of lantanoprost-induced iridial pigmentation as a function of eye color. *Survey of Ophthalmology* **41**, 129-138 (1997).
- 23 Friedman, D. S. *et al.* Using pharmacy claims data to study adherence to glaucoma medications: methodology and findings of the Glaucoma Adherence and Persistency Study (GAPS). *Investigative Ophthalmology & Visual Science* **48**, 5052-5057 (2007).
- 24 McIlraith, I., Strasfeld, M., Colev, G. & Hutnik, C. Selective laser trabeculoplasty as initial and adjunctive treatment for open-angle glaucoma. *Journal of Glaucoma* **15**, 124-130 (2006).
- 25 Samples, J. R. *et al.* Laser trabeculoplasty for open-angle glaucoma: a report by the american academy of ophthalmology. *Ophthalmology* **118**, 2296-2302 (2011).
- 26 Pham, H. *et al.* Argon laser trabeculoplasty versus selective laser trabeculoplasty. *Survey of ophthalmology* **53**, 641-646 (2008).
- 27 Dally, L. *et al.* The advanced glaucoma intervention study (AGIS): 11. Risk factors for failure of trabeculectomy and argon laser trabeculoplasty. *American Journal of Ophthalmology* **134**, 481-498 (2002).
- 28 Jay, J. & Murray, S. Early trabeculectomy versus conventional management in primary open angle glaucoma. *British Journal of Ophthalmology* **72**, 881-889 (1988).
- 29 Landers, J., Martin, K., Sarkies, N., Bourne, R. & Watson, P. A twenty-year follow-up study of trabeculectomy: Risk factors and outcomes. *Ophthalmology* **119**, 694-702 (2012).
- 30 Kim, E. A. *et al.* Long-term bleb-related infections after trabeculectomy: Incidence, risk factors, and influence of bleb revision. *Am J Ophthalmol* **159**, 1082-1091 (2015).
- 31 Patel, H. Y. & Danesh-Meyer, H. V. Incidence and management of cataract after glaucoma surgery. *Current opinion in ophthalmology* **24**, 15-20 (2013).
- 32 Greenfield, D., Liebmann, J., Jee, J. & Ritch, R. Late-Onset bleb leaks after glaucoma filtering surgery. *Archives of Ophthalmology* **116**, 443-447 (1998).
- 33 Hong, C. H., Arosemena, A., Zurakowski, D. & Ayyala, R. S. Glaucoma drainage devices: a systematic literature review and current controversies. *Survey of ophthalmology* **50**, 48-60 (2005).
- 34 Molteno, A. C. B. New implant for drainage in glaucoma. *British Journal of Ophthalmology* **53**, 606-615 (1969).
- 35 Molteno, A. C. B., Straughan, J. L. & Ancker, E. Long tube implants in the management of glaucoma. *South African Medical Journal* **50**, 1062-1066 (1976).
- 36 Huang, M. C. *et al.* Intermediate-term clinical experience with the ahmed glaucoma valve implant. *American Journal of Ophthalmology* **127**, 27-33 (1999).
- 37 Roy, S., Ravinet, E. & Mermoud, A. Baerveldt implant in refractory glaucoma: long-term results and factors influencing outcome. *International Ophthalmology* **24**, 93-100 (2002).
- 38 Hodkin, M. J., Goldblatt, W. S., Burgoyne, C. F., Ball, S. F. & Insler, M. S. Early clinical experience with the baerveldt implant in complicated glaucomas. *American Journal of Ophthalmology* **120**, 32-40 (1995).

## 5. Literature

---

- 39 Hill, R., Pirouzian, A. & Liaw, L. Pathophysiology of and prophylaxis against late ahmed glaucoma valve occlusion. *American Journal of Ophthalmology* **129**, 608-612 (2000).
- 40 Minckler, D., Shammam, A., Wilcox, M. & Ogden, T. Experimental studies of aqueous filtration using the molteno implant. *Transactions of the American Ophthalmological Society* **85**, 368-392 (1987).
- 41 Schocket, S. Investigations of the reasons for success and failure in the anterior shunt-to-the-encircling-band procedure in the treatment of refractory glaucoma. *Transactions of the American Ophthalmological Society* **84**, 743-798 (1968).
- 42 Epstein, E. Fibrosing response to aqueous; its relation to glaucoma. *British Journal of Ophthalmology* **43**, 641-647 (1959).
- 43 Schwartz, K., Lee, R. & Gedde, S. Glaucoma drainage implants: a critical comparison of types. *Current opinion in ophthalmology* **17**, 181-189 (2006).
- 44 Freedman, J. What is new after 40 years of glaucoma implants. *Journal of Glaucoma* **19**, 504-508 (2010).
- 45 Williams, D. F. On the mechanisms of biocompatibility. *Biomaterials* **29**, 2941-2953 (2008).
- 46 Johnson, W. W., B.S., D.D.S. & M.S. The history of prosthetic dentistry. *Journal of Prosthetic Dentistry* **9**, 841-846 (1959).
- 47 Thurston, A. J. Pare and prosthetics: the early history of artificial limbs. *ANZ journal of surgery* **77**, 1114-1119 (2007).
- 48 A.Lane, Lond, M. S. & Eng, F. R. C. S. On the advantage of the steel screw in the treatment of ununited fractures. *The Lancet* **201**, 1500-1501 (1893).
- 49 Scales, J. T., Winter, G. D. & Shirley, H. T. Corrosion of orthopaedic implants. *The Journal of Bone and Joint Surgery* **41 B**, 810-820 (1959).
- 50 Cramers, M. & Lucht, U. Metal sensitivity in patients treated for tibial fractures with plates of stainless steel. *Acta Orthopaedica Scandinavia* **48**, 245-249 (1977).
- 51 Firkins, P. J. *et al.* Quantitative analysis of wear and wear debris from metal-on-metal hip prostheses tested in a physiological hip joint simulator. *Bio-Medical Materials and Engineering* **11**, 143-157 (2001).
- 52 Zeh, A., Becker, C., Planert, M., Latke, P. & Wohlrab, D. Time-dependent release of cobalt and chromium ions into the serum following implantation of the metal-on-metal Maverick type artificial lumbar disc (Medtronic Sofamor Danek). *Archives of orthopaedic and trauma surgery* **129**, 741-746 (2009).
- 53 Cunningham, B. W. *et al.* The effect of spinal instrumentation particulate wear debris: an in vivo rabbit model and applied clinical study of retrieved instrumentation cases. *The Spine Journal* **3**, 19-32 (2003).
- 54 Hallab, N. J. *et al.* Effects of soluble metals on human peri-implant cells. *Journal of biomedical materials research. Part A* **74**, 124-140 (2005).
- 55 Niinomi, M. Recent metallic materials for biomedical applications. *Metallurgical and Materials Transactions A* **33**, 477-486 (2001).
- 56 Halliday, A. J., Moulton, S. E., Wallace, G. G. & Cook, M. J. Novel methods of antiepileptic drug delivery -- polymer-based implants. *Advanced drug delivery reviews* **64**, 953-964 (2012).
- 57 Liao, S. L., Kao, S. C., Tseng, J. H. & Lin, L. L. Surgical coverage of exposed hydroxyapatite implant with retroauricular myoperiosteal graft. *The British journal of ophthalmology* **89**, 92-95 (2005).
- 58 Weber, B., Zeisberger, S. M. & Hoerstrup, S. P. Prenatally harvested cells for cardiovascular tissue engineering: fabrication of autologous implants prior to birth. *Placenta* **32**, 316-319 (2011).

## 5. Literature

---

- 59 Chi, M.-H., Tsou, H.-K., Chung, C.-J. & He, J.-L. Biomimetic hydroxyapatite grown on biomedical polymer coated with titanium dioxide interlayer to assist osteocompatible performance. *Thin Solid Films* **549**, 98-102 (2013).
- 60 Scheerder, I. K. D. *et al.* Biocompatibility of polymer-coated oversized metallic stents implanted in normal porcine coronary arteries. *Atherosclerosis* **114**, 105-114 (1995).
- 61 Homsy, C. A. *et al.* Rapid in vitro screening of polymers for biocompatibility. *Journal of Macromolecular Science: Part A - Chemistry* **4**, 615-634 (1970).
- 62 Hegyeli, R. J. Limitations of current techniques for the evaluation of the biohazards and biocompatibility of new candidate materials. *Journal for Biomedical Materials Research* **1**, 1-14 (1971).
- 63 www.webofscience.com. *Web of Science*, <www.webofknowledge.com> (
- 64 Ramakrishna, S., Mayer, J., Wintermantel, E. & Leong, K. Biomedical applications of polymer-composite materials: a review. *Composites Science and Technology* **61**, 1189-1224 (2001).
- 65 Charnley, J. Tissue reactions to polytetrafluorethylene. *The Lancet* **282**, 1379 (1963).
- 66 Scales, J. & Stinson, N. Tissue reactions to polytetrafluoroethylene. *Lancet* **283**, 169 (1964).
- 67 Massia, S. & Hubbell, J. Human endothelial cell interactions with surface coupled adhesion peptides on a nonadhesive glass substrate and two polymeric materials. *Journal of Biomedical Materials Research* **25**, 223-242 (1991).
- 68 Williams, D. F. There is no such thing as a biocompatible material. *Biomaterials* **35**, 10009-10014 (2014).
- 69 Williams, D. *Essential biomaterials science*. (Cambridge University Press, 2014).
- 70 Ullah, F., Othman, M. B., Javed, F., Ahmad, Z. & Akil, H. M. Classification, processing and application of hydrogels: A review. *Materials science & engineering. C, Materials for biological applications* **57**, 414-433 (2015).
- 71 Cavallaro, G., Gianguzza, A., Lazzara, G., Milioto, S. & Piazzese, D. Alginate gel beads filled with halloysite nanotubes. *Applied Clay Science* **72**, 132-137 (2013).
- 72 Einerson, N., Stevens, K. & Kao, W. Synthesis and physiochemical analysis of gelatin-based hydrogels for drug carrier matrices. *Biomaterials* **24**, 509-523 (2002).
- 73 Pouyani, T., Harbison, G. S. & Prestwich, G. D. Novel hydrogels of hyaluronic acid: Synthesis, surface morphology, and solid state NMR. *Journal of the American Chemical Society* **116**, 7515-7522 (1994).
- 74 Lee, H. J. *et al.* Collagen mimetic peptide-conjugated photopolymerizable PEG hydrogel. *Biomaterials* **27**, 5268-5276 (2006).
- 75 Benedetto, F. D., Biasco, A., Pisignano, D. & Cingolani, R. Patterning polyacrylamide hydrogels by soft lithography. *Nanotechnology* **16**, 165-170 (2005).
- 76 Hong, K. H., Jeon, Y.-S., Chung, D. J. & Kim, J.-H. Drug release characteristics of modified PHEMA hydrogel containing thermo-responsive pluronic copolymer. *Macromolecular Research* **18**, 204-207 (2010).
- 77 Shalumon, K. T. *et al.* Sodium alginate/poly(vinyl alcohol)/nano ZnO composite nanofibers for antibacterial wound dressings. *International journal of biological macromolecules* **49**, 247-254 (2011).
- 78 Wichterle, O. & Lim, D. Hydrophilic gels in biologic use. *Nature* **185**, 117 (1960).
- 79 Drury, J. L. & Mooney, D. J. Hydrogels for tissue engineering: scaffold design variables and applications. *Biomaterials* **24**, 4337-4351 (2003).
- 80 Bassil, M., Davenas, J. & El Tahchi, M. Electrochemical properties and actuation mechanisms of polyacrylamide hydrogel for artificial muscle application. *Sensors and Actuators B: Chemical* **134**, 496-501 (2008).

## 5. Literature

---

- 81 Hill-West, J., Chowdhury, S., Slepian, M. & Hubbell, J. Inhibition of thrombosis and intimal thickening by in situ photopolymerization of thin hydrogel barriers. *Proceedings of the National Academy of Sciences of the United States of America* **91**, 5967-5971 (1994).
- 82 Corkhill, P., Hamilton, C. & Tighe, B. Synthetic hydrogels VI. Hydrogel composites as wound dressings and implant materials. *Biomaterials* **10**, 3-10 (1989).
- 83 Qiu, Y. & Park, K. Environment-sensitive hydrogels for drug delivery. *Advanced drug delivery reviews* **64**, 49-60 (2012).
- 84 Jen, A., Wake, C. & Mikos, A. Review: Hydrogels for cell immobilization. *Biotechnology and Bioengineering* **50**, 357-364 (1995).
- 85 Meiring, J. *et al.* Hydrogel biosensor array platform indexed by shape. *Chemistry of Materials* **16**, 5574-5580 (2004).
- 86 Crini, G. & Badot, P.-M. Application of chitosan, a natural aminopolysaccharide, for dye removal from aqueous solutions by adsorption processes using batch studies: A review of recent literature. *Progress in Polymer Science* **33**, 399-447 (2008).
- 87 Jamnongkan, T. & Kaewpirom, S. Potassium release kinetics and water retention of controlled-release fertilizers based on chitosan hydrogels. *Journal of Polymers and the Environment* **18**, 413-421 (2010).
- 88 Demitri, C., Scalera, F., Madaghiele, M., Sannino, A. & Maffezzoli, A. Potential of cellulose-based superabsorbent hydrogels as water reservoir in agriculture. *International Journal of Polymer Science* **2013**, 1-6 (2013).
- 89 Zohuriaan-Mehr, M. & Kabiri, K. Superabsorbent polymer materials: A review. *Irania Polymer Journal* **17**, 451-477 (2008).
- 90 Hoffman, A. S. Hydrogels for biomedical application. *Advanced Drug Delivery Review* **54**, 3-12 (2002).
- 91 Peppas, A., Bures, P., Leobandung, W. & Ichikawa, H. Hydrogels in pharmaceutical formulations. *European Journal of Pharmaceutics and Biopharmaceutics* **50**, 27-46 (2000).
- 92 Peppas, N. A., Hilt, J. Z., Khademhosseini, A. & Langer, R. Hydrogels in biology and medicine: From molecular principles to bionanotechnology. *Advanced Materials* **18**, 1345-1360 (2006).
- 93 Lin, Y. H., Liang, H. F., Chung, C. K., Chen, M. C. & Sung, H. W. Physically crosslinked alginate/N,O-carboxymethyl chitosan hydrogels with calcium for oral delivery of protein drugs. *Biomaterials* **26**, 2105-2113 (2005).
- 94 Boucard, N. *et al.* The use of physical hydrogels of chitosan for skin regeneration following third-degree burns. *Biomaterials* **28**, 3478-3488 (2007).
- 95 Sun, T. *et al.* Physical hydrogels composed of polyampholytes demonstrate high toughness and viscoelasticity. *Nature materials* **12**, 932-937 (2013).
- 96 Wischerhoff, E. *et al.* Controlled cell adhesion on PEG-based switchable surfaces. *Angewandte Chemie* **47**, 5666-5668 (2008).
- 97 Nash, M. E. *et al.* Ultra-thin spin coated crosslinkable hydrogels for use in cell sheet recovery—synthesis, characterisation to application. *Soft Matter* **8**, 3889-3899 (2012).
- 98 Nguyen, K. & Wesr, J. Photopolymerizable hydrogels for tissue engineering applications. *Biomaterials* **23**, 4307-4314 (2002).
- 99 Huynh, C. T., Nguyen, Q. V., Kang, S. W. & Lee, D. S. Synthesis and characterization of poly(amino urea urethane)-based block copolymer and its potential application as injectable pH/temperature-sensitive hydrogel for protein carrier. *Polymer* **53**, 4069-4075 (2012).

## 5. Literature

---

- 100 Palumbo, F. S. *et al.* In situ forming hydrogels of hyaluronic acid and inulin derivatives for cartilage regeneration. *Carbohydr Polym* **122**, 408-416 (2015).
- 101 Zheng Shu, X., Liu, Y., Palumbo, F. S., Luo, Y. & Prestwich, G. D. In situ crosslinkable hyaluronan hydrogels for tissue engineering. *Biomaterials* **25**, 1339-1348 (2004).
- 102 Shu, X. Z., Liu, Y., Luo, Y., Roberts, M. C. & Prestwich, G. D. Disulfide cross-linked hyaluronan hydrogels. *Biomacromolecules* **3**, 1304-1311 (2002).
- 103 Segura, T. *et al.* Crosslinked hyaluronic acid hydrogels: a strategy to functionalize and pattern. *Biomaterials* **26**, 359-371 (2005).
- 104 Maiti, B., Ruidas, B. & De, P. Dynamic covalent cross-linked polymer gels through the reaction between side-chain  $\beta$ -keto ester and primary amine groups. *Reactive and Functional Polymers* **93**, 148-155 (2015).
- 105 Jiang, Y., Chen, J., Deng, C., Suuronen, E. J. & Zhong, Z. Click hydrogels, microgels and nanogels: emerging platforms for drug delivery and tissue engineering. *Biomaterials* **35**, 4969-4985 (2014).
- 106 Gong, C. *et al.* Synthesis and characterization of PEG-PCL-PEG thermosensitive hydrogel. *International journal of pharmaceutics* **365**, 89-99 (2009).
- 107 Lipatov, Y. Polymer blends and interpenetrating polymer networks at the interface with solids. *Progress in Polymer Science* **27**, 1721-1801 (2002).
- 108 Holback, H., Yeo, Y. & Park, K. Hydrogel swelling behavior and its biomedical applications. 3-24 (2011).
- 109 Ganji, F., Vasheghani-Farahani, S. & Vasheghani-Farahani, E. Theoretical description of hydrogel swelling: A review. *Irania Polymer Journal* **19**, 375-398 (2010).
- 110 Anseth, K. S., Bowman, C. N. & Brannon-Peppas, L. Mechanical properties of hydrogels and their experimental determination. *Biomaterials* **17**, 1647-1657 (1996).
- 111 Reinhart, C. & Peppas, N. Solute diffusion in swollen membranes Part II. Influence of crosslinking on diffusive properties. *Journal of Membrane Science* **18**, 227-239 (1984).
- 112 Jeong, B., Bae, Y. & Kim, S. Drug release from biodegradable injectable thermosensitive hydrogel of PEG-PLA-PEG triblock copolymers. *Journal of Controlled Release* **63**, 155-163 (2000).
- 113 Burdick, J. A. & Prestwich, G. D. Hyaluronic acid hydrogels for biomedical applications. *Adv Mater* **23**, 41-56 (2011).
- 114 Hardingham, T. in *Chemistry and Biology of Hyaluronan* 1-19 (Elsevier Ltd., 2004).
- 115 Fraser, J. R. E., Laurent, T. C. & Laurent, U. B. G. Hyaluronan: its nature, distribution, functions and turnover. *Journal of Internal Medicine* **242**, 27-33 (1997).
- 116 Meyer, L. & Stern, R. Age-dependent changes of hyaluronan in human skin. *Journal of Investigative Dermatology* **102**, 385-389 (1994).
- 117 Laurent, U. Hyaluronate in aqueous humour. *Experimental Eye Research* **33**, 147-155 (1981).
- 118 Frenkel, J. S. The role of hyaluronan in wound healing. *International wound journal* **11**, 159-163 (2014).
- 119 Zhao, M. *et al.* Evidence for the covalent binding SHAP, heavy chains of inter-alpha-trypsin inhibitor, to hyaluronan. *The Journal of Biological Chemistry* **270**, 26657-26663 (1995).

## 5. Literature

---

- 120 Kogan, G., Soltes, L., Stern, R. & Gemeiner, P. Hyaluronic acid: a natural biopolymer with a broad range of biomedical and industrial applications. *Biotechnology letters* **29**, 17-25 (2007).
- 121 Hargittai, I. & Hargittai, M. Molecular structure of hyaluronan: an introduction. *Structural Chemistry* **19**, 697-717 (2008).
- 122 Laurent, T. C., Laurent, U. B. G. & Fraser, J. R. E. The structure and function of hyaluronan: An overview. *Immunology and Cell Biology* **74**, 1-7 (1996).
- 123 Atkins, E. & Meader, D. Model for hyaluronic acid incorporating four intramolecular hydrogen bonds. *International journal of biological macromolecules* **2**, 318-319 (1980).
- 124 Hascall, V. & Laurent, T. Hyaluronan: structure and physical properties. *Glycoforum* (1999).
- 125 Atkins, E. & Sheehan, J. Hyaluronates: Relation between molecular conformations. *Science* **179**, 562-564 (1973).
- 126 Haxaire, K., Braccini, I., Milas, M., Rinaudo, M. & Perez, S. Conformational behavior of hyaluronan in relation to its physical properties as probed by molecular modeling. *Glycobiology* **10**, 587-594 (2000).
- 127 Sheenan, J. & Almond, A. Hyaluronan: Static, hydrodynamic and molecular dynamic views. *Glycoforum* (2001).
- 128 Stern, R., Asari, A. A. & Sugahara, K. N. Hyaluronan fragments: an information-rich system. *European journal of cell biology* **85**, 699-715 (2006).
- 129 Laurent, T. C. & Fraser, J. R. E. Hyaluronan. *The FASEB Journal* **6**, 2397-2404 (1992).
- 130 Almond, A. Hyaluronan. *Cellular and molecular life sciences : CMLS* **64**, 1591-1596 (2007).
- 131 Liesegang, T. Viscoelastic substances in ophthalmology. *Survey of Ophthalmology* **34**, 268-293 (1990).
- 132 Balazs, E. in *Cosmetic and pharmaceutical applications of polymers* (eds C. Gebelein, T. Cheng, & V. Yang) 293-310 (Plenum Press, 1990).
- 133 Shiedlin, A. *et al.* Evaluation of hyaluronan from different sources: Streptococcus zooepidemicus, rooster comb, bovine vitreous and human umbilical cord. *Biomacromolecules* **5**, 2122-2127 (2004).
- 134 Miller, R. & Avila, L. in *Chemistry and Biology of Hyaluronan* 505-528 (Elsevier Ltd, 2004).
- 135 Shu, X. & Prestwich, G. in *Chemistry and Biology of Hyaluronan* 475-502 (Elsevier Ltd, 2004).
- 136 Blummel, J. *et al.* Protein repellent properties of covalently attached PEG coatings on nanostructured SiO<sub>2</sub>-based interfaces. *Biomaterials* **28**, 4739-4747 (2007).
- 137 Shu, X. Z., Liu, Y., Palumbo, F. & Prestwich, G. D. Disulfide-crosslinked hyaluronan-gelatin hydrogel films: a covalent mimic of the extracellular matrix for in vitro cell growth. *Biomaterials* **24**, 3825-3834 (2003).
- 138 Rolli, C. G. *et al.* Switchable adhesive substrates: revealing geometry dependence in collective cell behavior. *Biomaterials* **33**, 2409-2418 (2012).
- 139 Pitt, W. G., Morris, R. N., Mason, M. L., Hall, M. W. & Luo, Y. Attachment of hyaluronan to metallic surfaces. *Journal for Biomedical Materials Research* **68**, 95-106 (2004).
- 140 Brunette, D. M., Tengvall, P., Textor, M. & P.Thomsen. *Titanium in medicine*. (Springer, 2001).
- 141 Weeks, M. The discovery of the elements. *Journal of Chemical Education* **10**, 223-227 (1933).
- 142 Lütjering, G. & Williams, J. C. *Titanium*. (Springer, 2007).

## 5. Literature

---

- 143 Faller, K. & Froes, S. The use of titanium in family automobiles: Current trends. *The Journal of The Minerals, Metals & Materials Society* **53**, 27-28 (2001).
- 144 Fray, D. J. & Chen, G. Z. Reduction of titanium and other metal oxides using electrodeoxidation. *Materials Science and Technology* **20**, 295-300 (2004).
- 145 Boyer, R. An overview on the use of titanium in the aerospace industry. *Materials Science and Engineering* **213**, 103-114 (1996).
- 146 Wang, K. The use of titanium for medical applications in the USA. *Materials Science and Engineering* **213**, 134-137 (1996).
- 147 Le Guehennec, L., Soueidan, A., Layrolle, P. & Amouriq, Y. Surface treatments of titanium dental implants for rapid osseointegration. *Dental Materials* **23**, 844-854 (2007).
- 148 Long, M. & Rack, H. Titanium alloys in total joint replacement - a materials science perspective. *Biomaterials* **19**, 1621-1639 (1998).
- 149 Gonzalez, J. & Mirza-Rosca, J. Study of the corrosion behavior of titanium and some of its alloys for biomedical and dental implant applications. *Journal of Electroanalytical Chemistry* **471**, 109-115 (1999).
- 150 Khan, M., Williams, R. & Williams, D. In-vitro corrosion and wear of titanium alloys in the biological environment. *Biomaterials* **17**, 2117-2126 (1996).
- 151 Ratner, B. D. in *Titanium in Medicine* Ch. 1, 1-10 (Springer-Verlag, 2001).
- 152 Niinomi, M. & Narushima, T. *Advances in metallic biomaterials tissues, materials and biological reactions* (Springer Berlin Heidelberg, 2015).
- 153 Schueler, M., Trentin, D., Textor, M. & Tosatti, S. Biomedical interfaces: titanium surface technology for implants and cell carriers. *Nanomedicine* **1**, 449-463 (2006).
- 154 Bullock, E., Patthey, L. & Steinemann, S. Clean and hydroxylated rutile TiO<sub>2</sub> (110) surfaces studied by X-ray photoelectron spectroscopy. *Surface Science* **352-354**, 504-510 (1996).
- 155 Tengvall, P. & Lundström, I. Physico-chemical considerations of titanium as a biomaterial. *Clinical Materials* **9**, 115-134 (1992).
- 156 Collis, J. & Embery, G. Adsorption of glycoasminoglycans to commercially pure titanium. *Biomaterials* **13**, 548-552 (1992).
- 157 Höök, F. *et al.* A comparative study of protein adsorption on titanium oxide surfaces using in situ ellipsometry, optical waveguide lightmode spectroscopy and quartz crystal microbalance/dissipation. *Colloids and Surfaces B: Biointerfaces* **24**, 155-170 (2002).
- 158 Liu, X., Chu, P. & Ding, C. Surface modification of titanium, titanium alloys, and related materials for biomedical applications. *Materials Science and Engineering: R: Reports* **47**, 49-121 (2004).
- 159 Subramani, K. Titanium surface modification techniques for implant fabrication – From microscale to the nanoscale. *Journal of Biomimetics, Biomaterials, and Tissue Engineering* **5**, 39-56 (2010).
- 160 Rønold, H. J., Lyngstadaas, S. P. & Ellingsen, J. E. Analysing the optimal value for titanium implant roughness in bone attachment using a tensile test. *Biomaterials* **24**, 4559-4564 (2003).
- 161 Ratner, B. D. The catastrophe revisited: blood compatibility in the 21st Century. *Biomaterials* **28**, 5144-5147 (2007).
- 162 Huang, N. *et al.* Hemocompatibility of titanium oxide films. *Biomaterials* **24**, 2177-2187 (2003).
- 163 Nan, H. *et al.* Blood compatibility of amorphous titanium oxide films synthesized by ion beam enhanced deposition. *Biomaterials* **19**, 771-776 (1998).
- 164 Giorleo, L., Ceretti, E. & Giardini, C. Ti surface laser polishing: Effect of laser path and assist gas. *Procedia CIRP* **33**, 446-451 (2015).

## 5. Literature

---

- 165 Kern, M. & Thompson, V. Effects of sandblasting and silica-coating procedures on pure titanium. *Journal of Dentistry* **22**, 300-306 (1994).
- 166 Nanci, A. *et al.* Chemical modification of titanium surfaces for covalent attachment of biological molecules. *Journal of Biomedical Materials Research* **40**, 324-335 (1998).
- 167 Nishiguchi, S. *et al.* The effect of heat treatment on bone-bonding ability of alkali-treated titanium. *Biomaterials* **20**, 491-500 (1999).
- 168 Yoshida, K. *et al.* Thin sol-gel-derived silica coatings on dental pure titanium casting. *Journal of Biomedical Materials Research* **48**, 778-785 (1999).
- 169 Trögler, T. *et al.* Erosion resistance of CVD diamond-coated titanium alloy for aerospace applications. *Surface and Coatings Technology* **112**, 129-132 (1999).
- 170 Sevilla, P., Godoy, M., Salvagni, E., Rodríguez, D. & Gil, F. J. Biofunctionalization of titanium surfaces for osseointegration process improvement. *Journal of Physics: Conference Series* **252**, 012009 (2010).
- 171 Chua, P. H., Neoh, K. G., Kang, E. T. & Wang, W. Surface functionalization of titanium with hyaluronic acid/chitosan polyelectrolyte multilayers and RGD for promoting osteoblast functions and inhibiting bacterial adhesion. *Biomaterials* **29**, 1412-1421 (2008).
- 172 Xiao, S., Textor, M. & Spencer, N. Immobilization of the cell-adhesive peptide Arg-Gly-Asp-Cys(RGDC) on titanium surfaces by covalent chemical attachment. *Journal of Materials Science: Materials in Medicine* **8**, 867-872 (1997).
- 173 Rezania, A., Johnson, R., Lefkow, A. R. & Healy, K. E. Bioactivation of metal oxide surfaces. 1. Surface characterization and cell response. *Langmuir : the ACS journal of surfaces and colloids* **15**, 6931-6939 (1999).
- 174 Mani, G. *et al.* Drug delivery from gold and titanium surfaces using self-assembled monolayers. *Biomaterials* **29**, 4561-4573 (2008).
- 175 Nair, D. P. *et al.* The thiol-Michael addition click reaction: A powerful and widely used tool in materials chemistry. *Chemistry of Materials* **26**, 724-744 (2014).
- 176 Hagel, V. *et al.* Desmosine-inspired cross-linkers for hyaluronan hydrogels. *Scientific reports* **3**, 2043 (2013).
- 177 Halliwell, C. M. & Cass, A. E. G. A factorial analysis of silanization conditions for the immobilizations of oligonucleoties on glass surfaces. *Analytical Chemistry* **73**, 2476-2483 (2001).
- 178 Thierry, B., Winnik, F., Merhi, Y., Griesser, H. & Tabrizian, M. Biomimetic hemocompatible coatings through Immobilization of hyaluronan derivatives on metal surfaces. *Langmuir : the ACS journal of surfaces and colloids* **24**, 11834-11841 (2008).
- 179 Mukherjee, C., Maiti, G. & Misra, A. Regioselective ring opening of epoxides with thiols in water. *Archive for Organic Chemistry* **11**, 46-55 (2008).
- 180 Bruice, P. *Organic chemistry*. (Prentice Hall International, 2004).
- 181 Kwok, D. Y. & Neumann, A. W. Contact angle measurements and contact angle interpretation. *Advances in Colloid and Interface Science*, 167-249 (1999).
- 182 Brzoska, J., Azouz, I. & Rondelez, F. Silanization of solid substrates: A step toward reproducibility. *Langmuir : the ACS journal of surfaces and colloids* **10**, 4367-4373 (1994).
- 183 Walthall, W. K. & Stark, J. D. The acute and chronic toxicity of two xanthene dyes, fiorescein sodium salt and phloxine B, to *Daphnia pulex*. *Environmental Pollution* **104**, 207-215 (1999).
- 184 Sjöback, R., Nygren, J. & Kubista, M. Absorption and fluorescence properties of fluorescein. *Spectrochimica Acta Part A* **51**, 7-21 (1995).

## 5. Literature

---

- 185 Shiohara, A., Hoshino, A., Hanaki, K., Suzuki, K. & Yamamoto, K. On the cytotoxicity caused by quantum dots. *Microbiology and Immunology* **48**, 669-675 (2004).
- 186 Ogamo, A., Matsuzaki, K., Uchiyama, H. & Nagasawa, K. Preparation and properties of fluorescent glycosamino-glycuronans labeled with 5-aminofluorescein. *Carbohydrate Research* **105**, 69-85 (1982).
- 187 Kuo, J.-w., Swann, D. A. & Prestwich, G. D. Chemical modification of hyaluronic acid by carbodiimides. *Bioconjugate Chem.* **2**, 232-241 (1991).
- 188 Prestwich, G., Marecak, D., Marecek, J., Vercruyse, K. & Ziebell, M. Controlled chemical modification of hyaluronic acid: synthesis, applications, and biodegradation of hydrazide derivatives. *Journal of Controlled Release* **53**, 93-103 (1998).
- 189 Sehgal, D. & Vijay, I. K. A method for the high efficiency of water-soluble carbodiimide-mediated amidation. *Analytical Biochemistry* **218**, 87-91 (1994).
- 190 Vercruyse, K. P., Marecak, D. M., Marecek, J. F. & Prestwich, G. D. Synthesis and in vitro degradation of new polyvalent hydrazide cross-linked hydrogels of hyaluronic acid. *Bioconjugate Chem.* **8**, 686-694 (1997).
- 191 Son, G. M. *et al.* Self-assembled polymeric micelles based on hyaluronic acid-g-poly(D,L-lactide-co-glycolide) copolymer for tumor targeting. *International journal of molecular sciences* **15**, 16057-16068 (2014).
- 192 Ellman, G. L. A colorimetric method for determining low concentrations of mercaptans. *Archives of Biochemistry and Biophysics* **74**, 443-450 (1958).
- 193 Butterworth, P. H. W., Baum, H. & Porter, J. W. A modification of the ellman procedure for the estimation of protein sulphhydryl groups. *Archives of Biochemistry and Biophysics* **118**, 716-723 (1967).
- 194 Boehm, H. P. Acidic and basic properties of hydroxylated metal oxide surfaces. *Discussions of the Faraday Society* **52**, 264-275 (1971).
- 195 Martin, H. J., Schulz, K. H., Bumgardner, J. D. & Walters, K. B. An XPS study on the attachment of triethoxysilylbutyraldehyde to two titanium surfaces as a way to bond chitosan. *Applied Surface Science* **254**, 4599-4605 (2008).
- 196 Wu, L.-K., Chen, K.-Y., Cheng, S.-Y., Lee, B.-S. & Shu, C.-M. Thermal decomposition of hydrogen peroxide in the presence of sulfuric acid. *Journal of Thermal Analysis and Calorimetry* **93**, 115-120 (2008).
- 197 Tsukruk, V. V., Luzinov, I. & Julthongpipit, D. Sticky molecular surfaces: Epoxysilane self-assembled monolayers. *Langmuir : the ACS journal of surfaces and colloids* **15**, 3029-3032 (1999).
- 198 Balkenende, A. R., Boogaard, H. J. A. P., Scholten, M. & Willard, N. P. Evaluation of different approaches to assess the surface tension of low-energy solids by means of contact angle measurements. *Langmuir : the ACS journal of surfaces and colloids* **14**, 5907-5912 (1998).
- 199 Hozumi, A., Ushiyama, K., Sugimura, H. & Takai, O. Fluoroalkylsilane monolayers formed by chemical vapor surface modification on hydroxylated oxide surfaces. *Langmuir : the ACS journal of surfaces and colloids*, 7600-7604 (1999).
- 200 Tsierkezos, N. G. & Molinou, I. E. Thermodynamic properties of water + ethylene glycol at 283.15, 293.15, 303.15, 313.15. *Journal of Chemical and Engineering Data* **43**, 989-993 (1998).
- 201 Elender, G., Kühner, M. & Sackmann, E. Functionalisation of Si/SiO<sub>2</sub> and glass surfaces with ultrathin dextran films and deposition of lipid bilayers. *Biosensors & Bioelectronics* **11**, 565-577.

## 5. Literature

---

- 202 Chatani, S., Nair, D. P. & Bowman, C. N. Relative reactivity and selectivity of vinyl sulfones and acrylates towards the thiol–Michael addition reaction and polymerization. *Polymer Chemistry* **4**, 1048-1055 (2013).
- 203 Thompson, J., Vollman, R., Austin, D. & Kartchner, M. Prevention of hypertensive and renal complications of aortic surgery using balanced salt solution: Thirteen-year experience with 670 cases. *Annals of Surgery* **167**, 767-777 (1968).
- 204 www.bose-electroforce.com. *BOSE Electrofore Homepage URL*, <[http://worldwide.bose.com/electroforce/en\\_us/web/home/page.html?src=redirect](http://worldwide.bose.com/electroforce/en_us/web/home/page.html?src=redirect)> (
- 205 *ISI Web of Knowledge*, <[www.webofknowledge.com](http://www.webofknowledge.com)> (
- 206 Cai, S., Hu, Y., Zhao, X. & Suo, Z. Poroelasticity of a covalently crosslinked alginate hydrogel under compression. *Journal of Applied Physics* **108**, 113514 (2010).
- 207 Galli, M., Comley, K. S. C., Shean, T. A. V. & Oyen, M. L. Viscoelastic and poroelastic mechanical characterization of hydrated gels. *Journal of Materials Research* **24**, 973-979 (2011).
- 208 Holle, A., Chao, S., Holl, M., Houkal, J. & Meldrum, D. in *3rd Annual IEEE Conference on Automation Science and Engineering* 621-627 (IEEE, Scottsdale, 2008).
- 209 Rice, S. in *Comprehensive chemical kinetics: Diffusion-limited reactions* (Elsevier, 1985).
- 210 Belder, A. N. D. & Wik, K. O. Preparation and properties of fluorescein-labelled hyaluronate. *Carbohydrate Research* **44**, 251-257 (1975).
- 211 Zhu, X. Z. & Prestwich, G. D. in *Chemistry and Biology of Hyaluronan* Ch. 22, 475-504 (Elsevier, 2004).
- 212 Chang, C., Peng, J., Zhang, L. & Pang, D.-W. Strongly fluorescent hydrogels with quantum dots embedded in cellulose matrices. *Journal of Materials Chemistry* **19**, 7771-7776 (2009).
- 213 Mermoud, A. Ex-Press implant. *The British journal of ophthalmology* **89**, 395-396 (2005).
- 214 Khajavikhan, M. *et al.* Thresholdless nanoscale coaxial lasers. *Nature* **482**, 204-207 (2012).
- 215 Discher, D., Janmey, P. & Wang, Y. Tissue cells feel and respond to the stiffness of their substrate. *Science* **310**, 1139-1143 (2005).

---

## 6. Appendix

### 6.1. List of abbreviations

<b>POAG:</b>	Primary open-angle glaucoma
<b>IOP:</b>	Intraocular pressure
<b>PEG:</b>	Poly(ethylene glycol)
<b>PNIPAM:</b>	Poly(N-isopropylacrylamide)
<b>PHEMA:</b>	Poly (hydroxyethyl methacrylate)
<b>HA:</b>	Hyaluronic acid
<b>GAG:</b>	Glycosaminoglycan
<b>DTPH:</b>	Dithiobis(propionic hydrazide)
<b>DTBH:</b>	Dithiobis (butanoic hydrazide)
<b>DTT:</b>	Dithiothreitol
<b>FA:</b>	Fluoresceinamine
<b>HS-HA:</b>	Hyaluronic acid modified with thiol groups
<b>FA-HA:</b>	Hyaluronic acid modified with fluoresceinamine
<b>HS-FA-HA:</b>	Hyaluronic acid modified with thiol groups and fluoresceinamine
<b>BIS or MBAA:</b>	N,N'-Methylenebisacrylamide
<b>EDC:</b>	N-(3-Dimethylaminopropyl)-N'-ethylcarbodiimide
<b>NHS:</b>	N-Hydroxysuccinimide
<b>TG:</b>	Thiolation grade = Degree of substitution of HS-HA with thiol groups
<b>GPS:</b>	Glycidyloxypropyl)trimethoxy-silane
<b>PFS:</b>	1H,1H,2H,2H-Perfluoro-trichlorosilane
<b>APTES:</b>	(3-Aminopropyl)triethoxysilane
<b>PBS:</b>	Phosphate buffered saline
<b>BSS:</b>	Balanced salt solution
<b>TRIS:</b>	Tris(hydroxymethyl)aminomethane
<b>PEGDAA:</b>	Poly(ethylene glycol) diacrylamide
<b>BIS or MBAA:</b>	N,N'-Ethylenebis(acrylamide)
<b>CPA:</b>	Continuous pressure application
<b>HPA:</b>	Hydrostatic pressure application
<b>EP:</b>	Equilibrium pressure

<b>DTNB:</b>	(5,5'-dithiobis-(2-nitrobenzoic acid))
<b>PLA:</b>	Poly lactide
<b>PTFE:</b>	Polytetrafluorethen (Teflon)

## 6.2. Additional $^1\text{H}$ -NMR's of DTPH and unmodified hyaluronan

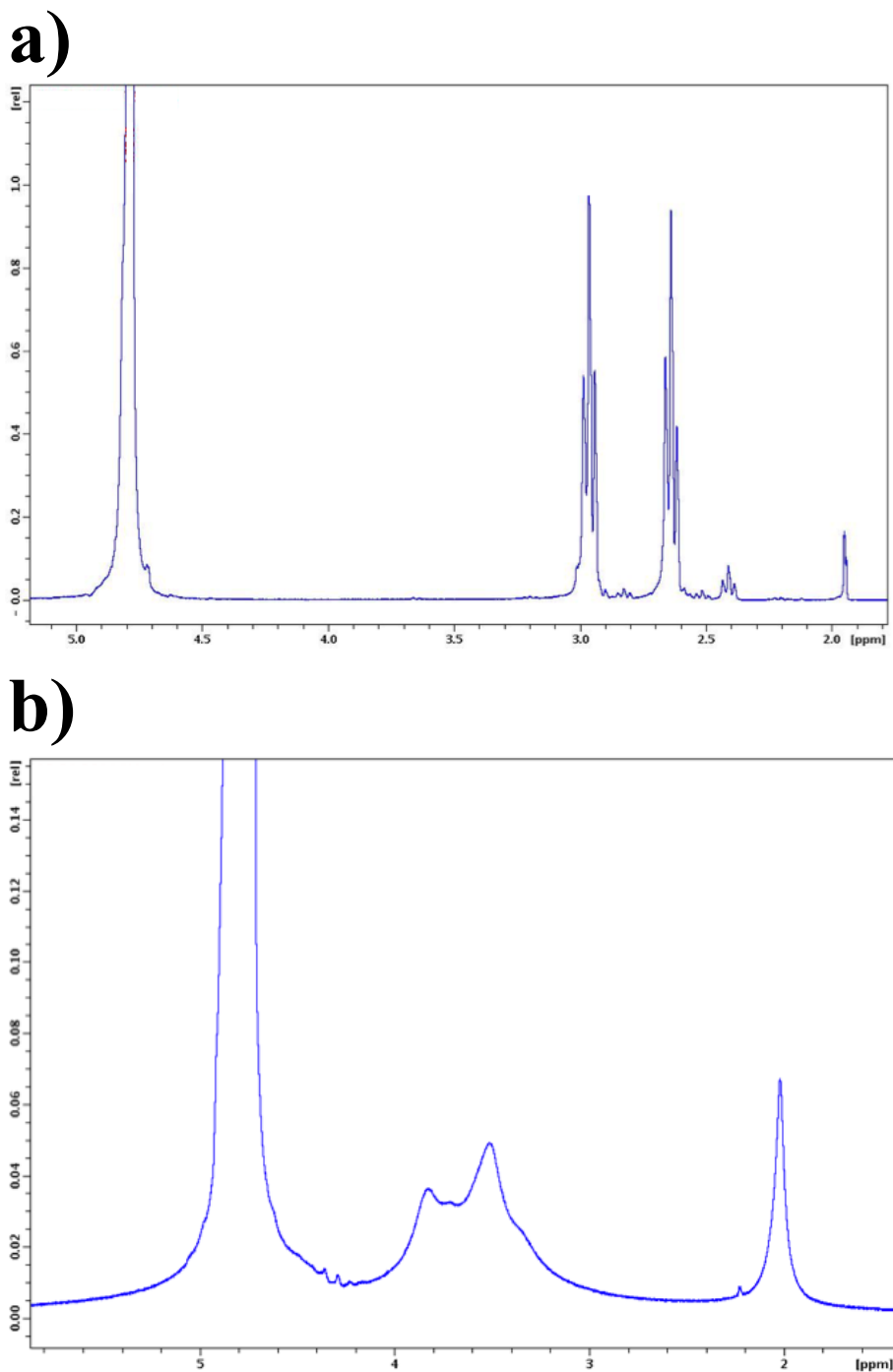


**Figure 82:** (a):  $^1\text{H}$ -NMR of DTPH. The triplets at  $\delta = 2.9631$  ppm and  $2.6376$  ppm belong to the  $-\text{CH}_2-\text{CH}_2-$  functions of DTPH. The smaller peaks were attributed to either  $^{13}\text{C}$  satellites or impurities. (b):  $^1\text{H}$ -NMR of unmodified HA ( $M_n = 60$  kDa). The multiplet at  $\delta = 4-3$  ppm belonged to the  $-(\text{CH})-$  groups of the polysaccharide backbone and the singlet at  $\delta = 2,1$  ppm was attributed to the  $-\text{CH}_3$  of the glycosamin.

### 6.3. pH changes in unbuffered BSS due to diluting HS-HA



**Figure 83:** Image of pH stripes immersed into an unbuffered BSS solution before (a) and after (b) the dissolution of HS-HA ( $M_n = 60$  kDa,  $\beta = 15$  mg/mL, TG = 0,18) illustrating the necessity of using buffers.

### 6.4. Blueprints of molds for creating macroscopic hydrogels

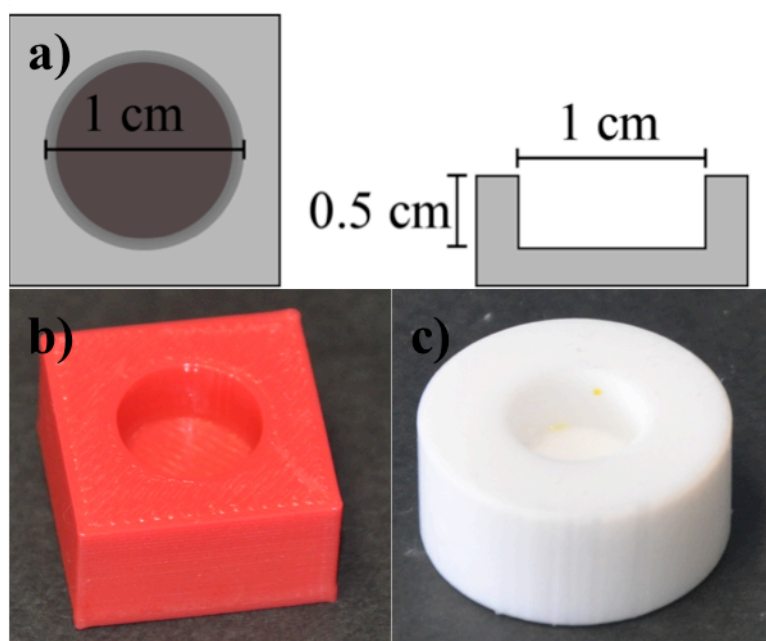


**Figure 84:** Blueprint (a) of molds used for creating the macroscopic hydrogels made from PLA (b) and PTFE (c).

6.5. Blueprints of sample holder for CPA measurements

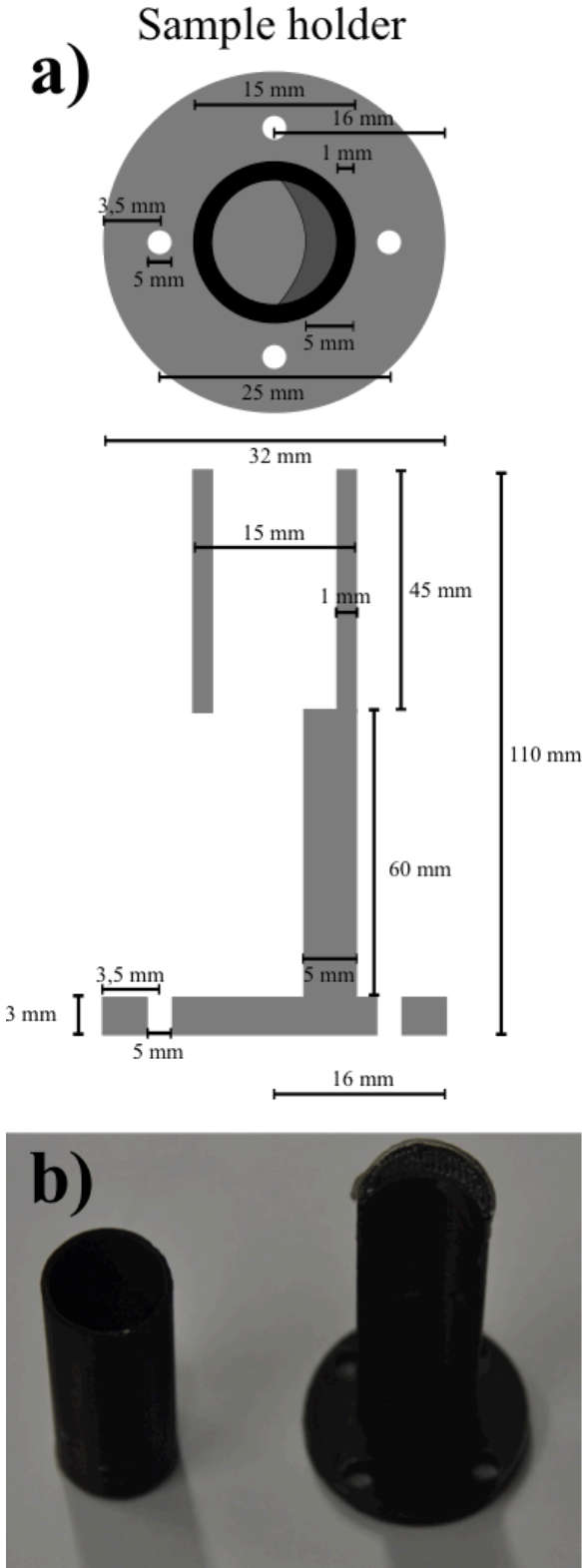


**Figure 85:** Blueprint (a) and image (b) of holder for CPA measurements. The holder was 3D printed in two parts as seen in (b) and glued together manually. The syringe could be inserted from the top as shown in Figure 44.

## 6.6. Blueprints of setup for partially silanizing glass and titanium slides

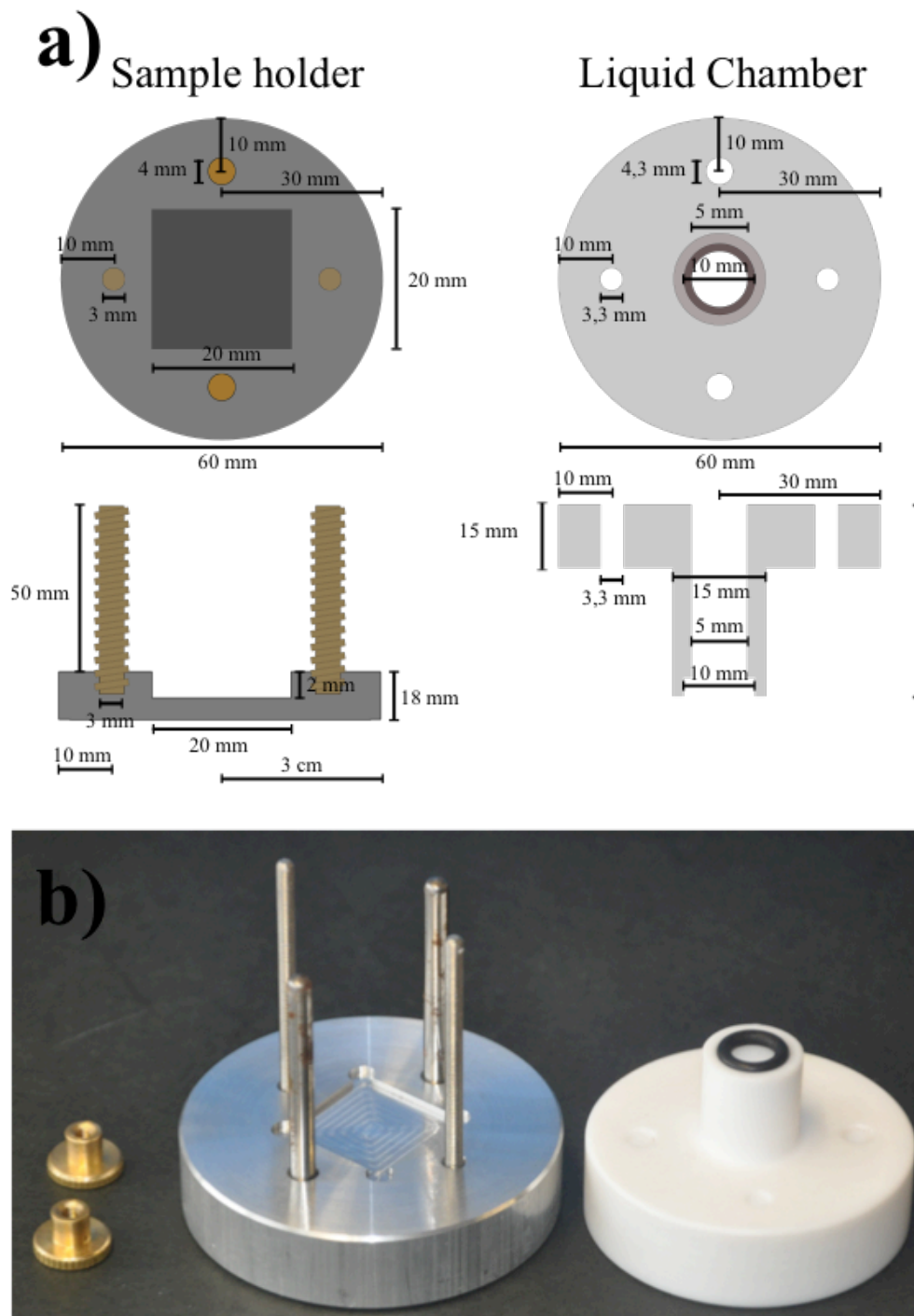


**Figure 86:** Blueprint (a) and image (b) of the setup used for partially silanizing flat glass and titanium slides.

**6.7. Blueprints for the setup for filling large glass tubes (ID = 5 mm; OD = 7 mm) with hydrogels**

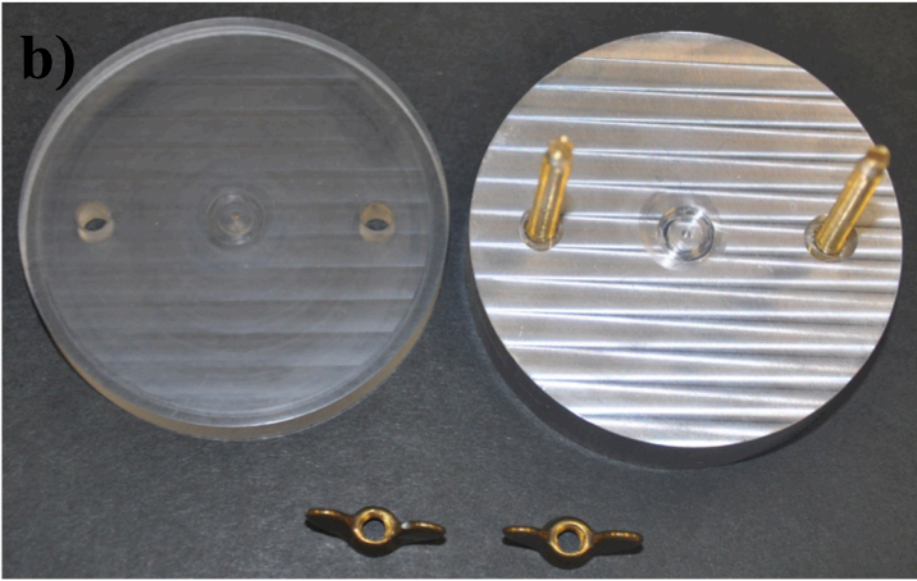
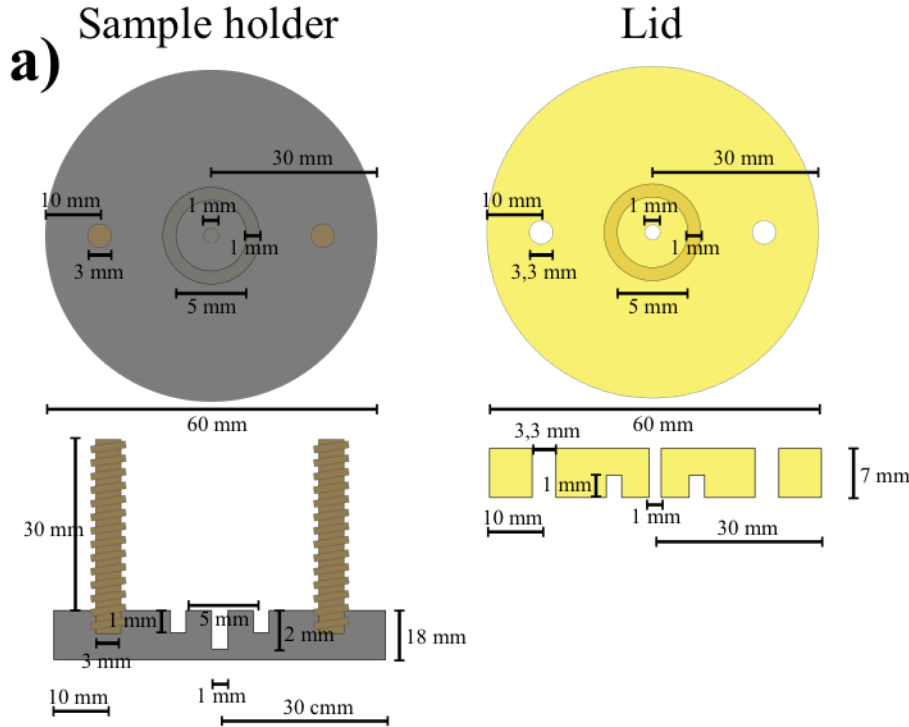


**Figure 87:** Blueprint (a) and image (b) of the sample holder used for immobilizing HA hydrogels within large glass tubes (L = 10 mm; ID = 5 mm; OD = 7 mm). The circular incisions were designed to exactly fit with the glass tubes. Holes were large enough to allow glass fibers to a maximum diameter of 0.9 mm.

---

## **6.8. Publication derived from this thesis**

European Patent Application:

Number: 15002024.6

Title: “Intraocular device and method for preparing the same”

Patent owner: Max Planck Society for the Advancement of Science

Inventors: Prof. Dr. J.P. Spatz, Dr. Fania Geiger, Michael Thaller, Dr. Heike Böhm, Dr. Christian Lingenfelder

---

## Danksagungen

Zuerst möchte ich mich bei Prof. Dr. Joachim Spatz und bei Dr. Fania Geiger bedanken, die mich während der gesamten Doktorarbeit begleitet haben. Bei Joachim dafür, dass er mir ermöglicht hat diese Doktorarbeit durchzuführen, die guten Anregungen und für die Freiheit die er mir gelassen hat meinen eigenen Ideen nachzugehen. Danke Fania, für deine Begleitung, Mühe und Hilfestellung während der gesamten Zeit und dass du mir immer mit Rat zur Seite standest wenn ich mal nicht weiter wusste. Selbst wenn du mal im Streß warst wenn deine Kinder dich auf Trab hielten.

Prof. Dr. Reiner Dahint gilt mein Dank dafür, dass er sich als Zweitgutachter für diese Doktorarbeit zur Verfügung gestellt hat.

Mein Dank gilt sowohl Dr. Heike Böhm, die mich mit ihrem Wissen über Hyaluronsäure in der Anfangsphase meiner Doktorarbeit mit ihrer Beratung sehr unterstützt hat, als auch den Mitgliedern ihrer Gruppe für die hilfreichen Diskussionen. Speziell Patricia Hegger möchte ich noch danken für die zahlreichen Diskussionen gegenseitigen Hilfestellungen.

Besonders bedanken möchte ich mich auch bei PD Dr. Günter Maier, der mir bei der Benutzung des Kernspinresonanzspektrometers sowie mehrerer Problemen physikalischer Art geholfen hat und Dr. Jan-Henning Dirks, der mir unter anderem die Nutzung des 3D Druckers sowie des BOSE Druckmessers ermöglichte und mir außerdem viele Tips bei der Herstellung verschiedener Messaufbauten geben konnte. Auch Christine Mollenhauer möchte ich danken für die regelmäßige Unterstützungen bei den kleinen Dingen während des Laboralltags und ihre immer fröhliche Art und Weise.

Weiterhin möchte ich Prof. Dr. Peer Fischer danken, der es mir erlaubte seine Geräte für meine Laserexperimente zu benutzen sowie Andrew Mark, der mir die Benutzung des Lasers beigebracht hat.

Mein Dank gilt auch Dr. Andrew Holle, dass er geholfen hat meine Doktorarbeit zu korrigieren, obwohl er selbst stets viel Arbeit zu erledigen hatte.

Weiterhin möchte ich mich auch bei meinen Kollegen, Dr. Markus Weiler, Dr. Christoph Stanglmair, Dr. Sarah Jahn, Wenwen Chen, Kim Clar und Dr. Jennifer Young bedanken, mit denen ich viel gemeinsame Stunden im Labor verbracht habe und die immer mit Rat und Tat zur Seite standen. Besonders Markus half mir sehr mit dem Erlernen verschiedenster Software und der Bereitstellung eigener Programme zur Bewältigung einiger Probleme. Auch Wenwen hat mir vor allem in der Anfangszeit sehr geholfen mich zurecht zu finden und war stets eine gute Freundin. Zusätzlich gilt mein Dank auch meinen Kollegen im Büro, Dr. Adria Sales, Galina Khachatryan und Hossein Riahinezhad, die immer für interessante Diskussionen und viel Spass sorgten, auch wenn die Arbeit mal weniger Spass machte. Auch bei den anderen Mitgliedern in der Gruppe, sowohl in Stuttgart als auch Heidelberg möchte Ich mich bedanken für die gute Arbeitsatmosphäre, die netten Gespräche und gemeinsamen Unternehmungen.

Auch Elisabeth Pfeilmeier, Sunsanne Sandbrink sowie Frau Petra Ziegler von der Universität Heidelberg möchte ich für ihre freundliche Hilfe bei administrativen Dingen danken. Weiterhin möchte ich hiermit den Mitarbeitern der Feinmechanik Werkstatt als

---

auch den Glasbläsern, die meinen z.T. aufwändigen Bedarf an experimentellen Aufbauten und speziellen Proben stets mit Freundlichkeit und Zuverlässigkeit erfüllen konnten meine Wertschätzung ausdrücken.

Zu guter letzt gilt mein besonderer Dank den Projektpartnern Dr. Christian Lingenfelder und Dr. Christoph Lindner von der alamedics GmbH & Co. KG, sowie Dr. Martin Udart vom ILM Ulm für den regelmäßigen Austausch und dem Bundesministerium für Bildung und Forschung, als auch dem VDI Technologiezentrum für die Finanzierung und Begleitung des Projekts.

---

## Eidesstattliche Versicherung

gemäß § 8 der Promotionsordnung der Universität Heidelberg für  
die Naturwissenschaftlich-Mathematischen Gesamtfakultät

1. Bei der eingereichten Dissertation zu dem Thema „**Hyaluronan hydrogel modified intraocular implants for glaucoma treatment**“ handelt es sich um meine eigenständig erbrachte Leistung.

2. Ich habe nur die angegebenen Quellen und Hilfsmittel benutzt und mich keiner unzulässigen Hilfe Dritter bedient. Insbesondere habe ich wörtlich oder sinngemäß aus anderen Werken übernommene Inhalte als solche kenntlich gemacht.

3. Die Arbeit oder Teile davon habe ich bislang nicht an einer Hochschule des In- oder Auslands als Bestandteil einer Prüfungs- oder Qualifikationsleistung vorgelegt.

4. Die Richtigkeit der vorstehenden Erklärungen bestätige ich.

5. Die Bedeutung der eidesstattlichen Versicherung und die strafrechtlichen Folgen einer unrichtigen oder unvollständigen eidesstattlichen Versicherung sind mir bekannt.

Ich versichere an Eides statt, dass ich nach bestem Wissen die reine Wahrheit erkläre und nichts verschwiegen habe.

\_\_\_\_\_  
Ort und Datum

\_\_\_\_\_  
Unterschrift

